WL-TR-95-2040

SOVIET SPACE POWER TECHNOLOGY

S. V. TIMASHEV
A. A. KULANDIN

SOUTHEASTERN CENTER FOR ELECTRICAL
   ENGINEERING EDUCATION
SPACE EXPLORATION ASSOCIATES, INC.

MARCH 1995
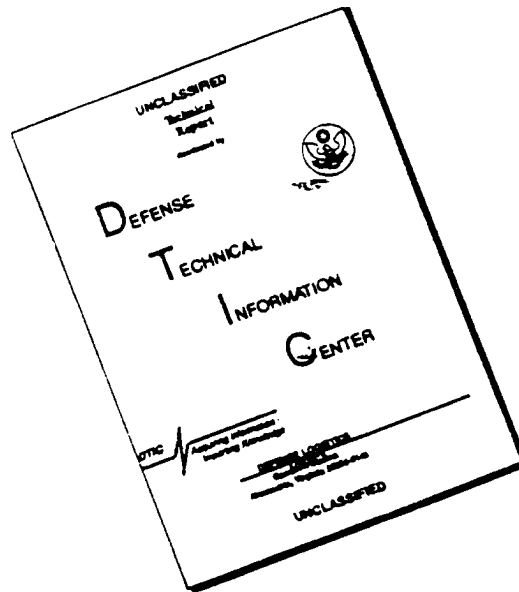
FINAL REPORT FOR 07/15/91-09/15/91

APPROVED FOR PUBLIC RELEASE; DISTRIBUTION IS UNLIMITED.

19960322 053
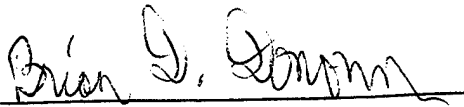
DTIC QUALITY INSPECTED 1

DISCLAIMER NOTICE

THIS DOCUMENT IS BEST QUALITY AVAILABLE. THE COPY FURNISHED TO DTIC CONTAINED A SIGNIFICANT NUMBER OF PAGES WHICH DO NOT REPRODUCE LEGIBLY.
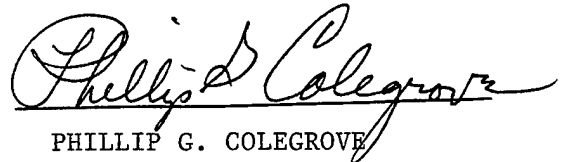
NOTICE

When Government drawings, specifications, or other data are used for any purpose other than in connection with a definitely Government-related procurement, the United States Government incurs no responsibility or any obligation whatsoever. The fact that the government may have formulated or in any way supplied the said drawings, specifications, or other data, is not to be regarded by implication, or otherwise in any manner construed, as licensing the holder, or any other person or corporation; or as conveying any rights or permission to manufacture, use, or sell any patented invention that may in any way be related thereto.

This report is releasable to the National Technical Information Service (NTIS). At NTIS, it will be available to the general public, including foreign nations.
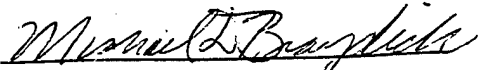
This technical report has been reviewed and is approved for publication.

BRIAN D. DONOVAN
Project Engineer
Power Generation and Thermal Management
Section

PHILLIP G. COLEGROVE
Chief
Power Generation and Thermal Management
Section

MICHAEL D. BRAYDICH, Lt Col, USAF
Chief
Aerospace Power Division

If your address has changed, if you wish to be removed from our mailing list, or if the addressee is no longer employed by your organization please notify WL/POOS-3, WPAFB, OH 45433-7251 to help us maintain a current mailing list.

Copies of this report should not be returned unless return is required by security considerations, contractual obligations, or notice on a specific document.

REPORT DOCUMENTATION PAGE

Public reporting burden for this collection of information is estimated to average 1 hour per response, including the time for reviewing instructions, searching existing data sources, gathering and maintaining the data needed, and completing and reviewing the collection of information. Send comments regarding this burden estimate or any other aspect of this collection of information, including suggestions for reducing this burden, to Washington Headquarters Services, Directorate for Information Operations and Reports, 1215 Jefferson Davis Highway, Suite 1204, Arlington, VA 22202-4302, and to the Office of Management and Budget, Paperwork Reduction Project (0704-0188), Washington, DC 20503.

1. AGENCY USE ONLY (Leave blank)	2. REPORT DATE MAR 1995	3. REPORT TYPE AND DATES COVERED FINAL 07/15/91--09/15/91

4. TITLE AND SUBTITLE SOVIET SPACE POWER TECHNOLOGY	5. FUNDING NUMBERS C F33615-90-C-2088 PE 63218 PR D812 TA 00 WU 01
6. AUTHOR(S) S. V. TIMASHEV A. A. KULANDIN	

7. PERFORMING ORGANIZATION NAME(S) AND ADDRESS(ES) SOUTHEASTERN CENTER FOR ELECTRICAL ENGINEERING EDUCATION SPACE EXPLORATION ASSOCIATES, INC.	8. PERFORMING ORGANIZATION REPORT NUMBER

9. SPONSORING/MONITORING AGENCY NAME(S) AND ADDRESS(ES) AERO PROPULSION AND POWER DIRECTORATE WRIGHT LABORATORY AIR FORCE MATERIEL COMMAND WRIGHT PATTERSON AFB OH 545433-7251	10. SPONSORING/MONITORING AGENCY REPORT NUMBER WL-TR-95-2040

12a. DISTRIBUTION/AVAILABILITY STATEMENT APPROVED FOR PUBLIC RELEASE: DISTRIBUTION IS UNLIMITED	12b. DISTRIBUTION CODE

13. ABSTRACT (Maximum 200 words)

This publication contains information on the space power experience fo the former Soviet Union. Topics covered include nuclear power generation, thermionic energy conversion, thermoelectrics, thermal management, and radioisotope generators. This document is intended to be an AIAA textbook.

14. SUBJECT TERMS SPACE POWER, REACTORS, THERMIONICS, THERMOELECTRICS	15. NUMBER OF PAGES 356
	16. PRICE CODE

17. SECURITY CLASSIFICATION OF REPORT	18. SECURITY CLASSIFICATION OF THIS PAGE	19. SECURITY CLASSIFICATION OF ABSTRACT	20. LIMITATION OF ABSTRACT
UNCLASSIFIED	UNCLASSIFIED	UNCLASSIFIED	UL

Table of Contents

List of Figures   Page

xi

List of Tables

1. GENERAL OBSERVATIONS ON SPACE POWER

Space power is an offshoot of ground-based power technology but it has a number of characteristic features which we will discuss below. At this point it is appropriate to comment on the general features of any power system such as devices for satisfying appropriate needs for different kinds of power (electrical, mechanical, thermal, etc.). We can cite many examples beginning with early steam machinery and ending with complex atomic electric stations. It is important here to emphasize something else. Power has always proven to be and will always prove to be a decisive factor in determining system characteristics and capabilities. Moreover, power exerts a revolutionary influence on the development of the means for which it is intended. Here are just a few characteristic examples. Conventional aerospace power technology came at the end of the 1940s to a dead end. Piston engines, although modernized, could not bring propeller aircraft even close to the speed of sound. The advent of jet engines by the beginning of the fifties allowed jet aircraft to approach the sound barrier and then transition to supersonic flight speeds.

Another example is the submarine fleet. Submarines with powerful diesel engines were always limited in the duration of submerged voyages. The situation rapidly changed with the development of powerful atomic steam turbine installations. Atomic powered undersea voyages became practically unlimited in duration.

The last example is in the space power area. All space systems to date are used principally for gathering information. The information is transmitted to earth (and in some cases into space) by way of weak electrical signals. They contain what we need to know; i.e. meteorological, navigational and other kinds of data. However, the advent of new and more efficient sources of power and principally of new converters of primary energy into electromagnetic radiation with a high energy density beam will turn the space vehicle from one of information to one of power. It will then be capable of long distance transmission of large amounts of energy that is far from in the nature of information.

The examples presented illustrate general characteristics of power. However, space power has its own specific characteristics. We need to discuss these, if only briefly. First of all, there are the conditions to which any space system, and, consequently, its power equipment, are subjected. These conditions are very well known: deep vacuum, weightlessness, space environmental factors (radiation of various kinds, flows of elementary and microparticles, radiation belts, and so on). Before proceeding with a summary of specific space power characteristics, we need to define terms in the area to be considered.

To begin with, all on-board systems of a space vehicle can be divided conventionally into two large groups: special purpose and support. The first group involves the accomplishment of specific tasks and it requires the supply of different forms of energy. The second group makes sure that this energy is provided. It includes thermal control systems, command and control, and electrical supply systems. Life support systems must be added to a manned space vehicle. The purpose of the electrical supply system is obvious. The thermal control system provides the temperatures needed by different on-board users. Command and control includes low thrust rocket engines (sometimes also electric thrusters). The purpose of these systems is to make sure that a

variety of space vehicle maneuvers can be accomplished in space, in particular, orbit correction, stabilization, orientation, etc. Later on we will examine the principles of an electrical supply system with nuclear sources of primary power, and in general the thermal control system which constitutes in part the equipment for rejecting heat to the external medium. The electrical control system includes not only sources of electrical power (these we call energy sources), but also different current converters and devices for stabilization, regulation and control. However, the central position in any electrical control system is occupied by the energy source. The power plant is the sum total of the source of primary energy, the conversion of this energy to electric energy, and finally the equipment for rejecting waste heat into space.

The purpose of any energy source to generate electrical power in response to a specific schedule. In the more general case, the make-up of the energy source may include piping systems with heat transfer fluids, pumps and other smaller components. Since our main attention later on will be paid to thermal nuclear power plants, we present their general schematic (Fig. 1.1). We note that the schematic is characteristic of any thermal power plant for stationary or transport purposes.

Now that we have provided a general definition of items in space power, it is wise to examine general requirements placed on them from the standpoint of the system mission.

1.1. Basic Aspects of Energy Expenditure in Space

The accomplishment of any task in space involves different ways of expending energy. The basic expenditures are electrical, thermal and mechanical energies. It is convenient to separate the expenditure of electrical energy and the demand it places on the electrical supply system into two independent groups by assigning to them the following principal requirements:

The first class of use is for spacecraft data processing. All spacecraft electronics produce heat in addition to their intended function as processing devices. Under ground-based conditions this situation does not cause any complications. This can, however, become a serious problem in space. Heat rejection can only occur by radiation to space in this situation. At low temperatures, very large radiators are required. There are, therefore, limitations on how much electrical power can be made available to satisfy the needs of the given group. In summarizing numerous studies in this area, we find that power requirements will probably be limited to around 30-50 kW and almost certainly less than 100 kW, at least for the foreseeable future.

The second group of users of electrical energy consists of equipment in which the greater part of the expended energy leaves the space vehicle. Typical examples are electric thrusters. In such engines (at their best performance level) up to 70 - 80% of the required electrical energy is transformed into kinetic energy of the working fluid flow which develops reactive thrust. Here there are virtually no limitations on electrical power requirements. Numbers in the hundreds of kilowatts and even tens of megawatts (such as in engine assemblies in Mars vehicle designs) are mentioned in the literature.

The expenditure of thermal energy generally involves heating of appropriate space vehicle compartments. Such an expenditure to room temperature levels is referred to as a

2
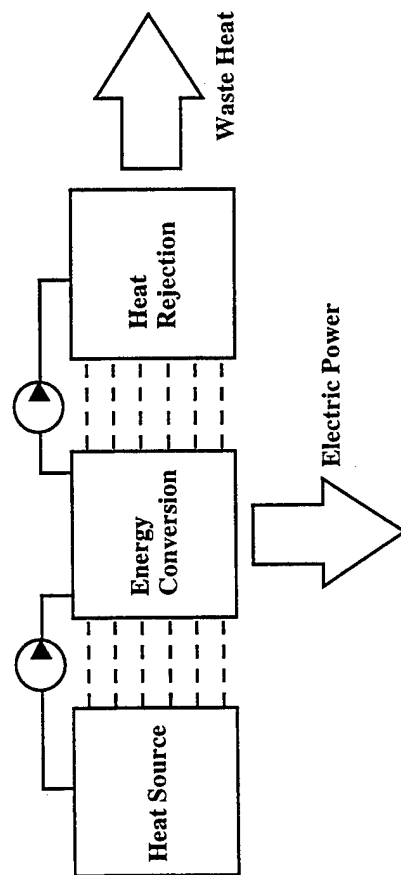
Fig. 1.1 General heat engine block diagram.

heating expenditure. However, if one has in mind the need to secure substantially lower temperatures all the way to cryogenic temperatures, then we do not talk about heating expenditures but about refrigeration expenditures. Such expenditures require the use of special refrigeration units. These units need also to consume electrical energy. The "cost" of the cooling done can, therefore, be quite high.

Finally, we have mechanical energy expenditures. Again in the general case, we can talk about the operation of some mechanical device (control equipment, control units of aerospace planes, etc.). However, the main form of mechanical energy expenditure involves that expended in accomplishing a variety of space vehicle maneuvers in the space environment. These expenditures are none other than flows of fuel (working fluid) through different kinds of engine units. The magnitude of the required flow is easily established from the Tsiolkovskiy equation. It results from the need to maintain characteristic velocities and may be responsible for a significant fraction of the launch weight of the space vehicle.

In our discussion we have been talking about average power requirements. Actual energy needs during one orbit around the earth are clearly marked by nonuniformities. In order to illustrate this, we present in qualitative form a load graph, i.e., a function in the form shown in Figure 1.2. As can be seen, the maximum power may significantly exceed the average requirement during a single orbit.

Such is the general view of energy expenditures in space. On-board power is required to satisfy them. As we have noted, our principal attention will be focused on the energy supply. Next, we present a retrospective overview of possible sources and converters of energy that make up an energy source.

1.2. Brief Characteristics of Primary Energy Sources.

Let's turn to the schematic in Fig. 1.1 which illustrates the basic components of any power plant. The first one is the source of primary energy. Such a source came from several classes which we will divide into two groups: on-board and external. On-board sources include mechanical, thermal, chemical and nuclear sources. Mechanical sources may be compressed gases, springs and flywheels and others. A feature that distinguishes mechanical sources is the extremely low values of stored specific energy (i.e., energy per unit mass of the source). Practical considerations limit this to 20 to 60 w/kg. This mechanical energy can easily and virtually without loss be transformed into electrical energy. An example is winding down a previously spun up flywheel with an electric generator. Such a system could be of interest in providing short duration maximum (peak) power. Here and later on we should keep in mind that the energy requirement for one revolution or orbit around the earth is clearly nonuniform. In addition to some constant power requirement, the need for peak power is encountered, although of short duration, that will exceed by several times the average requirement.

The simplest primary sources of thermal energy are different kinds of thermal energy storage devices. They work by melting and freezing appropriate substances.

Chemical sources of primary energy are found on board the space vehicle as stored (in principle, periodically replenished) fuel components. Their energy can be utilized in different ways. In short, these are the combustion reaction with the liberation of heat and
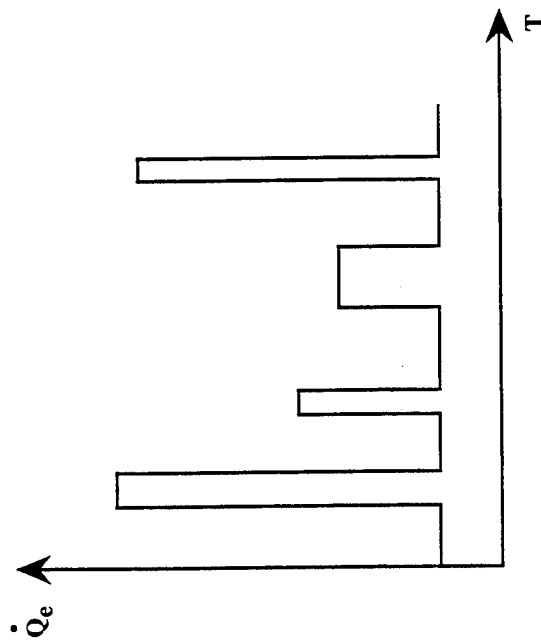
Fig. 1.2 Electric power demand usually consists of periods of peak demand and station keeping for most satellites.

the "cold" combustion reaction during which the chemical energy is converted directly into electrical.

Hydrogen-oxygen sources are most widely used in space power. Their energy capacity reaches hundreds to thousands of w/kg.

Nuclear sources of primary energy have a significantly greater energy capacity. The effects of different nuclear processes (reactions) can be used in liberating the following kinds of energies:

a. *Mechanical*, for example, by focusing the fission fragments being produced and in this manner develop reactive forces. The escape velocity of such a "working fluid" from these unique rocket engines may reach 10^7 cm/sec and higher. However, we have not found a practical application for such engines.

b. *Electrical*, by applying different electrical potentials during scattering from the reaction zone of oppositely charged elementary particles (for example, α particles and β particles). The difference in potentials can reach tens of kV. Atomic batteries are created in the laboratory based on this principle. However, in view of the low current density, the power of such atomic batteries does not exceed milliwatts, and the value of their practical use in space power has not been demonstrated.

c.. *Thermal*, due to the slowing down of fission fragments which at the instant of formation have colossal kinetic energies. This is the fundamental way in which nuclear energy produced in both fission reactors and radioisotope generators is used. The magnitude of the liberated energy lies in the range of tens of kilowatts per kilogram (in radioisotope generators) to millions of kilowatts per kilogram (in fission reactors).

Solar energy falls in the external source of primary energy category. The chief characteristic of solar radiation is its spectral composition, i.e., the distribution of radiation density as a function of the wavelengths that make up the spectrum (Fig. 1.3).

The total density of solar radiation, called the solar constant, is determined from the formula

$$E_s = \int_0^{\infty} \frac{E_s(\lambda)}{4\pi r^2} d\lambda \qquad (1.1)$$

where $E_s(\lambda)$ is the total amount of energy radiated by the sun at a wavelength λ, and r is the distance away from the sun. Its magnitude is characterized by the distance from the sun and at the limits of the earth's atmosphere it is about 1360 W/m^2. We note in passing that close to Mars the solar constant is about 680 W/m^2, and at Venus 2000 W/m^2.

Only the portion of the solar spectrum in the visible wavelength range (from 0.1 to 1.1 - 1.3 microns) is of practical use. Solar radiation as a primary source of energy is characterized by the following:

a. It is practically inexhaustible;

b. It is ecologically pure;

6
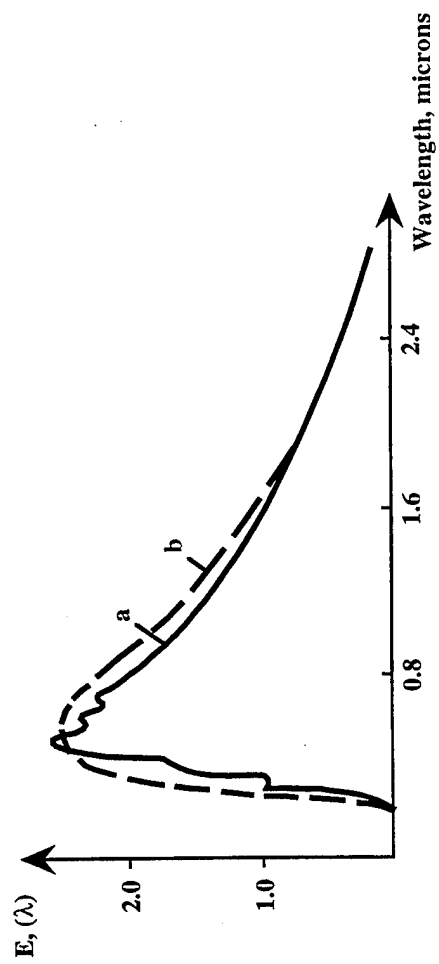
Fig. 1.3 Approximate wavelength-dependent solar energy flux.
a) actual; b) blackbody radiation curve.

c. It may be converted to many forms of energy.

The latter requires explanation. First, it is possible to obtain heat by in solar concentrator systems. Second, successes in the science and technology of semiconductor materials have allowed the development of efficient photoelectric converters of light energy into electrical. That is accomplished in solar cells. Third, it is possible also to use solar radiation in the direct production of thrust forces in the so-called photon engines ("solar sails"). Fourth, it is even possible to consider the direct conversion of solar energy to laser radiation, according recent studies.

These characteristics of solar radiation make it of great value in space power not only currently but also over the long term. For these reasons, solar radiation is a serious competitor with nuclear sources of energy. Thus, solar power must certainly be considered for any space power system.

In addition to solar radiation, there are different kinds of external flows such as cosmic radiation, magnetic fields of the Earth and of other planets, etc. Today it is also possible to consider remote transmission of energy via microwaves or laser beams.

1.3. Brief Characteristics of Energy Converters.

Processes of conversion of energy are accomplished in all on-board systems of the spacecraft for both special purposes and support. Below, we will briefly examine these processes with application to the energy source and only partially to the thermal control system by keeping in mind the conversion of heat at different temperature levels into thermal radiation to the surrounding medium.

Converters of primary energy that make up any energy source are divided into two groups: mechanical and direct converters. The first one is characterized by the fact that the primary (basically, thermal) energy is first transformed into mechanical energy mainly in devices operating within a closed gas (Brayton cycle) or a vapor (Rankine cycle) loop. Mechanical energy generated by gas or vapor turbines is converted into electrical energy by an electric generator. There are practically no losses in this process.

There are also other kinds of mechanical converters, for example, the well-known Stirling engine which is theoretically the most efficient of the mechanical converters. However, because this book is devoted primarily to nuclear energy sources with direct conversion of heat, we must discuss these especially in greater detail.

We can start by examining the principle of operation of direct converters of heat, chemical and solar energy. We will begin with the thermoelectric converter, using in our analysis a single thermoelement (Fig. 1.4), consisting of two semiconductors. The working process of the thermoelement is based on three thermoelectric effects: Seebeck, Peltier and Thompson. In a simplified examination of the principle of operation of the thermoelement (more detail on the operation of the thermoelectric converter will be provided later), it is sufficient to consider only the first effect. Essentially, when two semiconductors are joined, an electric current will arise when one of the junctions is heated and the other is cooled. When the circuit is interrupted by a gap, a difference potential (voltage) will exist across the gap. This is referred to as an electromotive force or thermal emf. Hence, when a temperature gradient exists along both semiconductors, a

8
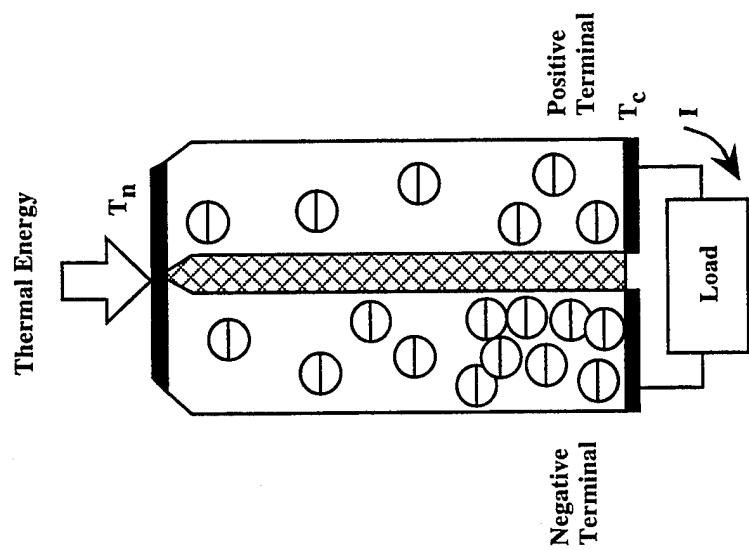
Fig. 1.4 Semiconductor thermoelectric element process diagram.

9

movement of charges (electrons) from the part with the higher temperature to the part with the lower temperature will begin. The electrical field that arises tries to reverse the electron flow, but since a temperature difference exists along the conductor, the concentration of electrons at the cold section will be higher than at the hot section. Since we agreed to consider only semiconductors, at any location (cross-section) of the column which they make up we will observe a difference in the concentration of electrons, which causes a thermal emf. If we now include in the circuit some load with a resistance R, an electric current I and a voltage V will be observed in the circuit. As a consequence, electrical work, I^2R, will be done.

Another direct converter of heat is the thermionic converter. Its operating process is based on the well-known thermionic effect, the emission of electrons by heated metals. It is not difficult to make such a diode. When there is a temperature differential between its electrodes (Fig. 1.5), in the one that is emitting electrons (the cathode, emitter) an electrical insufficiency (positive volume charge) will be created, and in the other (the anode, collector), a negative volume charge will accumulate. If such a diode is included in a circuit with a load R, a potential difference, or emf, will be observed across the open electrodes, and when they are closed, some voltage V and current I. The electrical power generated by such a diode will be equal to I^2R.

It is useful to make an analogy between a thermionic converter and any heat engine. In effect, at one of the electrodes heat is being conducted at a high temperature T_e and at the other it is being extracted at a lower temperature T_c. The difference between the conducted and extracted heat is, without accounting for losses, transformation to useful work. The working fluid of such a heat engine is an electron gas.

Fuel cells, another kind of direct energy converter, does not use heat but chemical energy to produce electrical energy. Power plants on this basis provided power from electrochemical generators in carrying out the "Apollo" lunar program and are used aboard the Space Shuttle Orbiter. The fuel cell also has two electrodes separated by some gap (electrolyte, ion membrane). A fuel is fed to one of the electrodes (Fig. 1.6). Owing to the catalytic properties of the electrode material, breaking of the chemical bond between the molecule and the atoms of the fuel occurs with the formation of positive ions of the fuel and free electrons. Ions migrate into the interelectrode gap, but the electrons remain at the electrode giving it a negative volume charge (the electrode becomes the anode). At the other electrode to which an oxidizer is fed, the process is similar. However, when the chemical bond of the molecule and the atoms of the oxidizer is broken, a combination occurs with the electrons from the electrode material with the simultaneous formation of negative oxidizer ions. This electrode takes on a positive charge and becomes a cathode. A potential difference is established between the cathode and the anode, the emf of the fuel cell. When the external (electron current) and the internal (ion current) circuits are closed, normal operation of the fuel cell begins with the development of useful work, I^2R, and the formation of reaction products by the interaction of positive ions of the fuel and negative ions of the oxidizer.

We observe that the working processes in fuel cells are similar to the working processes in thermionic converters of heat.

Last among the direct converters is the photoelectric converter, or solar cell which converts energy in the form of light into electrical energy. As shown in Fig. 1.7, it consists
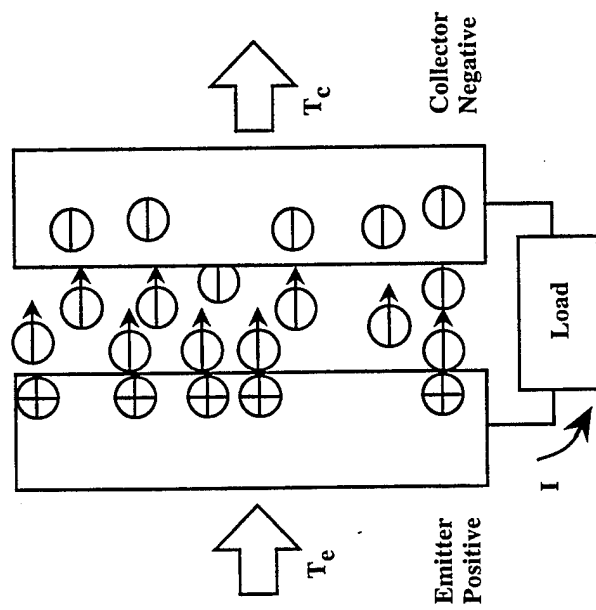
Fig. 1.5 Thermionic emitter process diagram.

11
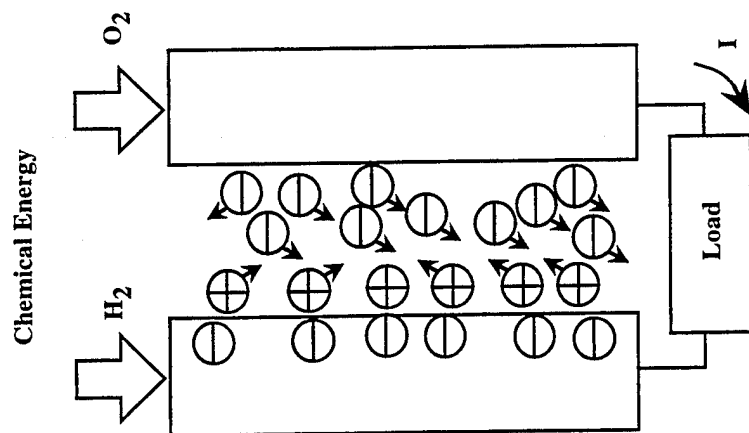
Fig. 1.6 Fuel cell process diagram.

of a diode (photodiode) with different properties that make up its electrodes. The partition between the electrodes behaves like a valve, i.e., it has the ability to let electrical charges pass freely through in one direction and to obstruct their movement in the other. As the result of absorption of solar radiation, additional charge carriers are formed (the well-known photoelectric effect). However, as the result of the valve properties of the layer bounding the diode, one part of the diode is negatively charged (a surplus quantity of electrons), and the other is positively charged (an insufficient quantity of electrons compared with the first one). Thus, a difference potential is created, the photoelectric emf, and by closing the circuit, an electric current I will flow in it doing useful work, I^2R.

At this point we could complete our consideration of the general principles of converters of primary energy into electrical. However, we want to mention still another, magnetohydrodynamic or MHD generators. A number of designs of such converters with nuclear sources are known, including also for space power. The essence of operation of the MHD converter is based on a well-known principle from electrical engineering. During the flow of a conducting fluid through a magnetic field, an electric current will arise in it. In this case, the conducting fluid is a plasma of any substance (liquid, gas), and its motion depends on purely gasdynamic properties, the conversion of potential (thermal) energy into kinetic energy. A simple schematic of an MHD converter is shown in Fig. 1.8.

For a variety of reasons (complex design requirements, the need to operate at high temperatures, etc.), such designs have not found practical application in space power. The reader may wish to consider the question: should such converters be classified as direct or indirect converters of thermal energy into electrical energy?

One should also consider thermal radiators that are not part of the primary power plant. To the number of energy converters on board the spacecraft one should also add thermal radiators (cooler-radiators) that are not used in primary energy power plants. A separate chapter in this book is devoted to their working processes.

The existence of all these possible sources and converters of primary energy make it possible to define an exceptionally broad spectrum of different classes and kinds of power plants.

1.4. Nuclear Power in Space: State of the Art and Prospects for the Development of Space Nuclear Power Plants.

The preceding sections provided a retrospective review of the principles of operation of different classes of space power plants. Many have found practical application (albeit not to the same degree), or offer significant promise for future use. Space nuclear power plants have also been mentioned briefly. However, specialists in a number of countries currently do not have a well-defined answer to the question of their use in space.

At the present time, a wealth of experience has been accumulated in the operation of nuclear power plants for both stationary and mobile applications. Unfortunately, while positive and highly acclaimed results have been achieved, some extremely negative events have also come about, at times tragic (for example, the Chernobyl atomic electric power station catastrophe in 1986).

13
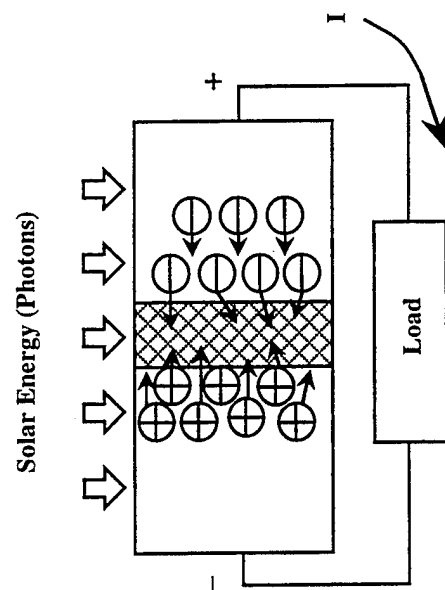
Fig. 1.7 Solar cell process diagram.

14
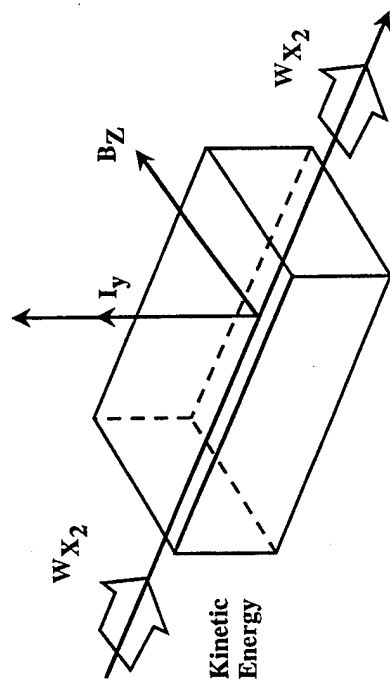
Fig. 1.8 Magnetohydrodynamic (MHD) generator process diagram.

Much anxiety developed throughout the world as a result of the accident on the Soviet space satellite "Cosmos-947" with its nuclear power plant. As is well known, this satellite fell in an uncontrolled manner through the dense layers of the atmosphere and certain components, including its nuclear reactor, impacted in the territory of Canada. Fortunately, dangerous consequences related to nuclear radiation were apparently avoided. Nevertheless, considerable doubt has arisen in scientific circles regarding the future use of nuclear power in space. In this connection, it is especially important to acquire detailed assessments of all aspects of the application, design and development of power plants with nuclear energy sources.

By correlating more than 30 years of experience in using nuclear power plants for different purposes in order to assess the future of nuclear power in general and in space in particular, we can with reasonable certainty single out three basic criteria for justifying the appropriateness in designing and developing power systems with nuclear energy sources for any purpose:

1) Nuclear energy must result in fundamental changes in the characteristics and nature of applications for which the use of nuclear energy is proposed. The importance of these changes must extend into military, political and economic spheres in the activities of humankind and must be supported at the highest government levels.

2) These fundamental, cardinal changes in these applications can come about *only* through the use of nuclear energy sources. Alternatives to their use must not exist.

3) The operation of any system with a nuclear energy source through its entire life cycle (including the burial of nuclear waste) must pose no danger or harm whatsoever to the earth's population.

Let's briefly examine the prospects for the development and use of space nuclear power in light of the above criteria.

We will not touch upon military-political goals although we could probably come up with some very convincing arguments (for example, the need for unlimited submerged travel of nuclear missile submarines). Regarding the first condition, let's turn our attention to economic and scientific objectives. Diminishing organic fuel reserves and the enormous difficulties in accessing them in remote regions (the Chukot region, the Far North, Alaska) and sharp (factors of 10) increases in cost make the development of nuclear power plants a national issue. Moreover, under these conditions the value of such power plants is increasing so much that they will permit new solutions to many economic problems.

A second example, which is illustrative of the first condition for the expedient development of nuclear power plants, pertains to space. At the present time and as the result of scientific and technical progress, the growing earth population increases the need for expanding communication and information links in all areas of life: commerce, education, medical services etc. Such services can be provided in a variety of ways:

a. By information exchange through new kinds of data links (video telephone, fax transmissions, electronic mail, etc.);

b. By global exchanges of computer software;

c. By monitoring and observing the movement of transport vehicles (aircraft, ships, and automobiles);

d. By supplying radar maps of the earth surface on request, etc.

All areas will experience an increase in the size of the territories served, an increasing number of subscribers and increasing exchange activities.

These needs can only be satisfied through the use of information systems in space. This can be accomplished only by increasing the strength of the signal used by the communications links. This, in turn, requires that the electrical power produced by the space vehicle be increased up to 20-30 kW and higher (possibly up to 100 kW in order to accomplish the radar mapping task). Power plants with nuclear energy sources are not only recommended in providing such power outputs, they are the only ones possible. There is still another advantage in using nuclear power plants in placing the "communications" satellites mentioned above in orbit. We know, for example, that the size of the payload placed in a geostationary orbit by using electric thrusters powered by a nuclear power supply will be significantly larger than that placed in the same orbit using liquid rocket engines.

A task of a special scientific nature, reflecting the realization of mankind's long dream, is the planned flight of a manned vehicle to Mars during the first quarter of the next century. Considerable research on a Mars vehicle and its power systems has been conducted during the past decades. A unique conclusion that can be drawn from these studies is that there is virtually no alternative to primary nuclear energy sources in supplying the entire range of energy for all stages of the flight. This, moreover, satisfies the second criterion for the development of nuclear power systems.

Numerous examples are appropriate here (recall again the comparison of atomic marine installations versus diesel generators for submarines). We will discuss only one. We know that radar mapping surveys of the earth surface are best accomplished from altitudes of 220-240 km. The electrical power requirement for radar mapping is in this case about 3 kW. Of course, such power levels can be satisfied in three different ways: by power plants that burn organic fuels (that is to say, hydrogen-oxygen fuel cells), solar cells and, finally, nuclear power plants. Note that when solar cells are used, thrusters will be needed in order to compensate for the aerodynamic drag of the solar cell panels. This drag can be substantial at the stated altitudes. Let's evaluate the time of active operation of such a spacecraft for each of the three classes of power plants. Turn to Table 1-1 and assume that the relative mass of the power and thruster system of the given spacecraft will not exceed 30% and that the mass of the spacecraft is less than 5 metric tons.

Table 1-1. Power System Mass Fraction

Operating Time, days	Fuel Cells	Photovoltaic Arrays	Nuclear Power
10	0.072	0.084	0.20-0.22
30	0.216	0.132	0.20-0.22
100	0.72	0.30	0.20-0.22
360	>1	>1	0.20-0.22

It is clear that beyond 100 days of active operation of the spacecraft there are no alternatives to nuclear energy sources.

Let's briefly discuss the third condition for the utility in developing and using nuclear power plants: the assurance of nuclear and radiation safety of nuclear power plants during their entire life cycle. A number of subsequent sections in this book are devoted to this important problem. Here we will only mention that even during the malfunctioning of "Cosmos-954" and "Cosmos-1900," no serious radiation consequences resulted. This holds true for the impact of satellite components from "Cosmos-954" in Canada and for the emergency transfer of "Cosmos-1900" into a radiation safe orbit. To this should be added the development of modern methods for providing nuclear and radiation safety of existing nuclear power plants (for example, Topaz) as well as of those planned in the future. We will discuss this more later.

Generally speaking, one can conclude that all the necessary conditions exist for the design and development of space nuclear power plants for a variety of applications, including lunar base. In addition, their role will inevitably increase as the number and complexity of space missions increase, including flights to the planets in the solar system.

It is now appropriate to discuss some historical aspects of the origin and modern development of space nuclear power.

These questions arose in the world immediately after the first launches of Sputnik and manned space vehicles as the 50's ended and the 60's began. These questions were also widely discussed in the USSR. Thus, during the mid 1960's numerous discussions were held in these areas at the Kurchatov Institute of Atomic Energy (IAE), at the Institute of Physical Power Engineering (IPPE) in Obninsk, and at various scientific and industrial organizations. The first All-Union scientific-technical conferences on problems of space power in 1963 - 1967 were held at the A. F. Mozhaiskiy Military Engineering Institute with the participation of prominent scientists and specialists from industry. Among the important decisions taken at these conferences, one should single out the thesis that the advent of new and more effective sources and converters of energy would open mainly new avenues to the use of cosmic space for a variety of purposes. The present has substantiated this prognosis. Currently, there are a number of competing projects for remote transmission of energy from space to satisfy a variety of requirements in space as well as on Earth. Other and still more practical results related to nuclear power have been obtained from the preferential development of nuclear power plants with direct conversion (thermoelectric and thermionic) of thermal energy into electrical. At the same time, in the USA preference has been given to the development of mechanical conversion using vapor and gas cycles. However, further design development and testing of individual components under test stand conditions have not taken place. In the Soviet

18

Union, on the other hand, specific power plant models with direct converters were developed, a number of which have repeatedly completed successful operation in space.

Variants of nuclear energy sources with thermoelectric conversion of thermal energy began to be studied in our country during the early 1960's. One of the first installations of this type was the "Romashka" facility, which was developed at the Kurchatov Institute of Atomic Energy (IAE). It was a high temperature fast reactor. High temperature fuel elements of dicarbide uranium with a 90% enrichment enclosed in graphite cartridges were used in the reactor. The reflector was made of metallic beryllium. The unused heat was radiated to the surrounding space from a finned radiator. The installation was brought to a calculated power of ~ 0.5 kW and successfully operated under test stand conditions for 15,000 hours. During this same time period, the SNAP-10A reactor was developed in the USA from the SNAP-2 reactor and it was tested in space for 40 days. However, thereafter work on the development of direct energy conversion came practically to a standstill. Further development in the USSR of nuclear energy sources with thermoelectric converters led to the development of installations with comparatively low powers (kilowatt level), which saw practical use in space and which did not lead to breaches in radiation safety (despite the well-known space objects, "Cosmos-954" and "Cosmos-1900").

The second direction in the area of nuclear energy sources with direct energy conversion was the use of the well-known phenomenon of thermionic emission.

One of the basic designs of a nuclear thermionic installation is the design with reactor-converters (Fig. 1.9), in which thermionic fuel elements (TFEs) are built into the reactor so as to create a single unit that generates heat and transforms that heat into electrical energy. Work on a nuclear energy source with single and multielement thermionic energy converters was conducted within the framework of the Topaz program and concentrated on the development of reactor-converters with cylindrical thermionic electrical generating channels. The work was done together with specialists from IAE, IPPE, NPO "Red Star," Central Design Bureau of Machine Building, now referred to as NPO Energiya) and other organizations. This joint development work on the nuclear energy source in the Topaz program led to a space demonstration.

Some parametric data on the Topaz-II unit and prospects for its development are shown in Tables 1-2 and 1-3.

Table 1-2. Topaz-2 Characteristics.

Electrical Power, kW	6
Thermal Power, kW	135
Output Voltage, v	28-30
Minimum Life, years	3
Mass of the Reactor Assembly, kg	1000
Length of the Reactor Assembly, m	3.9
Maximum Diameter, m	1.4

Fig. 1.9 Thermionic fuel element reactor, Topaz.

20

Table 1-3. Topaz Derivative Characteristics

	Topaz 3-61			Topaz 3-85			Topaz 3-97		
Number of TFEs	61			85			97		
Core Diameter, cm	31.5			37.0			38.5		
Reactor Mass, kg	430			565			600		
Electric Power per TFE, W	220	300	400	220	300	400	220	300	400
Reactor Output Power, kW	13.5	18.3	24	18.7	25.5	34	21	29	38
Reactor Assembly Mass, Metric Tonne	1.3	1.4	1.5	1.6	1.8	2.0	1.8	2.0	2.2

In 1987-1988, demonstration testing was successfully carried out during two flights of space vehicles in the "Cosmos" series. In order to assure safety, the experiments were done in high orbits. The results are still being analyzed. A preliminary result is that the practical operating capability of a nuclear energy source with thermionic emission during long, uninterrupted operation under cosmic space conditions was substantiated for the first time in the world. There was complete agreement of the parameters and their life behavior under natural conditions with characteristics obtained during ground testing.

There are two basic directions in the Soviet Union in the investigation of thermionic systems: low power reactors with zirconium hydride moderators and fast reactors with significantly higher powers. Up to now, the first direction has been given priority, and, therefore, our scientists and engineers have achieved the greatest results in this area.

The scientific potential that has been accumulated in the course of this work can be applied in the development of experimental models of nuclear thermionic energy sources in the 10-100 kW electric power output range (with thermal and intermediate reactors) and above 100 kW (with fast reactors).

Studies carried out in recent years and results of specific investigations show that the use of nuclear energy sources for a variety of space purposes are especially promising in energy-engine assemblies consisting of thermionic nuclear energy sources and high specific impulse electric thrusters. Such a combination allows one to accomplish highly efficient long duration and smooth satellite maneuvers, and as the energy supply and thrust of the engines grow, tasks involving transportation of loads into geostationary orbit and in interplanetary flight can be accomplished.

Investigations and preliminary analysis are also conducted of bimodal reactors capable of producing both electric power and propulsive thrust. The utility of applying nuclear energy sources for multiple functions will be determined by the possibilities offered by the nuclear rocket engine, which allows one to achieve exhaust velocity of up to 9000 m/sec in the engine mode with hydrogen as the working fluid. The advantages of nuclear energy sources will also be determined by the excellent thermal power, life and mass-size characteristics of nuclear energy-engine installations with closed power cycles.

We noted earlier that the work in the USA during the 1960s on the development of nuclear energy sources with mechanical converters of heat has been virtually discontinued, while in the USSR even simple design studies have generally not been conducted. This is due to the following reasons. In the vapor turbine design there are complexities in the management and separation of liquid phase and vapor phase working fluid under weightlessness, comparatively low efficiencies due to limitations on the turbine inlet temperature (especially with alkali metal vapors), the need for multiloop design configurations, etc.

Difficulties with the gas turbine design are the comparatively large dimensions of the radiator because of limitations on the turbine inlet gas temperature, and also the comparatively low development level of gas-cooled reactors.

Characteristic disadvantages of both kinds of power plants are gyroscopic moments caused by the rotating components (turbines, pumps, compressors), and also complexities in securing long rotor bearing life.

Currently, however, the position with regard to the development of nuclear energy sources with mechanical converters and the prospects for their application has changed substantially. This applies in particular to gas turbine designs that operate on the Brayton cycle. Gas-cooled reactors are being successfully developed. So-called petal shaped gas bearings with an operating life in excess of 10,000 hours have been developed. Of the greatest importance, however, is the advent of ceramic materials for gas turbine blades. One can now speak with confidence of turbine inlet gas temperatures at the 2000 degree Kelvin level and higher. Such temperatures, together with optimized compressor pressure ratios, will permit increases in gas turbine power plant efficiencies up to 20 - 25% and higher, i.e., gas turbine power plants will be fully competitive with thermionic reactor converters.

This completes our very short survey of the creation and development of specific items in space nuclear power. We note once more that we will return later to a more detailed examination of equipment and design of specific components in nuclear power. However, before we proceed with that it will be useful to acquaint the reader with fundamental and general information on nuclear energy sources from the nuclear physics point of view. We will present only the minimum information necessary to explain basic material on the theory and design of nuclear reactors for space nuclear energy sources, and partially in order to describe the principles of operation of isotope generators for space applications.

1.5. General Information on Nuclear Energy Sources.

In starting to study any item in nuclear power we need to turn our attention to the important situations we must deal with in terms of categories and topics pertaining to the submicroscopic world. Many of the laws that pertain to this world are not described by classical equations but by quantum mechanics. The theory of relativity is widely applied to this world. While familiar quantities are applied here, their measurement scales are quite unusual. The "tenants" of the "houses" in this world are elementary particles that rub shoulders with each other in a way peculiar only to their rules and laws. In order to enter into this world and in a general way become acquainted with its inhabitants, we need to

become familiar with (or restore in our recollection) a number of general premises in the science of nuclear physics.

1.5.1. General Information on Atomic Nuclei and Nuclear Forces.

The discovery of the structure of the atom and of the atomic nucleus were outstanding events in this century in the field of natural science. It allowed us not only to learn new laws of nature, but also to put them into service for the benefit of humankind. It allowed us to piece together an understanding of the worlds around us. In effect, everything that surrounds us in this world consists basically of three kinds of elementary particles: protons, neutrons and electrons. These particles can participate in only four known interactions: strong (nuclear), electromagnetic, weak and gravitational. These interactions differ substantially by the distances at which they manifest themselves noticeably, and also by their characteristic intensity. Thus, nuclear forces manifest themselves at distances between interacting particles on the order of 10^{-13} cm and in this region these forces are up to 10^3 times higher than electromagnetic forces.

Weak interactions (for example, neutron decay) occur at still shorter distances. At the same time, gravitational forces in nuclear processes can generally be neglected because their forces are comparatively small. Thus, any would-be phenomenon in nature we haven't discerned, or any would-be states of substances we haven't dealt with, will in the final analysis reduce to these basic interactions of several kinds of particles. For example, all atomic processes (combustion, chemical reactions) reduce to electromagnetic interactions of electrons with nuclei. In turn, all nuclear reactions are strong, electromagnetic interactions between elementary particles, basically, nucleons at "nuclear" distances. More intensive study of the properties of the nucleus led to the discovery of new elementary particles: mesons, pions, and others. They number more than a hundred at the present time. The study of elementary particles has now progressed to the point that there is hope of discovering the initial "building blocks" - super elementary particles with fractional electrical charges ("quarks") from which one could construct any microscopic or macroscopic object.

Elementary particles are notable for their high energies and they travel at high speeds that approach the speed of light. They interact, however, at very small distances. For this reason, they possess relativistic and quantum properties.

We are far from thinking about doing any detailed examination of this issue. We refer the student instead to appropriate materials usually presented in physics courses. We will only note that in energy calculations, together with the rest mass of elementary particles, the relativistic mass is also widely used. This can differ substantially from the rest mass.

We will often use one of the basic properties of the quantum world, the discrete standard structure of the energy spectra of atomic nuclei and elementary particles.

1.5.2. Fundamental Physical Quantities and Measurement Scales used in Nuclear Power.

Phenomena and processes are studied in nuclear physics that occur at small distances and at very high energies of the particle interactions. The upper limit on distance is the size of the atom, i.e., approximately 10^{-8} cm. The lower limit on energy involving single microparticles can be considered to be the electron binding energy in the atom, i.e., about 10^{-17} - 10^{-18} joule. Any lower limit on distance and higher limit on energy have not been established. Both of these limits are determined by experimental technology and measurement instruments. Advances in these areas will gradually change the limits. At the present time, the minimum length that can be measured is approximately 10^{-15} cm, i.e., five orders of magnitude smaller than the size of the atom. The maximum energy obtained experimentally involving a single particle falls in the range 0.6×10^{-7} to 0.8×10^{-7} joule. This is, of course, low for a macroscopic body but a lot for an elementary particle.

It is apparent that nuclear physics encompasses an enormous scale, five orders of magnitude in distance and 10 to 11 orders of magnitude in energy. While the fundamental unit of length in the SI system is one meter, in nuclear physics the unit of length used is basically one centimeter. A nonsystem unit, the fermi, which is equal to 10^{-13} m, is sometimes used. This unit is convenient because its order of magnitude is close to the size of the atomic nucleus. It is similar to the angstrom unit ($1 \text{ A} = 10^{-8}$ cm) which is also used in atomic physics because of its closeness to atomic sizes.

We must point out that not all elementary particles have sizes close to one fermi. This is the order of length (or distance) over which nuclear forces (strong interactions) act. The radii of electrons and of other elementary particles (weak interaction region) are so small that they still defy description by either measurement or observation.

The scale of distance is closely associated with the time scale. The most important notion of a time scale in nuclear processes is called nuclear time. It characterizes the time of flight of an elementary particle through an atomic nucleus. By supposing that the size of the nucleus is on the order of 10^{-13} cm, we obtain for nuclear time a magnitude of about 10^{-22} sec. Therefore, in nuclear processes $\tau > 10^{-22}$ sec is considered large and $\tau < 10^{-22}$ sec small.

The unit, 1 electron volt (eV) $= 1.6 \times 10^{-19}$ joule, is used in nuclear physics in measuring energy. This is the amount of energy acquired by an electron accelerated by a potential of 1 volt. Since nuclear interactions are characterized by much higher magnitudes of energy, either keV or MeV is often used. For example, in order to tear one proton or one neutron away from the nucleus one must expend about 10 MeV. With interaction energies of elementary particles on the order of 1 MeV the formation of an electron-positron pair is possible; with interaction energies up to 150 MeV, disintegration of the nucleus is possible; and at higher energies, the birth of new elementary particles can occur.

The so-called atomic mass unit (amu) is used in measuring the mass of atomic nuclei and elementary particles. The amu is defined as 1/12 the mass of a carbon isotope with a mass number A = 12. From this it is easy to obtain

$$\text{amu} = \frac{1}{12}\left(\frac{12}{A}\right) = \frac{1\,\text{atom}}{12}\left(\frac{12\,\dfrac{\text{g}}{\text{mol}}}{6.02 \times 10^{23}\,\dfrac{\text{atom}}{\text{mol}}}\right) = 1.66 \times 10^{-24}\,\text{g} \qquad .$$

The mass of the atomic nucleus ranges thus from about 1 amu in the case of hydrogen to over 250 for artificial trans-uranic elements.

Energy units of mass are often used in estimating the mass of an elementary particle. Their magnitudes in atomic units can easily be established from the fundamental Einstein principle which reflects the relationship between mass and energy. According to this principle, one amu = 931 MeV. The mass of elementary particles in reference tables is usually given in units of energy.

There are elementary "particles" (gamma quanta) the rest mass of which are equal to zero. From the theory of relativity, it follows that such particles, which do not have a nonrelativistic analog, must travel at a speed exactly equal to the speed of light.

We have looked at a number of fundamental physical quantities and measurement scales which are most frequently used in nuclear physics. In conclusion, we call attention to the fact that there are some other quantities that are used principally in various kinds of calculations in nuclear power. They are characterized by dimensions that do not correspond with our usual concepts. Thus, the probability of this or that interaction taking place are frequently expressed by the dimension of area (cm^2), and the probability of neutron escape from a reactor, frequently indicating an increasing number of neutrons, has dimensions of length squared (cm^2) etc.

In the subsequent sections we will briefly discuss such quantities and their measurement scales.

1.5.3. Basic Information on the Atomic Nucleus.

As is well-known, the atomic nucleus consists basically of nucleons, i.e., protons and neutrons. The nucleons in the nucleus are firmly held together by nuclear forces. Therefore, the energy (mass, by recalling Einstein's equation) of the nucleus is always less than the energy (mass) of the nucleons that make up the nucleus. Different nuclear models are in use today to describe the properties of the atomic nucleus. They differ in complexity and in the variety of phenomena that enter into the given investigation. The so-called "liquid drop" model is fully acceptable in realizing the aims of present day investigations. This model treats the nucleus as a very high density (up to 10^{14} g/cm^3) liquid drop made up of "nuclear material." The "nuclear material" resembles a liquid to a greater degree than a solid. One can, therefore, attribute properties of liquid drops to the nucleus-drop, namely, surface tension, breakup of droplets into smaller ones, or conversely, the combination of small droplets into larger ones, etc. In some cases, however, the liquid drop model does not explain specific properties of the atomic nucleus. More complex models are used in these situations. These models include nuclear shells according to which nucleons and elementary particles move according to the laws of quantum mechanics.

The physical quantities that characterize the properties of the atomic nucleus can be divided into statistical properties relevant to the unexcited state of the nucleus and to its subsequent nuclear transformations. Among the statistical characteristics of the nucleus that we need in discussing the material in the following sections are:

a. The composition of the nucleus, i.e., the number of protons, Z, neutrons, N, and the mass number, A = Z + N;

b. The size of the nucleus, the radius, R_n, and the nonsphericity factor, i.e., $\Delta R/R$. The radius of the nucleus can be determined from the simple relationship $R_n = R_0 A^{1/3}$, where $R_o = 1.2 \times 10^{-13}$ cm, the radius of a single nucleon;

c. Quantities that characterize mechanical properties, binding energy and spin characteristics. The spin characteristic is the inherent mechanical momentum of the nucleus which is equal to the sum of the momenta of the nucleons that make up the nucleus. The total momentum of each nucleon is, in turn, the sum of the spin and orbital momenta (i.e., it is associated with the motion of nucleons in specific trajectories within the nucleus).

While this is far from a complete description of atomic nuclei, we will return to using it later on.

1.5.4. Fundamental Properties of Nuclear Forces.

Nuclear forces are forces that act between individual nucleons. The nature of nuclear forces are unknown, however, many properties of these forces have been studied in depth. We will discuss the more essential ones.

a) Nuclear forces are forces of attraction. They retain the nucleons firmly inside the nucleus.

b) Nuclear forces are nonelectrical in nature. They act on all nucleons regardless of their electrical charge. They also are not related to any gravitational effects since these are negligibly small.

c) The region where nuclear forces appear is extremely small. Their radius of action is 1×10^{-13} to 2×10^{-13} cm, i.e. commensurate with the radius of the nucleus. The action of nuclear forces does not manifest itself at greater distances between nucleons. Thus, during the approach of two protons up to distances of 10^{-12} cm only repulsive electromagnetic forces are operating and nuclear attraction manifests itself only at distances less than 10^{-13} cm.

d) Nuclear forces are forces of great intensity. In the regions where they manifest themselves the quantities that characterize their intensity exceed by $\sim 10^3$ the electromagnetic interaction. One of the physical interpretations of the nature of nuclear forces is based on the so-called conversion characteristic of elementary particle interactions inside the nucleus. An analogy to such interactions is the interchange of neutrons and protons due to stripping or attachment by them of an electron or positron, respectively.

The most far reaching investigations of this issue, in particular by Academician E. Tamm, showed that the mass of the electron is so small that it can be explained by the two preceding properties of nuclear forces, short-range and intensive. A subsequent advance

was made in 1935 by the Japanese physicist, G. Yukavi. His reasoning was as follows. What must the mass of the converted particles be? According to the Heisenberg uncertainty principle, for a short time the energy of a particle can change to a very high value, $\Delta E = \sim h/\Delta\tau$. We shall select a time, $\Delta\tau$, such that the converted particle, moving at the speed of light, will successfully traverse the distance which is characteristic of nuclear force interactions, i.e., 1×10^{-13} to 2×10^{-13} cm. This time is approximately 0.5×10^{-23} sec, and, as we observed above, it is called the nuclear time. By substituting this time into the equation for ΔE, we obtain

$$\Delta E \sim \frac{6.56 \times 10^{-16}}{0.5 \times 10^{-23}} \sim 130 \text{ MeV}$$

Since the energy, 130 MeV, correlates with the mass, $m = \Delta E/c^2 \cong 300 m_e$, m_e is the rest mass of the electron. The result obtained can be evaluated as a manifestation for a short time interval ($\sim 10^{-23}$ sec) of the effect of a particle with a mass $\sim 300 m_e$. This "new" particle succeeds during the indicated time to traverse the distance between two interacting nucleons, i.e., on the order of 1×10^{-13} to 2×10^{-13} cm. Particles which exist for nuclear time periods in regions where nuclear forces are acting are called virtual particles. It is impossible for them to be present outside areas of nuclear interactions, i.e., separate from the nucleons. We should note that the particles referred to above were in reality discovered later on and were given the name π-mesons with a rest mass, $m_\pi = 273$ m_e.

e) Nuclear forces possess saturation properties similar to saturated valence bonds in the atom. These properties of nuclear forces appear when a single nucleon does not interact with all the nucleons in the nucleus but only with its closest neighbors.

f) Nuclear forces have a noncentral orientation. Nuclear interactions depend on the mutual position of the nucleons relative to their spin direction. Thus, in the deuterium nucleus the axes of the nucleons and the sum of their spin have the same direction and such a nucleus is the most stable. In other situations, the particle direction can differ and nuclear interactions become weaker.

g) Nuclear forces depend on spin orientation. It turns out, for example, that only with mutually parallel spins of a neutron and a proton can the stable nucleus of the deuterium atom, $_1H^2$, be formed.

Such are, in broad terms, the fundamental properties of nuclear forces. We need to know about these in discussing the physical essence and energy characteristics of the major nuclear reactions involved in nuclear power technology.

1.5.5. Binding Energy of the Nucleus. Stable and Radioactive Nuclei.

The binding energy of the nucleus is the energy which must be expended in breaking the nucleus up into its constituent neutrons and protons and removing them an infinite distance away. Accordingly, exactly this same energy is released during the synthesis of a nucleus from individual nucleons. Knowledge of the binding energy of the nucleus allows one to calculate an energy balance for not only seldom seen processes of complete disintegration of the nucleus but also for decay, fission, and other nuclear reactions. From Einstein's principle it follows that the binding energy of the nucleus $_ZX^A$, can be expressed by the difference in the mass (mass "defect") of the given nucleus and the mass of its constituent nucleons:

$$E_b = c^2 \left[Zm_p + (A - Z)m_n - m(z, A) \right] \qquad (1.2)$$

It follows from the equation that the mass of nucleus $_ZX^A$, is less than the sum of the masses of its constituent nucleons by $E_b(Z,A)/c^2$.

The binding energy of the nucleus is so large its magnitude can easily be measured directly. For example, an α particle with a binding energy, $E_b(2,4) \cong 28$ MeV, is lighter than the mass of the two protons and two neutrons composing it by

$$E_b(2,4)/c^2 \cong 4 \times 10^{-26} \text{ g,}$$

which is approximately equal to 0.7% of the mass of the α particle.

The nature and magnitude of the binding energy are determined largely by the properties of the nuclear forces that we have examined above. By using these properties, we will evaluate the factors that determine the binding energy of the nucleus. Keeping in mind that the nuclear forces of attraction act on nucleons independently of their electric charge, it is logical to propose that the sum total of their manifestation (i.e., energy of attraction) is directly proportional to the number of nucleons. In other words, $E'_{n,p} = a_1 A$. However, by taking into account the properties of nuclear force saturation, one must take into consideration that the nucleons located at the surface of the nucleus are more weakly bonded to each other than the nucleons that are inside the nucleus. For this reason, the energy of attraction E'_{na} ought to be reduced to a magnitude that is proportional to the surface of the nucleus (as a liquid spheroidal droplet), E''_{na}. Hence, $E'_{na} = a_2 A^{2/3}$, and, consequently, the total energy of nuclear attraction is the difference, $E_{na} = a_1 A - a_2 A^{2/3}$.

Another factor that characterizes the nuclear binding energy is electrostatic repulsion by identically charged particles, protons. The Coulomb energy of repulsion of a uniformly charged sphere is directly proportional to the square of the charge number, Z^2, and inversely proportional to its radius. By assigning to the repulsion energy the symbol, E_{rep}, we write $E_{rep} = a_3 Z^2 A^{-1/3}$. Naturally, this energy will lower the binding energy of the nucleus. A fourth factor that determines the nuclear binding energy is the presence in the nucleus of an unequal number of neutrons and protons. We consider it a fact that in the absence of Coulomb forces, the maximum specific binding energy, E_b/A, should be found at a level equal to $Z = N$ for all nuclei, i.e., that the nuclear forces act most intensively with an equal number of protons and neutrons in the nucleus. This fact is stipulated by the Pauli exclusion principle, and also by the fact that the energy of

28

interaction of neutrons and protons is on the average greater than the interaction energy of identical particles. The reduction in the binding energy of the nucleus that results from this has been found empirically and is given by the factor, $a_4[(N - Z)^2 A^{-2}]$. At Fermi's suggestion, this factor was designated as the isotope term, $E_{is} = -a_4[(N - Z)^2 A^{-2}]$.

Finally, it is necessary to determine the influence of the "pairing" phenomenon on the binding energy of the nucleus, i.e., in a certain sense the pairing of identical nucleons in the nucleus. As is known, even-even nuclei (an even number of protons and an even number of neutrons, etc.) are the most stable because the spin constituents of their nucleons are fully compensated. Conversely, in an odd-odd nucleus this effect is less apparent. Conventionally, this situation is evaluated by the term, $E_{pair} = a_5 A^{-3/4}$. It is surmised that for the even-even nucleus, $E_{np} > 0$, for the odd-odd nucleus, $E_{pn} < 0$, and for the even-odd and odd-even nuclei, $E_{pn} = 0$.

By combining the terms we discussed above, we obtain a final expression for the binding energy of the nucleus:

$$E_b = a_1 A - a_2 A^{2/3} - a_3 Z^2 A^{-1/3} - a_4 (N - Z)^2 A^{-1} - a_5 A^{-3/4} \qquad . \qquad (1.3)$$

This expression is to a known degree empirical since the coefficients $a_1 \ldots a_5$ are obtained mainly by experiment. Good agreement with test data is provided by the following values for these constants:

$$a_1 = 14 \text{ MeV}, \ a_2 = 13 \text{ MeV}, \ a_3 = 0.568 \text{ to } 0.615 \text{ MeV}, \ a_4 = 20 \text{ MeV}, \ a_5 = 33 \text{ MeV}.$$

In order to solve applied problems, it is of great value to have the latter equation written in terms of specific binding energy, i.e., energy pertaining to a single nucleon. For this purpose, the equation is rewritten in the form,

$$E_b/A = a_1 - a_2 A^{1/3} - a_3 Z^2 A^{-4/3} - a_4 (A - 2Z)^2 A^{-2} - a_5 A^{-7/4} \qquad . \qquad (1.4)$$

and its graphical relationship, $E_b/A = f(A)$, is shown in Fig. 1.10. We will now provide a qualitative analysis of this relationship.

The intensive increase in specific binding energy of the nucleus, E_b/A, is explained by a reduction in the negative effect related to the manifestation of saturation properties of the nuclear forces, which are attributed to a single interacting nucleon (despite the increase in this effect relative to the binding energy of the nucleus as a whole).

A gradual decrease in the specific binding energy is observed in large mass number regions. This is explained by the predominant influence of Coulomb forces of repulsion between the protons.

The maximum dependence of specific binding energy as a function of mass number is attributed to nuclei with mass numbers in the range $A = 50$ to 70.

The most stable nuclei in nature are grouped here. Against the background of a generally monotonic relationship, $E_b/A = f(A)$, one will find isolated spikes, in particular in regions with low values of A. This is either the most stable even-even nuclei, for example, $_2\text{He}^4$, $_6\text{C}^{12}$, $_8\text{O}^{16}$, or the least stable, such as $_3\text{Li}^6$, $_5\text{B}^{10}$. A number of important practical
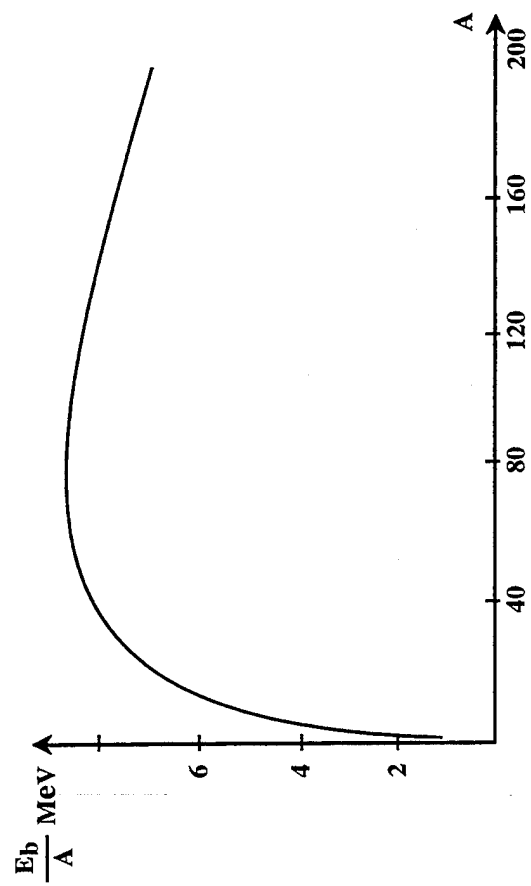
Fig. 1.10 Binding energy per nucleon as a function of atomic mass number. Light elements and heavy elements are less stable than elements in the mid-range.

conclusions can be drawn from analysis of this relationship. We will discuss some of them in more detail.

1. The specific binding energy for a majority of nuclei is 6 to 8 MeV. It is specifically this energy that must be expended to strip a nucleon from the nucleus. These numbers are useful in comparing analogous values that characterize the binding energy of electrons in the nucleus. We know that the binding energy of electrons in an atom is several eV, i.e., about 6 orders of magnitude lower than the binding energy of nucleons in the nucleus. Consequently, we can expect that a like amount of energy is liberated in nuclear processes where a mass "defect" of the nucleus occurs. In effect, during "burning" (i.e., complete transformation into energy) of 1 kg of uranium (mass "defect" of about 0.1 %) the same amount of energy will be liberated as it is in the burning of 1000 tons of coal. In other words, the energy capacity of uranium is $\sim 10^6$ that of the energy capacity of organic fuels.

2. Equation (1.4) makes it possible to establish the conditions for the existence of the most stable nuclei, i.e., nuclei in which the binding energy is the greatest. For this purpose, it suffices for nuclei-isobars (A = const) to solve the equation

$$\frac{\partial E_b}{\partial Z} = 0 \quad . \tag{1.5}$$

Hence, we obtain $a_3(ZA^{-1/3}) + 4a_4[(A - 2Z)A^{-1}] = 0$. If we substitute numerical values for a_3 and a_4 in the equation, we find the condition for the existence of the most stable nuclei (the condition for a stable nucleon region):

$$A_{stab} \cong A[(2 + 0.015A^{2/3})]^{-1} \quad . \tag{1.6}$$

3. Equation (1.6) and its graph make it possible to evaluate energy releases in different nuclear reactions, and also to point out ways in which nuclear energy can be used. We will discuss this important problem in more detail.

1.5.6. Ways in Which Energy from Nuclear Reactions Can be Used.

The physical essence of the possibility of utilizing the enormous energies in nuclear processes is based on two important facts: the presence of the mass defect in the nucleus and in its constituent nucleons, and also by the substantial difference in this defect between individual nuclei of the elements in Mendeleyev's periodic table. Thus, the mass defect in the hydrogen nucleus is obviously equal to zero since the hydrogen nucleus consists of a sole proton. The mass defect (consequently, in units of energy and binding energy) of deuterium (1p + 1n) is 0.1% of its rest mass. This is about 0.74% for the helium nucleus and 0.85% for oxygen. For nuclei with mass numbers of A = 50 - 70, the binding energy reaches 0.92% of the rest mass of the respective nuclei and for heavy nuclei (A > 230) it reduces again to about 0.78%.

We will now examine the ways in which we can use the energy in nuclear reactions which derives from the mechanisms mentioned. For this purpose, let's carry out the following mental experiment. Imagine a uranium-238 nucleus with its constituents of 92 protons and 146 neutrons. Now, mentally break this nucleus up into its 238 constituent nucleons and separate them from each other by a distance at which the nuclear forces of attraction have no effect. In order to do this, we have to expend an amount of energy numerically equal to the binding energy of the uranium-238 nucleus. This amount of energy equates to 0.8% of the rest mass energy of this nucleus. As a result, the mass of all the 238 nucleons exceeds this magnitude and is 1.008 times the rest mass of uranium-238. If we now mentally again collect all the nucleons into a single nucleus, then its mass will decrease by a factor of 1.008 and the energy released in this process will be exactly equal to what we expended. Naturally, there will be no gain or loss in the energy output. However, we will now try to synthesize the original uranium-238 nucleus into two new smaller and equal mass nuclei with the mass numbers, $A_1 = A_2 = 119$. The total mass of these two new nuclei will decrease to about 0.9% of the mass of the 238 nucleons, i.e., 0.1% greater than in the previous case. Thus, it seems that the total mass of the nuclei with mass numbers A_1 and A_2 is equal to 0.999 of the mass of uranium-238, i.e., less than the mass of the original nucleus by a factor of 1.001. In other words, the energy expended in disintegrating the uranium-238 nucleus into separate nucleons is less than the energy liberated in forming the two new nuclei. The difference in units of energy is 0.1% of the rest mass of $_{92}U^{238}$. This is the energy that is liberated in the reaction considered. It is quite clear that there was no need at all to first separate the uranium nucleus into its constituent nucleons, and then assemble them into two new ones. The same result can be achieved by splitting the uranium nucleus by any means (for example, by bombarding it with neutrons) into two fragments of approximately equal mass. This is the physical essence of liberating nuclear energy through fissioning of heavy nuclei.

Let's estimate the energy liberated in the fissioning of uranium-238. We will assume that two fragments of equal mass, $A_1 - A_2 = 119$ and $Z_1 = Z_2 = 46$, are formed in this process. Their specific energies are, according to Fig. 1.10, equal to 8.3 MeV, and the specific energy of the original uranium-238 nucleus is 7.4 MeV. By omitting the intermediate conversion, we can write

$$E_{release} = A[E_b(Z_1,A_1) - E_b(Z_1,A)] = (8.3 - 7.4)238 \cong 214\,MeV \quad . \qquad (1.7)$$

By comparing this magnitude with the energies of chemical reactions, it is apparent that it exceeds all of them (in eV units) by a factor of a million.

We now note that fission or conversion of heavy nuclei can be accomplished both artificially (nuclear reactor fission) and naturally (for example, radioactive decay). In reactor fission of heavy nuclei (U-235, Pu-239) the nuclear processes may be controlled over a wide range of energy output (nuclear power plants for a variety of purposes), or they may proceed virtually instantaneously (atomic bombs). Radioactive conversion of radioactive nuclei occurs in radioisotope generators of heat and electricity.

A second way of using nuclear energy is the fusion of light nuclei. From Fig. 1.10 it is apparent that one should select as light nuclei those with mass numbers that fall in the region to the left of the maximum specific binding energy. In this case, during fusion they

32

will form nuclei with greater specific binding energies. This, in turn, means that the mass of the new nuclei will be less than the mass of the original nuclei by about 0.5%. This mass defect changes into energy (thermonuclear). Note that this process yields significantly higher energies than fission of heavy nuclei. Elementary particle annihilation reactions will yield still greater energies. However, fusion reactions as well as annihilation reactions are still only of scientific interest. It is premature to discuss any industrial applications of these reactions.

1.6. Radioisotope Generators (RTGs)

The functional purpose of the power plants examined here derives from the name. The primary form of energy is heat obtained as a result of some kind of radioactive transformation. The stages in which heat is obtained can be limited by the functional design of such devices. Nevertheless, their areas of application are quite broad.

Of more general and wide use is the development of radioisotope generators that produce not only heat but also electrical power through the use of some kind of converter of heat. The converters of heat can be direct converters (thermionic, thermoelectric) and also mechanical converters (gas or vapor turbines, Stirling engines). The most widely used radioisotope generators are those with thermoelectric converters. These are referred to as radioisotope thermoelectric generators or RTGs.

In starting to discuss radioisotope generators it is useful to point out their advantages and disadvantages. Among the advantages are simplicity of construction and fabrication, operation that is independent of the surrounding environment, low weight and size, reliable and long operating life without degradation in output characteristics, etc. On the negative side, there is the high cost of radioactive isotopes, inability to influence the course of radioactive decay, the presence of high energy gamma-radiation for many radioactive isotopes, etc.

1.6.1. Equipment, Principles of Operation and Classification of Radioisotope Generators.

Radioisotope generator equipment is relatively simple and includes the basic components shown in Fig. 1.11.

The ampoule containing the radioactive isotope is hermetically sealed in order to provide radiation safety. The ampoule is, as a rule, inserted into one or two hermetically sealed containers which protect the isotope from mechanical damage and corrosion. The internal and external containers are fabricated from stainless steel, tantalum and other refractory materials. A characteristic feature of ampoules with radioactive isotopes is a free space for the accumulation of gaseous products of radioactive decay.

Various techniques are used to regulate the continuous liberation of energy: changing the heat transfer surfaces as a function of time, dummy resistances, etc.
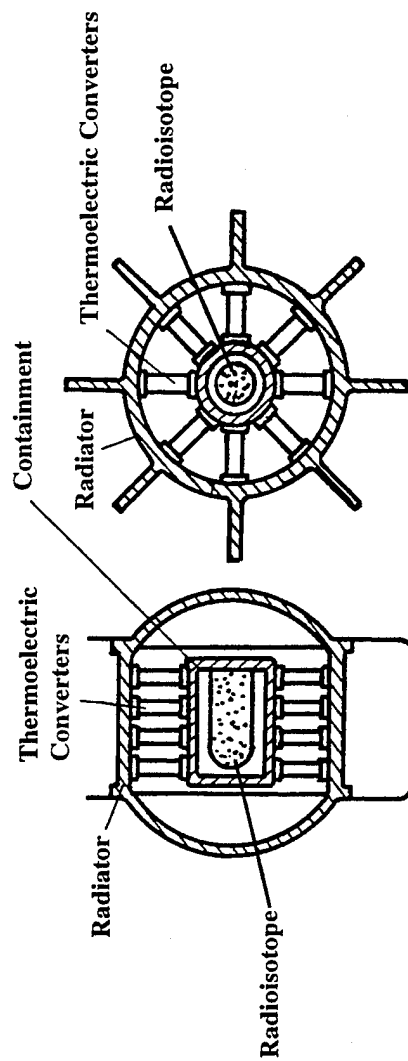
Fig. 1.11 Basic configuration of a radioisotope thermoelectric generator (RTG).

The principles of operation of radioisotope generators are not very complex. As we noted, the products of nuclear reactions (in this case, radioactive decay) possess high kinetic energies. This energy, as a result of slowing the reaction products down completely, is transformed into heat and then used in some other way.

Radioisotope generators can be classified by the names of the isotopes used and by the kind of radioactive decay. There are numerous naturally occurring and artificial radioactive isotopes. Several kinds of radioactive decay processes have been studied and are well known. Among these are:

α-decay in which the original nucleus emits α-particles (helium nuclei);

β-decay which, in turn, splits into two independent decay processes: electron decay with the emission of β$^-$ particles or electrons; positron decay with the emission of β$^+$ particles or positrons; and, finally, electron capture of an orbital electron from the K and L shell of the atom.

Spontaneous fission of certain of the heavy nuclei of elements is also possible. The majority of radioactive decay modes are accompanied by γ-radiation. These need to be heavily shielded to reduce the radiation field, as γ rays are very penetrating.

The α and β$^-$ radioactive isotopes are most widely used in autonomous power.

A second classification of radioisotope generators may be according to the kind of heat converter that is used. As we noted, the thermoelectric converter has been used the most. However, the push towards higher efficiencies caused by the high cost of radioisotopes has placed the use of more efficient converters on the agenda. Among these are thermionic converters as well as rotating machinery, in particular, the Stirling engine.

1.6.2. Fundamental Principles of Radioactive Decay.

The essence of the radioactivity phenomenon is the ability to spontaneously change the composition and state of the original nucleus by the emission of one or several elementary particles and γ-radiation.

It is apparent that the necessary (but not always sufficient) condition for radioactive decay processes is a resolution of differences in energy levels. This resolution of energy in the processes considered must be accompanied by a positive energy of decay, E_d. In other words, the mass of the original (mother) nucleus must exceed the mass of the new (daughter) nucleus and of the elementary particles formed during the given nuclear reaction. Radioactive decay is characterized by elapsed time, kinds of emitted particles and their energies.

Owing to the potential barrier, the existence of favorable energy conditions does not lead to instantaneous α-decay or spontaneous fission. This is observed more or less by the prolonged existence of nuclei capable of decay. β$^-$ decay is also not instantaneous, but for another reason. This process belongs to the so-called weak interaction processes. Such prolonged (often in nuclear time scales) existence of nuclei for which the energy conditions are favorable for decay is called radioactivity.

As we observed, the condition for the existence of nucleon stable regions is described by the equation shown graphically in Fig. 1.10.

We can make a number of important observations from an analysis of this graph. We will mention the most significant of them.

Light stable nuclei lie close to the line Z = N. A weakening in the binding energy of the nuclei shows up at Z > 40. This is due to the increasing effect of Coulomb forces of repulsion. In order to compensate for this factor and to provide conditions for nuclei stability, the nuclei must have a surplus of neutrons (relative to protons). Therefore, beginning with A = 20 to 30, the ratio N/Z, pertaining to the nucleon stability region, becomes greater than unity. For the last stable nucleus, bismuth-209, it reaches 1.52. This is the upper limit of the mass number A that corresponds to the nucleon stability region. In nuclei with Z > 83, the n-p, p-n, and p-p interactions cannot fully compensate for the Coulomb forces of repulsion of protons. Such nuclei are radioactive and undergo some form of radioactive decay (mainly alpha decay).

Alpha decay results in decreasing the number of neutrons by two and the number of protons by two. Beta decay (emission of a beta particle from a neutron) results in decreasing the number of neutrons by one and increasing the number of protons by one. These are the most common types of decays. Other, more rare, transmutations can include positron emission, electron capture, proton decay, etc. can also occur. Fig. 1.12 can be used to assist in visualizing these relationships.

Nuclei that fall below the nucleon stability curve contain a surplus of protons. As a result of a spontaneous change in composition, such nuclei will eject α particles (curve "b"), and in rare cases, individual protons or positrons (radioactive proton decay) and will shift to the left in the periodic table.

Experimental efforts in processing a large quantity of statistical data have established that the number of radioactive decays per unit of time (decay rate, activity) is proportional to the number of radioactive nuclei remaining at a given point in time. This is the law of radioactive decay which is written as

$$\frac{dN}{d\tau} = - \lambda N_n \qquad . \qquad\qquad (1.8)$$

where N_n is equal to the number of nuclei at any instant in time, and λ is the decay constant.

The unit rate of decay or activity is called the curie (in the SI system, the becquerel). One curie is 3.7×10^{10} decays/sec.

By integrating the equation, we obtain

$$N_n = N_n(0)\exp(-\lambda\tau) \qquad , \qquad\qquad (1.9)$$

where $N_n(0)$ is equal to the number of nuclei at an instant in time (that is to say, the moment the isotope is obtained), conventionally set equal to zero; i.e., $\tau = 0$.

The time it takes for the number of nuclei to reduce by one half is called the half-life, $T_{1/2}$. It is easy to see that $T = \ln(2)/\lambda$. The range of $T_{1/2}$ is extremely broad: from trillionths of a second to trillions of years.

36
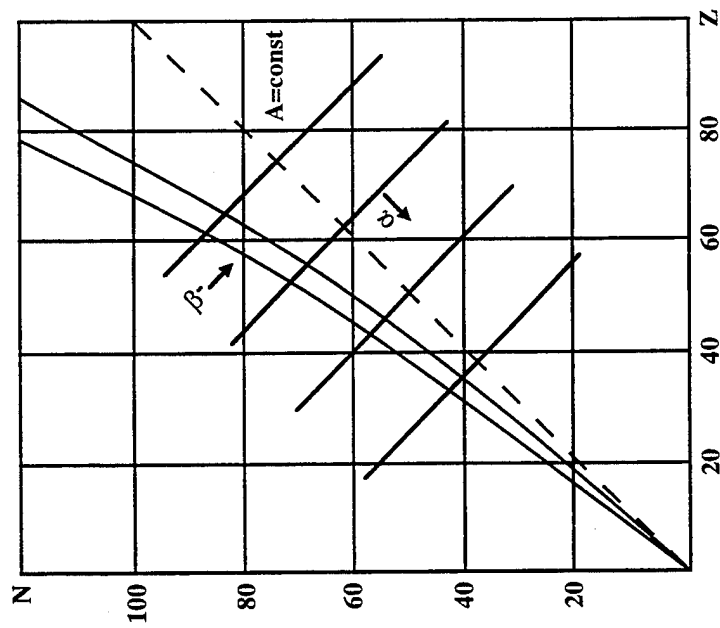
Fig. 1.12 Radioactive decay patterns. For β decay, the number of neutrons N decreases by one, while the number of protons Z increases by one. In alpha decay N and Z decrease by two. Aslo shown are lines of constant total nucleons A.

There are isotopes with nuclei that can decay in two or several independent ways. They are characterized by decay constants λ_1, λ_2,...λ_n. The overall decay constant is in this case equal to the sum

$$\lambda_{tot} = \sum_1^n \lambda_i \quad , \qquad\qquad (1.10)$$

and the overall half-life is determined from the equation

$$\left(\frac{1}{T_{1/2}} \right)_{tot} = \sum_1^n \left(\frac{1}{T_{1/2}} \right)_i \quad . \qquad\qquad (1.11)$$

Nuclei which are formed as a result of the decay of the original isotope can, in turn, be radioactive. In this case we are talking about the so-called radioactive nucleus. Three radioactive series are found in nature in protracted radioactive equilibrium. They begin with the long-lived isotopes, $_{90}Th^{231}$, $_{92}U^{235}$, and $_{92}U^{238}$, and are called the radioactive series of thorium and uranium, respectively.

1.6.3. Energy Characteristics of α-Decay.

The existence of α-decay was discovered during the study of natural radioactive substances, but the results that were obtained went far beyond the bounds of the initial task (thus, investigations of a-particle interactions with the atoms of different elements allowed Rutherford to formulate new hypotheses regarding the structure of the nucleus).

As we observed, during α-decay the original (mother nucleus) emits an α-particle, the nucleus of the helium atom, and transitions into a new (daughter) nucleus according to the following path:

$$_zX^A \rightarrow {}_{Z-2}Y^{A-4} + {}_2He^4 \quad .$$
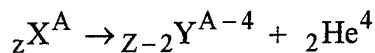
A typical example of α-decay is the decay of uranium-235 which proceeds along the following path

$$_{92}U^{235} \rightarrow {}_{90}Th^{231} + {}_2He^4 \quad .$$
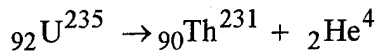
In like fashion, decays of the daughter nuclei may be found in excited states from which they transition to the original state by emitting γ quanta. A typical diagram for describing the entire process is usually like that shown in Fig. 1.13 where $_{92}U^{235}$ is used as an example.

The initial state of the daughter nucleus ($E_{dn}(\tau = 0) = 0$) is adopted as the starting point for reading the excitation energy levels. Its excitation energy is zero. The excitation energy of the $_{92}U^{235}$ mother nucleus is 4.559 MeV. The needed nomenclature and numbers that characterize the qualitative (in the given case, α) and quantitative (relative to
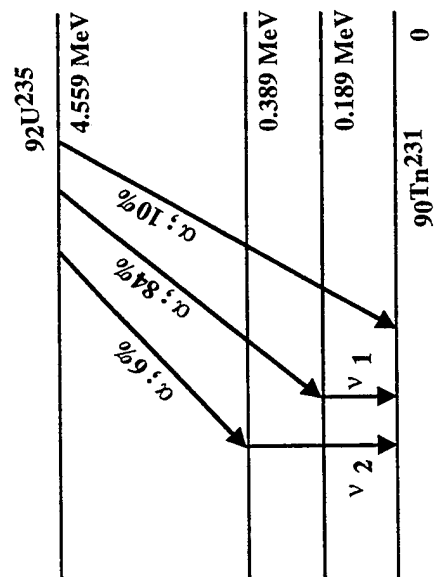
Fig. 1.13 Alpha decay paths for $_{92}U^{235}$.

$_{92}U^{235}$

4.559 MeV

0.389 MeV

0.189 MeV

$_{90}Tn^{231}$ 0

α; 10%

α; 84%

α; 6%

γ_1

γ_2

the number of nuclei decaying in the given manner) characteristics are written along the arrows that point to individual transitions. Horizontal lines show the magnitude of the excitation energy of the daughter nuclei.

Let's consider the energy that is liberated during α-decay, $E_{\alpha d}$. A positive value of $E_{\alpha d}$ exists only when the inequality $m(Z,A) > m(Z-2, A-4) + m(2,4)$ occurs. Then the energy of α-decay can be calculated from the equation:

$$E_{\alpha d} = c^2[m(Z,A) - m(Z - 2, A - 4) - m(2,4)] \qquad , \qquad (1.12)$$

or by taking into account the relationship between mass and energy, $E_b(Z,A) = c^2 \Delta m(Z,A)$, we obtain

$$E_{\alpha d} = E_b(Z - 2, A - 4) + E_b(2,4) - E_b(Z,A) \quad . \qquad (1.13)$$

With $E_{\alpha d} < 0$ decay is prohibited from an energy standpoint and the corresponding nucleus is stable. In order to secure a favorable energy state for α-decay ($E_{\alpha d} > 0$), the binding energy of the lighter daughter nucleus must be lower and not greater than the 28.3 MeV (the binding energy of the α-particles) binding energy of the mother nucleus.

Calculations using this equation show that unstable nuclei leading to α-decay can only exist at $A > 140$; i.e., in regions where the specific binding energy is decreasing as a function of the mass number A. Alpha decay is observed in experiments, however, in isotopes with $A > 209$. The problem is that with low values of energy, $E_{\alpha \delta}$, the activity produced is so low that it is very difficult to determine and put to practical use.

Let's examine the physical essence of nuclear processes associated with α-decay. For this purpose, we will first turn our attention to one feature of α-radiation. In practice, the set value of $E_{\alpha d}$ is, within relatively narrow limits, an average of about 5 MeV per decay. This value is significantly lower than would be obtained for a positively charged α-particle accelerated by an electrostatic field upon escape from the nucleus. Thus, according to calculations, an α-particle escaping from a uranium-235 nucleus can attain an energy of about 30 MeV, i.e., a factor of 6 greater value. This apparent contradiction is explained by quantum mechanics. Before the onset of α-decay there exists in many heavy nuclei an unstable association of two protons and two neutrons, i.e., α-particles. We will designate their energy inside the nucleus as E_α. Let's now examine the potential diagram for the protons in terms of the composite binding energies as a function of distance from the center of the nucleus, r (Fig. 1.14). As a proton approaches the nucleus from without, the potential energy of repulsion increases in proportion to the inverse of r. In the absence of nuclear forces of attraction, the energy of repulsion would increase without limit. However, as soon as the proton enters the interaction zone of the nuclear attraction force, the effect of repulsion changes to attraction (we recall the fourth property of nuclear forces), the potential energy of the proton changes sign and becomes negative. The positive part of the curve, $E_{rep} = f(r)$, is a barrier, and the negative part, due to the force of attraction, is a potential well of depth, E_0. Based on this principle, the two parts of the potential diagram are called, respectively, the potential barrier and the potential well. The

40
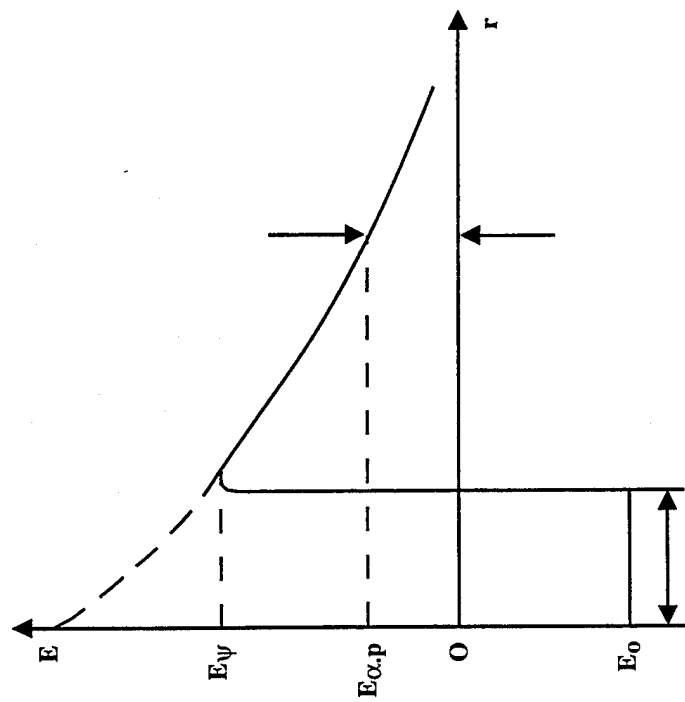
Fig. 1.14 Potential diagram for protons as a function of distance from the nucleus.

41

height of the potential barrier, E_Ψ, is equal to the maximum potential energy of repulsion of the proton, E_Ψ, at the boundary with the nucleus. If the potential barrier did not exist, then the α-particle would depart the nucleus with an energy, $E'_\alpha - E_0 = E_{\alpha d}$. Exactly this energy has been observed experimentally, and this means that the α-particle has paid no attention to the potential barrier. How can that be? According to quantum mechanics, α-particles have inherent wave properties. Therefore, in striking the wall of the potential barrier, the α-particle is reflected from it as a wave. Not all α-particles are reflected from this wall, a portion of them penetrate through the wall and depart the limits of the nucleus. This "tunneling through" is related to the penetration of α-particles through the barrier with energies lower than the height of the potential barrier. Thus, if this or another event pertains to energy resolution in the microworld ($E_{\alpha d} > 0$), it will inevitably occur. This is not so in the macroworld. Water in a glass will remain on the table and will never spill on the floor for any natural reason even though its potential energy on the table is higher than it would be on the floor. Spilling the water on the floor would settle this difference in energy level.

The probability that the α-particles will overcome the Coulomb potential barrier is higher the greater and more fully defined (discrete) the energy is that they possess inside the nucleus. Hence, we have the discrete energy level of the α-particles that escape from the nucleus. Based on this principle, α-active isotopes can eject two or more groups of the α-particles about which we have spoken above. The difference in the energies of α-particles of different groups is small, however, and amounts only to tenths and even hundredths of an MeV.

Let's proceed further with the problem of utilizing α-decay energy. In radioactive decays of any kind, in addition to the conservation of energy and charge, the total momentum is also conserved. By way of example, we will take α-decay during which γ-radiation is absent (Po-210, Pu-238). In this case, the daughter nucleus and the α-particle scatter with momenta that are of the same magnitude and exactly opposite in direction. Thus, based on the law of the conservation of momentum we can write, $m_d v_d = m_\alpha v_\alpha$. Therefore, the ratio of kinetic energy of the daughter nucleus and the α-particle is equal to

$$\frac{E_d}{E_\alpha} = \frac{m_d v_d v_d}{m_\alpha v_\alpha v_\alpha} = \frac{v_d}{v_\alpha} = \frac{m_\alpha}{m_d} \qquad (1.14)$$

Hence, it follows that the energy of α-decay is

$$E_{\alpha d} = E_\alpha + EA_\alpha = E_\alpha(1 + m_\alpha/mA_\alpha) \cong E_\alpha \quad , \qquad (1.15)$$

since the mass of the α-particle is negligibly small compared to the mass of the daughter nucleus. From the equation it follows that α-decay energy consists mainly in kinetic energy of the α-particles. As a rule, in one decay event about 5 MeV of energy is liberated. From the point of view of use in atomic power, the decay of polonium-210 and plutonium-238 makes the most sense. These are virtually free of α-radiation and proceed according to the following process:

$$_{84}Po^{210} \rightarrow {}_{82}Pb^{206} + {}_2He^4 \ ; E_{\alpha d} = 5.35\,MeV, \ T_{1/2} = 138\,days$$

42

$$_{94}\text{Pu}^{238} \rightarrow {}_{92}\text{U}^{234} + {}_2\text{He}^4 ; E_{\alpha d} = 5.5\,\text{MeV}, T_{1/2} = 88\,\text{years}$$
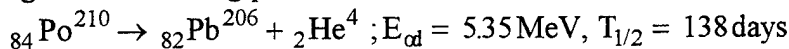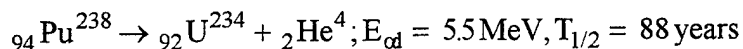
The range of an α-particle in a substance with a density ρ can be approximated from the formula

$$r_\alpha \approx 4 \times 10^{-3}\, \frac{E_{\alpha d}^{3/2}}{\rho} \qquad . \qquad (1.16)$$

Calculations show that the range of α-particles is small. For example, in metals with densities, $\rho = 8 \ldots 10$ g/cm^2, the ranges are hundredths and even thousandths of a mm.

Charged α-particles interact actively with electron shells of the atoms of the substances in which they are slowed down (the zone of heat liberation in a RTG). By capturing two electrons, the α-particle transforms into a neutral atom of helium,

$$(_2\text{He}^4 + 2\text{e} \rightarrow \text{He}) \qquad ,$$
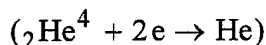
and its kinetic energy is converted to heat.

1.6.5. Energy Characteristics of β-Decay

Another type of radioactive decay is β⁻–decay, usually abbreviated as β–decay (when there is no superscript, it can usually be assumed that a β⁻ particle is being referred to, as this is by far more common than the positron β⁺). In this case, radioactive transformations of nucleons occur in such a manner that the mass number in the β-decays is maintained constant. For this reason, β-decay must be considered as a process that occurs inside nucleons and not externally as is the case with α-decay. The principal feature of β-decay is that it is due to weak interactions and not due to nuclear or electromagnetic forces. Hence, these decay processes are complex and inadequately understood. They may possibly occur over the whole range of the mass number A.

The β-decay process is written in the following form,

$$_Z\text{X}^A = {}_{Z+1}\text{Y}^A + \beta^- + \tilde{\nu} + \gamma .$$
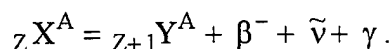
where $\tilde{\nu}$ is an antineutrino. The sum on the right represents $E_{\beta d}$.

Beta decay is virtually always accompanied by γ-radiation because the daughter nucleus is, as a rule, found to be in an excited state. An example is given in Fig. 1.15, β-decay of $_{27}\text{Co}^{60}$.

Daughter nuclei of nickel-60 are found in two excited states. Their transition to an unexcited state of the nucleus, $_{28}\text{Ni}^{60}$, is accompanied by the emission of three γ-quanta in succession with an overall energy of about 1.4 MeV. Thus, each fraction of γ-radiation and antineutrino account for about 1.47 MeV, i.e., approximately 50%. This is an important feature of β-decay.
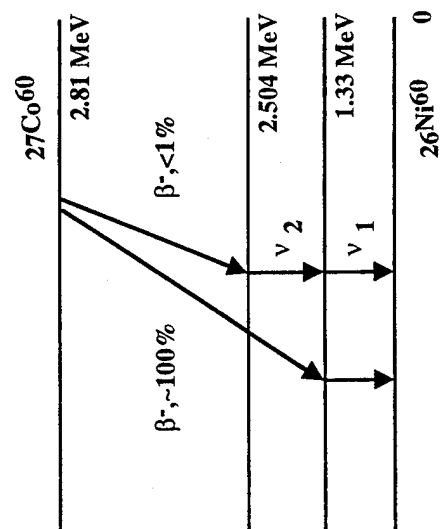
Fig. 1.15 Beta decay paths for $_{21}Co^{60}$.

$_{27}Co^{60}$

2.81 MeV

β-, <1%

2.504 MeV

1.33 MeV

$_{26}Ni^{60}$ 0

ν_2

ν_1

β-, ~100%

The question naturally arises: from where in the nucleus are the electrons taken? This question can be answered if it is assumed that in nuclei with excess neutrons which have a tendency to β-decay, conversion of a neutron into a proton takes place with the liberation of one electron in accordance with n → p + e. Such an assumption explains in a qualitative sense the kind of decay examined. There are, however, a number of quantitative characteristics calculated from this theoretical model which do not correspond with experimental data. Protons and electrons formed according to this process do not scatter precisely in opposite directions, as is required by the law of the conservation of momentum, but at some angle. Also, the energy spectrum of β-particles determined experimentally is not discrete as the laws of quantum mechanics require, but appears continuous. These contradictions were cleared up by Pauli, who, in his own words "attempted to rescue the laws of conservation." For this purpose, he assumed the existence of a previously unknown elementary particle formed in the neutron decay process. This particle, called the Fermi neutrino, can by his calculations have a zero electrical charge, possess a half-integral spin, travel close to the speed of light, and have a rest mass "seemingly" close to zero. Recently, Soviet scientists determined that the rest mass of the neutrino is not equal to zero but is about 40 keV in energy units of mass. The calculated characteristics of the neutrino explain its exceptionally high penetrating capability which for a long time made it impossible to discover even in very delicate experiments. The neutrino was identified experimentally only during the mid 1950's in experiments with superhigh energy particles.

In addition, supplementary processes of neutron disintegration by new elementary particles (in the β-decay process, the antineutrino in accordance with the condition for the existence of particles and antiparticles), i.e. n → p + e + ṽ, have led to complete agreement between the theoretical and experimental data about which we spoke above.

The fact is that the theoretical discovery and subsequent experimental verification of the antineutrino is a brilliant confirmation of the well known assumption of the indestructibility of matter. It is also a clear illustration of the indirect paths which physics sometimes takes into in order to solve many and often seemingly insoluble problems.

Next, we will examine the condition under which β-decay is energetically feasible. Similar to α-decay, this condition is determined by the inequality

$$m(Z,A) > m(Z + 1, A) + m_e.$$

In this case, the energy of β-decay can be determined from the equation,

$$E_{\beta d} = C^2 \left[m(Z,A) - m(Z + 1, A) - m_e \right] \qquad . \qquad (1.17)$$

with the assumption that $m_v = 0$.
Or the energy can be found from the binding energies,

$$E_{\beta d} = E_b(Z + 1, A) + E_b(\beta) - E_b(Z,A) \qquad . \qquad (1.18)$$

Since the binding energy of the β particles is $E_b(\beta) = c^2(m_n - m_p - m_e)$, and the mass of the neutron, proton, and electron equal, respectively, 1.008665, 1.007278 and 0.000549 MeV, then $E_b(\beta) = 0.875$ MeV. Thus, β–decay is energetically advantageous when the binding energy of the daughter nucleus exceeds, is equal to or less than (but by no more than 0.875 MeV) the energy of the mother nucleus.

One of the features of β-decay is a continuous energy spectrum of the β particle ranging from a minimum to some maximum value of $E_{\beta\text{-max}}$. As has been noted, based on the notion in quantum mechanics that elementary particles have discrete energy levels, this situation is inexplicable. The simultaneous ejection, however, of antineutrinos with the β particles disposes of this contradiction because the antineutrino takes with it a portion of the energy liberated in the β–decays. Since the energy of the antineutrino can, according to statistical laws, be some random value, it should also be expected that the β particles will carry away some portion of the energy. For this reason, the energy spectrum of β particles becomes continuous (Fig. 1.16).

Since, as we noted, γ radiation and β–decays can have a number of discrete energy levels, several β particle groups with different energies, $E_{\beta max}$, will appear. The sum $E_\beta + E_\nu$ remain constant. On the average, β particles carry away energy of about 1/3 $E_{\beta max}$. This can be put to use because the antineutrino will virtually not interact with the medium. One can also, but for a different reason, neglect the kinetic energy of the daughter nucleus. In fact, according to the conservation of momentum, the energy contribution by the daughter nucleus is proportional to the ratio m_β/m_{dn} This can be neglected because it is so small compared to unity.

In addition, in β decays the γ radiation energy fraction can be significant and must be accounted for in calculations. Thus, the useful energy derived from a single β decay can be determined from the sum,

$$E_{\beta_{tot}} = \frac{1}{3}\sum_1^n E_{\beta_{i max}} a_i + b\sum_1^n E_\gamma a_i \qquad , \qquad (1.19)$$

where a_i is the relative number of nuclei radiating β particles with a maximum energy, $E_{\beta imax}$, and γ quanta with energy, $E_{\gamma i}$; b is the fraction of γ radiation absorbed in the zone where thermal energy is liberated; typically in the range of 0.5 to 0.9.

For example, for $_{55}Cs^{137}$ with b = 0.5 we obtain $E_{\beta_{tot}}$ = 1/3 x (0.51 x 0.92 + 0.08 x 1.17) + 0.5 x 0.66 x 0.92   0.5 MeV. The antineutrino and the unabsorbed γ quanta carry away the energy, $E_{\beta d_{tot}} - E_{\beta d} = 1.17 - 0.5 = 0.67$ MeV.

The range of the β particle in a substance can be determined from the following empirical equations:

$$R_\beta \approx \frac{1}{\rho}\left(0.54E_\beta - 0.13\right) \text{ for } 0.8 \le E_\beta \le 3\,\text{MeV} \qquad , \qquad (1.20)$$

$$R_\beta = \frac{0.41\left(E_\beta\right)^{0.14}}{\rho} \text{ for } 0.15 \le E_\beta \le 0.8\,\text{MeV} . \qquad (1.21)$$
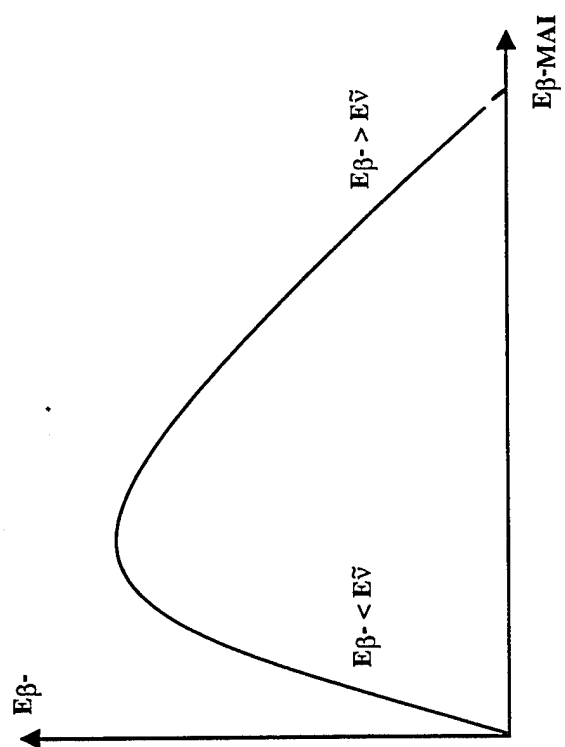
Fig. 1.16 Energy of beta particles (β-). The total decay energy is carried by the β- partical and an antineutrino $\tilde{\nu}$.

Eβ-

Eβ- < E$\tilde{\nu}$

Eβ- > E$\tilde{\nu}$

Eβ-MAI

The range of the β particle in the heat liberating region of materials used in practical work is, as with α–decay, small. It is, however, greater than the range of the α particle. With E_β = 2 MeV, the range of β particles in steel is about 1.2 mm. Gamma radiation energy in β decays (unlike α radiation) makes a significant contribution to the total useful thermal power. Therefore, materials that are used in designs for the generation of thermal power must be chosen based on their capacity to absorb γ radiation.

The attenuation in energy of γ radiation as it passes through a substance is described by the exponential law,

$$I(x) = I_0 \exp(-\mu x) \qquad , \tag{1.22}$$

where μ is a linear attenuation constant which represents the sum of the partial attenuation constants, μ_{ph}, μ_c, μ_{pp}. These characterize, respectively, the three fundamental interactions of γ-quanta with substances: photoelectric effect, Compton scattering and positron-electron pair formation.

In β decays the range of the β particle in substances is usually significantly less than the thickness of the layer in which the basic portion of the γ radiation energy is absorbed. Based on the allowable γ radiation level, this layer determines the dimensions of the heat liberation region and, in essence, the size of the RTG as a whole.

1.6.6. Thermal Power of an RTG.

The energy that is released in radioactive decays can be used in different ways. The thermal energy that is obtained by slowing down α and β particles and by the interaction of γ radiation with substances is of the greatest interest in satisfying needs for autonomous power. By calling the thermal energy that is liberated in one single decay E_d, it is not difficult to determine the thermal power of a given RTG,

$$Q_t = E_d \frac{dN}{d\tau} = E_d \lambda N_0 \exp(-\lambda\tau) \qquad . \tag{1.23}$$

If we have 1 gram of a pure isotope, then the specific thermal power generated by it during radioactive decay will be

$$Q_t = \frac{A}{\mu} E_d \lambda \exp(-\lambda\tau) \qquad , \frac{MeV}{g\ sec} \tag{1.24}$$

$$Q_t = \frac{A}{\mu} E_d \lambda \exp(-\lambda\tau) \cdot 1.6 \times 10^{-13} \qquad , \frac{Joule}{g\ sec} \tag{1.25}$$

$$Q_t = \frac{9.63 \times 10^{10}}{\mu} E_d \lambda \exp(-\lambda\tau) \qquad , \frac{W}{g} \tag{1.26}$$

where μ is the molecular (atomic) mass of the pure isotope.

48

Radioactive fuels are frequently not pure isotopes, but are chemical compounds or mixtures with stable elements. The specific thermal power is in this case reduced in proportion to the mass fraction of the pure isotope.

1.6.7. Production of Radioactive Isotopes and Product Requirements.

An overwhelming quantity of isotopes that are suitable for use in autonomous power is produced artificially. The extraction of radioactive isotopes from natural ores that contain radioactive series does not make sense because such ores can be found only in very small quantities. Artificial radioactive isotope production methods can be divided into the three groups given below:

1. Isotopes which derive from by-products of the nuclear industry. Such isotopes are produced by different radiation chemistry techniques. Among such isotopes are Sr-90, Pm-149, Ce-144, and Cs-137.

2. Isotopes that are formed as a result of bombarding the nuclei of stable elements with neutrons. Co-60 and Po-210 are among these. They are produced in the following reactions:

$$_{26}Co^{59} + _{0}n^{1} \rightarrow _{26}Co^{60} \qquad , \text{ or,}$$

$$_{83}Bi^{209} + _{0}n^{1} \rightarrow _{83}Bi^{210} \rightarrow _{84}Po^{210} + \beta^{-} + \tilde{\nu} + \gamma \qquad .$$
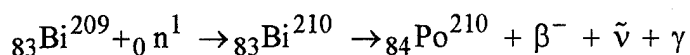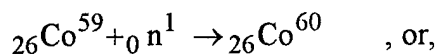
3. Isotopes which are produced by neutron bombardment of by-products from the uranium and plutonium cycles. By way of example, we will show you the production of the radioactive isotope $_{94}Pu^{238}$:

$$_{93}Np^{237} + _{0}n^{1} \rightarrow _{93}Np^{238} \rightarrow _{94}Pu^{238} + \beta + \tilde{\nu} + \gamma \qquad .$$
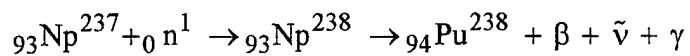
Other isotopes that are produced in this manner are Am-243, Cm-242, Cm-244, and others.

In choosing radioactive isotopes for use in autonomous power it is necessary to take into account the following factors: half-life, decay energy, γ radiation, robustness, compatibility with structural materials, chemical stability, melting point, fabrication technology, cost, etc. Generally, the half-life must not be less than several months. Several years is desirable. An excessively short half-life will result in a rapid decrease in activity as a function of time. This is unacceptable for a number of reasons: control of the RTG is difficult, the initial quantity of the isotope required increases, the period the isotope can be kept is limited, etc. Another disadvantage occurs when the half-life of the isotope is too long: the initial activity is low. The above factors are usually taken into account in estimating the specific thermal energy release from the above equation. It is customary that the initial specific power ($\gamma = 0$) should not be less than 0.1 watt/gram.

49

In order to improve the stability of the fuel, such as increasing the melting point and the like, different compounds are used instead of pure isotopes. The remaining requirements are sufficiently obvious and there is no sense in dwelling on them. The practical uses of isotopes in autonomous power have evolved through the application of a limited number of isotopes. These include Co-60, Sr-90, Cs-137, Po-210, Pu-238, Cm-244, and others.

Radioactive isotopes with a half-life of a year and longer are called long life isotopes (Co-60, Sr-90, Cs-137, Pu-238). Accordingly, isotopes with a half-life of less than one year are called short life isotopes (Po-210).

1.6.8. Control of the Power of an RTG.

Energy liberation by radioactive isotopes is not subject to control but obeys the laws of radioactive decay. A characteristic reduction in thermal power, determined from equation (1.26), is shown in Fig. 1.17.

In addition, the electrical power generated by the RTG should, as a rule, be kept constant or be at some given level after a prescribed operating period, τ_{op}. This requirement can be satisfied by dumping excess electrical power during the time prior to actual operation, dumping excess electrical power over the entire time, or combinations of the two methods. We will now consider the optimization of some parameters in controlling an RTG by dumping thermal power.

In this case, the thermal regime and the parameters of the converters of heat are maintained constant over the time interval 0 to τ_{op}. By solving the equation

$$\frac{\partial Q_e}{\partial \lambda \tau} = 0 \quad ,$$

(1.27)

it is easy to show that the electrical energy produced during the time τ_{op} is

$$Q_e = Q_t \varepsilon \tau_{op}$$

(1.28)

where ε is the thermal conversion efficiency which is a maximum for $\tau_{op}\lambda = 1$.

Consequently, an operating time of $\tau_{op} = 1/\lambda = 1.44 T_{1/2}$ is most advantageous for the given isotope. With this as the operating time, it is prudent to select from among the isotopes that have approximately identical values of the parameter Q_t, or one for which $\lambda_{opt} = 1/\tau_{op}$ or $(T_{1/2})opt = 0.693 \tau_{op}$.

The maximum electrical energy and the constant electrical power generated are, respectively

$$Q_e = 9.63 \cdot 10^{10} \frac{E_d}{\mu e} \varepsilon \; ; \quad \dot{Q}_{elec} = 9.63 \cdot 10^{10} \frac{E_d}{\mu e \tau_{op}} \varepsilon \quad .$$

(1.29)

It should be noted that the maximum Q_e slopes gently as a function of $\tau_{op}\lambda$. Thus, a deviation of 10% in τ_{op} or λ from the optimum will lead to only ~ 1% reduction in E_{elec}.
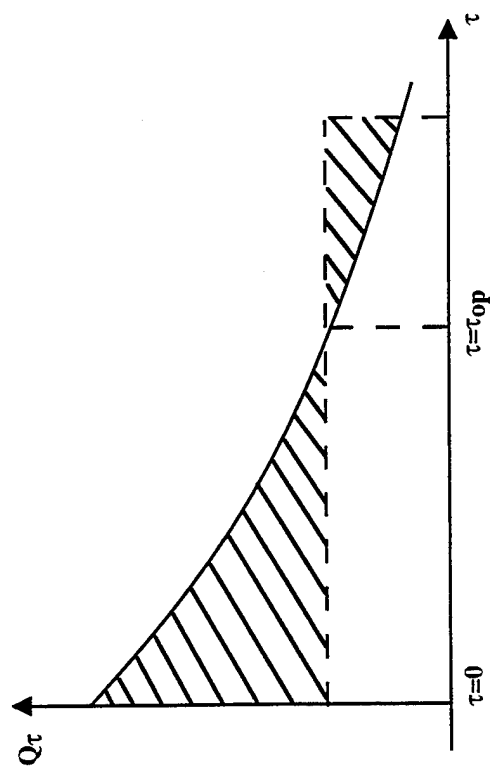
Fig. 1.17 Exponential dependence of radioisotope thermal power with time. The power must be kept above some minimum threshold during its prgrammed operating period τ_{op}.

We will estimate the order of magnitude of Q_e max for $\varepsilon = 0.05$. For β emitters having on the average $\mu = 100$ and E_d 1 MeV, we obtain a mass normalized value of

$$Q_{e,max} \approx 9.63 \cdot 10^{10} \frac{0.05}{100 \cdot 2.72} \cdot \frac{1}{3600} = 4000 \frac{kWhr}{kg} \qquad . \qquad (1.30)$$

This exceeds by more than a factor of 3 the energy capacity of the best chemical energy source, the fuel cell.

There are several design options for removing the time-varying excess thermal power from the heat generation region. A possible design for such equipment is shown in Fig. 1.18. Here the sensitivity of the damper actuator regulates the temperature changes in the heat generation zone. The damper opening needs to be adjusted in order to keep the temperature constant during a given power plant operating period.

A large number of radioisotope generators have been developed to date which use thermoelectric converters of heat. These include, for example, the power plants in the odd-numbered SNAP series which range in power from tens to hundreds of watts. All of them have been used successfully on space vehicles. The last of them was a power plant using the Pu-238 isotope. It was mounted on the interplanetary probe "Magellan," which was launched by the USA in 1990.

Auxiliary Radiator Surface

Moveable Thermal Shield

Radioactive Heat Source

Thermoelectric Converters
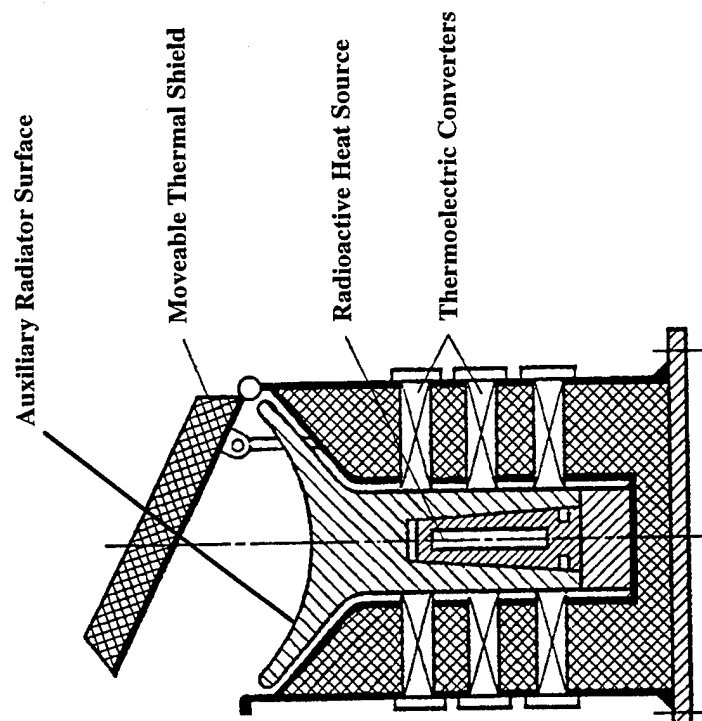
Fig. 1.18 Possible thermal regulation system.

2. PHYSICAL PRINCIPLES OF WORKING PROCESSES IN SPACE NUCLEAR POWER PLANTS

2.1. Designs and Classifications

The author assumes that the reader is generally familiar with the equipment and make-up of nuclear reactors and the function of their basic components. Nevertheless, the author considers it worthwhile to briefly dwell on a number of characteristics and classes of reactors for space power plants, to identify those that have practical applications and, especially, to identify those that are promising in the development of future space hardware.

A nuclear reactor is a device in which neutrons sustain a controlled fission chain reaction that releases different kinds of energies. The bulk of these energies is converted into thermal energy which is used to satisfy a variety of needs. The design of a nuclear reactor is not complicated (Fig. 2.1). It includes the reactor vessel, the core, neutron reflectors, a heat transfer system, a control system and shielding and, in the general case, external shielding.

The core consists of the nuclear fuel and the moderator, although sometimes there is no moderator. The function of the core is to create conditions that will sustain a controlled nuclear fission chain reaction.

The purpose of the reflectors (end and side) is to reduce the number of neutrons that leak from the core. Shielding is necessary in order to attenuate the energy of the neutrons that escape from the reactor vessel as well as the energy of the attendant γ radiation to levels that are within safe limits for maintenance personnel, instruments and materials.

Different kinds of nuclear reactors can be used in space nuclear power applications depending on a number of specific requirements that arise from the conditions under which they are to be used.

The fundamental requirement on reactors for space nuclear power use is to achieve the minimum possible mass and size. The reactor dimensions determine the size and mass of the shielding needed to protect on-board equipment (for an unmanned spacecraft) from neutron flux and γ radiation. As a consequence, the reactor size determines to a significant degree the dimensions and mass of the spacecraft as a whole.

Naturally, this limitation imposes a requirement to generate as much power as possible within the core volume. In the majority of cases, minimum reactor dimensions are not determined by conditions critical to sustaining fission, but by the thermal power required. This circumstance demands the selection of the most effective liquid metal coolant, design and core materials.

It follows from the above that reactors for space nuclear power plants must operate at high temperatures. This means that refractory materials must be used in the core, such as stainless steels, carbides, and metallic ceramics. In order to reduce the unproductive (relative to the fission reaction) expenditure of neutrons, highly enriched uranium must be used as the fissioning material, and the moderator must be a material which doesn't capture neutrons readily.
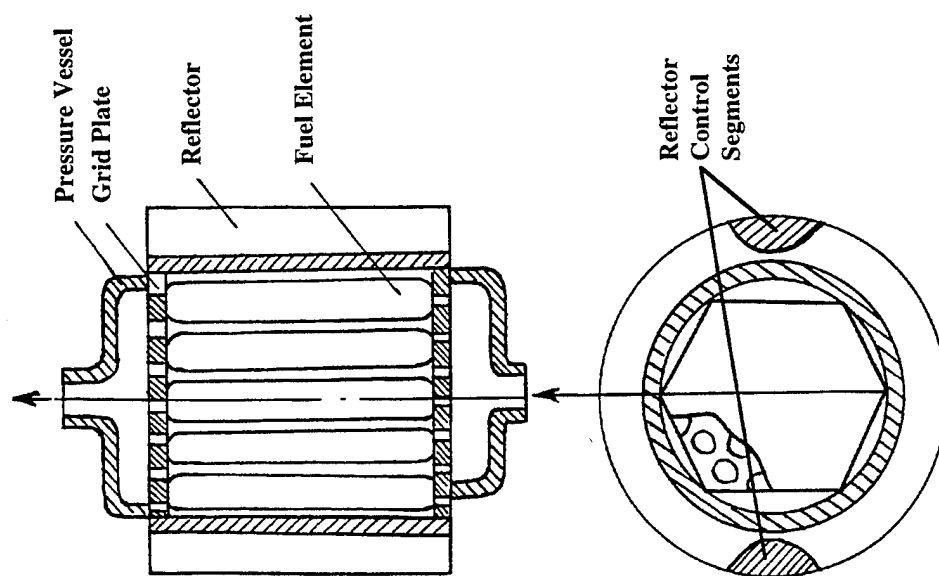
Fig. 2.1 Basic design of a compact nuclear reactor.

The basic characteristics used in classifying nuclear power reactors are the following:

1. Neutron energies that sustain the fission reaction: megaelectron volts (fast neutrons), tenths of electron volts (thermal neutrons) and from tenths to thousands of electron volts (epithermal neutrons).

2. The distribution of nuclear fuel and moderator. In heterogeneous reactors the nuclear fuel is distributed locally in the moderator, and in homogeneous reactors the fuel and moderator constitute a uniform mixture.

3. The state of the fuel (solid, liquid, gas) in the core.

4. Methods for heat removal (transfer of heat to where it is needed): different kinds of coolants, heat pipes, direct contact heat transfer or thermal radiation.

Considering the requirements mentioned above for space nuclear power reactors, homogeneous and heterogeneous reactors with fast and epithermal neutrons and with a solid core are most advantageous for use in space. The thermal energy liberated in these reactors is removed by using a coolant (principally, a liquid metal), heat pipes, or by thermal conductance.

The working process and its basic characteristics (heat generation and its change with time, the composition of products of reaction and nuclear radiation, etc.) in any power reactor are determined directly by neutron interactions with nuclei in the reactor. We will, therefore, discuss these interactions in sufficient detail beginning with the fundamental laws upon which reactor processes are based.

2.2. Neutron Interactions with Nuclei.

In a broad sense, a nuclear reaction is any process that begins with the collision of two, seldom several, microparticles (simple or complex) and which, as a rule, results in strong interactions (nuclear or electromagnetic). While there are a large number of different nuclear reactions, we are interested mostly in neutron interactions with nuclei. Since neutrons do not carry an electrical charge, they will not be stopped by the Coulomb potential barrier as they approach the nucleus. As a consequence, even neutrons that possess comparatively low energies, i.e., thermal or slow neutrons, can interact with the nucleus. Moreover, the probability of interaction with the nucleus by slow neutrons is significantly higher than by fast neutrons. This is easily explained by classical physics: slow moving neutrons remain in the vicinity of the nucleus for a longer average time than fast moving neutrons. Thus, one can assume that the probability of neutron interaction with the nucleus will be higher in the first case than in the second. In quantum mechanics, the collision of a neutron with a nucleus is considered as the interaction of a neutron wave with a barrier - the nucleus. The effective wave length of a neutron is known to be inversely proportional to its velocity. Consequently, the wave length of a slow neutron is

greater than that of a fast neutron, and the probability of interaction is correspondingly higher.

Neutron interactions with nuclei are complex processes that involve restructuring of the atomic nucleus. There are numerous different interpretations of the mechanism of nuclear reactions. We will examine only the simplest of these.

Any neutron interaction with a nucleus can be represented as a collision of a nucleus at rest (target nucleus) with a fast moving elementary particle - the neutron. At the initial instant of collision a compound nucleus is formed, which has a comparatively long (in nuclear dimensions) life time: 10^{-14} - 10^{-15} sec. The explanation is that a neutron impacting with a nucleus, instead of directly traversing the distance equal to the diameter of the nucleus, is "trapped" among other particles and exchanges energy with them. Hence, the comparatively long life time of the compound nucleus. The condition for the existence of the compound nucleus like any real system is satisfied in this way.

All particles are "equal" in the compound nucleus as they are in the ordinary nucleus. The compound nucleus is always excited because the neutron that impacted with it contributes excess energy. This energy consists of the neutron binding energy (about 8 MeV) and the kinetic energy of the neutron. The excitation energy is distributed among all the nucleons of the compound nucleus. This distribution is subject to statistical laws and, in general, the distribution obeys Maxwell's law of energy distribution in an ideal gas. The temperature of the compound nucleus is quite high. Thus, for example, a neutron penetrating into the nuclei of elements that lie in the middle of the Mendeleyev table (A= 80-100) excites them by 8-10 MeV. The average excitation energy of a single nucleon is about 0.1 MeV, which corresponds to a temperature of about 10^9 K. A phenomenon can occur in such a "heated" nucleus, which is analogous to the evaporation of a molecule from a liquid droplet. The surplus energy or a significant portion of it can in time be concentrated in some single particle, and this particle "evaporates," i.e., escapes from the nucleus. It is specifically for this reason that one can speak of nuclear processes occurring in two stages:

1) formation of a compound nucleus; 2) transformation of the compound nucleus. Such a model of nuclear reactions, first introduced by Niels Bohr in 1936, can be represented by the following:

$$_Z X^A + _0 n^1 \rightarrow \left[_Z X^{A+1} \right]^*$$

$$\left[_Z X^{A+1} \right]^* \rightarrow \text{Yield of the reaction.}$$
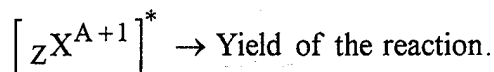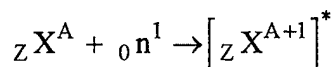
An important consequence of the prolonged existence of the compound nucleus is that the probability of subsequent processes is independent of how the compound nucleus was formed. Thus, depending on the excitation energy of the compound nucleus, the duration of its existence, the composition of the nucleons that constitute it and so on, different kinds of nuclear reactions that follow will occur with different probabilities. Hence, there are several kinds of neutron interactions with nuclei. Those of the greatest importance from the standpoint of nuclear power are elastic and inelastic neutron

scattering, radiative capture or absorption reactions of neutrons, and, finally, fission reactions. Neutrons play a role in all of these reactions. We will, therefore, briefly discuss methods for producing and keeping track of neutrons.

Production of neutrons and methods for counting neutrons. There are many different methods for producing neutrons. The following are the basic ones used in nuclear power:

1. Alpha particle interaction with beryllium (such as the so called polonium-beryllium sources). These nuclear reactions proceed as follows:

$$_4Be^9 + _2He^4 \rightarrow 3\left(_2He^4\right) + _0n^1 \quad ;$$

$$_4Be^9 + _2He^4 \rightarrow _6C^{12} + _0n^1 \quad .$$
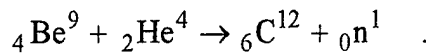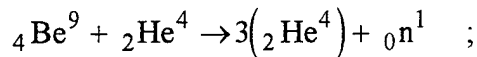
2. Gamma radiation interaction with beryllium (the so called photonuclear sources). The reaction proceeds in accordance with

$$_4Be^9 + \gamma \rightarrow _4Be^8 + _0n^1 \quad .$$
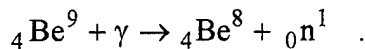
Photonuclear sources are capable of producing monoenergetic neutrons, but the neutron yield is lower than in the preceding process.

3. Fission of heavy nuclei with the formation of neutrons in quantities adequate to sustain a chain reaction at a given level.

The first two processes are used in bringing a reactor to a controlled minimum power level.

There are also several methods for counting neutrons and determining their energies. The choice of method takes into account the weak interaction of neutrons with the electron shell of the atoms of substances. For this reason, the degree of direct ionization of atoms by neutrons is negligibly small. The operation of the detectors is, therefore, based on secondary effects, such as the absorption of neutrons by the nucleus with the ejection of a charged particle and the absorption of neutrons with the formation of a radioactive isotope and the emission of γ quanta.

The first effect is seen in the so called ionization chamber. The volume of the chamber is filled with a gaseous boron compound, for example, BF_3. The reaction proceeds as follows:

$$_5B^{10} + _0n^1 \rightarrow _3Li^7 + _2He^4 \quad .$$
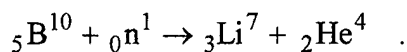
The neutrons are counted and their energies are calculated from the ionization current generated by the α particles.

The second effect is accomplished by direct measurement of the γ radiation energy, for example, in the reaction

$$_{92}U^{238} + {}_0n^1 \rightarrow {}_{92}U^{238} + \gamma .$$
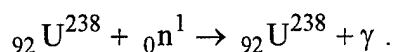
and the neutron energy is then calculated.

Both effects are used simultaneously in order to arrive at a more accurate determination of neutron density and energy. Several standard neutron detectors (counters) are used in observing each of these effects and their readings are then averaged.

Fundamental characteristics of neutron interactions with nuclei. During the penetration of neutrons through matter contained in the reactor core all of the neutron interactions with nuclei mentioned above may occur. The probability of each of these taking place is, however, different and is determined by the average number of processes that occur during the interaction of one neutron with a single nucleus. This parameter, which is measured in units of area, is called the microscopic effective cross section and is designated by σ. In order to clarify this in a physical sense, let's assume an area of 1 cm^2 (Fig. 2.2) containing a number of nuclei, N_n, located in a single layer. Let a neutron flux of density I (sec^{-1}cm^{-2}) be incident on this surface. Then the number of neutrons that interact with nuclei on the prescribed area per unit time (collision rate) is $C = \sigma N_n I$, i.e., $\sigma = C/(N_n I)$ is the probability of a single interaction, cm^2.

The product σN_n can be interpreted as the relative area occupied by all nuclei on the designated 1 cm^2 area. If $\sigma N_n = 1$, then $C = I$, i.e., all neutrons incident on the prescribed area will participate in nuclear interactions.

Since the probability of specific kinds of neutron interactions with nuclei is different and depends on the neutron energies, then the microscopic cross sections of like nuclei will differ. The probability that any of the above neutron interactions with nuclei will occur is determined by the sum of the probabilities (microscopic cross sections) of the individual nuclear interactions: $\sigma = \sigma_s + \sigma_c + \sigma_f$, where σ_s, σ_c, σ_f are the microscopic cross sections of scattering, radiative capture and fission, respectively.

The sum $\sigma_c + \sigma_f$ is sometimes designated by the symbol σ_a and it characterizes reactions associated with neutron absorption. It is useful to compare the microscopic cross section with actual nuclear dimensions, σR^2_n. Since the radius of the nucleus is proportional to the mass number A and $R_n = 1.2 \times 10^{-13}A$ (in centimeters), then the actual cross section falls in the range from 0.05×10^{-24} cm^2 (0.05 barn) to 1.2×10^{-24} cm^2 (1.2 barn). Note that these values differ in a number of cases from the microscopic cross sections of these nuclei by several orders of magnitude.

As has been noted, the probability of different neutron interactions with nuclei depends to a significant degree on neutron energy. In addition, handbook references usually give the value of σ for standard conditions ($E_n = 0.025$ eV; $T_n = 293$ K). For the purpose of calculating the microscopic cross sections at other neutron energies (temperatures), σ can usually assumed to be inversely proportional to the neutron velocity (energy), or since energy is proportional to the square of velocity,
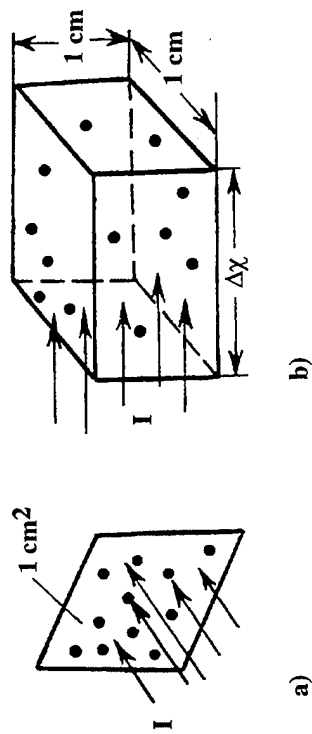
Fig. 2.2 Models for visualizing neutron flux and a) microscopic cross section and b) macroscopic cross section.

$$\sigma \propto \frac{1}{\sqrt{E_n}} \quad .$$

It is then necessary to account for the neutron energy distribution which obeys Maxwell's energy spectrum. Since the average neutron energy used in the calculations differ from the most probable by a factor of $\sqrt{\pi}/2$, this circumstance must be taken into account in all formulas.

According to this, one can write the following expression for the average microscopic cross section $\bar{\sigma}$

$$\bar{\sigma} = \sigma_0 f \sqrt{\frac{293\,\pi}{4\,T_n}} \tag{2.1}$$

where σ_0 is the microscopic cross section at $T_n = 293$ K, f is a factor which takes into account the deviation of the relationship $\sigma(T_n)$ from the relationship assumed, $\sigma \propto 1 / \sqrt{E_n}$. In addition to microscopic cross sections in evaluating neutron interactions with nuclei, macroscopic cross sections are also examined. These characterize interactions that take place within the volume of the material rather than on its surface. The macroscopic cross section is defined as

$$\bar{\Sigma} \equiv N_n \bar{\sigma} \quad ,$$

where N_n is the nucleus density, i.e., the number of nuclei in 1 cm^3 of material. The units of macroscopic cross section are inverse centimeters (cm^{-1}).

By expressing the nuclear density through the mass density ρ of the given isotope, the Avogadro number N_A and the atomic mass m, we can write

$$\bar{\Sigma} = \frac{\rho N_A \bar{\sigma}}{m} \quad .$$

In those cases when the isotope of interest to us is contained in the reactor core as an alloy or a chemical compound, its nuclear density is determined by the equation:

$$N_{n,tot} = \sum_{i=1}^{n} N_{n,i} = \frac{\rho_i}{m_i} N_A v_i \quad , \tag{2.2}$$

where ρ_i is the mass density of the ith constituent in the alloy or the chemical compound; v_i is the volume fraction of the i-th element in the alloy; n_i is the number of atoms of the i-th element in a molecule of the chemical compound; m_i is the atomic mass of the i-th constituent; and N_A is Avogadro's number, 6.022 x 10^{23} atoms/mol.

The macroscopic cross section of the alloy or chemical compound is determined by the sum

$$\bar{\Sigma} = \sum_{i=1}^{n} N_{n,i}\sigma_i$$

The total macroscopic cross section, taking into account all possible kinds of neutron-nuclei interactions, will be

$$\bar{\Sigma} = \bar{\Sigma}_s + \bar{\Sigma}_c + \bar{\Sigma}_f$$

The quantity, the inverse macroscopic cross section, is called the mean free path, $\bar{\lambda} = 1/\bar{\Sigma}$.

In addition to the neutron beam density I in determining neutron interactions with nuclei, there is also a parameter called the neutron flux, ϕ_n. It is equal to the product of the number of neutrons contained in a 1 cm^3 volume (neutron density, N_n) and the average velocity of the neutrons, $\bar{v}_n$. The neutron flux is used conveniently in calculations that involve monoenergetic neutrons. In a physical sense, the neutron flux is the number of neutrons per second passing through a 1 cm^2 target.

Typically, the product $\phi_n \bar{\Sigma}$ is also frequently encountered in calculations. It determines the average number of given neutron interactions with nuclei in a 1 cm^3 volume per second. Another physical interpretation is that it is the ratio of the overall distance per second, $N_n \bar{v}_n$, to the average mean free path length of a single neutron..

We conclude at this point our enumeration of the fundamental characteristics that describe specific kinds of neutron interactions with nuclei and proceed with a more detailed discussion of each kind.

2.3. Neutron Scattering (Moderating) Reactions.

In the majority of neutron sources neutrons are "born" with energies from tens of keV to several MeV. At the same time, the majority of neutrons of importance in applications that have the highest probability of interacting with nuclei are those with very low neutron energies. This circumstance is of great importance in the theory of thermal reactors (reactors with thermal neutrons). This is because the average crow-flight distance over which a fast neutron is thermalized determines the amount of neutron leakage from the core during the moderation process. We will take a look at this in some detail later.

Elastic scattering, which occurs without the formation of a compound nucleus, is of the greatest significance among the scattering reactions of neutrons during collisions. Such collisions can be looked at from the point of view of classical mechanics by assuming that the neutron and the scattering target nucleus behave like ideal elastic spheres. By using the laws of conservation of mass and energy, one can establish a relationship between the angle of scatter and the neutron energy before and after collision with the nucleus. Then, by using certain empirical scattering laws, one can obtain results of practical importance.

We will examine this problem in a simplified manner and, in particular, we will discuss only the head-on collision of a neutron with a nucleus during which the travel of the neutron and the nucleus is in a straight line (Fig. 2.3). The target nucleus is assumed to

a)

Neutron (M_n, V_1)

Nucleus (M_n)

Energy: $\dfrac{M_n V_1^2}{2}$

Momentum: $M_n V_1$

b)

Neutron (M_n, V_2)

Nucleus (M_n, V)

Energy: $\dfrac{M_n V_2^2}{2} + \dfrac{M_n V^2}{2}$

Momentum: $-M_n V_1 + M_n V$
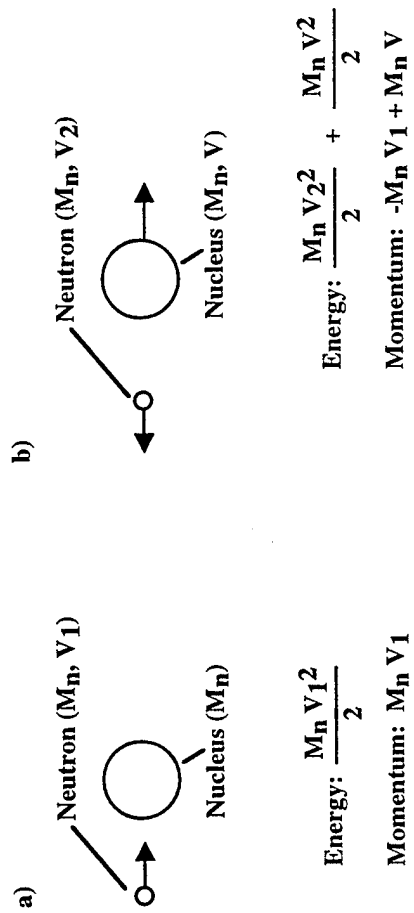
Fig. 2.3 Energy and momentum balance for a collision between a neutron and a nucleus initially at rest; a) before collision; b) after collision.

be at rest prior to the collision. We write the laws of conservation of energy and momentum by assuming that in atomic mass units the mass of the neutron is $m_n \cong 1$, and the mass of the nucleus is $M_n \cong A$:

$$E_1 = \frac{v_1^2}{2} = \frac{Av^2}{2} + \frac{v_2^2}{2} \quad ; \quad v_1 = Av - v_2 \quad . \quad (2.3)$$

After a number of transformations, we obtain

$$\frac{E_2}{E_1} = \left(\frac{A-1}{A+1} \right)^2 \quad ,$$

where E_1 and E_2 are the neutron energies before and after the collision, respectively. The maximum energy loss in a single collision is

$$\Delta E_{max} = E_1 - E_2 = E_1 \frac{4A}{(A+1)^2} \quad . \quad (2.4)$$

It follows from this equation that the largest neutron energy loss occurs during collisions with nuclei of light elements. Thus, in a head-on collision of a neutron with a hydrogen nucleus, the neutron loses all its energy. In a head-on collision of a neutron with a carbon nucleus ($A = 12$), it loses $0.28E_1$, and with a uranium nucleus ($A = 238$), it loses only $0.016E_1$. Thus, the moderation of neutrons deteriorates with increasing mass numbers.

In addition, head-on collisions will cause neutrons to deflect at an angle, $\theta = 180°$; upon off-center collisions, $0 < \theta < 180°$, during which $\Delta E < \Delta E_{max}$.

If the probability of neutron scatter in all possible directions is the same, then the scattering is called isotropic. Neutrons scatter, however, more frequently at an angle $\theta < 90°$ and rarely at an angle $\theta > 90°$ (Fig. 2.4). Such scattering is called anisotropic. Anisotropic neutron scatter is characterized by an average scattering angle cosine, $\overline{\mu} = \cos \overline{\theta}$. For isotropic scattering $\overline{\mu} = 0$, and for anisotropic scattering $\overline{\mu} > 0$. At relatively low neutron energies the average cosine of the scattering angle depends only on the mass number and can be assumed to be $\overline{\mu} = (2/3)A$. The greatest anisotropic scattering is observed in hydrogen and deuterium nuclei. With increasing mass numbers, the value of $\overline{\mu}$ approaches zero. The scattering by nuclei with mass numbers $A > 10$ can, therefore, be approximated as isotropic scatter.

The predominant scattering at an angle $\theta < 90°$ increases somewhat the free path compared to the isotropic scattering assumption; i.e., for $\overline{\lambda}_s = \frac{1}{\overline{\Sigma}_s}$. In practice, therefore, the so called transport (actual) mean free path is used. It is calculated from the equation:

$$\bar{\lambda}_{tr} = \frac{\bar{\lambda}_s}{1 - \bar{\mu}} \qquad (2.5)$$

This equation is easily obtained through the following simple argument. Let's examine neutron travel initially in a direction along the x-axis by assuming the angles θ_1, θ_2 ... and so on as small, and $\sin\theta_1$, $\sin\theta_2$ are consequently small. After the initial collision, the neutron is deflected at an angle θ_1, after the second, at an angle $\theta_1 + \theta_2$, and so on. The projection of the segment λ_1, λ_2 ... on the x-axis will, after the first collision, be $\bar{\lambda}_s\cos\theta_1$, after the second, $\bar{\lambda}_s\cos\theta_1\cos\theta_2$, etc. (this assumes that the segments λ_1, λ_2, ..., λ_n are equal and equal to $\bar{\lambda}_s$).

We note further that by assuming $\theta_1 = \theta_2 = \theta_n = \bar{\theta}$, $\cos\bar{\theta} = \bar{\mu}$, after the n-th collision, the projection is equal to $\bar{\lambda}_s\cos^n\bar{\theta}$, etc.

By summing the individual segments, we obtain

$$\bar{\lambda}_{tr} = \bar{\lambda}_s + \bar{\lambda}_s\cos\bar{\theta} + \bar{\lambda}_s\cos^2\bar{\theta} + ... \bar{\lambda}_s\cos^n\theta + .. \quad ; \text{ or,}$$

$$\bar{\lambda}_{tr} = \lambda_s\left(1 + \bar{\mu} + \bar{\mu}^2 + ... \bar{\mu}^n\right) \qquad .$$

Since $\bar{\mu} < 1$, the sum considered represents an infinitely decreasing geometric progression thus confirming the equation.

The macroscopic cross section corresponding to the transport mean free path of the neutron will be $\bar{\Sigma}_{tr} = \dfrac{1}{\bar{\lambda}_{tr}}$.

Different moderators and their selection requirements are described by a number of characteristics. We will take a look at those that are important. The reduction in neutron energy during collisions with moderator nuclei is in practice evaluated from the mean logarithmic neutron energy loss in a single collision. This is the so called neutron moderation parameter ξ. It is equal to the average difference in the natural logarithmic neutron energies before and after a collision:

$$\xi = \ln\overline{E}_1 - \ln\overline{E}_2 = \ln\frac{\overline{E}_1}{\overline{E}_2} \qquad (2.6)$$

The moderation parameter ξ is frequently called the average logarithmic energy decrement per collision. It depends only on the mass number and the scattering angle of the neutrons. Based on the laws of conservation of energy and momentum, the following expression for ξ can be obtained by assuming isotropic scattering:

$$\xi = 1 + \frac{(A-1)^2}{2A}\ln\left[\frac{A-1}{A+1}\right] \qquad . \qquad (2.7)$$

65

A better approximation, valid for $A > 10$, is provided by the simple equation

$$\xi \cong \frac{3}{A + \frac{2}{3}}$$
(2.8)

The moderation parameter is independent of energy. This makes it easy to calculate the average number of collisions, n_c, that are necessary to reduce the neutron energy from an energy E_1 to some energy E, to wit $n_c = \ln(E_1/E_2)/\xi$. Thus, in order to moderate a neutron from its average energy at the moment of formation, E_0 (in most calculations, E_0 2 MeV), to thermal energy in hydrogen, an average of 18 collisions are required, in beryllium, 87, and in carbon, 115.

We will substitute the difference $\ln(E_1/E) = \ln(E_0/E) - \ln(E_0/E_1)$ for the logarithm of the ratio E_1/E in the equation for n_c. $\mathrm{Ln}(E_0/E)$ is called the logarithmic energy or lethargy. We will designate u_1 and u_2 as the neutron lethargies with respect to E_1 and E_2. Accordingly, we can write $u_2 - u_1 = \ln E_1 - \ln E_2 = \xi$. Thus, ξ is the average change in lethargy per collision (Fig. 2.5). Since $E = E_0 e^{-u}$, the average value of neutron energy loss in earlier scattering events is higher than in subsequent events.

We will now turn our attention to requirements established for moderators. A good moderator should not only have a large moderation parameter ξ, but also a large macroscopic scattering cross section, i.e. the highest possible number of scattering events per unit time in a unit volume. From this standpoint, the significant parameter is $\xi \Sigma_s$, which is the moderating capability of the medium in which the moderation process is accomplished.

The moderating capability of alloys or chemical compounds is determined (in cm^{-1}) from the equation

$$\xi \bar{\Sigma}_s = \xi_1 \bar{\Sigma}_{s1} + \xi_2 \bar{\Sigma}_{s2} + \ldots \xi_n \bar{\Sigma}_{sn} \quad ,$$
(2.9)

where ξ_1, ξ_2, ..., ξ_n are the moderation parameters of the substances contained in the alloy or chemical compound; $\bar{\Sigma}_{s1}$, $\bar{\Sigma}_{s2}$, ...$\bar{\Sigma}_{sn}$ are the average macroscopic scattering cross sections taking into account the relative volume or mass density of the moderator.

A high moderating capability is not the only requirement of moderators. It is also necessary to consider its absorption capability. For example, the moderating capability of boron exceeds that of carbon, but boron is an excellent absorber of neutrons and is never used as a moderator. Therefore, an additional parameter enters into the picture. It estimates the property of the moderator in toto and is called the moderation factor

$$\kappa = \frac{\xi \bar{\Sigma}}{\bar{\Sigma}_{at}} \quad ,$$
(2.10)

where $\bar{\Sigma}_{at}$ is the macroscopic cross section of thermal neutron absorption by the nuclei of the substance used as the moderator.

Water, carbon, beryllium, and alkali metal hydrides are excellent moderators. Table 2.1 presents data on the parameters discussed above for several moderators used in practical applications. It is obvious that heavy water is the best moderator. Due to its high cost and for a number of other reasons it has not seen wide practical use. Low cost moderators, such as graphite and water, are used, and alkali metal hydrides are used in space power plants because of the high operating temperatures.

Table 2.1

Moderator	ξ	$\xi \overline{\Sigma}_s$, cm^{-1}	κ
Water	0.924	1.35	70
Heavy water	0.515	0.188	2000
Beryllium	0.209	0.154	159
Graphite	0.158	0.064	170
Alkali metal hydrides	0.900	1.540	51

A most important characteristic of the moderation process is the duration of the moderation process as expressed by the quantity $\sqrt{\tau}$. The units of τ (cm^2) does not correspond with its name, the age of neutrons. (The actual life time of a neutron from the moment of formation to the moment of moderation, i.e., reduction in energy to thermal energy levels, is short and is, for example, during moderation in lead only about 4×10^{-4} sec). The origin of this term is related to the form of the equation for the age of neutrons, first derived by Fermi. The age equation establishes a connection between the moderation density (i.e., the number of neutrons contained in 1 cm^3 and which, during moderation, pass through a given energy level in one second) and the distance from the fast neutron source to the elementary volume in which the moderation process is examined. Solution to the age equation is found by assuming that the moderation density is the product of two different functions. One of these is a function of the distance δ from the neutron source and the other is a function of τ only. Hence, the similarity of this equation to the thermal conductivity equation, in which the role of time is played by τ, gives rise to the concept of the term "age."

It is usually of interest to determine the point at which the neutron becomes thermalized, and, accordingly, the age of the neutron, i.e., to take a look at the sequence of the moderation process. A precise calculation of the moderation process is very complicated. Even if the neutron source is monoenergetic, during moderation the neutrons acquire different velocities and traverse different distances from the source. The following equation is used in approximate calculations for practical purposes in determining the age of neutrons:

$$\tau = \frac{\ln\left(\dfrac{E_o}{E}\right)}{3\left(\xi \overline{\Sigma}_s\right)\Sigma_s\left(1 - \overline{\mu}\right)} \qquad (2.11)$$

The age of neutrons is illustrated geometrically by 1/6 the average square distance δ^2_m on a straight line along which a neutron travels during moderation from the point where it was formed as a fast neutron to the point where it became thermalized (Fig. 2.4).

Some idea of the age of neutrons during moderation in different substances is provided by the following numbers in Table 2.2.

Table 2. 2 Neutron Age of Various Materials

Moderator	H_2O	D_2O	Be	Alkali Metal Hydrides
τ, cm^2	31	125	86	313

It is obvious from these parameters that water is the best moderator. This explains its wide use in water-water reactors in marine power plants and in atomic electric stations. In addition to the reasons stated earlier, the use of water as a moderator in space nuclear power plants is not feasible. Therefore, these use moderators with large values of τ, such as beryllium and alkali metal hydrides.

2.4. Radiative Capture Reactions.

In general, radiative capture reactions proceed as follows:

$$_Z X^A +_0 n^1 \rightarrow \left[_Z X^{A+1} \right]^* \rightarrow \left[_Z X^{A+1} \right] + \gamma \qquad .$$
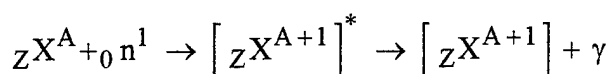
The new nucleus, which is an isotope of the original chemical element, transitions from an excited state to a normal or ground state by the ejection of a batch of γ quanta. The probability of this reaction taking place depends on several factors including the energy of the neutrons.

It was discovered in neutron-nuclei interaction experiments that when the interacting neutron possesses a certain kinetic energy, its probability of capture by the target nucleus increases rapidly. This phenomenon, which is especially noticeable in slow neutron interactions, is called resonance capture. It is generally accepted that resonance capture occurs when the compound nucleus, formed as a result of the absorption of a neutron with a given kinetic energy, is in an excited state close to the energy of one of its quantum energy levels. The resonance capture effect can be illustrated by using Fig. 2.5 in which the lines on the right represent the quantum energy levels of the composite nucleus.

The dashed lines on the left represent the energy of a composite nucleus which has absorbed neutrons with different kinetic energies (i.e., the energy of the ground state of the composite nucleus plus the binding energy of a neutron in its nucleus plus its kinetic energy). The E'_0 level corresponds to the condition when the kinetic energy of the neutron is zero. Apparently, the energy E_1 corresponds to one of the quantum levels of the compound nucleus and, consequently, a neutron with a kinetic energy $E_n = E_1 - E'_0$ undergoes resonance capture. The next resonance capture occurs with a neutron energy of $E_2 - E_0$ when the new energy of the composite nucleus corresponds to a different quantum level.

68
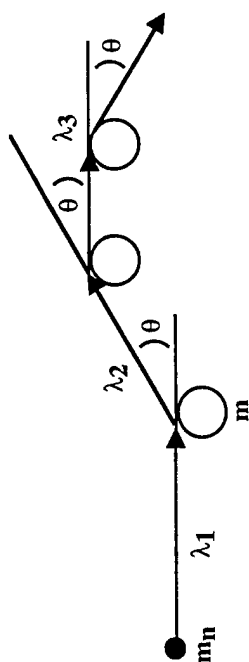
Fig. 2.4 Neutron scattering conceptual illustration. For anisotropic scattering, θ is usually less than 90°.
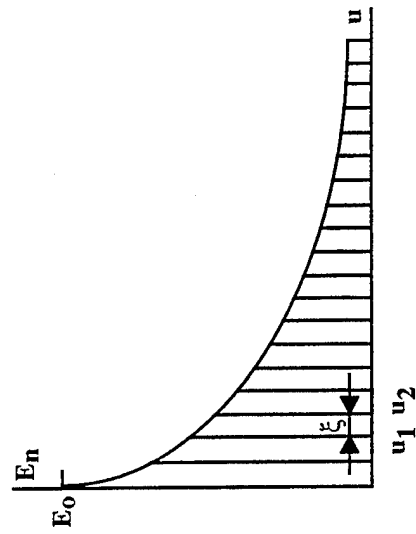
Fig. 2.5 Neutron energy as a function neutron lethargy. Moderating of neutron energy occurs most rapidly at high energies.

It should be emphasized that the quantum energy levels of the compound nucleus in Fig. 2.6 are not shown precisely.

In reality, each energy level has a finite band width. There exists, therefore, a certain energy interval of the interacting neutrons within which resonance capture is observed. If the width of the quantum levels is greater than the average distance between them (i.e., when different energy levels overlap), the concept of resonance capture loses meaning. Experimental data show that the distance between quantum energy levels of compound nuclei with moderate and large mass numbers is approximately 1 to 10 eV. One should therefore expect to observe resonance capture of neutrons with energies of this magnitude. If the neutrons possess substantially higher energies, i.e. in units of MeV and higher, then the compound nucleus will have a surplus of energy in excess of the ground state by about 8 to 10 MeV. In this region, the energy level widths of the compound nucleus are significantly greater than the distance between them and the concept of resonance capture loses its meaning.

Fig. 2.7 shows a typical relationship between the microscopic absorption cross section of uranium-238 and neutron energy. As is apparent, a sharp increase in the absorption cross section is observed in the neutron energy region $E_n = 6$ to 8 eV. This phenomenon must be taken into account in the moderation of neutrons.

In radiative capture reactions (including resonance) a compound nucleus in the excited state can transition to the ground state in different ways, for example, through ejection of neutrons and γ quanta (inelastic scattering), ejection of α-particles or protons, and finally, ejection of only portions of γ quanta (the latter transition to the ground state is the most typical occurrence in neutron interactions with nuclei). Thus, radiative capture reactions are in the overwhelming majority of cases detrimental from the position of the number of neutrons that participate in the fundamental nuclear processes--heavy nuclei fission reactions. Resonance absorption of neutrons is especially significant at resonance peaks of uranium-238. The same process is, however, useful in reactions for the purpose of producing new nuclear fuels.

We will now discuss these two processes (resonance absorption of neutrons by uranium-238 nuclei and the formation of new fuels from uranium-238).

Resonance absorption of neutrons by uranium-238. In thermal reactors with slow neutrons, uranium-238 has a large tendency to absorb neutrons in the resonance region. The resonance region consists of a number of resonance peaks which lie in the neutron energy range from roughly 1 eV to about 1 keV.

Let's examine resonance absorption of neutrons in a homogeneous infinite reactor consisting of a moderator and U^{238}. Migrating neutrons in this system are either scattered by the moderator or absorbed by uranium-238. We will assume that the first resonance peak is confined within a narrow lethargy interval, $\Delta u_1 = u_2 - u_1$. Let the neutron flux per unit interval of energy close to the lethargy u be equal to $\phi(u)$, then in the interval Δu_1 it will equal $\phi(u)\Delta u_1$. During collisions with the moderator nuclei the neutron will on the average change its logarithmic energy by the moderation parameter ξ. The probability that the neutron will depart the resonance interval after scattering by the collision is equal to the ratio $\xi/\Delta u$. If $\xi > \Delta u$, a single collision is sufficient for a neutron to depart the interval. If $\xi < \Delta u_1$, a neutron will pass through the resonance interval per
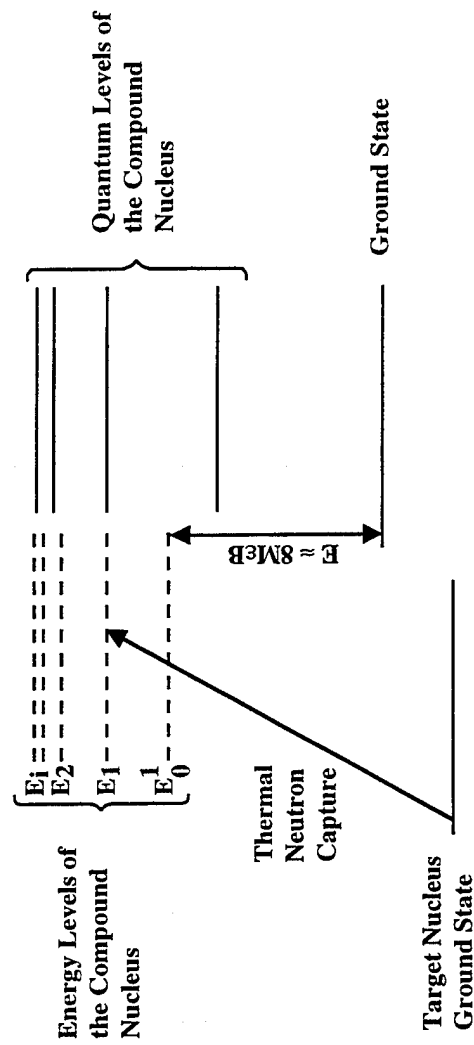
Fig. 2.6 Energy level diagram for a nucleus undergoing neutron resonance absorption.

72
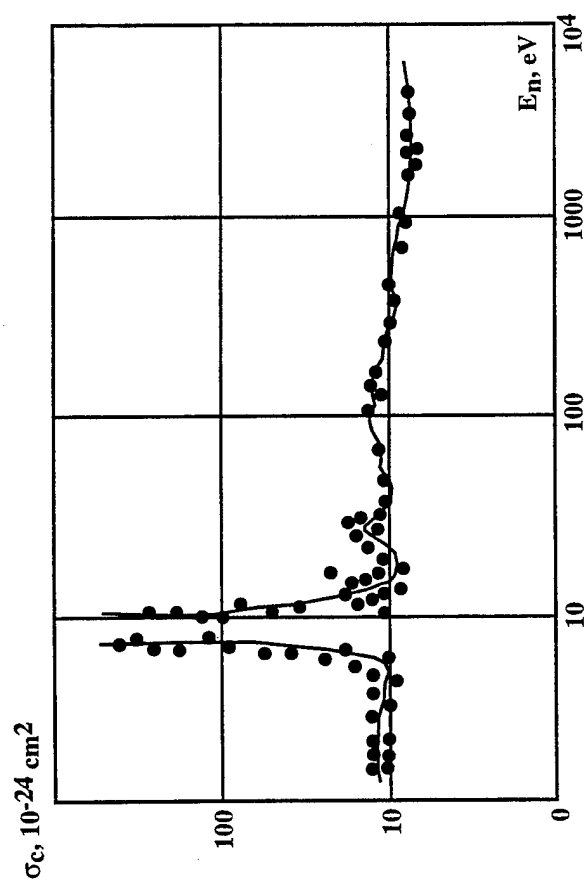
Fig. 2.7 Capture cross section of U-238 as a function of neutron energy. Note resonance absorption at ~ 8 eV.

$\Delta u_1/\xi$ of the collisions. The total number of collisions in a unit volume occurring in the interval Δu_1 will equal $\Sigma_s\phi(u)\Delta u_1$. As a result of the collisions in this interval, $\xi\bar{\Sigma}_s\phi(u)$ neutrons will be moderated. Collisions with U^{238} nuclei in the resonance interval results in neutron absorption. If $N(U^{238})$ is the concentration of U^{238} nuclei, then at the first resonance level $N(U^{238})\bar{\sigma}_{a1}\phi(u)\Delta u_1$ neutrons will be absorbed, where $\bar{\sigma}_{a1}$ is the average resonance absorption cross section. The total number of collisions during which the neutrons are either moderated or absorbed in the resonance interval will equal

$$\xi\bar{\Sigma}_s\phi(u) + N(U^{238})\bar{\sigma}_{a1}(u)\Delta u_1$$

Consequently, the fraction of neutrons being moderated below the first resonance level will be

$$\phi_1 = \frac{\xi\bar{\Sigma}_s\phi(u)}{\xi\bar{\Sigma}_s\phi(u) + N(U^{238})\bar{\sigma}_{a1}\Delta v_1}$$

and after division of the numerator and denominator by $\xi\bar{\Sigma}_s\phi(u)$.

$$\phi_1 = \frac{1}{1 + \left(\dfrac{N(U^{238})}{\xi\bar{\Sigma}_s}\right)\bar{\sigma}_{a1}\Delta u_1}$$

In thermal reactors the ratio $N(U^{238})/\xi\bar{\Sigma}_s$ is approximately equal to 0.005 barn^{-1} while the product $\bar{\sigma}_{a1}\Delta u_1$ is ~12 barn. As a result, the second item in the denominator turns out to negligibly small and the expression for ϕ_1 can be written in exponential form:

$$\phi_1 = \exp\left(\frac{-N(U^{238})\bar{\sigma}_{a1}}{\xi\bar{\Sigma}_s}\right)$$

Neutron absorption occurs in the second, third and in other peaks. The neutron fraction that escapes absorption in any k-th resonance peak is equal to

$$\phi_k = \exp\left(\frac{-N(U^{238})\bar{\sigma}_{ak}\Delta u_k}{\xi\bar{\Sigma}_s}\right)$$

where $k = 1, 2, 3, \ldots$ n is the number of resonance peaks.

Of N_n neutrons entering the resonance region, $N_n\phi_1$ neutrons will remain after the first resonance, $N\phi_1\phi_2$ after the second, and so on. $N^t_n = N_n\phi_1\phi_2 \ldots \phi_n$ neutrons will pass through the resonance region in the moderation process and become thermalized. The fast neutron fraction that has become thermalized,

$$\phi = \frac{N_r^T}{N_r} = \phi_1, \phi_2, \dots \phi_n \qquad ,$$

is called the probability of resonance capture escape. The expression for

$$\phi = \phi_1 \phi_2 \phi_3 \cdots \phi_n$$

can now be written as

$$\phi = \exp\left(\frac{N(U^{238})}{\xi \Sigma_s} I\right) \qquad , \qquad (2.12)$$

where $I = \bar{\sigma}_{a,1} \Delta u_1 + \bar{\sigma}_{a,2} \Delta u_2 + \dots \bar{\sigma}_{a,n} \Delta u_n$ is called the resonance integral. It portrays the absorption of neutrons by individual nuclei in the resonance region and is measured in barns.

The use of the resonance integral simplifies quantitative calculations of resonance absorption without a detailed examination of neutron interactions during the moderation process. The resonance integral J is usually determined experimentally. It depends on the concentration of uranium-238 and the mutual distribution of uranium and moderator. At the same time, there are empirical equations convenient for practical use in calculating the resonance integral for homogeneous mixtures. In heterogeneous reactors the resonance integral depends on the diameter of the fuel elements. It can also be calculated from appropriate empirical formulas.

The breeding of nuclear fuels as a useful product of radiative capture reactions. The formation of new fuels in radiative capture reactions proceed according to the following:

$$_{92}U^{238} + {}_0n^1 \rightarrow \left[{}_{92}U^{239} \right]^* \rightarrow {}_{92}U^{239} + \gamma \qquad ;$$

$$_{92}U^{239} + {}_0n^1 \xrightarrow{\beta} {}_{93}Np^{239} \xrightarrow{\beta} {}_{94}Pu^{239} \qquad .$$
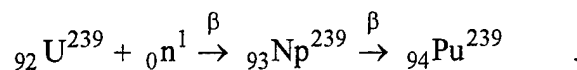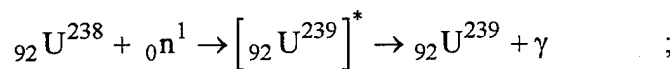
Thus, as a result of a secondary ß⁻ decay of the radioactive isotope $_{92}U^{239}$ a new nuclear fuel, plutonium-239, is formed. The process becomes possible if more than two new neutrons are formed during fission of uranium. A quantitative estimate of the process of forming new fuels makes use of the breeding factor K_B. This is the ratio of newly formed fissioning nuclei to the quantity undergoing fission. In thermal reactors it is difficult to breed nuclear fuel because in one neutron capture in the core no more than 2 - 2.5 new fission neutrons will be emitted. In fast reactors each neutron capture is accompanied by the emission of 2.5 - 3 neutrons. One neutron is needed to sustain the chain reaction, and the remaining 1.5 - 2 neutrons can be used in producing plutonium.

The breeding ratio for a fast reactor depends on the unproductive neutron capture by the nuclear fuel and structural materials and on the neutron leakage. At the present time, fast breeder reactors are being designed in which the unproductive expenditure of neutrons is reduced to a minimum. As a result, the breeding ratio reaches about 1.8 - 2, i.e., each kilogram of uranium-238 fuel burned will accumulate 1.8 - 2 grams of plutonium. Considering the limited supply of uranium on the earth and its very low uranium-235 isotope content, the artificial production of such a fuel as plutonium-239 is becoming of greater and greater importance.

2.5. Fission of Heavy Nuclei

Fission of heavy nuclei is the most important neutron-nuclei interaction process. It is the fundamental operating mechanism in nuclear power plants designed for any purpose. From the standpoint of the early 1980s (a period of vigorous nuclear power development in several countries in the world), it is useful to discuss briefly some historical landmarks in the discovery of heavy nuclei fission, the main event in physics during the first half of the 20th century.

At the end of the 1930s, a group of physicists under the leadership of Enrico Fermi conducted experiments on irradiating heavy uranium-238 nuclei with neutrons. The objective of these experiments was to produce transuranic elements by possible ß⁻ decay of an excess of neutrons of heavy nuclei, i.e., elements with an atomic number Z = 93. In fact, in the experiments Fermi converted uranium by neutron interactions into hitherto unknown isotopes. In 1938, Fermi was awarded the Nobel Prize in physics for the discovery of new radioactive elements obtained by neutron irradiation of uranium. In 1939, however, the sensational work of the German physicists, L. Maitner and O. Hahn, appeared: "Fission of uranium by neutrons--a new kind of nuclear reaction." In this work, which explained Fermi's experiments, it was shown that the elements formed in the reaction were not transuranic elements but radioactive isotopes which fell in the middle of the Mendeleyev periodic table. Thus, the Fermi group had unsuspectingly split such a "monolith" as the atomic nucleus with a tiny neutron. This was equivalent to shattering a piece of granite by tapping on it with a pencil! The rock not only shattered, it liberated a large quantity of energy stored within it. Einstein's first law, which correlates mass and energy through the relationship $E = mC^2$, was quantitatively substantiated. Later, Fermi loved to joke that the first Nobel Prize in physics was awarded for an incorrect interpretation of a discovery.

Several decades have passed since then. Tens of atomic electric stations have been built throughout the world and ships are plying the oceans with atomic power plants. Nuclear power plants are used in space. As we all know, there have been some extremely bad consequences. It is, therefore, so important to understand in a few words the principles of operation and design of nuclear reactors. We need to know how to operate nuclear power systems wisely and completely avoid any kind of accident and catastrophe during their operation.

Let's return now to the mechanism of heavy nuclei fission. We know that any time the mass of the nucleus exceeds the mass of the fragments that could be formed as a result of fission, there is a definite probability that the original nucleus will undergo a fission

reaction. This is because the process is accompanied by a decrease in mass and the liberation of energy, i.e., there is an energy resolution. This condition is satisfied by all nuclei with mass numbers $A > 100$. Consequently, they are theoretically capable of undergoing spontaneous fission. In practice, however, such processes are extremely rare. In order for the fission reaction to occur, a certain critical energy must be delivered to the nucleus. It is called the activation energy, E_{ac}.

For substances with mass numbers $A < 210$ this energy is so great that fission can occur only when the energy of the particles (neutrons, protons, and others) that bombard the target nuclei exceeds 50 MeV. Thus, the magnitude of the activation energy is an important indicator of the capability of the nucleus to undergo fission. A definitive idea of the critical energy can be obtained from the droplet model of the atomic nucleus.

Let's examine a liquid droplet which by some method is brought into a state of oscillation. The system can in this case pass through a number of phases, some of which are shown in Fig. 2.8.

At first, the droplet has a spherical shape "a," then it elongates and becomes an ellipsoid "b." If the energy delivered to the droplet is insufficient to accomplish the next stage in its transformation, i.e., insufficient to overcome the surface tension force, the droplet will return to its original shape. If the deformation force is sufficiently great, the liquid droplet will assume a shape similar to that of the dumbbell "c." If the droplet reaches this phase, it is unlikely to return to its spherical shape and will rapidly divide into two droplets. They will be somewhat deformed "d" at first and then assume the spherical shape "e."

The situation in the fission of a nucleus-drop is analogous to that just described. A target nucleus absorbs a neutron and forms a compound nucleus. The excitation energy of the compound nucleus is equal to the binding energy of the neutron plus the kinetic energy of the neutron prior to capture by the target nucleus. It can be expected that this excess energy will cause the compound nucleus to pass through a number of phases similar to those described above. If the excitation energy is insufficient to lead to phases that exist beyond the state at "b," the intranuclear forces will compel the nucleus to return to its original form "a," and the excess energy will be removed by the expulsion from the target nucleus of either a particle or γ quanta. However, if the nucleus has gained enough energy from neutron absorption to cause it to turn into the dumbbell shape "c," the restoration of the intitial state "a" becomes improbable. This is because the electrostatic repulsion between the protons at the two ends of the deformed nucleus "c" can now overcome the nuclear forces of attraction at work in the connecting region. The system then passes rapidly from state "c" to "d" and then to state "e" after forming two "fragments" that fly away in opposite directions. Thus, the critical energy or activation energy is the energy that must be added to the target nucleus in order to deform it to the state "c." Thereafter, fission inevitably occurs.

Let's now evaluate the factors that influence the activation energy. We will assume that the composition of the nucleus does not change (A = const) and that the nucleus, when it is in the excited state, can change its shape. Since the volume of the nucleus does not change, then during deformation from the original spherical shape to, let's say, an ellipsoid, the change in energy of the nucleus will be determined by only two factors: the effective surface tension and the forces of coulomb repulsion. The surface tension effect
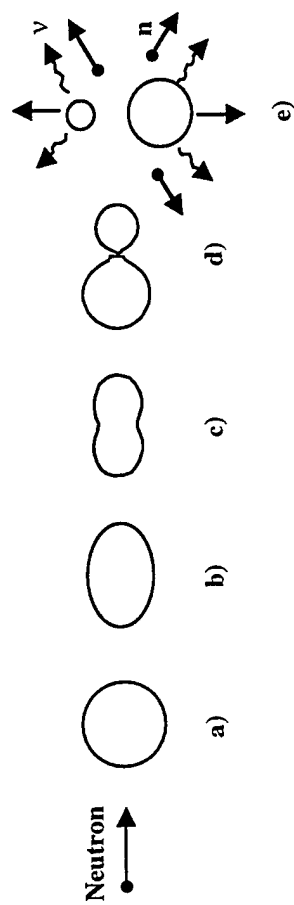
Fig. 2.8 Oscillating liquid droplet model of nuclear fission.
a) spherical shape; b) ellipsoid; c) dumbbell;
d) division; e) fission.

increases with deformation of the nucleus since the surface area will increase with the volume remaining constant. At the same time, the coulomb forces of repulsion will diminish since the protons move away from each other slightly. To sum up, with an increase in mass number A and with the number of protons remaining the same, the activation energy must increase. On the other hand, with an increasing Z and a simultaneous increase in the mass number A, the coulomb forces of repulsion will increase so much that at some value of A (the portion of the curve to the right, $E_b/A = f(A)$), they will prevail over the surface tension forces. Hence, the inverse relationship of the activation energy to the number of protons. From a comparison of these forces (surface tension and coulomb repulsion), the following expression was obtained for the activation energy:

$$E_{ac} = 0.9A^{2/3} - 0.02\frac{Z}{A^{1/3}} \approx A^{2/3}(0.9 - 0.02\frac{Z^2}{A}) \qquad . \qquad (2.13)$$

In this equation, the first term portrays the surface tension effect, the second the electrostatic energy of repulsion.

From eq. (2.13) one can establish conditions for spontaneous fission of a nucleus. In order for this to occur, the activation energy must be equal to zero or be a negative quantity. This is always possible when $Z^2/A > 45$. Such a condition is satisfied by nuclei with mass numbers $A > 260$, which, of course, do not exist in nature.

Let's write the fission reaction for uranium-235 when acted upon by slow neutrons. One possible fission variant looks like the following:

$$_{92}U^{235} + {_0}n^1 \rightarrow \left[_{92}U^{236} \right]^* \rightarrow {_{57}}La^{147} + {_{35}}Br^{87} + 2{_0}n^1 + \gamma \qquad . \qquad (2.14)$$
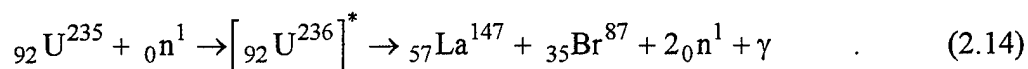
As can be seen, both fragments, the nuclei of the lanthanum and bromine isotopes, are much lighter than the uranium-235 nucleus and differ from each other in mass number. More detailed studies of the fission of uranium-235 show that it fissions in more than 30 different ways. The mass numbers of the fission fragments fall in the range from 72 (zinc isotope) to 158 (samarium isotope). However, the most probable (yielding ~6% of the possible fission variants compared with $10^{-5}\%$ for the extreme cases) is the formation of fragments with mass numbers $A = 95$ and $A = 139$, respectively. Analogously, the quantity of neutrons produced in each act of fission also differ and averages $\overline{v} = 2.5 \pm 0.1$.

Neutrons that are produced during fission of the uranium nucleus can be divided into *prompt* and *delayed* neutrons. The first of these comprise about 99% of the neutrons produced. They are produced virtually instantaneously in 10^{-14} to 10^{-15} sec. Delayed neutrons, representing less than 1% of the total number of neutrons produced, are associated with the formation of radioactive fission products, the neutron-rich isotopes found in the middle of the Mendeleyev table. The duration of delayed neutron production per single act of fission is on the average about a tenth of a second. It differs, however, for different groups of delayed neutrons and fall in the range from 0.07 sec with a relative yield for any one group of 0.02% of the total quantity of neutrons being produced to 30

sec with a relative yield of 0.026%. The most probable duration of delayed neutron production is from 2 to 30 sec with a relative delayed neutron yield of ~0.2%.

It is important to emphasize that although the quantity of delayed neutrons is small, their role in nuclear reactor control is extremely great.

The energy of prompt neutrons falls within a broad range from more than 10 MeV to hundreds of eV. However, the majority of prompt neutrons have energies that lie within a comparatively narrow range of 1 to 3 MeV and their average energy is assumed to be 2 MeV in most calculations. The energy liberated during fission is concentrated mainly in the fission fragments, but also in the elementary particles and γ radiation produced by the reaction.

The table 2.3 shows the distribution of energy liberated during fission.

Table 2.3 Average Energy Released per Fission

Fission fragment energy (kinetic)	162 MeV
Beta decay energy	5 MeV
Gamma decay energy	5 MeV
Neutrino energy	11 MeV
Fission neutrons	6 MeV
Gamma ray energy	6 MeV
Total fission energy	195 MeV

The kinetic energy of the fission fragments is transformed into thermal energy almost instantaneously. The energy of instantaneous γ radiation is also dissipated very rapidly. In addition, the energy of ß radiation and of γ quanta during beta decay is liberated gradually (during several tens of seconds) as radioactive decay of fission fragments. As a consequence, the energy liberated in the initial instant is about 174 MeV. When the delayed release of energy is accounted for, the energy then becomes 184 MeV. However, because the energy carried by the neutrinos is irretrievably lost, the energy of practical use that is liberated in a single act of fission in uranium-235 is about 180 MeV. This exceeds by many times the energy liberated in radioactive decay processes.

In conclusion, let's look at the fission of $_{92}U^{235}$ and $_{92}U^{238}$ nuclei when acted upon by slow and fast neutrons and from this formulate nuclear fuel requirements. For this purpose, let's determine the activation energy for uranium-235 and natural uranium-238 nuclei. As one would expect, the activation energy in the first case is 6.5 MeV, and in the second 7.0 MeV. Now let's evaluate the excitation energy of the nucleus under consideration by assuming initially that the kinetic energy of the absorbed neutron is zero. In this case, the excitation energy of the compound nucleus can be calculated from the difference in binding energies of the compound nucleus and the original nucleus. Hence, we obtain for the excitation energy of uranium-235:

$$E_e(U^{235}) = E_e(U^{236}) - E_e(U^{235}) = 6.8 \text{ MeV}$$

and for uranium-238

$$E_e(U^{238}) = E_e(U^{239}) - E_e(U^{238}) = 5.5 \text{ MeV}$$

It is obvious that the excitation energy in the first case is higher than in the second. Let's now compare the excitation energy of both nuclei with their activation energies. It is not difficult to see that neutrons of any energy can cause uranium-235 nuclei to fission. At the same time, the kinetic energy of the neutrons should be no lower than 1.5 MeV to cause fission of natural uranium-238 nuclei. In other words, the fission of natural uranium is possible only with fast neutrons.

The reason for the appreciable difference in the above binding energies of the two isotopes of uranium indicated by the last term of the equation is due to the nuclear "spin" effect (the coupling of paired or unpaired nucleons that make up the nucleus). Since the compound nucleus $_{92}U^{236}$ has an even-even nature, the spin component makes a positive contribution to the binding energy by 0.55 MeV. At the same time, this contribution is zero for a target nucleus of $_{92}U^{235}$, which has an even-odd nature. The compound nucleus $_{92}U^{239}$ is even-odd and its spin effect is zero while the spin effect of the even-even target nucleus $_{92}U^{238}$ contributes 0.55 MeV to the binding energy. Consequently, this effect by itself causes a difference in excitation energies of U^{235} and U^{238} by 1.3 MeV. Hence, one can formulate the requirement on nuclear fuels. These should consist of either even-odd or odd-odd nuclei. Since the odd-odd nucleus is unstable and is not found in nature, the odd-even nucleus is recommended for use in nuclear power. Such nuclei make up the isotopes $_{92}U^{233}$, $_{92}U^{235}$, and $_{94}Pu^{239}$. These isotopes are found in different combinations with natural uranium-238 and are used in practical applications.

2.6. Neutron Diffusion in the Reactor core.

Let's now take a look at neutron interactions with nuclei in their entirety. Keeping the composition of the core in mind, it is not difficult to see that neutrons, after being produced in the fission process and migrating (diffusing) throughout the volume of the core, can undergo scattering (moderation) and all kinds of absorption. It should be added that the probability of any interaction of a neutron with a nucleus is a complex function of neutron energy since it characterizes the micro- and macroscopic cross sections of any interaction. Temperature also influences the nuclear density of different substances and this must also be taken into account in calculations.

The study of the nature and laws of neutron interactions with nuclei is one of the central tasks in the theory and design of nuclear reactors.

The law of neutron conservation or balance lie at the foundation of any nuclear reactor theory. The essence of this law is that a change in the number of neutrons (N_n) in a given volume per unit time is equal to the number of neutrons generated (N_{gen}) in the volume less the number leaking from the volume (neutron loss, N_{leak}) and being absorbed in it (N_{abs}) during the same time interval.

Consequently, the general conservation equation expressing this balance can be written as

$$\frac{dN_n}{dt} = \frac{dN_{gen}}{dt} - \frac{dN_{leak}}{dt} - \frac{dN_{abs}}{dt} \qquad (2.15)$$

This equation is called the kinetic Boltzmann equation because of its complete analogy with the equation used by Boltzmann in studying the diffusion of gases. The dependent variable in this equation is the neutron distribution function which determines the number of neutrons at any point (x,y,z) moving at a velocity v. The solution to this kinetic equation requires knowledge not only of the point coordinates but also of the direction of the neutron velocity vectors as a function of time. The solution is complicated and is recommended only for precise design calculations of reactors for actual applications.

Since the purpose of this book is to teach methods, we will make some assumptions in order to simplify the solution to the kinetic Boltzmann equation. We already made one such assumption in our examination of the neutron flux $\phi_n = \rho_n \bar{v}_n$ and the product $\phi_n \Sigma$ when we proposed using the average neutron velocity $\bar{v}_n$ (monoenergetic neutrons). We will now add the following assumptions:

a. The neutron velocity vector distribution is uniform (isotropic) and does not depend on the neutron energy. In this case, the desired neutron distribution function in the core volume can be reduced to scalar flows;

b. Neutron moderation occurs virtually instantaneously. Possible neutron loss during moderation by leakage from the core is accounted for by the probability of nonleakage, an expression first derived by Fermi;

c. Neutron loss due to resonance absorption during moderation is accounted for by equation (2.10).

These assumptions do not result in a true map of the neutron flux distribution in the core volume. However, the assumptions make the essence of the complex processes that take place in the reactor far easier to understand and, consequently, the objective of this book is satisfied.

The neutron diffusion problem is essentially a statistical one, however, as in the kinetic theory of gases, one can construct a macroscopic theory describing the behavior of a large number of neutrons. In all diffusion phenomena, such as the diffusion of gas molecules, the diffusing substance propagates from a region of high density to a region of low density. Neutrons behave similarly because in regions where their density is high, a large number of collisions occur and after the collisions, the neutrons move away from the scattering centers.

Let's examine further the diffusion of monoenergetic neutrons because the results of such an examination provide a first approximation of the diffusion of thermal neutrons. If necessary, we can then take a look at the diffusion of neutrons of any energy.

The diffusion of monoenergetic neutrons can be described by Fick's law. According to this law, the net number of neutrons J (neutron beam density) passing through a unit area per unit time normal to the direction of the neutron flux is expressed

by the equality $J = -D_o \nabla N_n$, where D_o is the diffusion coefficient. The minus sign indicates that the neutron flux is in the direction of decreasing density; $\nabla N_n = \dfrac{dN_n}{dr}$ is the neutron density gradient in a direction normal to r. Since the monoenergetic neutron flux is $\phi_n = N_n \bar{v}$, then we obtain

$$J = -D \nabla \phi_n$$

where $D = D_o / \bar{v}$ is the diffusion factor for the neutron flux. This factor can, for a relatively weak absorption medium (the substance in the core), be determined from the formula,

$$D = \frac{\bar{\lambda}_s}{3(1-\bar{\mu})} = \frac{\bar{\lambda}_{tr}}{3} \qquad (2.16)$$

Next, let's proceed with a successive examination of the terms on the right side of equation (2.15), beginning with the last term. The neutron leakage rate from an elementary volume $dV = dxdydz$ (Fig. 2.9), a parallelepiped, can be determined from equation (2.16). We will consider two facets of this parallelepiped with the parallel planes xy, each with an area dxdy. The net neutron beam passing per unit time through the isolated facets in the direction of the z-axis is:

$$J_{z+dz} - J_z = -D \left[\left(\frac{\partial \phi_n}{\partial z} \right)_{z+dz} - \left(\frac{\partial \phi_n}{\partial z} \right)_z \right] dxdy \qquad .$$

If we replace the difference in the square brackets by the second derivative of the neutron flux with respect to the z coordinate, we obtain

$$J_{z+dz} - J_z = -D \frac{\partial^2 \phi_n}{\partial z^2} dzdxdy = -D \frac{\partial^2 \phi_n}{\partial z^2} dV$$

Similarly, the neutron leakage from the volume of the parallelepiped in the x and y directions through the area dydz and dxdz is determined from the expressions $-D \dfrac{\partial^2 \phi_n}{\partial y^2} dV$ and $-D \dfrac{\partial^2 \phi_n}{\partial x^2} dV$, respectively.

The neutron leakage from the elementary volume dV per unit time (leakage loss rate) is

$$\frac{dN_{leak}}{dt} = -D \left(\frac{\partial^2 \phi_n}{\partial x^2} + \frac{\partial^2 \phi_n}{\partial y^2} + \frac{\partial^2 \phi_n}{\partial z^2} \right) dV \qquad .$$

83
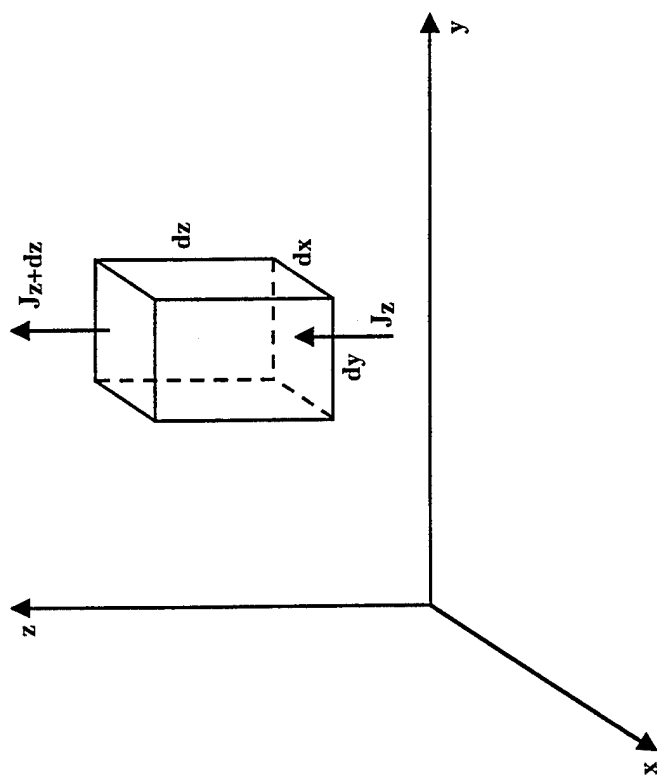
Fig. 2.9 Volume element for consideration of neutron leakage.

By assuming next that the elementary volume dV is equal to unity (for example, 1 cm^3), we finally obtain

$$\frac{dN_{leak}}{dt} = \frac{d\rho_n}{dt} = -D\nabla^2 \phi_n(x,y,z) \qquad . \qquad (2.17)$$

In the practical design of reactors, which are for the most part cylindrical, the Laplacian operator is conveniently examined in cylindrical coordinates:

$$\nabla^2 = \frac{\partial^2 \phi_n}{\partial r^2} + \frac{1}{r}\frac{\partial \phi_n}{\partial r} + \frac{1}{r^2}\frac{\partial^2 \phi_n}{\partial y^2} + \frac{\partial^2 \phi_n}{\partial z^2} \qquad .$$

By virtue of angular symmetry of the neutron flux distribution, the third term does not depend on the angle φ and $\dfrac{1}{r^2}\dfrac{\partial^2 \phi_n}{\partial y^2} = 0$. In this case, the Laplacian operator takes

the form $\nabla^2 = \dfrac{\partial^2 \phi_n}{\partial r^2} + \dfrac{1}{r}\dfrac{\partial \phi_n}{\partial r} + \dfrac{\partial^2 \phi_n}{\partial z^2}$ and thus:

$$\frac{dN_n}{dt} = -D\nabla^2 \phi_n(r,z) \qquad . \qquad (2.18)$$

An examination of the second term of the right side of equation (2.15) presents no difficulty because this term characterizes the number of neutrons absorbed in a unit volume per unit time by all the absorbers that make up the core. According to the foregoing, the number of neutrons absorbed can be determined from the equation

$$\frac{dN_{abs}}{dt} = \bar{\Sigma}_{at}\phi_n(r,z) \qquad .$$

where $\bar{\Sigma}_{at}$ is the total macroscopic absorption cross section of thermal neutrons in the given unit volume.

Next, let's designate the first term on the right side of equation (2.15) with the symbol S and let it be the number of neutrons produced in a unit volume per unit time. This is called the capacity of the neutron source. As a result, the neutron balance equation acquires the form:

$$\frac{dN_n}{dt} = -D\nabla^2 \phi_n(r,z) - \Sigma_{at}\phi_n(r,z) + S \qquad . \qquad (2.19)$$

This is called the elementary diffusion equation for monoenergetic neutrons.

Let's continue in more detail with an analysis of the capacity of neutron sources. Neutron sources in a unit volume can consist of the following: an extraneous source (for example, polonium-beryllium) for the purpose of bringing the reactor to a minimum power

level, breeding media, i.e. fissioning substances and, finally, the moderation process from which neutrons enter into the volume considered. Since we are examining monoenergetic neutrons, the latter process is absent. No thought will be given to extraneous sources of neutrons because they function only during reactor startup. Thus, the only neutron source in the isolated volume will be the fission of nuclear fuel in the breeder medium.

Let's examine initially a reactor with slow neutrons in a homogeneous core of infinite size. An "infinite" reactor experiences no neutron leakage. As has been noted, the fission reaction that results from the absorption of a single neutron produces ν new neutrons.

Thus, at any instant in time $\overline{\Sigma}_f \phi_n(r, z)$ fission events occur in a unit volume of the core, and $\nu \overline{\Sigma}_f \phi_n(r, z)$ fast neutrons are produced. A portion of them can interact with the nuclei and cause them to fission. Thus, the number of neutrons produced and which will participate in fission after being moderated, must be increased by the factor ε (ε is the fast fission factor, defined as the ratio of the total number of fission neutrons produced by fast and thermal fission to the number produced by fission alone. Typically, it is equal to 1.00-1.03). During moderation the neutrons may experience radiative (resonance) capture. Thus the number of neutrons produced by a given number of fissions must be multiplied by the factor p, the resonance escape probability; i.e., the probability a neutron will not be absorbed at resonance (epithermal) energies while it is slowing down to thermal energies. Thus, p < 1.

As a result, the capacity of a neutron source in a reactor of infinite size is

$$S = \nu \overline{\Sigma}_f \phi_n(r, z) \varepsilon p$$

Let's multiply and divide the right side of this equation by the product of the two factors $\overline{\Sigma}_{at}^{fuel} \overline{\Sigma}_{at}$ (the macroscopic absorption cross section of thermal neutrons by fuel nuclei, and by the nuclei of all absorbers in the core). The capacity of the neutron source can then be written as

$$S = \nu \frac{\overline{\Sigma}_f}{\overline{\Sigma}_{at}^{fuel}} \frac{\overline{\Sigma}_{at}^{fuel}}{\overline{\Sigma}_{at}} \varepsilon p \overline{\Sigma}_{at} \phi(r, z) \quad .$$

Next, let's designate $\eta = \nu \overline{\Sigma}_f / \overline{\Sigma}_{at}^{fuel}$ as a factor that characterizes the fast neutron yield by the absorption of a single thermal neutron; $f = \overline{\Sigma}_{at}^{fuel} / \overline{\Sigma}_{at}$ the thermal neutron utilization factor which accounts for neutron absorption by not only the fuel nuclei, but also by all absorbers in the core.

As a result, the expression for the capacity of a neutron source in an infinite size reactor becomes:

$$S = \eta \varepsilon p f \overline{\Sigma}_{at} \phi_n(r, z)$$

or

$$S = k_\infty \bar{\Sigma}_{at} \phi_n(r,z) \qquad , \qquad\qquad\qquad (2.20)$$

where k_∞ is the neutron multiplication factor in an infinite size reactor, $k_\infty = \eta \epsilon pf$.

In a physical sense, k_∞ is the ratio of the number of neutrons produced in a given act of fission and capable of sustaining this reaction (i.e., having avoided all kinds of absorption and resonance capture) to the number of neutrons causing the given act of fission. In other words, each neutron capture will produce k_∞ new neutrons during fission which will ensure that the given fission reaction continues. The equation $k_\infty = \eta \epsilon pf$ is frequently referred to in the literature as the "four factor equation."

In transitioning from an infinite reactor to a reactor of finite size it is necessary to account for possible neutron leakage from the core during moderation from an average energy $E_0 = 2$ MeV (at the instant of generation) to thermal energy. By designating the probability of leakage avoidance during moderation as $p_{nonleak}$, the following expression for the capacity of a neutron source in a finite size reactor is obtained:

$$S = k_\infty p_{nonleak} \bar{\Sigma}_{at} \phi_n(r,z) \qquad .$$

By substituting this expression in equation (2.19), we get

$$\frac{dN_n}{dt} = D\nabla^2 \phi_n(r,z) - \bar{\Sigma}_{at}\phi_n(r,z) + k_\infty \phi_n(r,z) \qquad\qquad (2.21)$$

Three reactor states are possible, and consequently, there are three possible values of $\frac{dN_n}{dt}$, specifically

$$\frac{dN_n}{dt} > 0, \quad \frac{dN_n}{dt} = 0, \quad \text{and} \quad \frac{dN_n}{dt} < 0 \; .$$

These are the supercritical, critical (steady state), and subcritical states, respectively.

One can be certain that the steady reactor state ($\frac{dN_n}{dt} = 0$) is reached if the capacity of the neutron source is decreased beforehand by $k > 1$ and if the parameters chosen for this extreme case characterize its working process. In this case, one can create steady state reactor conditions over the entire range from 1 to k by way of a control system.

Let's now rewrite the equation in the form

$$D\nabla^2\phi_n(r,z) - \bar{\Sigma}_{at}\phi_n(r,z) + \frac{k_\infty p_{nonleak}}{k}\bar{\Sigma}_{at}\phi_n(r,z) = 0 \qquad . \qquad (2.22)$$

We then divide the left side of the equation with the diffusion factor D and designate the ratio $D / \bar{\Sigma}_{at} = L^2$. This ratio, which is equal to $(1/3)\bar{\lambda}_{tr}\bar{\lambda}_{at}$ is the square of the thermal neutron diffusion length in the core. Numerically, the square of the neutron

diffusion length is $L^2 = (1/6)\bar{r}_d^2$; i.e., it is a measure of the average migration of a neutron in a straight line from the point where it became thermalized to the point of its absorption. Let's return to equation (2.22) and rewrite it in the form:

$$\nabla^2 \phi_n(r,z) - \frac{1}{L^2} \phi_n(r,z) \left[\frac{k_\infty p_{nonleak}}{k} - 1 \right] = 0 \qquad (2.23)$$

Let's designate the factor $B^2 = \frac{1}{L^2} \left[\frac{k_\infty p_{nonleak}}{k} - 1 \right]$ and assume that it is independent of the coordinates r and z. This makes it possible to rewrite the equation as

$$\nabla^2 \phi_n(r,z) + B^2 \phi_n(r,z) = 0 \qquad (2.24)$$

Let's reason as follows. The algebraic gain in the number of neutrons in 1 cm^3 in 1 sec due to their diffusion in the core in a volume element with the coordinates (r, z) is, according to (2.18), $-D\nabla^2\phi_n(r,z)$, and according to (2.24) it is $B^2 D\phi_n(r,z)$. At the same time, the number of thermal neutrons absorbed in 1 cm^3 in 1 sec is equal to $\bar{\Sigma}_{at}\phi_n(r,z)$. Consequently, the ratio of the thermal neutron leakage during the diffusion process after moderation p_{leak} to the number absorbed in the same volume p_{abs} is equal to

$$\frac{p_{leak}}{p_{abs}} = \frac{DB^2}{\bar{\Sigma}_{at}} = B^2 L^2 \qquad .$$

Next, one can obtain an expression for the ratio of the number of absorbed neutrons in the volume considered N_{abs} to the total number of all neutrons moderated to thermal energy, $N_{abs} + N_{leak}$. This ratio is equal to $1/(1 + B^2L^2)$.

Thus, $1/(1 + B^2L^2)$ characterizes the probability that a neutron will remain in the reactor after it has been moderated. Consequently, the given ratio is nothing more than the thermal neutron nonleakage probability during diffusion (i.e., up to the instant of absorption by some nucleus).

Let's return to the equation

$$B^2 = \frac{1}{L^2} \left[\frac{k_\infty p_{nonleak}}{k} - 1 \right]$$

and solve it for k. Hence,

$$k = \frac{k_\infty p_{nonleak}}{1 + B^2 L^2}$$

It is obvious that the product $\dfrac{p_{\text{nonleak}}}{1 + B^2L^2}$ characterizes the total neutron nonleakage probability during moderation and diffusion.

The neutron nonleakage probability during moderation is determined from Fermi's neutron growth equation. This equation together with the diffusion equation (2.15) will yield for p_{nonleak} the following expression, first derived by Fermi:

$$p_{\text{nonleak}} = e^{-B^2\tau}.$$

Thus, the expression for k acquires the form

$$k = k_{\text{eff}} = \frac{k_\infty e^{-B^2\tau}}{1 + B^2L^2} \qquad .$$

This is known as the neutron multiplication factor, k_{eff}. In a physical sense, k_{eff} is the ratio of the number of neutrons produced in a given act of fission that have escaped all kinds of absorption and leakage (i.e., capable of sustaining fission) to the number of absorbed thermal neutrons.

Equation (2.23) is of great value in practical applications because it allows one to establish the neutron flux distribution in the core volume, determine reactor criticality conditions, and solve a number of other important problems. In addition, as has been noted above, this equation was derived for a very simplified case - on the assumption of constant neutron energy. In reality, neutron energies vary over a wide range. Strong resonances (characteristic of heavy isotopes) should also be kept in mind. These resonances will cause microscopic and macroscopic cross sections to change abruptly with very small changes in energy. Thus, the monoenergetic concept of neutron flux is clearly an approximation. It does not provide a true picture of neutron distribution throughout the core volume.

In order to obtain more reliable results, it is necessary to know the neutron energy spectrum. This means that the neutron history in all energy intervals must be traced, the probability of absorption and moderation during elastic and inelastic collisions must be taken into account, and leakage from the core during moderation and diffusion must be accounted for. The multigroup diffusion equation is used in solving such problems.

The multigroup neutron diffusion equation. In order to construct this equation, the energy intervals are broken up into a large number of subintervals, i.e., a distribution of all neutrons into separate groups as a function of energy is carried out. The average effective cross sections are determined for each group. The number of groups used depends on the purpose of the calculations and may vary from several tens to several hundred.

By assuming that the effective cross section as a function of energy is known, equation (2.19), which expresses Fick's law, can be written as

$$\frac{1}{3}\nabla\phi(r,E) + \Sigma_t(E)J(r,E) = \int \Sigma_s(E'\rightarrow E)J(r,E)dE' \quad .$$

where $\Sigma_t(E)$ is the total macroscopic cross section of neutron interaction with a medium at energy E; $\Sigma_s(E'\rightarrow E)$ is the macroscopic neutron scattering cross section during transition from a group at energy E' to a group at energy E.

If we assume that

$$\int \Sigma_s(E\rightarrow E')J(r,E)dE' = \int \Sigma_s(E'\rightarrow E)J(r,E)dE'$$

i.e., we assume isotropic scattering, then from (2.25) we obtain Fick's law in a form similar to (2.16),

$$J(r,E) = -D(E)\nabla\phi(r,E)$$

By using the neutron balance equation (2.15), we can write the diffusion equation without external neutron sources in the form

$$D(E)\nabla\phi(r,E) + \Sigma_t(E)\phi(r,E) = \int \Sigma_s(E'\rightarrow E)\phi(r,E')dE'$$
$$+ \frac{1}{k_{eff}}\chi(E)\int \nu(E)\Sigma_f(E')\phi(r,E')dE' \qquad (2.26)$$

where $\chi(E)$ is the neutron fission spectrum, i.e., the probability density that a neutron with an energy E will be generated during fission; accordingly

$$\int_0^\infty \chi(E)dE = \quad ;$$

and $\nu(E)$ is the average number of secondary neutrons produced by neutrons with a given energy E'.

In the derivation of equation (2.26) an expansion of the Boltzmann equation into spherical harmonics was used. This permitted the elimination of the angular distribution of neutron flux. In this regard, equation (2.26) is applicable in regions sufficiently far removed from surfaces where the angular distribution of neutron flux is strongly anisotropic (for example, external reflectors, strong absorbers, etc.). This is not, however, the case with such moderators as hydrogen where the collision energy losses can be very large. The equation applies fully to heavy moderators, for example, graphite or beryllium.

As has been noted, in order to obtain a picture of a neutron flux distribution that is close to reality all neutrons must be separated into discrete energy groups. Accordingly, the multigroup diffusion equation is written as

$$D_i\nabla\phi(r) + \Sigma_{ti}(E)\phi_i(r) = \sum_{k=1}^N \Sigma_{s,k\rightarrow i}\phi(R) + \frac{1}{k_{eff}}\chi_i\sum_{k=1}^N \nu_k\Sigma_{fk}\phi_k(r) \qquad (2.27)$$

90

where N is the number of groups.

For a complete solution to the problem, it is necessary to assign boundary conditions to the neutron flux at the reactor surface. Equation (2.27) with the boundary conditions (2.28) can be solved analytically only in exceptional cases when the geometry of the reactor core and the boundary conditions are quite simple. Moreover, the simplified analytical solution is very useful as an initial estimate of neutron flux distribution in the reactor core.

3. NUCLEAR REACTOR DESIGN

3.1. General Problems and Types of Designs.

The fundamental objective of general reactor design is to establish a set of geometric, thermal-hydraulic and other parameters which will ensure normal operation over a given time period. Thus, one can define several independent reactor design calculations, in particular:

a. Neutron physics, the principal task being to provide conditions for a normal sustained nuclear fission chain reaction;

b. Thermal-hydraulics, the common task being to provide a given heat transfer regime at given temperatures of the principal components of the nuclear power plant;

c. Endurance, the principal task being to assure a safe operating life of the reactor and, in general, of the nuclear power plant as a whole.

All these design calculations are closely interconnected. Thus, arbitrary changes in geometric data and in physical and engineering constants of the core components may facilitate the assurance of reactor reliability and endurance, but they may also degrade neutron physics characteristics substantially. They may, for example, result in an unwarranted increase in the uranium-235 concentration in the nuclear fuel. Or, for example, based on the given heat transfer conditions, the fuel element geometry in the reactor core may prove to be unsuitable in achieving critical mass and effective operation of the control system, etc.

Thus, the choice of final design parameters and reactor dimensions is possible only after all kinds of interactive design calculations. Nevertheless, it is advisable to perform this variety of design calculations in any development project, i.e. separate neutron physics, thermal, hydraulic, strength and reliability calculations. An optimum is then selected based on a comparative analysis of the results. These are then verified in order to refine the characteristics of the power plant being designed. This is followed by rough design and experimental verification of individual reactor components, especially of fuel elements (in so called loop tests in stationary reactor assemblies). The objective of all the design and experimental work is to develop an experimental reactor which then undergoes design refinements until output characteristics are attained that match the desired conditions. Only then can operations to complete the project begin.

It is not our task here to present the sum total of all kinds of design calculations needed to complete the design and construction of specific reactors. Our main objective is to present the physical essentials and fundamentals involved in these calculations. By way of example, we have chosen a homogeneous reactor with a uniform distribution of nuclear fuel concentration in the core volume.

Moreover, the basic methodology for more in-depth and precise design of reactors for specific purposes is contained in the recommended reference literature at the end of this book.

3.2. Neutron physics calculations

It is necessary to investigate the neutron physics characteristics of a reactor in different stages of its design. This, together with other calculations, will substantiate or repudiate the design decisions made. The influence of fabrication technology on the neutron physics parameters of individual reactor components are evaluated at the same time. The degree and depth of neutron physics calculations depend on the reactor design stage. A determination of neutron physics characteristics is made repeatedly in order to obtain the relationships needed in the given and subsequent stages of reactor development.

The basic stages in reactor neutron physics calculations are the following:

a. Establishment of a picture of the neutron flux distribution and of the corresponding energy liberation throughout the volume (height and radius) of the core;

b. Establishment of reactor criticality conditions and an analysis of the factors that influence them;

c. Determination of the time-temperature coefficients of reactivity taking into account fuel burnup, reactor contamination, etc.;
- investigation of reactor transients (the kinetics of the processes for the purpose of setting control system requirements).

In general, the investigation of reactor neutron physics characteristics requires the use of very complex models and numerical calculation techniques. However, in order to understand the meaning of reactor neutron physics calculations, the use of simpler models is justified. This book serves this particular purpose. Let's take a step-by-step look at the above stages in neutron physics calculations.

Neutron flux distribution in the core. Remember that we will examine the diffusion of monoenergetic thermal neutrons in a "bare" (without reflectors) homogeneous reactor.

Let's turn to equation (2.24).

We note that the equation is a wave differential equation of the second order. In the general case, it will not provide a specific picture of the neutron flux distribution in r, z coordinates because its general solution contains arbitrary integration constants. In order to determine these constants, one must impose specific boundary conditions on the possible solution to equation (2.24). These boundary conditions stem from the particulars of the problem being solved. In our case, these conditions can be the following:

1. In the region where the diffusion equation is applicable the neutron flux must be finite and nonnegative;

2. At each point in the plane of separation of two media with different diffusion properties (the reactor core and the surrounding space) the net neutron fluxes in the direction normal to the plane are identical.

3. Near the boundary between the core and surrounding space (Fig. 3.1) the neutron flux changes in such a manner that by linear extrapolation it goes to zero at a certain distance from the plane of the boundary separation;

$$\delta_{ex} = \frac{2\bar{\lambda}_{tr}}{3} \qquad .$$

(3.1)

Thus, by linear extrapolation the neutron flux will go to zero at a distance equal to 2/3 the transport path length of the neutron from the plane separating the diffusion medium from its surrounding space. In other words, the following boundary conditions hold:

$$\phi_n(z, \frac{D}{2} + \delta_{ex}) = 0 \qquad ;$$

$$\phi_n(r, H/2 + \delta_{ex}) = 0 \qquad .$$

The solution to the differential equation (2.24) is accomplished by the method of separation of the variables $x(g)$ and $y(z)$. Omitting the details of this solution, the final results for the diffusion of monoenergetic neutrons are:

$$\phi_n(r, z) = \phi_n(0,0) J_0 (\frac{2.405r}{R_{ex}}) \cos(\frac{\pi z}{H_{ex}})$$

(3.2)

$$B_g^2 = \left(\frac{2.405}{R_{ex}}\right)^2 + \left(\frac{\pi}{H_{ex}}\right)^2$$

(3.3)

where J_0 is the zeroeth order of the first Bessel function; $R_{ex} = R + \delta_{ex}$; $H_{ex} = H + 2\delta_{ex}$, and B_g^2 is a geometric parameter - the eigenvalue of the arbitrary constants in the solution to equation (2.24), which correspond with the boundary conditions assumed.

In reality, with $r = R_e$, $I_0 = 0$, the neutron flux at the lateral surfaces of the reactor (conventionally, "extrapolated") is equal to zero. Analogously, with $z = R_e/2$, $\cos \pi/2 = 0$, it is also equal to zero at the end surfaces of the conventional reactor (H_e, D_e).

Equations (3.2) and (3.3) provide a picture of the monoenergetic neutron flux distribution in the core volume.

These are only simplified calculations of the distribution of neutron flux in the volume of the core. These simplified methods do not permit, naturally, a precise calculation of the distribution in the reactor. For this objective, it is necessary to use multigroup calculation theory. The simplified one-group calculations are not very accurate, and dimensions calculated are typically no more accurate than 10-15%. However, for the aim of this instruction, the results of these simplifying assumptions are quite sufficient.

94
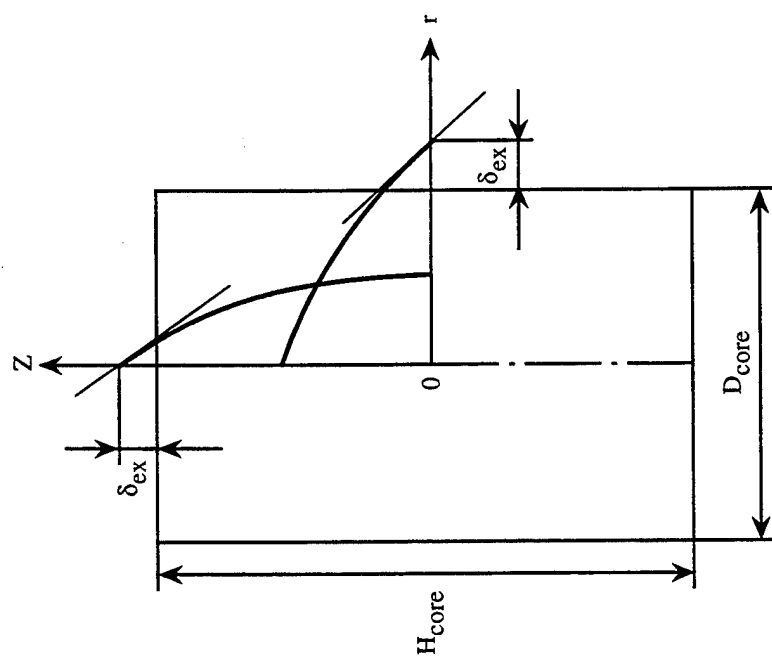
Fig. 3.1 Radial and axial neutron flux. The use of the extrapolation distance results in a better fit of a simple curve to the experimental valves.

Some basic multigroup calculation techniques. As has been noted, an examination of only monoenergetic neutrons does not provide a true picture of the neutron flux distribution in the core volume. Multigroup techniques are therefore used in neutron physics reactor design calculations. It is not our objective to examine these in detail, we will discuss only the nature and characteristics of the solution to such problems. With this in mind, let's turn to equation (2.22) and show by way of example its solution for two- and three-dimensional geometries by the finite difference method which is easily handled by a computer. It is convenient to write equation (2.22) in the following form:

$$D_i \nabla^2 \phi_i - \Sigma_{tr} \phi_i + S = 0 \qquad , \qquad (3.4)$$

where

$$S = \sum_{k=1}^{n} \left(\Sigma_{s,k \to i} + \frac{1}{k_{eff}} \chi_k \nu_k \Sigma_{fk} \right) \phi_k$$

Equation (3.4) assumes the form of a single group for each group which relates group i with all remaining groups k in the multigroup case when S is the source.

The reactor is divided up into a large number of calculation cells. Their boundaries are determined by fixed values of one of the coordinates; for example, in xyz three-dimensional geometry such boundaries are the planes x = const, y = const, z = const. The parameters in equation (3.4) must be constant within each calculation cell but may change from cell to cell.

The division of the reactor into cells is called a difference matrix and the boundary points of the cells are called matrix nodes. The neutron flux can be calculated at the matrix nodes or at the center of the cells.

Let's initially consider a plane geometry with a total number of spatial points, M (Fig. 3.2). In this case,

$$D_i = \frac{d^2 \phi_i}{d^2 x} - \Sigma_t \phi_i + S = 0 \qquad . \qquad (3.5)$$

Let's integrate this equation over the interval Dm corresponding to point x_m:

$$\int_{x_m + \frac{x_m - x_{m-1}}{2}}^{x_m + \frac{x_{m+1} - x_m}{2}} D_i \frac{d^2 \phi_i}{dx^2} dx + \int_{x_m + \frac{x_m - x_{m-1}}{2}}^{x_m + \frac{x_{m+1} - x_m}{2}} \left(S_i - \Sigma_{t,i} \phi_i \right) dx$$

We then obtain for each node
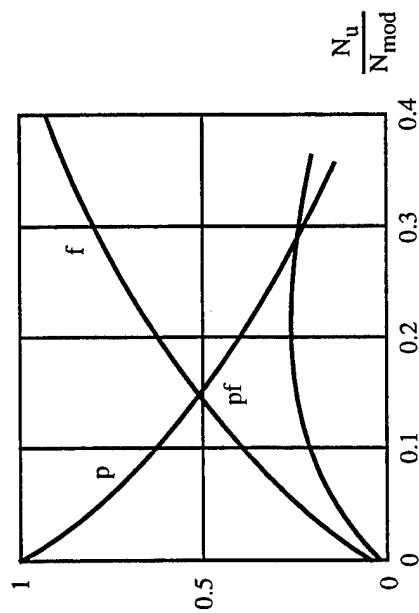
Fig. 3.2 Variation of resonance escape probability and thermal utilization as a function of the ratio of uranium atoms to moderator atoms. Generally it is desirable to maximize the product pf.

$$D_i\left(\frac{\phi_i(x_{m+1}) - \phi_i(x_m)}{x_{m+1} - x_m} - \frac{\phi_i(x_m) - \phi_i(x_{m-1})}{x_m - x_{m-1}}\right)$$

$$-\Sigma_{ti}\phi_i(x_m)\Delta m + S(x_m)\Delta m = 0$$

After a simple conversion, we finally obtain

$$D_i\left[\frac{\phi_i(x_{m+1}) - 2\phi_i(x_m) + \phi_i(x_{m-1})}{(\Delta m)^2}\right] - \Sigma_{ti}\phi_i(x_m) + S(x_m) = 0 \qquad . \qquad (3.6)$$

Thus, the differential equation is replaced by an algebraic equation, which is frequently called the difference equation.

In practical applications, the reactor core has a cylindrical geometry. In a two-dimensional cylindrical coordinate system equation this equation may be written in the following form:

$$D_i\left(\frac{\partial^2\phi_i}{\partial r^2} + \frac{1}{r}\frac{\partial\phi_i}{\partial r} + \frac{\partial^2\phi_i}{\partial z^2}\right) - \Sigma_{ti}\phi_i + S = 0 \qquad .$$

We find the appropriate difference equation by performing the same operations as previously. We obtain

$$D_i\left(\frac{\phi_i(r_{m+1}) - 2\phi_i(r_m) + \phi_i(r_{m-1})}{\Delta m^2} + \frac{1}{r_m}\frac{\phi_i(r_{m+1})}{\Delta m} + \frac{\phi_i(z_{\ell+1}) - 2\phi_i(z_\ell) + \phi_i(z_{\ell+1})}{h^2}\right)$$

$$-\Sigma_{t_i}\phi_i(r_m, z_\ell) + S(r_m, z_\ell) = 0 \qquad . \qquad (3.7)$$

where l is the number of nodes along the z-coordinate; h is the distance between two adjoining nodes along the g-axis.

There is a simple and convenient method for solving the difference equation (3.4). This method is called the allowance method and is a variant of the method for eliminating unknowns. Let's initially examine the allowance method in the one-dimensional problem of calculating the neutron flux in a reactor with a cylindrical geometry.

In this case, the difference equation assumes the form

$$D_i\left(\frac{\phi_i(r_{m+1}) - 2\phi_i(r_m) + \phi_i(r_{m-1})}{\Delta m^2} + \frac{1}{r_m}\frac{\phi_i(r_{m+1})}{\Delta m}\right) - \Sigma_{t_i}\phi_i(r_m) + S(r_m) = 0. \qquad (3.8)$$

We can rewrite this equation in the form

$$\phi_i(r_{m+1}) - B_m\phi_i(r_m) + C_m\phi_i(r_{m-1}) = F_m \qquad . \qquad (3.9)$$

where

$$B_m = \frac{2r_m + \Delta m}{r_m + \Delta m} + \frac{\Delta m^2 r_m}{D_i} \Sigma_{t_i} \quad ; \qquad C_m = \frac{r_m}{r_m + \Delta m} \quad ;$$

$$F_m = \frac{\Delta m^2 r_m}{(r_m + \Delta m)D_i} S(r_m) \quad .$$

In order to form the computational algorithm based on the allowance method, we can rewrite equation (3.8) in the form

$$\phi_i(r_m) = \beta_{m+1}\phi_i(r_{m+1}) + \eta_{m+1} \quad , \tag{3.10}$$

where β_{m+1} and η_{m+1} are determined from the recurrent equations

$$\beta_{m+1} = \frac{1}{B_m - \beta_m C_m} \quad ; \tag{3.11}$$

$$\eta_{m+1} = \beta_{m+1}(\eta_m C_m + F_m) \quad . \tag{3.12}$$

The coefficients β_m and η_m are called the allowance coefficients.

The validity of this notation can be determined by substituting equations (3.11) and (3.12) in equation (3.10). This substitution leads to equation (3.8).

By using equations (3.10)-(3.12), one can calculate the neutron flux in all energy groups at all nodes of the difference matrix chosen. The sequence of the calculations can be as follows: first, beginning at the "left" boundary of the region under investigation, determine in succession the allowance coefficients at all calculation nodes from equations (3.11) and (3.12);

then from equation (3.10) calculate, beginning at the "right" boundary, all values of $\phi_i(r_m)$. β_1, η_1 and $\phi_i(r_m)$ are determined from the boundary conditions (2.28) for equation (3.8), which are also represented in finite difference form by equations similar to equation (3.10).

In this manner, each equation in (3.8) can be solved if at each node of the matrix the value of S, determined from equation (3.4), is known. The latter can be determined only after calculating the entire neutron flux, therefore, the problem is solved only by iteration methods.

For this purpose, it is necessary to know some initial neutron source distribution which is determined from the equation

$$S(r) = \sum_{i=1}^{n} v_f \Sigma_{fi} \phi_i \quad . \tag{3.13}$$

This makes it possible to compute the neutron flux, determine a new value of S from equation (3.4) and again calculate the neutron flux. When organized in this manner, the process of successive approximations will converge. The effective neutron multiplication factor is determined as the limit:

$$k_{eff} = \lim_{n \to \infty} \left(\frac{S^n(r)}{S^{n-1}(r)} \right) .$$

where n is the number of approximations.

The expression for k_{eff} is the neutron multiplication factor for the entire reactor. Similarly, one can obtain the local k_{eff} for each calculation node, m:

$$k_{eff\,m} = \lim_{n \to \infty} \left(\frac{S^n(r_m)}{S^{n-1}(r_m)} \right) . \tag{3.14}$$

Usually, k_{eff} converges faster than the $k_{eff,m}$ distribution. For this reason, two conversion criteria are used in practice. The iterations will come to an end when

$$\left| \frac{k_{eff}^n - k_{eff}^{n-1}}{k_{eff}^n} \right| < \varepsilon_1 \quad \text{and} \quad \left| \frac{k_{max}^n - k_{min}^n}{k_{max}^n} \right| < \varepsilon_2 \quad ,$$

where k_{max}^n and k_{min}^n are the maximum and minimum values of the set, $k_{eff,m}$.

The number of iterations required depends on the initial distribution conditions assumed. However, the form of these conditions is of minor importance with the use of modern high-speed computers and for simplicity usually $S^0(r) = const$. The method examined for calculating neutron flux can be run quite easily on a computer. However, we are talking about the solution to a one-dimensional system of diffusion equations. The problem becomes extremely complicated when we transition to a multidimensional geometry. In this case, it is of great importance to limit the number of calculations. Many so called economical approaches have been proposed in recent years. These allow one to solve a number of complex problems in physics and engineering.

In equation (3.7) the matrix can be represented as a set of nodes with the numbers $i_2 = 0, 1, 2, \ldots M$ arranged on "rows" along the R-axis, and with the numbers $i = 0, 1, 2, \ldots K$ arranged on "columns" along the z-axis. The basic idea in economical methods is a successive solution to a one-dimensional problem along rows and columns.

The most clear-cut expression of this concept is the longitudinal-transverse scheme (the implicit variable directions method). The solution is accomplished by iteration methods in two stages with half step iterations. First, equation (3.7) is solved implicitly in the z-direction and explicitly in the R-direction. It is then solved implicitly in the R-direction and explicitly in the z-direction. The solution is accomplished by the trial and error method at each half step of the iteration.

It is impossible to apply the implicit method of variable directions to a three-dimensional geometry problem. The longitudinal-transverse scheme will be unstable. Special methods are required here. General purpose methods applicable to the solution of diffusion equations with variable coefficients in arbitrary regions and any number of measurements will not be discussed here.

Thus, the finite difference method allows one to solve neutron flux diffusion equations in a multigroup approximation for reactors of varying geometry.

Critical size and critical mass of a reactor. Let's turn to the complex variable $\frac{1}{L^2}\left(\frac{k_\infty p_{nonleak}}{k_{eff}} - 1\right) = B^2$. This transcendental equation is called the reactor criticality equation since it determines its state: when $k_{eff} > 1$ it is supercritical; when $k_{eff} < 1$ it is subcritical; when $k_{eff} = 1$ it is steady-state. The reactor size and core mass that correspond to $k_{eff} = 1$ are called critical because in this case the number of neutrons being generated during fission is exactly equal to the number of neutrons lost due to leakage, capture and other processes.

Let's examine in more detail the conditions for ensuring that $k_{eff} = 1$. For this purpose, we will turn to an analysis of the factor k_∞. The neutron multiplication factor for an infinite reactor, k_∞ is determined from the four factor formula. Let's discuss each of these separately. The factor, which characterizes the fast neutron yield, $\eta = \frac{\nu \overline{\Sigma}_f}{\overline{\Sigma}_a}$ is the ratio of the number of neutrons formed in a given fission reaction to the number of neutrons captured by the fuel nuclei (i.e., the fact that not all neutrons captured by the fuel nuclei cause fission to occur is taken into account). This factor can be determined for a mixture of several nuclear fuels, for example, U-235 and Pu-233, from the equation

$$\eta = \frac{\overline{\Sigma}_f^{235}\nu^{235} + \overline{\Sigma}_f^{239}\nu^{239}}{\overline{\Sigma}_a^{235} + \overline{\Sigma}_a^{239}} \qquad , \qquad (3.15)$$

where $\overline{\Sigma}_f^{235}$, $\overline{\Sigma}_f^{239}$ are the macroscopic cross sections of uranium-235 and plutonium-239 nuclei with their mass fractions taken into account; ν^{235}, ν^{239} are the average numbers of fast neutrons produced during a single fission of U-235 and Pu-239; and $\overline{\Sigma}_a^{235}$, $\overline{\Sigma}_a^{239}$ are the macroscopic absorption cross sections of U-235 and Pu-239 nuclei.

If there is only one fissioning material in the core, then equation (3.15) simplifies to

$$\eta = \frac{\nu \overline{\Sigma}_f}{\overline{\Sigma}_a} \qquad .$$

The next factor, ε, is called the fast fission factor. This factor is introduced in order to account for the fact that a portion of the fast neutrons after their production can cause fission without first being moderated. The factor ε always exceeds unity, although not by much. Typically, $\varepsilon = 1.03$ for thermal reactors; $\varepsilon = 1$ for a fast reactor.

The thermal neutron utilization factor

$$f = \frac{\bar{\Sigma}_a^{Fuel}}{\bar{\Sigma}_a^{Total}}$$

(3.16)

indicates what fraction of thermal neutrons is absorbed by the fuel nuclei. It is always less than unity because a portion of the neutrons is lost in the moderator and other materials that make up the core. For example, for the U-235 + U-238 fuel mixture

$$f = \frac{\bar{\Sigma}_a^{235} + \bar{\Sigma}_a^{238}}{\bar{\Sigma}_a^{Total}} \qquad ,$$

(3.16)

where $\bar{\Sigma}_a^{Total}$ is the total macroscopic absorption cross section of all components that make up the core.

The factor that characterizes the resonance escape probability (the factor, p) is determined basically by the density of the U238 nucleus and the moderating capability of the medium $\xi\bar{\Sigma}_s$. We examined its significance earlier.

As is apparent from (2.12), p depends on the quantitative relationship of uranium-238 and moderator in the homogeneous mixture. If the ratio N_U/N_{mod} (Fig. 3.2) is quite small, i.e., there is a large degree of uranium dilution in the moderator, then the average macroscopic absorption cross section $\bar{\Sigma}_a$ becomes negligibly small in comparison with the average macroscopic scattering cross section $\bar{\Sigma}_s$ and the probability of resonance escape will be close to unity. On the other hand, when the indicated ratio is large, $p \approx 0$, because the probability that a neutron possessing resonance energy will be captured by uranium-235 nuclei is much greater than the probability of elastic scattering by moderator nuclei.

Unfortunately, the factors that increase the probability of resonance escape will at the same time decrease the thermal neutron utilization factor. Therefore, one attempts to find a combination and arrangement of fuel and moderator such that the maximum product of pf is found. In a system consisting of uranium fuel and graphite or other moderator, an increase in pf is achieved through an appropriate heterogeneous lattice arrangement of uranium fuel elements in the moderator. As will be observed later, the probability of resonance escape is in this case greater than in a homogeneous mixture of uranium and moderator in the same proportion.

One way to increase k_∞ is to use enriched uranium fuel which contains a higher percentage of the fissioning uranium-235 isotope than the natural mixture.

In concluding the analysis of reactor criticality conditions we note that criticality does not depend on the neutron flux. This, in turn, means that a steady state reactor power ($k_{eff} = 1$) is possible at any power level (neutron flux). This property allows one to carry out a number of operations in testing reactor capability at a minimum tolerable power level when the danger of ionizing radiation is insignificant. This is very important in start-up preparations of a reactor.

Influence of reflectors on reactor critical size. All of the relationships obtained earlier pertain to the so-called bare reactor which does not have reflectors. Analysis of equation (2.23) indicates that the critical reactor size must decrease when the core is surrounded by reflectors which are fabricated from such scattering materials as graphite, beryllium, alkali metal hydrides and others.

The effectiveness of a reflector is estimated by its albedo: the ratio of the number of neutrons reflected back into the core by reflectors to the number of neutrons escaping the core into the reflectors.

In order to calculate the neutron flux in a reactor, which is equipped with side and end reflectors, one can use the same elementary diffusion equation (2.23) by writing it separately for the core (S $\neq$ 0) and the reflector (S = 0). Thus, the problem reduces to solving two partial wave differential equations with the following boundary conditions:

1) The neutron flux goes to zero at the extrapolation boundary of the reflector which is determined not by the extrapolation addition δ_{ex} but by the so called effective addition δ_{eff}, which will be discussed below;

2) the neutron fluxes at the boundary between the core and the reflectors are equal.

A typical neutron flux distribution picture along the radius of a cylindrical reactor with reflectors is shown in Fig. 3.3. As can be seen, a reactor with reflectors has a number of noticeable advantages over a "bare" reactor. Thus, in a reactor without reflectors the neutron flux goes to zero at the extrapolation boundary (R_{ex}, H_{ex}). In a reactor with reflectors the neutron flux curve in the core flattens out and the peripheral regions of the core are used more effectively. Since the maximum neutron flux is often decisive in establishing the thermal power level, a reactor with reflectors will provide a greater average flux. Consequently, the nuclear fuel is used more effectively.

The material presented above is not completely accurate since it is based on a one energy group (average value) approximation. Naturally, the true neutron flux distribution picture will be different in an actual reactor. Thus, one can obtain a qualitative result from an illustration of neutron flux and energy distribution that considers only thermal monoenergetic neutrons. As has been observed earlier, however, such an approach satisfies the purposes of this textbook.

We note further that a reflector fabricated from a material with low atomic weight is capable of moderating fast neutrons that escape from the core and then returning them. In the peripheral core regions of a reactor with reflectors one can also observe some increase in the neutron flux in comparison with a "bare" reactor.

In addition, an excessive increase in reflector size, i.e., thickness, is not efficient. In order to evaluate this situation, one must consider the change in the overall size of a reactor with reflectors as a function of the side reflector thickness (Fig. 3.4). As is apparent, starting with some value of δ_{ref} a further increase in reflector thickness does not lead to a noticeable reduction in the overall radial dimensions of the reactor and can even cause them to increase. This thickness is also used as the calculated δ_{ref}.
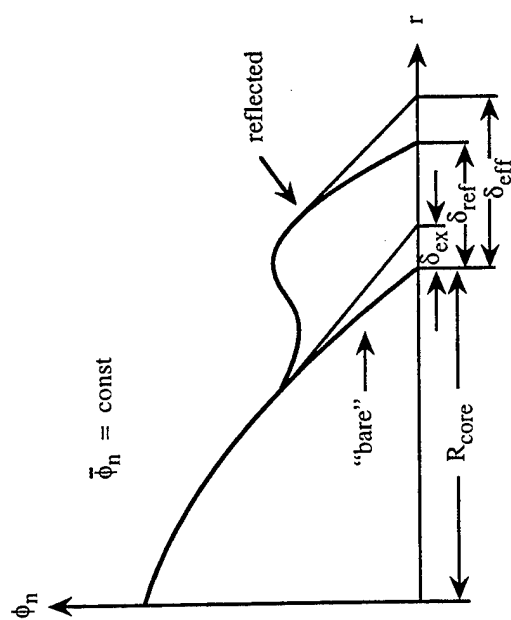
Fig. 3.3 Neutron flux for a reactor with a reflector.
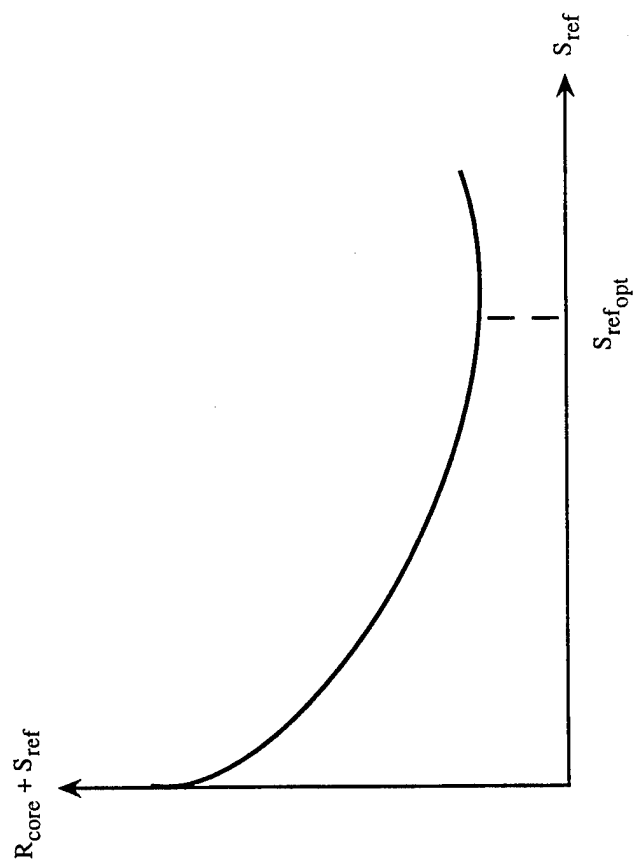
Fig. 3.4 Overall reactor size as a function of reflector thickness.

In determining the extrapolation additions to the geometric dimensions of the core, the following equation is used in practice:

$$\delta_{eff} = 1.2\lambda \tanh\left(\frac{\delta_{ref}}{\lambda}\right) \quad , \tag{3.17}$$

where λ is the thermal neutron diffusion length in the core.

Thus, in solving the diffusion equation (2.24) one must use δ_{eff} instead of δ_{ex}, namely, $H_{eff} = H + 2\delta_{eff}$; $R_{eff} = R + \delta_{eff}$, since δ_{eff} is always greater than δ_{ex}. As a result, the geometric parameter

$$B_g^2 = \left(\frac{2.405}{R_{eff}}\right)^2 + \left(\frac{\pi}{H_{eff}}\right)^2$$

will be less than that for a "bare" reactor. Consequently, the probabilities of neutron non-leakage, $p_{nonleak, mod}$ and $p_{nonleak,diff}$, will increase.

In conclusion, we can make the simplified neutron-physics calculations more precise, namely, the first two stages of those indicated above. As has been noted, neutron-physics reactor calculations are a way of checking the proposed geometric dimensions of the core, in particular, its diameter D and height H. The variable parameters are the characteristics that describe the composition of the core relative to the quantity and nature of the moderator in a homogeneous mixture and the uranium-235 fuel enrichment. Physics and engineering constants are also needed. The sequence of the calculations is as follows:

1. The neutron flux distribution (3.2) in the reactor core with reflectors is determined. As a first approximation, δ_{ref} is given from the considerations expressed above, and the effective addition δ_{eff} is calculated from equation (3.17).

2. The macroscopic cross section of nuclei of individual components and of the core as a whole is calculated (2.6) with the known geometry and composition of the core. The growth in neutrons is calculated from equation (2.15) and the thermal diffusion distance λ is also calculated.

3. The neutron multiplication factor k_∞ is determined for an infinite reactor and for different core compositions.

4. The geometric parameter B_g^2 is calculated for given D and H and also the assumed value of δ_{eff}.

5. k_{eff} is determined from the values of k_∞, B_g^2, τ and λ obtained.

6. The critical geometric parameter $B^2_{g,crit}$ is determined graphically from the reactor critical state condition ($k_{eff} = 1$). Next, the computations are repeated for other combinations of D, H, δ_{ref} and remaining variables in order to find the most reasonable variants.

Heterogeneous reactors differ from homogeneous reactors in that the nuclear fuel and moderator is distributed throughout the core volume in individual lumps (or blocks). This feature, called the lumped moderator, affects the neutron flux distribution in the reactor core volume (Fig. 3.5) and it also influences the four factors that determine k_∞. Thus, the fast fission factor ε will increase because the fast neutron flux that causes U238 fission is greater in the lump than the average flux in a homogeneous reactor. The coefficient p, which characterizes the resonance noncapture probability, will increase due to an abrupt reduction in resonance neutrons in the lump during neutron moderation between the lumps. In addition, the thermal neutron utilization factor f will diminish somewhat due to an increase in the neutron flux in the moderator and a rise in neutron absorption.

As a result, $\eta_{het} \cong \eta_{hom}$; $\varepsilon_{het} > \varepsilon_{hom}$; $p_{het} > p_{hom}$; $f_{het} > f_{hom}$; and, finally, $k_{eff,het} > k_{eff,hom}$.

The "homogenization" method is used in calculating neutron flux distribution. The essence of this method is that the macroscopic cross section of nuclei of materials in the core is calculated with cross section averaging taken into account not only relative to neutron energy but also relative to the volume of an elementary cell. The relationships needed to carry out this calculation are given in the reference literature. However, the structure of the equations for calculating k_∞ and k_{eff} remains unchanged.

Margin of reactivity taking reactor poisoning into account. As we noted above, one of the steps in reactor neutron-physics calculations is the determination of the margin of reactivity with fuel burnup and the accumulation of fission products in the core taken into account. The reactivity margin is denoted by the difference $k_{eff} - 1$ and the ratio

$$\frac{k_{eff} - 1}{k_{eff}} = \rho$$

is called the reactivity.

There are a number of reasons for which k_{eff} and, as a consequence, ρ will change with time during the operation of a reactor. For example, the burning of nuclear fuel and the accumulation of fission fragments, which are capable of absorbing neutrons, will cause a reduction in k_{eff}. On the other hand, the formation of new fuel, for example, Pu-239, will lead to an increase in k_{eff}. Furthermore, a temperature effect is observed, due to the effect of temperature upon neutron absorption.

The decrease with time in reactivity due to absorption of neutrons by products of the radioactive decay of fission fragments is called reactor poisoning. Quantitatively, reactor poisoning is evaluated from the ratio of neutrons absorbed by the total number of fission fragments from the *i*th isotope to the number of neutrons absorbed by the fuel:

107
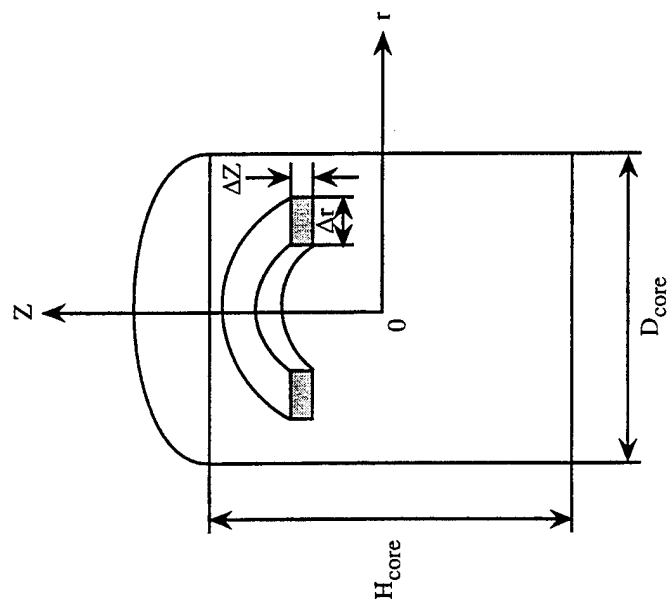
Fig. 3.5 Reactor core volume element.

$$W = \frac{\bar{\Sigma}\rho_i\sigma_{ci}}{\bar{\Sigma}_{at}}$$

The determining factor is poisoning by xenon-135 and samarium-149. During interaction with neutrons, xenon-135 is transformed into xenon-136 which has a small microscopic capture cross section. Equilibrium develops then with time between the formation and decrease in Xe-135, which corresponds to a constant value of W. However, after shutting the reactor down the formation of Xe-135 will predominate over its decrease for a certain length of time due to the continuing decay of fission fragments - radioactive iodine-135 according to ${}_{53}I^{135} \xrightarrow{\beta^-} {}_{54}Xe^{135} + \gamma$. As a result, the concentration of Xe-135 and reactor poisoning will reach a maximum and then decrease. This phenomenon is sometimes called the "iodine well" and it must be taken into account in the calculations. Subsequent reactor startup is possible only after the passage of a certain period of time until the formation of Xe-135 fragments ceases. This time can take several hours.

The decrease in reactivity due to burnup and poisoning is compensated for by a prescribed fuel reserve and the operation of two systems: fuel burnup compensation when substances that absorb neutrons burn in addition to the fuel, and a reactor control system.

The required uranium reserve taking burnup into account is easily determined from the following simple considerations. It is known that in order to obtain a thermal energy of 1 Mw·day in a thermal reactor it is necessary to expend about 1 g of uranium-235. Consequently, for a reactor thermal power of $\dot{Q}_t$ (in kW) and an operating time of t (in hours), it is necessary to have a reserve of uranium,

$$M_{burn}^{235} \approx 0.5 \cdot 10^{-4}\dot{Q}_t t.$$

A decrease in the reactivity margin due to poisoning (mainly by Xe-135 and Sm-149 fragments) can be determined from the empirical equation

$$\Delta k_{pois} = \frac{k_\infty}{2.07}P_0\left(1 - \frac{B^2L^2}{1+B^2L^2}\right) \qquad ,$$

where $P_0 = 0.12 + 8 \cdot 10^{-15}\phi_n(0,0)$. By knowing Δk_{pois} it is not difficult to determine the additional loading ΔM_{pois}^{235*} of uranium-235. As a result, the total uranium-235 loading taking burnup and poisoning into account is $M_0 = M_{cr}^{235} + \Delta M_{burn}^{235} + M_{pois}^{235}$, where M_{cr}^{235} is the critical uranium-235 loading determined from the criticality equation in which, obviously, $k_{eff} = 1$.

The relationship of k_{eff} to the average core temperature is calculated from the following simple and quite obvious equation:

$$k_{eff}(T) = k_{eff}(T_0)[1 + \alpha T]$$

where $k_{eff}(T_0)$ is the effective multiplication factor for a "cold" reactor; α is the temperature coefficient.

With an increase in temperature, k_{eff} can either decrease ($\alpha < 0$) or increase ($\alpha > 0$). This is explained by two factors: on the one hand, the average neutron energy changes which influences the absorption interaction cross section (nuclear temperature effect) and, on the other hand, the density of all materials in the core changes (the temperature density effect) which will result in changes in such parameters as neutron growth and diffusion length. Both factors influence k_{eff} in different ways. This also explains the temperature effect, which characterizes the relationship of k_{eff} to the average core temperature. The effort is made in reactor design to operate at temperatures where the temperature coefficient α is negative. This results in reactor self-stabilization. That is, suppose k_{eff} increases for some reason. This will lead to an increase in reactor power, and, consequently, in the reactor temperature. If α is negative, k_{eff} will decrease and the reactor will return to its original state. A similar situation occurs if there is an arbitrary reduction in power and, thus, a reduction in k_{eff} of the reactor. As a result, the reactor will have the property of self-stabilization.

Reactor kinetics. In conclusion, let's turn to the last step in the neutron-physics calculations which relates to the operation of the reactor control system. For this purpose, we will examine the transient process in the reactor, i.e., the change in neutron flux with time. This process is called reactor kinetics.

A change in neutron density with time can be established from the following. In the supercritical reactor state, the increase in neutron density in a single generation of neutrons with an average life time $\bar{l} = \rho_n(k_{eff} - 1)$.

Consequently,

$$\frac{\Delta\rho}{\Delta t} = \frac{\rho(k_{eff} - 1)}{\bar{l}} \quad ,$$

and in the limiting case, the reactor kinetics equation is obtained,

$$\frac{d\rho}{dt} = \frac{\rho(k_{eff} - 1)}{\bar{l}} \quad . \tag{3.18}$$

Keeping mind that $\phi = \rho\bar{v}$ for monoenergetic neutrons and integrating (3.18), we can write the kinetics equation in the form

$$\phi(t) = \phi_0 \exp\left(\frac{k_\infty - 1}{\bar{l}}t\right) \quad . \tag{3.19}$$

where ϕ_0 is the neutron flux at time $t = 0$.

The time during which the neutron flux increases by a factor of e is called the reactor period,

$$T = \frac{\bar{l}}{k_{eff} - 1}.$$

Thus, equation (3.19) can be represented in the form,

$$\phi(t) = \phi_0 \exp\frac{t}{T} \quad .$$

Let's examine the operation of a control system by supposing initially that all neutron fissions are instantaneous with an average life time $\bar{l}_{inst}$ = 10-3 sec. By assuming an instantaneous reactivity margin k_{eff} -1 = 0.01, one can determine the reactor period, T = 0.1 sec. This means that in one second the neutron flux as well as the reactor power will increase by a factor of e^{10}. It is difficult to imagine a control system which could cope with such rapid changes in power.

In reality, approximately 0.75% of the total neutron yield is not prompt neutrons, rather, neutron emission occurs for tens of seconds or longer. These are the delayed neutrons mentioned earlier and they consist of several groups. The average life time of these neutrons is $\bar{l}_{delayed}$ = 12.24 sec. The average life time of all neutrons, i.e., prompt and delayed neutrons, with consideration given to their fractions of the total is determined from the equation

$$\bar{l}^* = \bar{l}_{prompt}\left(1 - \beta\right) + \bar{l}_{delayed}\beta$$

where ß is the number of delayed neutrons divided by the total number of neutrons in a given generation; the delayed neutron fraction.

Hence, $\bar{l}^*$ = 0.001 x 0.9925 + 12.24 x 0.0075 = 0.0928 sec. The margin of reactivity k_{eff} - 1 = 0.01 and the reactor period will be 9.28 sec. This means that the reactor power will increase by about 20% in 1 sec. The control system must handle this increase in power at the same rate.

It should be noted that the estimate made of the reactor period is purely illustrative and very approximate. Nevertheless, it allows one to demonstrate reasonable limits of changes in k_{eff}. By showing k_{eff} as the sum of the effective multiplication factors for prompt ($k_{eff,prompt}$) and delayed ($k_{eff, delayed}$) neutrons, we get

$$k_{eff} = k_{eff,prompt} + k_{eff,delayed} = k_{eff}\left(1 - \beta\right) + k_{eff}\beta \quad .$$

If $k_{eff,prompt}$ < 1, the chain reaction will depend on prompt and delayed neutrons. In this case, without fission by delayed neutrons the chain reaction will attenuate (subcritical reactor state). If $k_{eff,prompt}$ ≥ 1, the chain reaction can proceed with prompt neutrons and without help from the delayed neutrons. The reactor power will rise rapidly (prompt supercritical reactor state) and the reactor becomes uncontrollable.

A reactor with a neutron multiplication factor $k_{eff,prompt}$ = 1 is called prompt critical. In this case, ß = ρ. At this point, the neutron flux will increase extremely rapidly

and reactor control systems will not be react. Hence, it follows that the maximum reactivity control limits of a power plant reactor must never exceed 0.0075, i.e.,

$$k_{eff} < 1.0075$$

The neutron flux, and, consequently, the reactor power is changed through the use of control equipment. The latter can consist either of rods, plates or drums containing materials that are strong absorbers of neutrons or which periodically expose sections of the surface of the core, thus regulating the number of neutrons that escape from its confines.

3.3. Thermal-Hydraulic Design Calculations.

Thermal-hydraulic reactor design involves two kinds of design calculations, thermal and hydraulic. Each of these are determined by the layout and type of reactor, the kind of coolant used, etc. Hence, there are a large number of design calculation variants, however, the overall objective remains the same.

The principal task in thermal design calculations is to find the geometric and thermophysical parameters of the core that will provide a given thermal power output at given reactor inlet and outlet temperatures, the allowable temperatures of the most thermally stressed components, etc.

The hydraulic design task is basically to determine reasonable flow rates of the coolant, often a liquid metal, and also to determine the required pumping power with pressure losses taken into account.

Thermal and hydraulic design calculations are done in order to verify a given reactor layout, kind of core, etc. The variables are: geometrical - H, D, δ_{eff}, n_{fuel} d_{fuel} (number, grid spacing and diameter of fuel elements) and others; thermophysical - $\bar{c}$, $\bar{\Sigma}$, $\bar{\rho}$, $\bar{\lambda}$, $\bar{\alpha}$ (average heat capacity, cross section, coolant density, thermal conductivity and thermal reactivity coefficient, etc.).

The given parameters include $\dot{Q}$, T_{in}, T_{out} (reactor power, coolant temperatures at inlet and outlet).

The given reactor thermal regime must be ensured within specific limits, for example, wall temperature (T_w) and fuel element centerline temperature ($T_{fuel,cl}$), etc.

This, then, is the general approach to thermal and hydraulic design calculations. We will now discuss in more detail reactor thermal design calculations for a thermal neutron reactor with a homogeneous core.

Thermal design calculations of a homogeneous reactor. Such a reactor consists of an assembly of cylindrical fuel elements immersed in a flowing coolant (Fig. 2-1).

The reactor thermal power is determined from the equation

$$\dot{Q}_t = \dot{M}_c \bar{c}_p (T_h - T_c) = h A_{fuel} \Delta T \qquad (3.20)$$

112

where $\dot{M}_c$ is the coolant mass flow per second through the core; ΔT is the average temperature drop; $\bar{c}_p$ is the specific heat, A_{fuel} is the total fuel element surface area over which the coolant flows.

By taking the continuity equation into account, $\dot{M}_c = \rho A_{flow} \bar{v}$, where A_{flow} is the cross sectional area of the core perpendicular to the coolant flow, $\bar{v}$ is the average coolant flow velocity, we obtain the following relationship:

$$\frac{A_{fuel}}{A_{flow}} = \frac{4 d_{fuel} H n_{fuel}}{D^2 \bar{\varepsilon}_c} = \frac{\rho \overline{vc} (T_{out} - T_{in})}{\bar{\alpha} \Delta \bar{T}} \quad , \tag{3.21}$$

where n_{fuel} is the number of fuel elements, and $\bar{\varepsilon}_c = \dfrac{4 A_{flow}}{\pi D^2}$ is the effective area for the coolant passages.

Equation (3.21) associates the geometrical parameters of the core (the left side of the equation) with the thermal and hydraulic parameters of the coolant. However, using this equation in practical situations is possible only by knowing the relationship between ΔT and the initial data, T_{in}, T_{out}.

Let's look at the solution to this problem. Let's consider heat liberation in a unit volume (for example, 1 cm³) of the core. By designating the thermal power of this unit volume as $\dot{Q}'''$, we can write

$$\dot{Q}''' = E_f \phi(r,z) \bar{\Sigma}_f \quad , \tag{3.22}$$

where $E_f = 3.1 \times 10^{-11}$ joules, the energy liberated in a single act of fission and which is converted into heat.

By assuming further that $\bar{\Sigma}_f$ is constant over the core volume and taking equation (3.12) into account, equation (3.22) becomes

$$\dot{Q}''' = \dot{Q}_c''' J_0 \left(\frac{2.405 r}{R_{eff}} \right) \cos\left(\frac{\pi z}{H_{eff}} \right) \quad , \tag{3.23}$$

where $\dot{Q}_c'''$ is the maximum power per unit volume, in the center of the core ($r=0$; $z=0$).

$\dot{Q}_c'''$ can be determined from the following consideration. Analogously with (3.22), we can write the expression for the reactor thermal power as a whole:

$$\dot{Q}_t = E_f \bar{\phi}(r,z) \bar{\Sigma}_f V_f \tag{3.24}$$

where V_f is the volume occupied by the homogeneous mixture which contains nuclear fuel; $\bar{\phi}(r,z)$ is the average neutron flux.

The factors in equation (3.24) can be written in the form

$$V_f = \frac{\pi D^2}{4} H(1 - \bar{\varepsilon}_c) \quad ; \quad \bar{\phi}(r,z) = \bar{\phi}(0,0)\bar{\kappa}_R \bar{\kappa}_H \quad ,$$

where

$$\bar{\kappa}_R = \frac{1}{R^2} \int_0^R J_0\left(\frac{2.405r}{R_{eff}}\right) dr \quad ; \quad \bar{\kappa}_H = \frac{1}{H} \int_{-H/2}^{H/2} \cos\left(\frac{\pi z}{H_{eff}}\right) dz \quad ,$$

are the neutron flux averaging factors along the radius and height of the core.

As a result, equation (3.24) becomes

$$\dot{Q}_t = \dot{Q}_t''' \bar{\kappa}_R \bar{\kappa}_H \frac{\pi D^2 \left(1 - \bar{\varepsilon}_c\right)}{4} H$$

or

$$\dot{Q}_t = \dot{Q}_t''' \bar{\kappa}_R \bar{\kappa}_H \frac{\pi d_{fuel}^2}{4} H \quad . \tag{3.25}$$

For reasons of brevity, we will designate

$$J_0\left(\frac{2.405r}{R_{eff}}\right) = f_1(r) \quad ; \quad \cos\left(\frac{\pi z}{H_{eff}}\right) = f_2(z) \quad .$$

Next, let's isolate (Fig. 3.6) an annular volume $\Delta A \Delta z = \left[\pi(r + \Delta r)^2 - \pi r^2\right]\Delta z$ in the cross section along the height z. The thermal power liberated in this volume is

$$\dot{Q}_{t,\Delta} = \dot{Q}_t''' (1 - \varepsilon_c)\Delta A \Delta z \quad , \tag{3.26}$$

where $\varepsilon_c = \Delta A_{cool}/\Delta A$ is the local porosity for the coolant which, in the general case, can change along the core radius depending on the fuel element grid spacing.

In the steady reactor operating mode, the thermal power liberated should be completely removed by the coolant that flows through the isolated volume:

$$\Delta Q_t = \dot{M}_c \bar{c}_p \Delta T \quad . \tag{3.27}$$

where $\dot{M}_c$ is the coolant mass flow per second through the cross section ΔA; ΔT is the heating of the coolant in the segment Δz.

By equating (3.26) and (3.27), we obtain

$$\Delta T = \dot{Q}_t''' \frac{(1 - \varepsilon_c)\Delta A \Delta z}{\bar{c}_p \Delta \dot{M}_c} \quad . \tag{3.28}$$
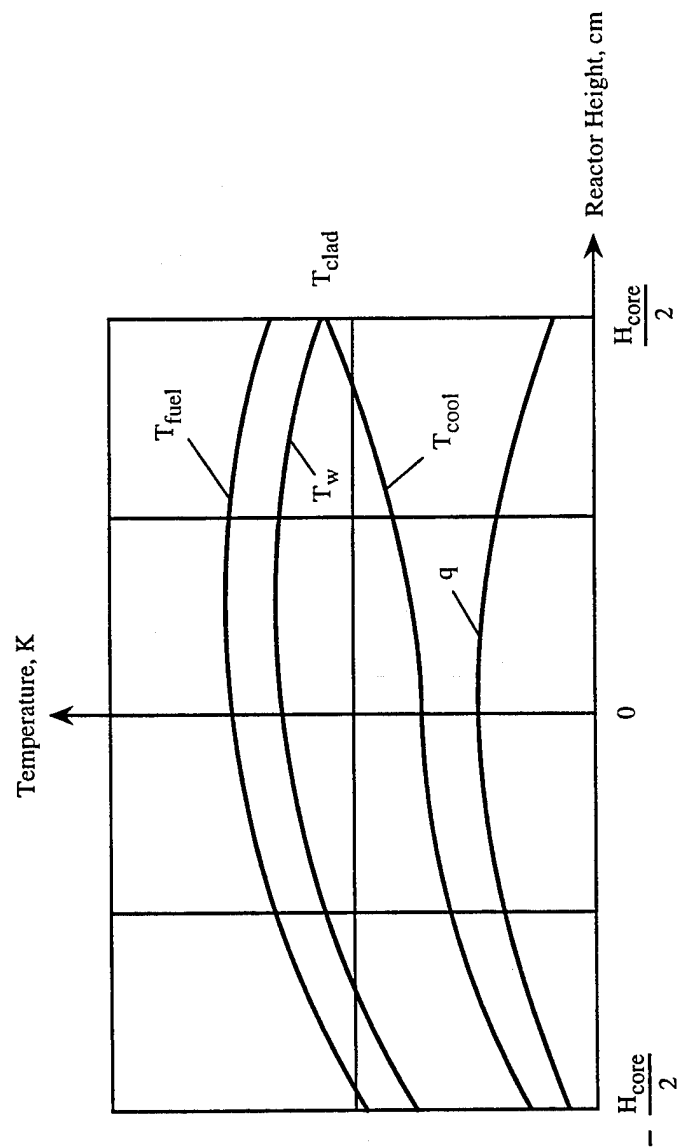
Fig. 3.6 Temperature variation along the length of a reactor.

115

$\Delta \dot{M}_c$ can be obtained from the equation for the coolant flow through the cross section ΔA by expressing the product $\overline{\rho v}$ in terms of the variables in the continuity equation,

$$\Delta \dot{M}_c = \frac{4 \dot{M}_c \Delta A \varepsilon_c}{\pi D^2 \overline{\varepsilon}_c}$$

If we substitute $\Delta \dot{M}_c$ into equation (3.28) and also take (3.23) into account, we obtain

$$\Delta T = \frac{\dot{Q}_t'' f_1(r) f_2(z)(1 - \varepsilon_c) \Delta A \pi D^2 \overline{\varepsilon}_c \Delta z}{4 \overline{c}_p \dot{M}_c \Delta A \varepsilon_c}$$

By introducing the variable

$$\chi(r) = \frac{f_1(r)(1 - \overline{\varepsilon}_c) \varepsilon_c}{\overline{\kappa}_R (1 - \varepsilon_c) \overline{\varepsilon}_c}$$

into our examination and using (3.25), we finally obtain

$$\Delta T = \frac{Q_t''' \chi(r) f_2(z) \Delta z}{\overline{c} \dot{M}_c \overline{\kappa}_H H}$$

If we go to the limit and integrate the latter relationship over the limits from the inlet cross section, where $T = T_{in}$, to some cross section along the height z, we obtain the equation of interest to us that describes the coolant temperature distribution along the height of the core:

$$T(z) = T_{in} + \frac{Q_t \chi(r) \int_{-H/2}^{z} f_x(z) dz}{\dot{M}_c \overline{c}_p \overline{\kappa}_H H} \qquad (3.29)$$

Next, if we keep in mind that $Q_t = \dot{M}\overline{c}_p(T_{out} - T_{in})$, equation (3.29) can be written differently:

$$T_{cool}(z) = T_{in} + \frac{(T_{out} - T_{in}) \chi(r) \int_{-H/2}^{z} f_x(z) dz}{\overline{\kappa}_H H} \qquad (3.30)$$

In order to establish how the fuel element clad temperature changes along the radius of the core, we will examine how the heating of the coolant in the earlier isolated annular volume can be determined. In order to do this, we will write

$$T_{clad} - T_{cool} = \frac{\Delta Q_T}{\overline{\alpha} \Delta A_{fuel}} \qquad , \qquad (3.31)$$

where ΔA_{fuel} is the total lateral surface area of the fuel elements over which the coolant flows in the isolated volume.

Next, we write the equality

$$\frac{\Delta A_{fuel}}{A_{fuel}} = \frac{4 \Delta A (1 - \varepsilon_c) \Delta z}{\pi D^2 (1 - \overline{\varepsilon}_c) H} \qquad . \qquad (3.32)$$

Following a number of transformations using equations (3.23), (3.25), (3.26) and (3.32), equation (3.31) becomes

$$T_{clad} = T_{cool} + \frac{Q_t f_1(r) f_2(z)}{\overline{\alpha} A_{fuel} \overline{\kappa}_R \overline{\kappa}_H} \qquad .$$

Since $Q_t = \overline{\alpha} A_{fuel} \Delta \overline{T}$, the latter equation can be rewritten in a form which is more suitable for analysis:

$$T_{clad} = T_{cool} + \frac{f_1(r) f_2(z) \Delta \overline{T}}{\overline{\kappa}_r \overline{\kappa}_H} \qquad . \qquad (3.33)$$

Equations (3.30) and (3.33) make it possible to determine the temperature of the coolant and the fuel element clad at any point in the core and to compare it with the allowable temperature. Obviously, the maximum temperature will be in the central fuel element and in the coolant that flows over it. This fuel element is usually taken as the design fuel element.

In order to equalize the temperature regime along the core radius, it is necessary to satisfy, as a minimum, two conditions.

First, one must assure a constant coolant cross sectional area fraction, i.e. $\varepsilon_c = \overline{\varepsilon}_c = $ const. This is easily accomplished by maintaining a constant fuel element grid spacing (geometric profiling). Second, it is necessary to strive for a $\overline{\kappa}_R$ that is close to unity. This can be achieved by varying the uranium-235 concentration from the center to the periphery (nuclear profiling).

Similar procedures can be used in profiling the heat liberation along the height of the core.

Thus, for a given pattern of heat liberation in the core volume one can find the condition for which the fuel element clad temperature will reach a maximum. The latter,

117

in turn, makes it possible to establish the average temperature drop which enters into equation (3.20).

Let's by way of example consider a simplified variant which, through nuclear profiling, successfully satisfies the condition $f_2(z) = 1$ and, correspondingly, $\overline{\kappa}_H = 1$. Then, according to (3.20), we obtain

$$T_{cool} = T_{in} + \left(T_{out} - T_{in}\right)\frac{\chi(r)}{H}\int\limits_{H/2}^{z} dz$$

The maximum temperature of the coolant and the fuel element clad is obtained at the core outlet ($z = H/2$). According to (3.33),

$$T_{clad} = T_{in} + \left(T_{out} - T_{in}\right)\chi(r) + \frac{f_1(r)\Delta\overline{T}}{\overline{\kappa}_R}$$

and the average temperature drop for the maximum allowable clad temperature ($T_{clad} = T_{clad,max}$) is

$$\Delta\overline{T} = \left[T_{clad} - T_{out} - \left(T_{out} - T_{in}\right)\chi(r)\right]\frac{\overline{\kappa}_R}{f_1(r)} \qquad . \qquad (3.34)$$

If we assume additionally that $f_1(r) = 1$, $\overline{\kappa}_R = 1$ (i.e., we examine the most thermally stressed central fuel element), then equation (3.31) reduces to $\Delta\overline{T} = T_{clad,max} - T_{out}$. In the general case, however, the functions $T_{cool}(z)$ and $T_{clad}(z)$ obey more complex patterns, and $T_{clad,max}$ is not reached at the outlet cross section but at a certain distance from it.

Such a general case is described by the following equation:

$$T_{clad} = T_{in} - \left(T_{out} - T_{in}\right)\frac{\chi(r)H_{eff}}{\overline{\kappa}_R H}\left(\sin\frac{\pi z}{H_{eff}} + \sin\frac{\pi H}{2H_{eff}}\right) + \frac{f_1(r)\cos\left(\dfrac{\pi z}{H_{eff}}\right)}{\overline{\kappa}_R\overline{\kappa}_H} \qquad . \qquad (3.35)$$

Two parameters that are of interest, in addition to the fuel element clad temperature and the coolant temperature, are the heat flux q" and the fuel element centerline temperature. The heat flux passing through the lateral surface of an elementary cylindrical volume ΔV of radius r is

$$q" = \frac{\dot{Q}_t'''\Delta V}{A_{fuel}} = \frac{\dot{Q}_t'''\pi r^2\Delta z}{\pi d_{fuel}\Delta z} = \frac{\dot{Q}_t''' r}{2} \qquad . \qquad (3.36)$$

and it can also be calculated from an equation similar to (3.2), i.e.,

118

$$q''(r, z) = q''(0,0) J_o \left(\frac{2.405 r}{R_{eff}} \right) \cos \left(\frac{\pi z}{H_{eff}} \right) \qquad . \qquad (3.37)$$

In order to determine the temperature at the center of the fuel element, one must solve the planar axisymmetrical problem of heat transfer by thermal conductance from the fuel element center to its periphery. According to Fourier's law, we can write

$$d\dot{Q}_{cond} = -\bar{\lambda} \frac{dT}{dr} 2\pi r dz \qquad .$$

where $\dot{Q}_{cond}$ is the thermal power transferred by thermal conductance from the fuel element center to its periphery.

On the other hand, a thermal power of $\dot{Q}_t''' \pi r^2 dz$ is liberated in the volume $\pi r^2 dz$. By equating the liberated and transferred thermal powers, we can write

$$\dot{Q}_t''' \pi r^2 dz = -k \frac{dT}{dr} 2\pi r^2 dz$$

and, consequently,

$$dT = -\frac{\dot{Q}_t''' r dr}{2k} \qquad .$$

If we integrate the latter equation in the limit from 0 to r_{fuel}, we obtain

$$T_{fuel} = T_w + \frac{\dot{Q}_t'''}{4k} r_{fuel}^2 \qquad .$$

By using equation (3.36) and the expression for q through the temperature drop $q'' = h(T_{clad} - T_{cool})$, we finally obtain (without accounting for the fuel element clad)

$$T_{fuel} = T_{cool} + q'' \left(\frac{1}{h} + \frac{d_{fuel}}{4k} \right) \qquad . \qquad (3.38)$$

Thus, the thermal design of a reactor as a heat exchanger reduces to solving the equations presented above, the principal ones being (3.21), (3.30), (3.33), (3.35), (3.37) and (3.38). The qualitative nature of changes in the parameters $T_{cool}(z)$, $T_{clad}(z)$, $q''(z)$, and T_{fuel} is shown in Fig. 3.7.

As is apparent, the basic characteristics that describe the thermal regime of a reactor can be secured through different combinations of geometric and thermophysical parameters of the core. In the process of completing design variants, those characteristics

119
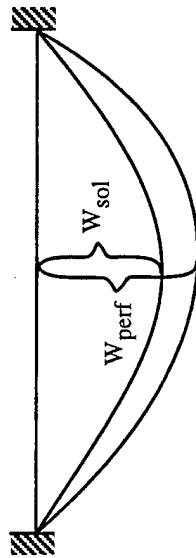
Fig. 3.7 Relative buckling of a solid and perforated plate.

will emerge which to a greater degree result in minimum reactor size and mass and which simultaneously satisfy neutron-physics design conditions.

Hydraulic reactor design calculations. Hydraulic design calculations do not present any difficulties when the coolant is an incompressible fluid (in the majority of nuclear power plants, liquid metals are used as the coolant). When, by virtue of a constant cross-sectional flow area, the fluid flow velocity, $\bar{v}$, is also constant, the pressure loss is determined from the well-known equation

$$\Delta p = \xi \frac{\overline{\rho v}}{2} \frac{H}{d_{hyd}} \qquad ,$$

where ξ is the pressure loss coefficient (found in reference handbooks); d_{hyd} is the hydraulic diameter of the channel.

When gas coolants are used as, for example, in certain gas turbine power plants, the well studied gas dynamic problem of the flow of heated gases with friction in constant area channels arises. The crux of this problem in the given case is that equation (3.29) describes the temperature change along the height of the core, z. By solving simultaneously Bernoulli's equation, the equations of continuity and state,

$$\frac{dp}{\rho} + vdv + \xi \frac{v^2}{2} \frac{dz}{d_{hyd}} = 0 \quad ; \quad \frac{d\rho}{\rho} + \frac{dv}{v} = 0 \quad ; \quad \frac{dp}{p} = \frac{dT_{cool}}{T_{cool}} + \frac{d\rho}{\rho} \qquad ,$$

one can obtain an equation which relates velocity and temperature:

$$RT_{cool} \left(\frac{dT_{cool}}{T_{cool}} - \frac{dv}{v} \right) + vdv + \xi \frac{v^2}{2} \frac{dz}{d_{hyd}} = 0 \qquad . \qquad (3.39)$$

In combination with equation (3.29), this allows one to find the relationship between T_{cool} and v (generally, by using a computer).

In order to avoid critical flow problems in the channel, it is advisable to assume as input data the gas parameters at the exit cross section of the core, ρ_{out}, v_{out}, p_{out}. These parameters should be used in equation (3.21). The gas parameters at the inlet to the core and, consequently, the total pressure drop in the core, $\sigma = \dfrac{p_{out}}{p_{in}}$, are then determined by solving equation (3.39).

3.4. Some Problems in the Design of Reactors for Endurance.

As has been noted earlier, the design of a reactor for endurance (strength calculations) is a part of overall reactor design. Strength calculations of reactor components and of the reactor as a whole are usually of two kinds: preliminary design

calculations and design verification. The first is carried out in the early stages when there are still no specific limitations on the basic data set (i.e., geometric, thermophysical and other parameters). Design verification is done when the specified parameters are well understood from neutron-physics and thermal calculations. Thus, the purpose of design verification is to establish agreement between these parameters and conditions for securing a factor of safety for those components which are being evaluated for use in a reactor with a given operating life in a power plant assembly. In those situations where any component does not satisfy these conditions, its parameters must be changed appropriately. However, this requires that the first two kinds of reactor design calculations be repeated, not arbitrarily, but with the conclusions from the strength calculations taken into account.

Naturally, reactor strength calculations as a whole consists of a number of separate design calculations pertaining to individual reactor components (housing, support structure, containment, fuel clad, etc.). One should realize that all these components experience individual load conditions and that, in the final analysis, they determine to a large extent the reactor design strength as a whole.

In keeping with the purpose of this book, we will discuss only briefly some principal problems in the verification of nuclear reactor strength calculations by selecting for this purpose the support grid to which the fuel elements are attached and the fuel element clad.

Generally speaking, strength calculations for any reactor component are done in three successive stages, in particular:

a. Analysis of component loading and selection of the components stressed the most during operation;

b. Selection of a component design scheme and computation of the stresses and deformations caused by the acting forces and moments;

c. Comparative analysis of the stresses and deformations found, comparison of these with the allowable values, determination of the safety factor, compilation of appropriate conclusions.

By keeping in mind orbit insertion processes and the operating life in space of a spacecraft with a nuclear power plant, one can define the two most important reactor component load regimes:

Regime I - orbit insertion and concomitant loads that affect the component under evaluation;

Regime II - the duration of operation in orbit comparable to the calculated operating regime of the nuclear power plant.

In the first regime, the loading along the longitudinal axis can reach 10 g's (i.e., 10 times the force of earth gravity). These forces, however, act for a comparatively short time interval, no more than 10 to 15 minutes. Strength calculations in this regime are carried out using the theory of elasticity

$$\sigma = E\varepsilon \qquad ,$$

where σ is the stress (with units of pressure), E is the material modulus (also in units of pressure), and ε is the relative strain.

The second regime is characterized by extremely small loads along any axis ($n_x \sim n_y \sim n_z \leq 0.05$ g). For this reason, the basic loads considered are those caused by pressure forces. These forces, although smaller than the forces in regime I, act during the entire orbit operation of the nuclear power plant. They must, therefore, be taken into account in the design calculations. The influence of high temperatures, characteristic of the reactor operating process, must also be included. Thus, one cannot justify restricting the examination to only elastic deformation. The basic kind of deformation the components are subjected to here is creep deformation. The relationship between stress and deformation is nonlinear and changes with time. Let's turn to an examination of strength calculations of support grids.

3.4.1. Strength Calculations of Support Grids.

The support grid is a perforated plate of constant thickness. Design calculations of such a plate involves the substitution of an equivalent solid plate with a given thickness. The following conditions apply. Above all, one must keep in mind that a perforated plate, weakened as it is by holes for retaining the fuel elements, will experience greater axial buckling than a solid plate of the same thickness under the same load. It has been established experimentally that the relative buckling of both plates at congruent points (Fig. 3.8) will be the same:

$$\gamma = \frac{W_{sol}}{W_{perf}} = \text{const} \quad ,$$

where W_{sol}, W_{perf} are the buckling of the solid and perforated plates, respectively.

It is permissible in our calculations to assume that $W \propto \dfrac{1}{h^3}$ (h is the plate thickness). Thus, one can assign a thickness to the perforated plate such that its buckling will the same as for a solid plate and call this conditional plate the equivalent of the original plate (support grid).

$$W_{eq} = W_{perf} \quad . \quad \gamma = \frac{W_{sol}}{W_{perf}} = \frac{h_{eq}^3}{h_{perf}^3} \quad ; \quad h_{eq} = h_{perf}\sqrt{\gamma}$$

The following relationship exists for γ:

$$\gamma = \frac{3+\kappa}{4}\left(1-\mu^2\right)\left(1-\frac{d}{t}\right) \quad , \tag{3.40}$$
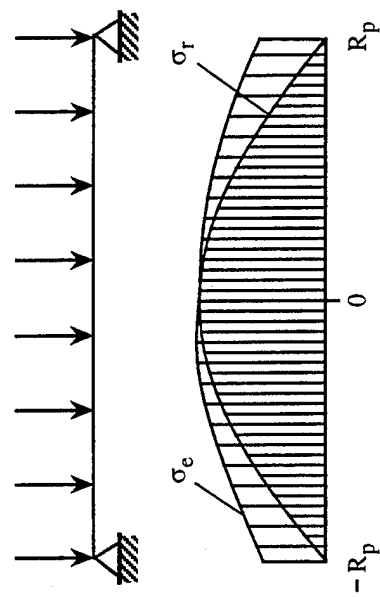
Fig. 3.8 Stress diagram for a reactor support grid.

where d is the hole diameter for retaining the fuel element; t is the fuel element pitch; μ is Poisson's ratio; κ is the plate stiffness factor;

$$\kappa = \frac{1.41}{1 + \left(n_{perf}/t - d\right)^2}$$

In other words, it appears possible for us to carry out calculations applicable to a perforated plate by using a solid plate of a smaller thickness.

Next, we will assume that in all regimes the support grid will be subjected to loads that are uniformly distributed over its surface. In regime I, the support grid is loaded by its own mass forces and with the operating load n_x taken into account. We will only consider the top support grid since it is loaded the most. In this case, the specific load on the support grid will be

$$q_{grid}^I = \frac{\left(m_{grid} + m_{fuel}\right)g_o n_x}{\pi R_{grid}^2 - A_{holes}} \tag{3.41}$$

where m_p, m_{fuel} are the masses of the support grid (plate) and the fuel element assembly, respectively; R_p is the radius of the support grid; A_{hole} is the total area of the holes for the fuel elements; g_o is the acceleration due to gravity.

In the second regime (II), the support grid is loaded by the coolant pressure differential before and after the grid (Δp_{cool}). Of course, this loading also occurs in regime I but it is negligible in comparison with the mass forces. So, in regime II the resultant force acting is $p_{res} = \Delta p_{cool} R_{grid}^2$, and the specific load on the support grid is

$$q_p^{II} = \frac{p_{res}}{\pi R_p^2 - A_{holes}} = \frac{\Delta p_{cool}}{1 - \dfrac{A_{holes}}{\pi R_p^2}} \tag{3.42}$$

Let's determine the stress in the support grid by the load considered. There are two methods for securing the support grid in the reactor vessel (Fig. 3.9). The first method is the free-floating support grid. It is the most stressed and we select it for examination. The following equations for σ_θ and σ_r can be used for the free support grid:

$$\text{For} \quad r = 0, \quad \sigma_r = \sigma_\theta = \frac{3}{8}\frac{qR_p^2}{n_{ex}^2}\left(3 + \mu\right) \quad ;$$

$$\text{For} \quad r = R_p, \quad \sigma_r = 0, \quad \sigma_\theta = \pm\frac{qR_r^2}{n_{ex}^2\left(1 + 2\mu\right)}$$

$$W_{max} = \frac{qR_p^4\left(5 + \mu\right)}{64D\left(1 + \mu\right)} \quad ; \quad D = \frac{Eh_{eq}^3}{12\left(1 - \mu^2\right)}$$
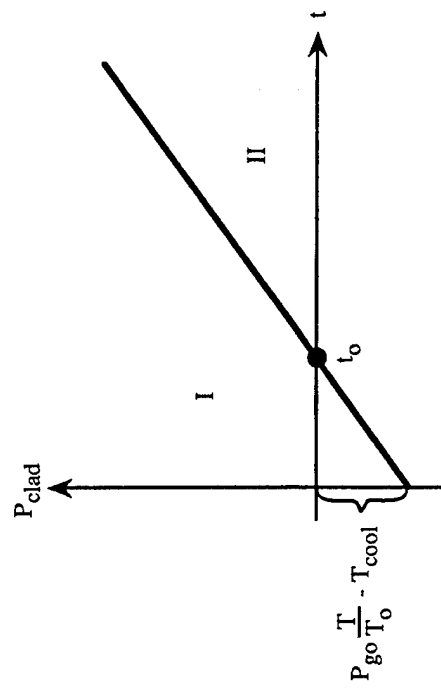
Fig. 3.9 Cladding pressure as a function of time. Initially the clad is acted on by compressive forces from the coolant, but as fission gasses accumulate, internal pressure builds up.

is the rigidity of the grid in buckling.

The calculations are performed in the following sequence:

First, the parameters k, γ and h_{eq} are determined from the geometry of the perforated plate; then, the stresses σ_r and σ_θ in both load regimes are analyzed for the equivalent support grid; then a certain total equivalent stress is determined for the complex stress state

$$\sigma_{eq} = \sqrt{\sigma_r^2 - \sigma_r \sigma_\theta + \sigma_\theta^2}$$

In conclusion, a comparison is made between the σ_{eq} obtained and the allowable stress and the safety factor is determined. A given creep limit for the material is assumed ($\sim$0.2% creep, $\sigma_{0.2t}$, and the endurance limit is $\sigma_{0.2t}^\tau$, that is σ_{creep} and σ_{limit}). The safety factor will in this case be equal to

$$n_1 = \frac{\sigma_{0.2t}}{\sigma_{eqv}} \quad ; \quad n_2 = \frac{\sigma_{0.2t}^\tau}{\sigma_{eqv}}$$

Normal operation of the support grid is assumed when n_1 and n_2 are greater than about 1.1.

Otherwise, the calculations need to be repeated with new materials data and new geometric parameters for the support grid.

3.4.2. Strength Calculations of Fuel Element Clad.

The fuel element clad determines to a significant degree the life of the given component. The most pertinent load regime is regime II - nuclear power plant operation in space. We will examine a fuel element clad (Fig. 3.10) with a gas space which provides for the accumulation of gaseous fission products (krypton and xenon) from nuclear fission. The volume of this space is V_g. The exterior of the clad is loaded by the coolant pressure. To sum up, a pressure differential $\Delta p_{clad} = p_g - p_{cool}$ acts on the clad.

In general, the gas pressure is that of the original gas that fills the gas space, usually helium. To this must be added the pressure of all the fission gases, $\sum_{i=1}^{n} p_{gi}$, where p_{gi} is the partial pressure of the ith fission product.

The volume of the gas space can change due to material creep and nuclear fuel swelling. These factors, however, can be neglected entirely because of their small influence on V_{go} and it is assumed that $V_{go} = V_g = $ const. In this case, the change in pressure of the original gas as a function of temperature is determined from the equation

$$p_{go}' = p_{go} \frac{T}{T_o}$$

127
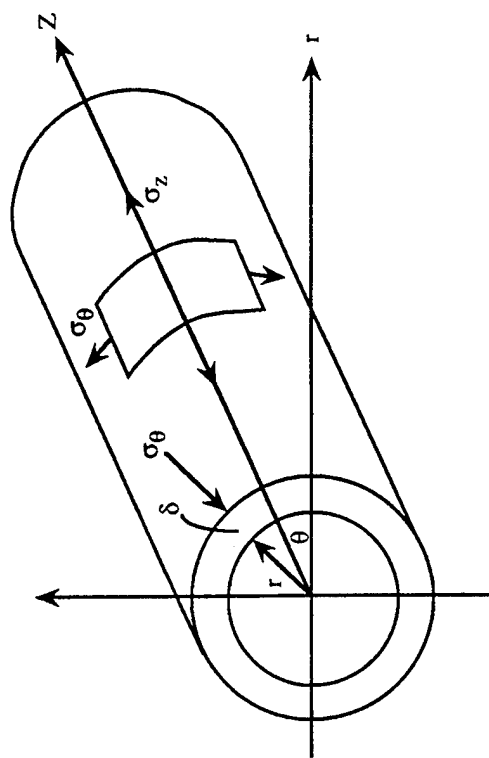
Fig. 3.10 Stress diagram for thin walled shell.

where p_{go} and T_o are the original pressure and temperature, respectively; and T is the current temperature).

The cladding pressure is

$$p_{clad} = p_{go} \frac{T}{T_o + At - p_{cool}} \qquad (3.43)$$

The factor A is assumed to be known from empirical results.

This equation is shown graphically in Fig. 3.9. As can be seen, at $t < t_o$ the clad is acted upon by forces basically from the coolant side. These are small, compressive forces. At $t > t_o$, the clad elongates and its material "creeps" with the time t. It is of interest to know at what time t the elongation of the fuel element clad will exceed the allowable. Let's turn to the design calculation scheme for the clad (Fig. 3.10). As is known, the state of a thin-walled shell under an internal pressure p_{clad} is described by the following equation:

$$\sigma_r = 0 \quad ; \quad \sigma_\theta = \frac{p_{clad} \, r}{\delta_{clad}} \quad ; \quad \sigma_z = \frac{p_{clad} \, r}{2\delta_{clad}}$$

In cylindrical coordinates, we can write

$$\sigma_{cr} = \frac{1}{3}\left(\sigma_\theta + \sigma_z + \sigma_r\right) \qquad ;$$

$$T = \frac{1}{\sqrt{\sigma}}\sqrt{\left(\sigma_\theta - \sigma_z\right)^2 - \left(\sigma_z - \sigma_r\right)^2 - \left(\sigma_r - \sigma_\theta\right)^2}$$

is the tangential stress.

After substitution, we can write

$$\sigma_{cr} = T = \frac{p_{clad} \, r}{2\sigma_{clad}} \qquad .$$

The rate of deformation in the complex stress state is now:

$$\dot{\varepsilon} = \frac{d\varepsilon}{dt} = B_1 \sigma^m \qquad .$$

where B_1 is the creep factor and m is the creep exponent.

In sections with established creep the rate of deformation is constant and for the computation of $\dot{\varepsilon}_\theta, \dot{\varepsilon}_z, \dot{\varepsilon}_r$ the relationship $\varepsilon = f(\sigma_r, \sigma_\theta, \sigma_z, B_1, m)$ exists.

Since, as has been observed, $P_{clad} = f(t)$, then one can also find the inverse relationship, which is the relationship between changes in clad dimensions and the

corresponding loading time. By omitting intermediate transformations, we can write this relationship in the following form:

$$t = \left(\frac{m+1}{(2m-1)\bar{f}} \left(1 - \left(\frac{r_0}{r} \right)^{2m-1} \right) \right)^{\frac{1}{m+1}} \quad ;$$

$$\bar{f} = \frac{1}{2} B \left(\frac{A r_0}{2\delta_{clad}} \right)^m \quad ; \qquad B = B_1 3^{\frac{m+1}{2}}$$

Thus, one can establish the operating time of the clad under given load conditions when the deformation will begin to exceed the allowable, that is $r > r_{allow}$. This time limit depends on many factors. In the event this time interval is less than the scheduled operating period of the nuclear power plant, the strength calculations must be repeated using new initial geometric data and materials properties.

3.5. Design of Nuclear Reactors.

3.5.1. General Requirements and Characteristics

The general requirement of reactors for any purpose is quite obvious: the generation of a given power output over a given operating life with complete nuclear and radiation safety. An additional requirement is placed on reactors for space power: minimum size and weight. In addition, considering all stages in the life cycle of space nuclear power reactors, there is an urgent need to consider the consequences of nuclear incidents. In fact, immediately after the launch of a rocket with a nuclear power plant payload the reactor could accidentally fall back to earth and initiate an uncontrolled startup. To this we can add the impact on earth by individual fragments (such as was the case following the accident on the "Cosmos-954" satellite) resulting from the unscheduled reentry into the earth's atmosphere of a spacecraft with a nuclear power plant. These circumstances place additional requirements on the design of nuclear reactors to ensure nuclear safety under any possible accident situations. All of these problems require special attention and we will discuss them below.

Depending on the class of thermal energy converters used, reactors can be divided into reactors with liquid metal and gas coolants (gas turbine nuclear power plants, nuclear rockets). There are also reactors which contain in-core direct converters of thermal energy (thermoelectric and thermionic) and reactors with no additional components in the core. We will devote our discussion to the latter kind of reactor because its properties are generally the most characteristic. Some characteristics of reactors that combine the thermal energy source with electric energy converters will be examined in the sections that deal with thermoelectric generators and reactor-generators that operate on the thermionic energy conversion principle.

The construction of the reactor under consideration consists of the following basic components: reactor vessel, heat liberating elements (fuel elements), neutron moderator

(in thermal reactors), radial and end reflectors, control system, as well as systems for ensuring nuclear and radiation safety. Let's examine these.

3.5.2. The Reactor Vessel.

The reactor vessel is the basic structural component that receives and transmits the loads that occur during the acceleration of the spacecraft and during the operation of the nuclear power plant. It combines in a single assembly all the basic components of the reactor. In addition, the reactor vessel also serves as a flow channel in the nuclear power plant because heat transfer between the fuel elements and the coolant takes place within the reactor. In accomplishing its function, the reactor vessel must maintain its dimensions within prescribed limits during its lifetime. In other words, it must be strong and durable during its entire operating life.

The basic structural elements of the reactor vessel are: shell, end plates or plenums and support grids, as can be seen in Fig. 3.11.

The shell, the lateral (or side) portion of the reactor vessel, is cylindrical and fabricated from welded sheet metal. Depending on the design of the reactor flow channel, the shell can be a single-walled or double-walled structure. In the latter case, corrugated stiffeners are inserted between the outer and inner walls of the shell.

At the locations where the shell is connected to the load bearing components of the reactor vessel (the support grids, diaphragms, attachment lugs, etc.), forged struts are welded to the shell. These pick up and transmit to the shell forces from the core components and the neutron reflectors, increase the stiffness of the shell and maintain the positioning of the reactor vessel components.

At the locations where they are welded to the shell, the struts should have cylindrical positioning rings to insure that the components being welded are positioned radially. These rings will also prevent the ejection of molten metal from the back of the seam and improve seam quality. For these purposes, during butt welding when the seam (welding quality) cannot be monitored from both sides, a special liner ring must be provided. The edges of shell and tubing to be butt welded should undergo preparatory machining.

The shell and plenums (end plates) form the sealed cavity of the reactor. The plenums can be spherical or elliptical. Inlet and outlet coolant tubing must first be welded to them. In order to reduce the axial dimension of the reactor and its mass, the plenums sometimes curve inside the reactor. When a plenum is used that is shaped by coupling the arcs of different radii circles, the plenum section is strengthened by fabricating it in sections.

The support grids are designed to hold the fuel elements in place, receive the fuel element assembly forces and transmit them to the reactor shell. The grids also shape the coolant flow around the fuel elements. The fuel elements are rigidly attached to one of the two grids (as a rule, the front one) and are free to shift axially relative to each other. Considering how the fuel elements are fastened and the loads are taken up, the front support grid must have a high stiffness and bending strength. The rear support grid picks up lateral forces from the fuel elements and axial forces caused by differences in coolant pressure. This grid plate has a lesser bending strength and thickness.
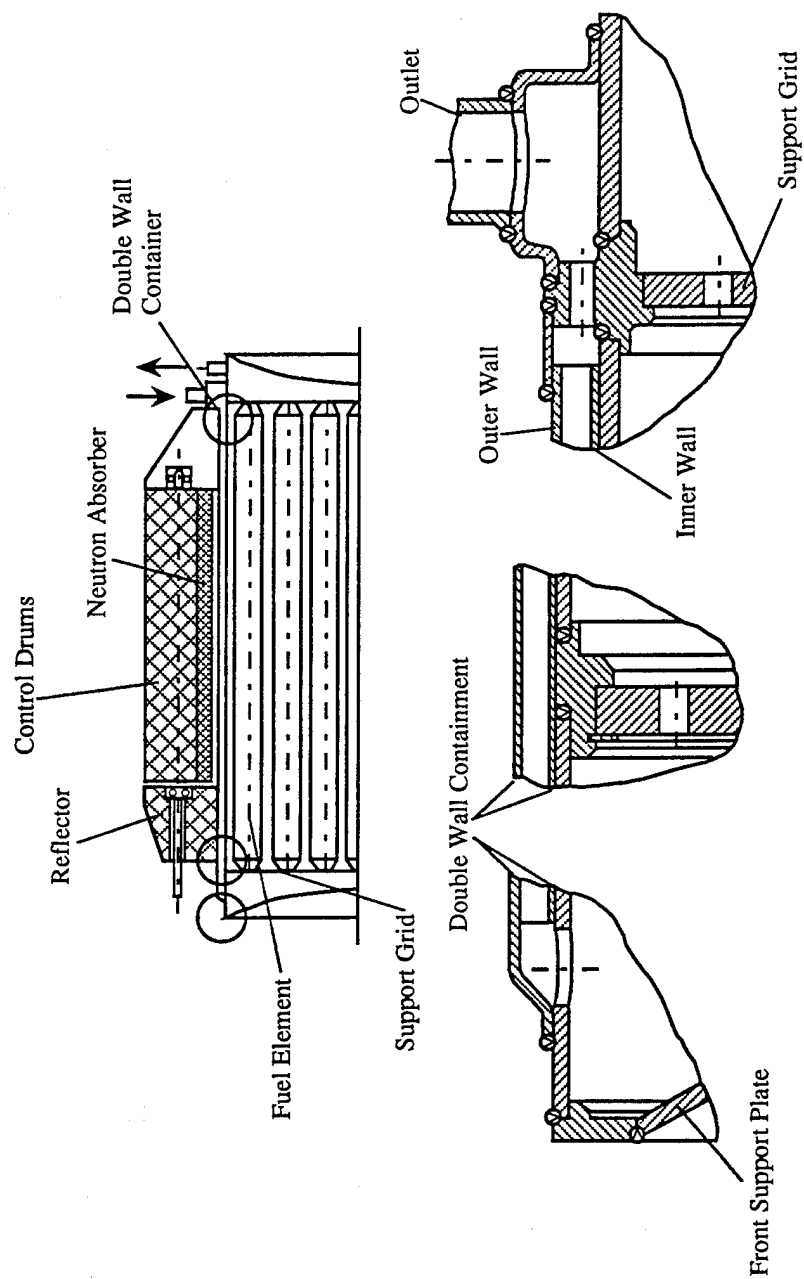
Fig. 3.11 Structural design of a compact honogeneous core nuclear reactor.

132

There are holes in the support grids for retaining the fuel elements according to the positioning arrangement selected. Holes are also provided for the coolant flow (Fig. 3.12). The rear support grid is welded to the shell. The front support grid is removable and in order to eliminate axial movement relative to the reactor vessel, it can be fastened by bolts, a spring-loaded collar, thrust liners, etc.

In order to decrease weight but maintain rigidity, grids of a finned construction can be used. Double-layered support grids are used for this purpose with large diameter cores. In such structures, the panels which form the grids, are joined together by rings and cylindrical sleeves. These are welded to the panels and serve as fuel element retainers and coolant passages.

When relatively long fuel elements are used, backup structures fastened to the inside of the shell can be employed. These will prevent bending due to lateral loads and maintain proper clearance between the fuel elements.

Inlet and outlet connecting pipes for the coolant are welded to the shell of the reactor vessel. The use of several such connecting pipes spaced along the surface of the shell will promote uniform coolant flow distribution in the core.

Reactor fastening studs are welded to the shell at the location of the reinforcement fins. These provide a strong connection between the reactor and the radiation shield. The reactor fastening studs are made from forgings.

3.5.3. Fuel Elements

The fuel elements distribute nuclear fuel in the core and transfer the liberated heat to the coolant by means of heat pipes or by direct heating of the heat conversion elements.

These fuel rods can be of different construction depending on the heat transfer method. They include rod, ring-shaped, tubular, plate, prismatic and spherical elements.

Fuel elements for reactors with liquid metal coolants are fabricated principally into cylindrical rods with smooth surfaces. Finned fuel elements are used in gas-cooled reactors in order to intensify heat transfer. In order to remove heat by heat pipes, the fuel elements are fabricated into six-sided prisms with openings for the heat pipes, or the fuel elements may be made into plates. These have openings for the heat pipes and are distributed over the entire transverse cross section of the core.

As a rule, fuel elements consist of a fuel core, a clad, end caps and spacer plugs (Fig. 3.13). The clad and the end covers form the sealed container which is filled with fuel. The sealed container prevents contact by the fuel core with the coolant. This prevents fuel particles and fission fragments from entering the coolant and protects the core from corrosion and erosion by the coolant.

There are different kinds of fuel element containers depending on the type of bond between the fuel core and the clad. These include the container-type fuel element which has a gap between the fuel and the clad that is filled with a heat conducting medium (liquid metal, helium), and fuel elements with a diffusion bond between the clad and the fuel.

The end plugs are made from a material which reflects neutrons. When the entire fuel assembly is placed in the reactor, these make up the neutron end reflectors. Fuel pellets are used in container-type fuel elements. The fuel pellets can be of any shape and they provide cavities within the fuel core for the accumulation of gaseous fission products.
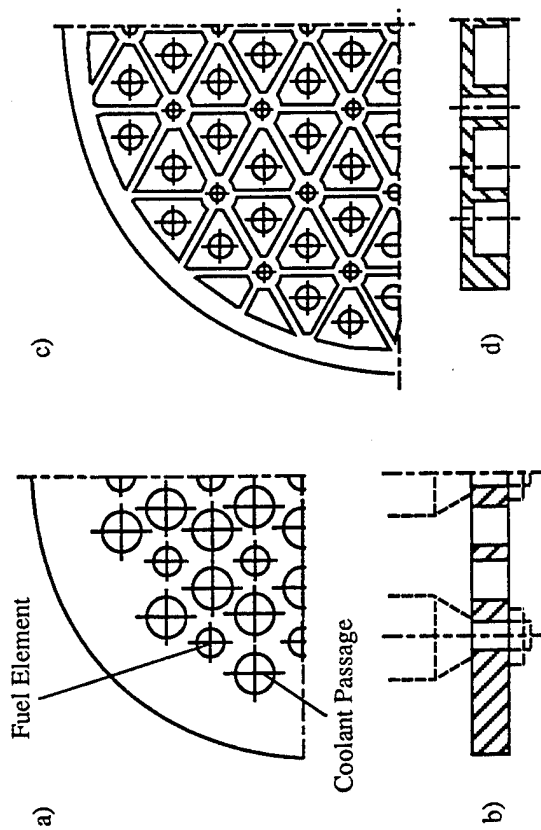
Fig. 3.12 Inlet plenum and support grid. a) radial perspective of inlet plenum; b) profile of inlet plenum; c) radial perspective of support grid; d) profile of support grid.

134
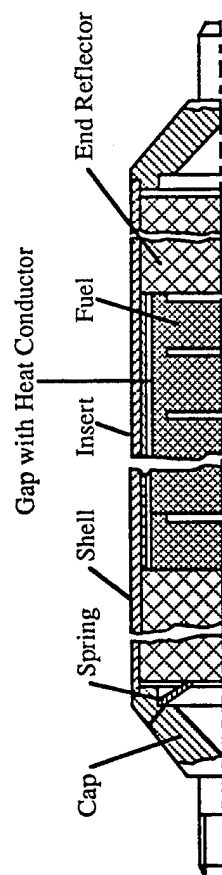
Fig. 3.13 Schematic of a cylindrical fuel element for a nuclear reactor.

Cavities may also be provided in the end sections of the fuel elements. In order to compensate for thermal expansion of the core and clad and to prevent free migration of fuel along the fuel element, the fuel core is compressed by springs.

The end caps, which together with the clad form a sealed container for the fuel, serve also as the support grid fastening points. Stems are added to the tips for this purpose. The most common method of joining the stems to the clad is by welding and subsequent mechanical finishing.

As we noted earlier, the fuel element clad can be finned. Clad with straight longitudinal fins are fabricated by forming or milling. Helical fins are obtained by twisting clad with straight longitudinal fins. The fins on the clad surface enhance heat transfer and serve as spacers to prevent mutual contact of the closely packed fuel elements. The fins also serve as spacers when fuel elements are set in special tubular channels in a heterogeneous core.

The characteristic construction of fuel elements that employ heat pipes in transferring thermal energy is that the fuel element material does not make contact with any kind of coolant fluid (the working fluid is enclosed in a sealed heat pipe). In addition, the fuel elements must be designed such that reliable thermal contact is achieved with the heat pipes. The fuel element design configuration is driven by the need for close packing and the smallest possible temperature gradients in the fuel material.

One possible way of coupling fuel elements with heat pipes is shown in Fig. 3.14. This design assumes there is a significant difference in the coefficient of linear expansion of the heat pipe material (Mo) and the fuel (90%UC + 10%ZrC). The block of fuel is divided into sections both cross-sectionally and axially. The clearances between the sections compensate for increases in volume due to fuel swelling and heating. The fuel element clad (Mo) is joined to the fuel sections in the block and promotes reliable thermal contact between the heat pipe and the fuel. It should be noted that the difference in the coefficient of linear expansion of the heat pipe material, the clad and the fuel excludes the possibility of thermal contact with the weld seams or the diffusion coupling.

The presence of sections in the fuel block along the length of the heat pipe permits nuclear profiling in the core in order to equalize heat generation. When dispersed ceramic-metallic fuel (referred to as *cermet* fuel; for example, UO_2 + Mo) is used, the need for a radially sectioned fuel block is eliminated.

A layered fuel element configuration can be used with low thermal conductivity fuel. In such fuel elements the fuel is made in pellets which are applied on layers of molybdenum disks. These are fitted with openings for the heat pipes. The molybdenum disks function as heat conducting shunts through which the heat from the fuel is transferred to the heat pipes. The heat pipes are interference fitted into the openings thus providing the necessary thermal contact with the panels. The thickness of the fuel pellet is small (1.5 -6.0 mm) and does not result in an appreciable temperature drop in the fuel. Heat transfer from the fuel to the panels is accomplished by thermal conductance (due to their direct contact) and by radiation.

Failure of heat pipes in the core of such a design does not lead to a significant temperature surge in the fuel. The contact with the panels allows the heat from the damaged heat pipes to be transferred to the adjoining pipes.

Radial View

Support Structure

Thermal Insulator

Heat Pipe

End Reflector

Thermal Neutron Absorber

Fuel Blocks

Wick

Cap

Axial View

Support Structure
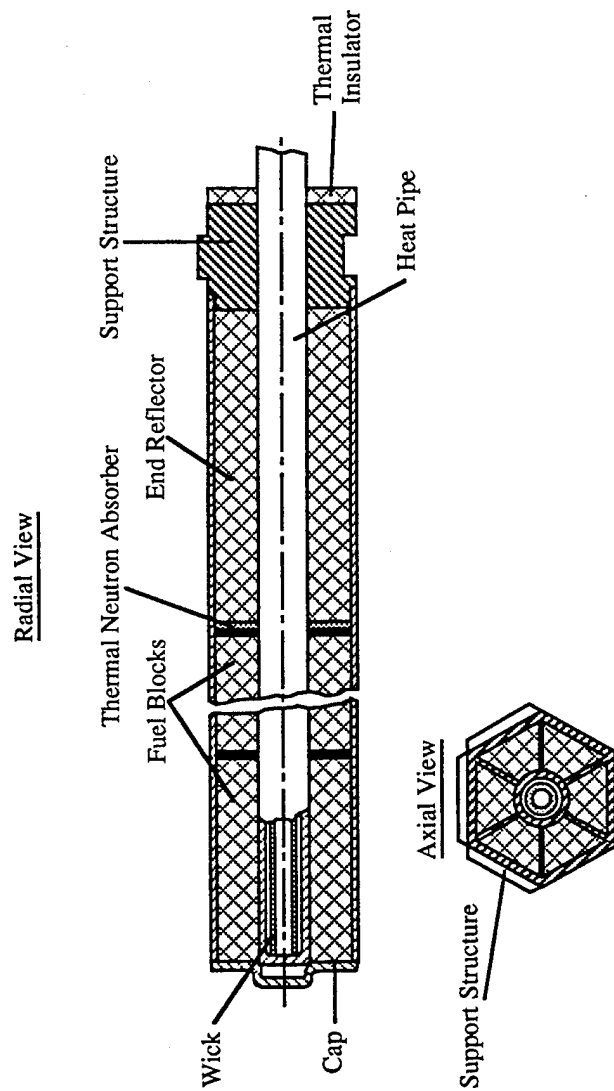
Fig. 3.14 Schematic of heat pipe cooled nuclear fuel element based on a Los Alamos National Laboratory concept.

Disadvantages of fuel elements with continuous heat conducting panels are complexities in core assembly and in inspecting the quality of the assembly. In addition, the integrity of the panels makes it difficult to pulverize and disperse the core in the dense layers of the atmosphere in the event an emergency requires the destruction of the reactor. In this regard, it is advisable to use fuel elements with contact panels made in annular segments. However, such a design configuration degrades the redistribution of heat in the event of heat pipe failures.

The need for sealed reactor vessels lessens when reactors with heat pipes are used. This situation allows one to design the reactor differently. Fig. 3.15 shows one solution to this problem. Here the axial forces from the fuel elements are transmitted to special locks formed during the assembly of the panels and connected to the core support ring. The radial core forces are transmitted to the lateral panels of the vessel and then through a system of radial rods and the reflector blocks to the force ring and fastening studs of the reactor.

Direct contact of the lateral panels of the vessel with the fuel elements enhances the problem of redistributing heat in the event of failure of the peripheral heat pipes. In order to decrease the heat loss from the core to the reflector, a laminated shielded vacuum insulator can be used. A layer of boron carbide surrounding the core serves to moderate surges in heat liberation in the boundary regions. This is accomplished by absorption of a portion of the thermal neutrons, which are moderated and reflected by the reflector material. This layer decreases the probability of reaching reactor criticality during accidental submersion in water. Possible variants in the design of the reactor include replacing the lateral panels of the vessel with several rings or bands that encircle the core.

Structural materials. The choice of structural materials is made by considering the effects which the fuel elements are subjected to during operation. Among the main damaging factors are changes in shape and size of the fuel core due to radiation and gas swelling, cyclical temperature changes and allotropic transformations, as well as damage to the clad by corrosion and erosion processes, diffusion interaction of fuel and clad material, and overheating of individual sections.

These diversely damaging factors place rigid requirements on the fuel and structural materials and on the structural design of the fuel elements.

The structural materials must provide a stable shape and stable dimensions of the fuel elements during the entire operating life of the reactor. They must be compatible and possess adequate corrosion and erosion resistance during contact with the coolant and have neutron absorption cross sections that are as small as possible.

Fuel cores are fabricated from metallic uranium alloys, refractory chemical compounds (ceramic fuels), and from mechanical mixtures of ceramic fuel and refractory metals or compounds (matrices). The latter fuel form is called dispersed fuel.

Uranium alloys include U-Fe, U-Al, U-Si, U-Cr, U-Mo, U-Zr, U-Nb, etc. Uranium alloy fuels are subjected to ionizing radiation, gas swelling, and changes in shape caused by cyclical temperature changes. The substantial dependence of damage intensity on temperature limits the temperature region where uranium alloys can be used at no higher than 900-1000 K.
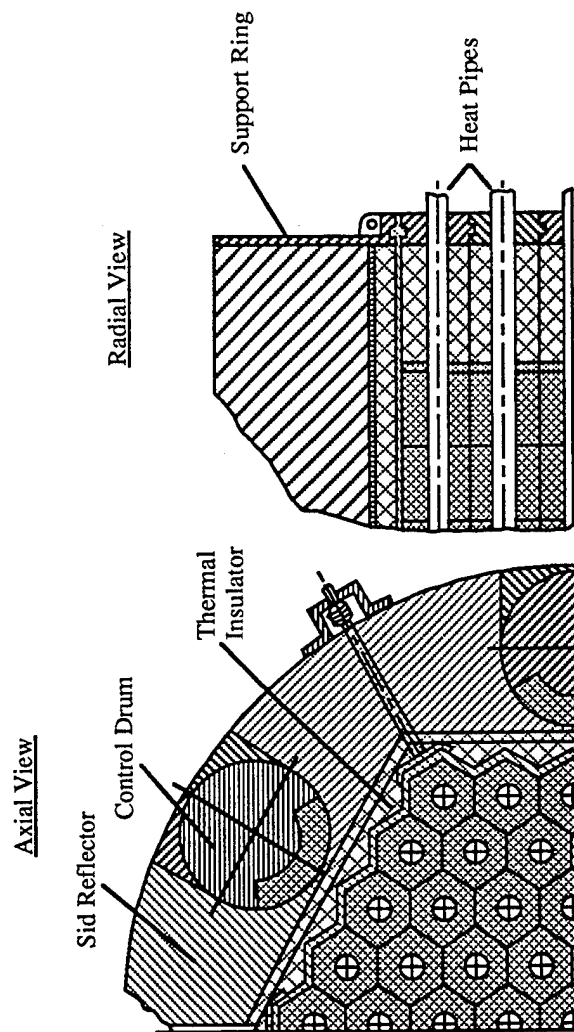
Fig. 3.15 Illustration of a heat pipe cooled reactor core.

Ceramic fuels are the most resistant to damage during operation. Potential fuels among the chemical compounds of uranium are oxides, carbides, nitrides, silicides of uranium and others. However, at the present time only UO_2 and UC-based fuels have found practical applications.

Uranium dioxide has a high melting point (3150 K), an isotropic cubic lattice, irradiation stability up to temperatures close to the melting point and, in addition, compatibility with numerous structural materials. A significant disadvantage is the low thermal conductivity of uranium dioxide.

Uranium monocarbide has a high melting point (2640 K), a thermal conductivity which is 8-10 times higher than uranium dioxide, and a much higher uranium content. The isotropic cubic lattice structure provides excellent radiation stability at high temperatures and burnup. A basic disadvantage is brittleness.

A dispersed fuel is a heterogeneous mixture of ceramic nuclear fuel in an inert diluent (matrix) that does not interact with it. Matrix materials include the refractory metals Mo, Nb, W and also Be and graphite.

Dispersed fuels have a high resistance to swelling. Fission products are localized in the nuclear fuel particles, which are included in the matrix material.

Structural materials of the reactor core components operate under conditions that are exceedingly complex. Principal among them are the effects of load forces, neutron irradiation, and the presence of different working media (argon, helium, hydrogen). Taking the stated circumstances into consideration, the requirements on structural materials are as follows:

a. Radiation stability under radiation doses up to 10^{25} neutrons/m² and at energies En > 1 MeV at high temperatures;

b. Corrosion resistance in inert media at high temperatures;

c. Resistance to hydrogen embrittlement;

d. Minimum hydrogen permeability.

The combined effects of such factors as radiation and hydrogen-containing media present the greatest danger to the operating capability of reactor materials and structures as a whole.

Analytical studies of the choice of structural materials have shown that the following alloys look promising: FeCr20Ni16NMnMo systems, dispersed-solid alloys of vanadium, molybdenum and tungsten. Experimental investigations have determined that:

a. Nickel base dispersed-solid alloys can be used under radiation doses of up to 10^{24} neutrons/m² ($E_n \geq 1$ MeV) in the 77-773 K temperature range in inert media;

b. Vanadium base alloys exceed significantly the radiation stability of Ni55Cr20WMo nickel base alloys at temperatures of 1173-1223 K and are the preferred structural materials at such temperatures;

c.   Molybdenum base alloys Mo-Zr-C, Mo-V-C are advisable for use at temperatures above 1273 K since radiation doses of about 10^{25} neutrons/m² will result in strong embrittlement of these materials at lower temperatures.

3.5.4. Reflectors and Moderators

The neutron reflector is intended to reduce neutron leakage from the reactor core and is made from materials with a high scattering cross section. Beryllium or beryllium oxide are usually used in nuclear space power plants. Beryllium oxide has a higher thermal stability and is therefore used in high temperature portions of the reflector.

The side reflector consists of a thin-walled shell surrounding the lateral surfaces of the core. Lateral (or side) reflectors are usually made in individual units with recesses to accommodate the reactor control components. The units are fastened to the reactor vessel with easily detachable connectors, for example, clamping strips.

The unit design of the reflector and its simple fabrication process promotes reactor breakup during reentry into the dense layers of the atmosphere. In addition, rupture of the clamping strips and separation of the reflector decreases the danger of the core becoming supercritical in the event the reactor falls and impacts with a solid obstacle.

As has been noted, the end reflectors in fast reactors and in homogeneous reactors are arranged in individual units at the ends of the fuel elements. Heterogeneous core reactors have reflectors that are formed from the end sections of the fuel elements and the reflector units, which are placed on the ends of the moderator.

The design of the heterogeneous core incorporates separate fuel and moderator units. Moderating materials used are graphite, beryllium, beryllium oxide, zirconium hydride, yttrium, calcium, cerium, etc. Zirconium hydride and yttrium are the most widely used moderators in space reactors. These materials have a high moderating capability, but they dissociate at high temperatures and are incompatible with liquid metal coolants. This requires that the moderator be inserted in a special sealed cavity, isolated from the coolant. The cavity is formed by the shell of the reactor vessel and two diaphragms through which coolant tubes pass and the fuel elements are positioned. The cavity must be filled with an inert gas in order to suppress thermal decomposition of the hydrides.

The moderator can be composed of individual plates (disks) with diameters equal to the core diameter and with openings for the coolant channels. With large core diameters, it is advisable to make the moderator stack from separate hexagonal units with central openings. Units of appropriate thickness that are made of a neutron-reflecting material are usually attached at both sides to the ends of the moderator. These units, together with the end sections of the fuel elements, form the end reflectors.

3.5.5. Control Elements

The control elements are used in reactor start-up and in bringing the reactor to its nominal operating regime. They maintain reactor criticality during operation and transition the reactor to the subcritical state during shut-down.

Space nuclear power reactors are usually controlled by regulating neutron leakage through the side surfaces of the core. This is accomplished by either changing the thickness or the scattering properties of the side reflectors in individual sections.

The reflector thickness is changed by moving a portion of the reflector relative to the core. This movement can be accomplished by different methods. Some of them are shown in Fig. 3.16. Stepwise movement of portions of the reflector can be done in directions that are parallel or perpendicular to the axis of the reactor (Fig. 3.16a,b). Turning of the reflector sections can be done either around an axis that is parallel to the side reflector (Fig. 3.16b) or around an axis that is perpendicular to it (Fig. 3.16c).

These control methods are quite effective, but they have a substantial disadvantage in that the movement of the reflectors changes the overall dimensions of the reactor. As a result, the size of radiation shielding must be increased, leading to an increase in reactor system size and mass. The use of compensating rotating control drums (Fig. 3.16d) containing inserts (segments) of a material with a high neutron absorption cross section (for example, B_4C) will eliminate this disadvantage. Reactor control is accomplished by changing the position of the neutron absorbing segments relative to the core. The least reactivity of the core is reached when the absorbing segments are closest to it. When the drums are rotated relative to this position, the core reactivity will increase due to a decrease in the neutron fraction absorbed. It should be noted that when the absorbers are at the greatest distance away from the core, they will still absorb neutrons. This is a disadvantage of this method of control. Despite this disadvantage, rotating control drums have found wide application in practical reactor construction.

3.5.6. Problems in Providing Nuclear and Radiation Safety of Nuclear Reactors for Space Power Plants.

In accordance with recommendations in documents approved by the UN Committee on the Peaceful Uses of Outer Space the use of nuclear reactors in high and low orbits are permitted. However, the recommendations set the following conditions:

a. Low orbit spacecraft (comparatively short duration spacecraft) must be provided with a system for parking in high orbits;

b. High orbits must provide complete radiation protection;

c. A reactor must only use uranium-235;

d. Only a subcritical reactor can be deorbited;

e. Reactor startup can only be done after it has reached its operational orbit.

Reactor subcriticality under any emergency condition is achieved by incorporating auxiliary devices in the reactor together with the control drum system. This involves the use of safety rods which are inserted in the core at the factory and which are only withdrawn after the reactor has reached operational orbit and after the orbit parameters
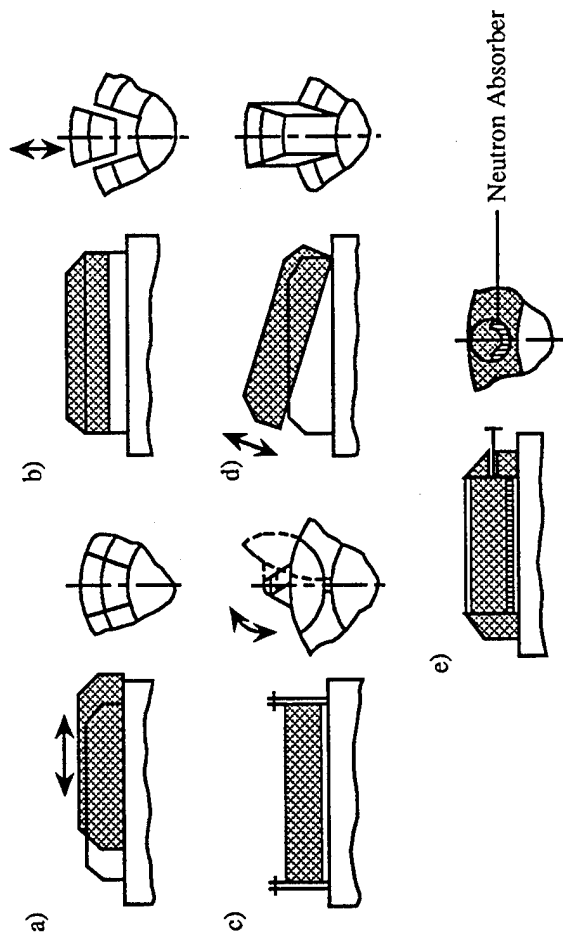
Fig. 3.16 Illustrations of various types of reactor controls: a) axial sliding reflector; b) radially sliding reflector; c) radially hinged reflector; d) axial hinged reflector; e) rotating control drum.

143

have been verified by direct trajectory measurements. Possible results of emergency situations during all stages of departure from operational orbit are:

a. Filling of all reactor voids with water;

b. Compression of the reactor vessel until the fuel elements are so densely packed that no space exists between them;

c. Effects of explosion and combustion of rocket fuels at the highest possible temperatures.

Considering these circumstances, the design of the safety rods and the rotating drums must be based on these requirements:

a. The safety rod mechanism must ensure that the rods remain in the core under any conditions (impact effects, etc.);

b. The effectiveness of safety rods and rotating drums in intermediate neutron reactors must be such that the reactor will remain subcritical under any conditions. These objectives are reached in fast reactors by introducing resonance absorbers in the fuel that yield a significant negative contribution to reactivity in the event the reactor is filled with water;

c. The indicated control organs must also secure nuclear safety following any operator errors and failures in the control and test equipment during preparation of the spacecraft for launch.

Securing radiation safety. Radiation safety of spacecraft with nuclear power plants used in high orbits is provided in a natural manner by a long term passive stay of the spacecraft in these orbits. In this case, the radioactivity of individual components of the spacecraft will decay to allowable levels. By an allowable level we mean an activity level at which the γ-radiation dose that an individual person will receive on the earth's surface is less than 0.5 rem/yr. This condition is completely satisfied by using the so called "century-long" orbits where the spacecraft remains for more than 300-400 years.

Radiation safety of low orbit spacecraft with nuclear power plants is provided by the above mentioned orbit parking system and also by a system for dispersal (special destruct system) of the reactor and its components in the event the orbit parking system fails to act. This dispersal system contains command and control organs with their own sources of electrical power, engines for orbit transfer, and the necessary rocket fuel. The system for placing the nuclear power plant in a parking orbit completes the following operations: shutting the reactor down, separation of the nuclear power plant compartment from the spacecraft, orientation and stabilization of the compartment for transfer to a parking orbit, and, finally, starting the parking orbit transfer engines.

The system for dispersal of the nuclear reactor of a power plant on a low orbit spacecraft is designed on the premise that the structure will break up into its component parts. This considers that optimum conditions will be reached for aerodynamic heating,

thermal breakup, oxidation, melting and evaporation of the reactor materials into a cloud of microparticles. This cloud will dissipate completely in the atmosphere and the radioactive fallout on earth will be less than 0.5 rem/yr. Possible failures in the system for removal of the nuclear power plant from low orbit and in the system for breaking up the reactor structure are considered in all stages of operation of these systems including failure in portions of the command and control devices. The probability of the simultaneous failure of all systems, which are independent of each other, is estimated to be 10-4. This substantiates the reliability in ensuring radiation safety when nuclear power plants are used in low orbits.

The actual development of a system for placing the nuclear power plant in a parking orbit and for separating the reactor structures for aerodynamic disintegration of its components was accomplished by the "Cosmos-1900" satellite. This satellite was launched on December 12, 1987. The situation on the satellite after losing radio contact with earth on April 9, 1988 and after the command for parking orbit transfer failed on April 13, 1988 was described as follows:

There was no response to a command from earth for nuclear power plant orbit transfer; there was no response to commands from earth for orbit corrections; the orientation and stabilization system operated normally based on flight trajectory measurements; and the nuclear power plant operated normally.

During lowering of the satellite orbit to an altitude of 100 km under stable flight conditions the system for parking orbit transfer of the nuclear power plant can be made to operate by two commands that derive from an indication of a voltage drop in the electric power supply and an indication of a mismatch in the stabilization angles of the spacecraft.

The flight of the satellite at an altitude of 95-100 km is characterized by an additional aerodynamic heat flux on the space radiator. This leads to a reduction in the temperature drop in the thermoelectric converters and a corresponding drop in power and voltage below allowable limits.

During descent in the 90-95 km altitude range, the aerodynamic heat flux results in automatic operation of the system for separating the reactor structure and ejection of the fuel element assembly by command from the aerodynamic heating recorders.

The "Cosmos-1900" satellite entered the atmosphere on September 30, 1988 at an altitude of 100 km. This had been predicted to occur on October 5, 1988. During the night of September 30, 1988 in the initial portion of the next revolution at an altitude of about 180 km, the system for reactor separation proceeded to operate and it placed the reactor in a parking orbit. The parking orbit has an apogee of 773 km and a perigee of 725 km, which provides an orbit residence time of about 200 years. The fuel element assembly was ejected from the reactor vessel into a parking orbit with an apogee of 764 km and a perigee of 708 km, which provides a residence time of more than 300 years. The indicated orbit lives are entirely adequate to reduce the radioactivity of the reactor components to acceptable levels. Thus, radiation safety was assured on the "Cosmos-1900" satellite.

4. EQUIPMENT FOR HEAT REMOVAL IN SPACE

4.1. General Description of Conditions and Means for Heat Removal.

The basic removal of heat from a space vehicle, which is equipped with a nuclear power plant, involves the unused (always a significant) portion of the thermal energy generated by the nuclear reactor or radioisotope generator. With the relatively low thermal energy conversion efficiencies, the heat rejected to surrounding space is up to 80-90% of the thermal power of the primary energy source.

In general, the heat rejected also includes that from the on-board equipment. When it operates, the larger portion (up to 90%) of the required electrical power is turned into thermal energy. Compared with the nuclear power plant, however, the heat rejected from payload equipment must be accomplished at substantially lower temperatures. This pertains also to life support systems on manned space stations.

Heat rejection from a space vehicle without expending any kind of coolant is possible only by radiation. This method is, therefore, the only one applicable during long term operation of a nuclear power plant or radioisotope generator.

As is known, a plane surface with area A at a constant temperature T in the vacuum of space will radiate, according to the Stefan-Boltzmann law, a thermal power

$$q'' = \dot{Q}/A = \varepsilon \sigma T^4 \qquad , \qquad (4.1)$$

where ε is the emissivity, and $\sigma = 5.72 \times 10^{-8}$ w/m²K^4.

In earth orbit, however, one must account for various heat fluxes which influence the operation of the surface under consideration and which decrease the thermal power rejected. Such heat fluxes include direct solar radiation, solar radiation reflected from earth (especially in the polar regions), and earth's own thermal energy radiation. At comparatively low altitudes (less than 200 km), one must also account for aerodynamic heating due to interaction with the surrounding medium (albeit a very rarefied medium).

As a result, the surface will absorb a certain specific thermal flux q_a'' which depends on the absorption coefficient α_n and the orientation of the surface in space.

The specific thermal power radiated from a unit surface will then equal

$$q'' = \varepsilon \sigma T^4 - q_a'' = \varepsilon \sigma T^4 \left(1 - \frac{q_a''}{\varepsilon \sigma T^4} \right) \qquad . \qquad (4.2)$$

We will designate the ratio $q_a''/\varepsilon\sigma = q_a^*$ and call the dimensionless parameter q_a^*/T^4 the surrounding medium parameter. Typically, the value of q_a^* lies in the range 7×10^9 K^4 to 9×10^9 K^4.

It is of interest to analyze the influence of the temperature T_i on the magnitude of the surrounding medium parameter. Let's turn to an analysis of the graph in Fig. 4.1. From this analysis, we can arrive at the following conclusions:
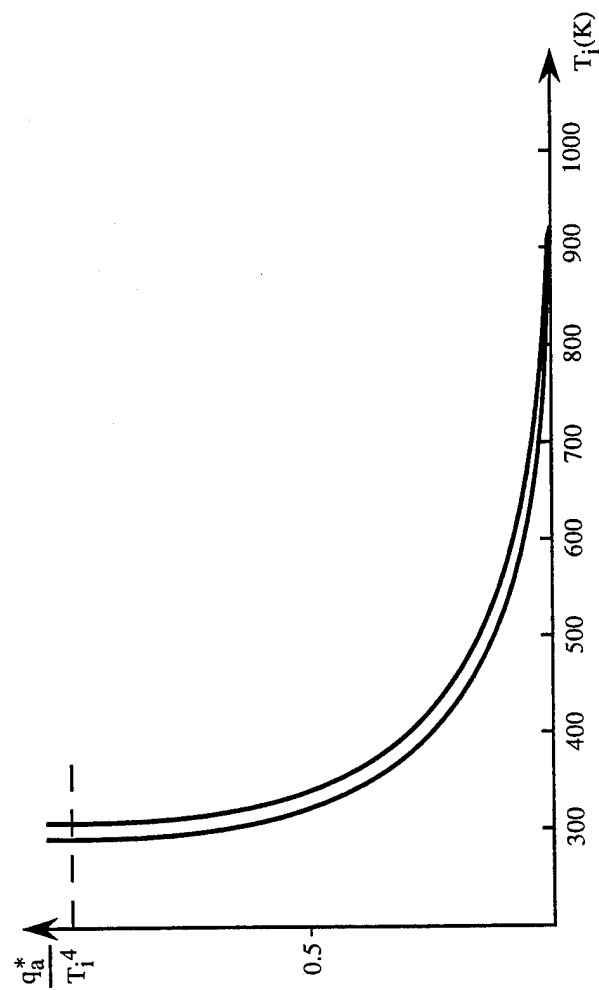
Fig. 4.1 Variation of surrounding medium parameter as a function of T_i, indicating that higher temperatures dramatically decrease radiator area requirements for a given amount of heat rejection.

a. At temperatures $T_i > 600$ K, the parameter q_a^*/T^4 is small compared to unity and its influence on the radiated power can be neglected. This result pertains to all classes of nuclear power plants and radioisotope generators, which significantly enhances investigations of their output data;

b. At temperatures below 300 K, the parameter $q_a^*/T^4 > 1$ and, consequently, heat rejection by radiation is impossible, rather, it will be necessary to employ other means. We will discuss the features of these below.

There are a number of methods for decreasing q_a^*. First of all, there are special so-called "selective coatings" for radiating surfaces which possess low absorption capabilities (absorption coefficient $\alpha = 0.15 - 0.20$) and high emissivities, $\varepsilon = 0.95 - 0.98$. We will discuss the optical characteristics of radiating surfaces in more detail.

The fact is that in space, in addition to natural factors characteristic of space (different forms of cosmic radiation, micrometeorites), man-made factors have come to play a not insignificant role. The latter reflect the great increase in space waste which consists of space vehicle fragments and organic fuel residue. Such man-made material can have a significant effect on space vehicle components upon impact with the waste in given orbits. Thus, finely dispersed space waste particles can alter optical characteristics (coefficient of absorption and emissivity) of heat radiating panels. This, in turn, shows up in the quantity of heat rejected from the space vehicle, especially at the low temperatures of the cooled component.

For obvious reasons, it is very difficult to obtain reliable and comprehensive data on changes in optical characteristics of heat radiating panels by direct experiment in space. Experimental investigations conducted on earth are of particular value in this connection. We will not discuss the essentials of such work, but will instead only provide some general conclusions. Thus, metallic powders, which are characteristic of space vehicle and rocket structures, were used as finely dispersed particles in one such experiment. These included powders of titanium alloys, aluminum, tungsten, and several others. The velocity of encounter with the target (radiator panels) reached "cosmic" velocities, i.e., on the order of up to 8 km/sec. The parameter selected to characterize the effect of micrometeor particle impact was the specific particle kinetic energy $E_{ke}'' = \dfrac{fv^2}{2}$, where f is the flux density, kg/cm², and v the average impact velocity, m/sec). The coating applied on the heat radiating surfaces was enamel, which is normally used in practical applications.

Some results showing changes in the absorption coefficient α and emissivity ε in as function of the kinetic energy parameter E_{ke}'' are presented in Table 4.1.

Table 4.1 Variation of α and ε as a Function of Kinetic Energy Parameter E_{ke}''

E", J/m²	0	10	20	40	80
α	0.18	0.55	0.75	0.85	0.86
ε	0.86	0.85	0.84	0.83	0.80

An idea of certain specific changes in the optical characteristics of the majority of coatings used on radiating surfaces due to the effect of micrometeorite particles is provided by the following experimental data: $\varepsilon = 0.9$ to 0.65, $\alpha = 0.15 - 0.9$.

On the basis of these data, one can conclude that degradation (worsening) of the optical characteristics of radiator panels can be very significant and must be accurately accounted for in design studies. This is specially important in cooling low temperature components.

An obvious method of reducing q_a^* is orient the heat rejection surfaces such that they are shaded from heat sources such as the sun and earth. One must, however, consider that this additional orientation of the heat radiating panels requires the expenditure of energy which will increase the mass of the spacecraft.

At temperatures lower than ~300 K, heat rejection is either impossible ($q_a^*/T^4 > 1$) or the required heat radiating surface becomes prohibitively large. Cooling can in this case be accomplished in two ways: by increasing the temperature of the radiating surface using a refrigerator (heat pump), or, instead of radiating heat, by using materials which will absorb heat by virtue of their heat capacity, latent thermal phase changes and endothermic chemical reactions. The first method requires the expenditure of energy, and the second requires a supply of heat absorbing materials which, therefore, cannot be used in long duration operation of spacecraft in which heat liberation is constant over time.

In view of the characteristics of thermal radiation, a rational configuration for a radiating surface is one that works under conditions other than convective heat transfer in a gas or liquid medium. A traditional configuration of a radiator surface in which convective heat transfer plays the predominant role is one with comparatively short and thick fins. It is not advisable to use such a configuration in radiating heat. That's because of mutual radiation by closely placed parallel fins, their lateral surfaces radiate almost no heat to the outside. The effective radiating surface is an equivalent plane the area of which is practically equal to the projection of the finned surfaces.

In addition, the surface area of the component being cooled is often too small to reject the required heat. Since one cannot do without fins, the shape of the fins and their arrangement must be such that mutual radiation is as low as possible (Fig. 4.2). The optimum fin is thin and long with a decreasing thickness toward the periphery. Mutual radiation is entirely absent when only two fins are located in single plane (Fig. 4.2a). However, a larger number of fins is more advantageous from a weight and size standpoint despite mutual radiation (Fig. 4.2b). The optimum number of fins is close to six, which, owing to the design in Fig. 4.2b, is used in many radioisotope generators.

The component being cooled often approximates the shape of a regular polyhedron (cube, octahedron, etc.) or a short cylinder.

One possible kind of optimum fin arrangement for such components is shown in Fig. 4.2c. If the component has only one flat radiating surface which is nearly circular, then an advantageous fin configuration is that shown in Fig. 4.2d.

In the majority of situations (basically, nuclear power plants), however, heat rejection is not accomplished directly but through the use of a coolant or heat pipes. The coolant, a liquid, vapor or gas, is pumped through the space radiator. The space radiator is independent of the power plant and it is equipped with radiating surfaces. It can be completely subordinated to conditions for optimum heat rejection.
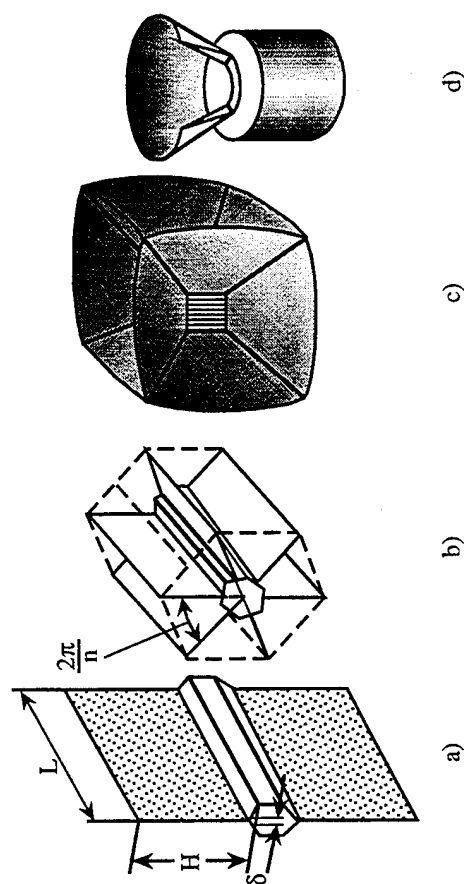
a) Single-plane geometry
b) Six fins, optimal for minimum mass
c) Fin arrangement for polyhedral heat source
d) Fin for a disk heat source

Fig. 4.2   Radiator fin configurations.

It is natural to assume that the radiating surfaces, henceforth called the space radiator, should be a rectilinear channel radiating from both sides (Fig. 4.3a). Mutual radiation is completely absent in this case.

This simple design of a space radiator will radiate the maximum possible specific thermal power q" for a given coolant temperature and external conditions. The required radiating surface area A is a minimum. This single criterion is inadequate, however, in an overall assessment of its effectiveness. An important parameter is also the mass, or more accurately, the specific weight of the radiator, which is the ratio of the mass to the radiated thermal power.

$$M_{sp} = \frac{m}{q"} \qquad . \qquad (4.3)$$

To reduce this parameter, it is advisable to install connectors (fins) between individual channels which can participate in heat radiation. For one and the same radiated power the number of channels can be reduced which will result in a reduction in the mass of the space radiator. In truth, the radiating surface area will increase because the average fin temperature will be lower than in the previous design. However, the loss in specific surface area is not much and for a given connector (fin) length, the overall specific characteristics (we will look at these later on in more detail) will remain optimum.

The circular channel design is a more easily manufactured structure than the rectilinear channel. Thus, the tube-fin space radiator is the preferred design. In the practical development of nuclear power plants, tube-fin radiator panels look like truncated cones. Recently, practical interest has risen in the use of heat pipes in heat rejection equipment.

Space radiators using heat pipes. A new kind of heat transfer device, the so called heat pipe, offers great promise in sharply increasing the effectiveness of heat rejection in space. The heat pipe (Fig. 4.4) consists of a sealed tube which operates on the closed evaporation-condensation cycle in thermal contact with an external source and a heat flux. In this sense, the heat pipe can be considered as a simple vapor generator with distinctive parts. The heat received from an external source by the heat pipe is expended in evaporating a working fluid which is confined inside the heat pipe container. The energy expended in evaporation is equal to the latent heat of vaporization. This energy is transmitted by the vapor flow to the cooled portion of the pipe (condenser) where the vapor condenses and liberates the latent heat of vaporization. The heat liberated in the condenser is carried to the outer surface of the heat pipe and, depending on the design employed, the heat is radiated to surrounding space. The condensate returns to the evaporation region by capillary action, which is provided by a wick structure inside the heat pipe. When the heat pipe operates in the steady state, the coolant (the working fluid inside the heat pipe) flows continuously in the gas phase from the evaporation region to the condensation region and returns as a liquid via capillary action in the wick structure to the evaporation region. In order to insure transfer of the coolant as a vapor and as a liquid, an appropriate pressure gradient must be established. The transfer pressure in the vapor ΔP_v arises as a result of maintaining the condenser temperature somewhat lower than the evaporation temperature.
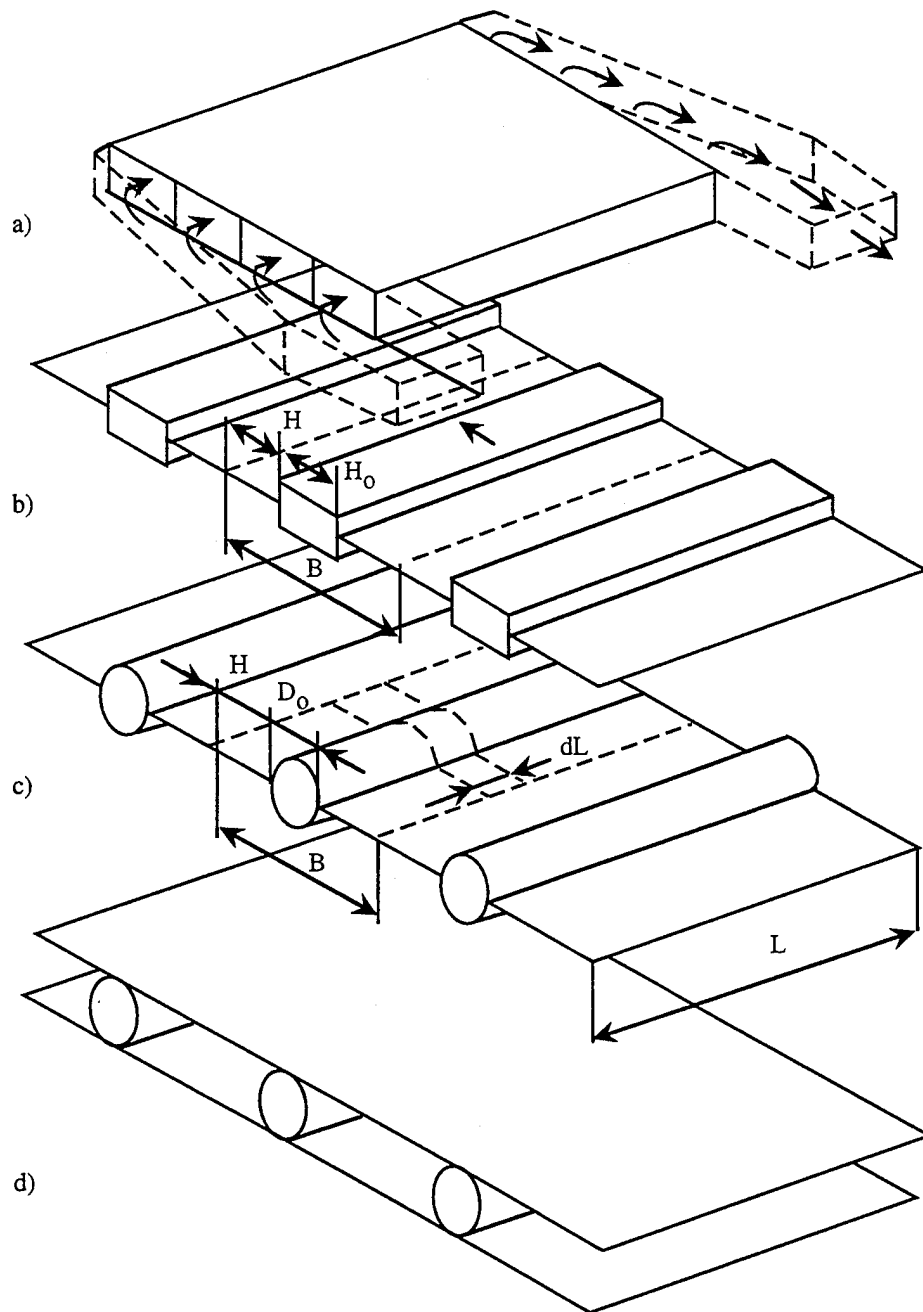
a) Two-sided channel radiator panel; notions
b) Rectilinear channels with fins
c) Cylindrical channels with fins
d) Cylindrical channels with external fine/micronetioroid armor

Fig. 4.3 Space radiator panel configurations.
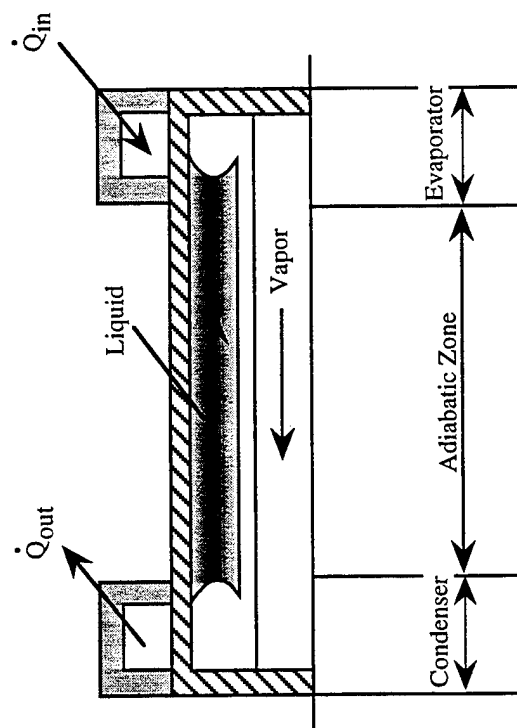
Fig. 4.4 Heat pipe schematic.

In this case, the saturated vapor pressure in the evaporation region is higher than in the condensation region. The liquid pressure drop is caused by capillary forces.

The needed pressure balance requires that the pressure on the liquid side at the liquid-vapor interface be greater than the pressure on the vapor side along the entire length of the pipe. Thus, in addition to the usual heat transfer mechanism that obtains in metallic heat conductors, the heat pipe uses molar processes of vapor generation and condensation. The latent heat of vaporization is several orders of magnitude higher than the quantity of heat that can be transferred as enthalpy of the working fluid in the usual convective systems. Therefore, the heat pipe can transfer a larger heat flux with a small temperature difference between the evaporation and condensation regions. No special energy expenditure is required in transferring the working fluid in its different phases. The latent heat of vaporization of applicable working fluids is in hundreds and thousands of joules per gram of the substance and with the evaporation of on the order of grams per second of liquid, the vapor can transmit heat fluxes on the order of tens of kilowatt. Thus, the heat pipe has an effective thermal conductivity several orders higher than the thermal conductivity of metal rods of the same size. In addition, other advantages of the heat pipe include simplicity of fabrication and construction, isothermal heat exchanger surfaces, etc.

Heat pipe theory is currently well developed and heat pipe design methods have been published in a variety of papers, textbooks, handbooks, etc. In this section, we consider it useful to discuss the physical principles of heat pipe processes and general design and construction fundamentals.

Some problems in theory. In the steady operating regime of the heat pipe, the coolant (working fluid) circulates continuously from the evaporation section to the condenser section and reverts to the vapor and liquid phases, respectively. In order to provide such a circular motion, it is necessary to create a vapor pressure drop along the vapor channel ΔP_v and a pressure drop in the liquid flow ΔP_l. The necessary condition for steady state operation of a heat pipe is satisfied by the equality

$$\left(\Delta p_{cap}\right)_{max} \ge \Delta p_{liq} + \Delta p_v \qquad , \qquad (4.4)$$

where $(\Delta P_{cap})_{max}$ is the maximum capillary gradient.

By using known properties of capillarity as motive forces in transporting the liquid in a heat pipe, one can obtain an expression for $\left(\Delta p_{cap}\right)_{max} = \dfrac{2\sigma}{r_{cap}}$. Here σ is the liquid surface tension, and r_{cap} is the effective radius of the pores in the wick).

If the above condition is not satisfied, then the wick will dry up in the vaporizer and the heat pipe will cease to function.

The flow regime in the heat pipe liquid phase is almost always laminar. With steady laminar flow of an incompressible fluid with a constant viscosity μ in a circular pipe of radius r at a velocity v, the liquid pressure drop Δp_{liq} over a section of length L can be calculated from the simple expression,

$$\frac{\Delta p_{liq}}{L} = \frac{8\mu v}{r^2}$$

(4.5)

Since the liquid channel is generally not rectilinear and may not have a circular cross section, expression (4.5) must be changed to reflect these circumstances.

The total pressure drop in the vapor phase is equal to the sum of the pressure drops in three regions, in particular, in the evaporator Δp_{ev}, the adiabatic section Δp_a, and in the condenser Δp_{con}. The problem of calculating the pressure drop in the vapor phase in the evaporation and condensation regions is compounded by radial vapor flows in these regions. However, the solution to such problems is currently well known and has been published in the appropriate technical literature. We will restrict ourselves to presenting the final expression for the total vapor pressure drop

$$\Delta p_{tot} = \frac{8\mu_v \dot{M}}{\pi \rho_v r_{cap}^4} \left(\frac{L_{evap} + L_{cond}}{2} + L_a \right)$$

(4.6)

where μ_v is the vapor viscosity, $\dot{M}$ is the mass flow rate, ρ_v is the density, r_v is the radius of the vapor channel.

This equation is widely used in practice for calculating the pressure drop in the vapor phase in heat pipes. Various limitations on the heat flux transferred are possible in processes of operating heat pipes. The basic ones of these are: attainment of the sonic velocity by the vapor, an insufficient capillary gradient, burnout in the evaporator (blockage in the wick), the effect of viscous forces at low temperatures, coolant droplet breakaway from the wick surfaces due to vapor flow effects. We will dwell on the stated limitations in more detail. Blockage in the wick can occur in the evaporator region at elevated temperatures. This happens when the vapor reaches the sonic velocity. The sonic heat flow limit can be calculated from the equation

$$q_{sonic}'' = 0.474 L_v \left(\rho_v p_v \right)^{1/2}$$

(4.7)

where L_v is the latent heat of vaporization, which is in good agreement with experimental data.

Viscous forces predominate in vapor flows at low temperatures. The heat flow in the axial direction will increase rapidly as the condenser pressure decreases. The maximum heat flow is reached when the pressure is reduced to zero. The magnitude of this heat flow can be calculated from the equation

$$q'' = \frac{r_v L_v \rho_v p_v}{16 \mu_v L_{eff}}; \quad L_{eff} = L_a + \frac{L_{evap} + L_{cond}}{2}$$

(4.8)

Here, ρ_v and p_v pertain to the vapor region.

Tangential pressures arise at the wick-vapor flow interfaces during the flow of vapor from the evaporator to the condenser. Their magnitudes depend on the vapor

properties and its velocity. Tangential pressures will result in the breakaway of liquid droplets and their entrainment in the vapor flow towards the condenser end. Droplet entrainment is, as has been noted, one of the limiting factors in the heat transfer capability of the heat pipe. The axial heat flow limit based on acceptable droplet entrainment is determined from the equation

$$q_{entrain}^{"} = \sqrt{\frac{2\pi\rho_v L_v \sigma_{liq}}{z}} \quad , \tag{4.9}$$

where z is determined by the pore spacing in the wick. The value of the product $\pi_v L^2 \sigma_{liq}$ is a measure of the inclination of a given working fluid to droplet entrainment.

Burnout heat transfer can occur with high radial heat fluxes in the evaporator. Naturally, this is to be avoided. A similar limitation pertains also to the condenser. Some values of critical radial thermal fluxes are presented in Table 4.2.

Table 4.2 Critical Radial Heat Flux for Several Heat Pipes.

Coolant	Wick	Vapor Temp, °C	Radial Heat Flux, W/cm^2
Potassium	Steel Felt	750	230
Sodium	Stainless Screen	775	1250
Lithium	Nb-1%Zr Felt	1250	205
Lithium	W-26%Re Artery	1600	120

Some structural characteristics of heat pipes. In general, the construction of the heat pipe (Fig. 4.4) is not marked by any great complexity. Its basic components are the heat pipe container itself, a capillary system (wick) and the heat transfer fluid that changes phase. The quantitative and qualitative characteristics of the heat transfer process depend to a significant degree on the properties of the working fluid. For this reason, we will spend some time on the selection of working fluid properties. It is necessary to take into account the following conditions under which the heat pipe in question will operate: the operating temperature, the maximum heat flow conducted, the allowable heat flux, the geometric dimensions, life and reliability requirements. Taking these conditions into account, the following requirements must be placed on the working fluid:

1. It must be chemically compatible with the wick and container materials.

2. A large latent heat of vaporization and a high thermal conductivity.

3. Low liquid and vapor viscosities.

4. High surface tension.

5. An acceptable melting point.

A convenient characteristic for a rapid comparison of working fluids is provided by the so called "quality criterion," which is calculated from the equation

$$\Phi = \frac{\sigma_{liq} L_v \rho_{liq}}{\mu} \quad , \qquad (4.10)$$

where σ_{liq} is the surface tension, L_v is the heat of vaporization; ρ_{liq} is the liquid density, and μ is the viscosity.

Some values for the criterion Φ (W/m²) is given in Table 4.3.

Table 4.3 Φ (W/m²) for Several Working Fluids and Temperatures.

	600 K	1000	1500
Mercury	1.1×10^{12}		
Potassium		5×10^{11}	
Sodium		2×10^{12}	
Lithium			7×10^{13}

High temperature organic working fluids, such as Dowtherm, can be used in the 500-600 K temperature range. Dowtherm is a working fluid which is a eutectic mixture of diphenyl and diphenyl oxide with a boiling point of 533 K at atmospheric pressure. This fluid, however, has a low surface tension and a low latent heat of vaporization. Like many other organic compounds, diphenyl easily decomposes at some temperature exceeding a critical value. Unlike many other organic mixtures which have the same operating temperature range, Dowtherm has a characteristic boiling point and a region with no boiling.

The thermodynamic properties of mercury are appropriate in the 500-900 K range. Mercury is in the liquid state at room temperature, which simplifies the fabrication of heat pipes and filling them. However, mercury is very toxic which complicates its handling. In addition, difficulties arise in wetting the wick and the walls.

The use of the alkali metals, cesium, potassium, sodium, is preferable at much higher temperatures. Lithium as well as silver are the most applicable at temperatures above 1400 K.

Wick construction. The purpose of the wick is the following: the creation of the necessary channels for the return of condensed fluid to the evaporation region; provision for the required capillary pressure by the pore surfaces at the liquid-vapor interface; provision for thermal contact between the internal walls of the heat pipe container and the liquid-vapor interface surface.

Different porous structures can serve as wicks, such as wire gauze, fiber glass, baked metallic powder materials, narrow channels cut on the inside surface of the container wall.

The most efficient wick structure must have small size surface pores which provide large capillary pressures, large internal pores (in a direction normal to the liquid flow) for minimum resistance to liquid flow, reliable thermal contact with a high thermal

conductivity through the entire wick cross section in order to maintain a small temperature drop between the internal wall of the heat pipe container and the liquid-vapor interface boundary.

Because of these requirements, wicks can differ in construction. It can be divided in two basic classes, in particular: homogeneous and compound (composite) wicks.

Some homogeneous wicks are shown in Fig. 4.5.

Wicks made of screen netting and convoluted into the heat pipe are easy to fabricate and are highly reliable (see Fig. 4.5a). The size of the pores on the surface of such a wick is inversely proportional to the porosity, which is the quantity of pores per unit length. The hydraulic resistance to the flow of liquid in such a wick can be regulated by changing the density of the wick twist. This provides flexibility in construction. However, the temperature drop in the transverse cross section can be large.

If it is necessary to provide a low temperature drop in the wick cross section, one can use a porous material made from baked metallic powder (Fig. 4.5b). The pores in the baked porous metal are usually small. They create large capillary forces at the liquid-vapor interface surface which ensure fluid flow. However, with small internal pores, the hydraulic resistance in the wick channels is often high.

A wick made by axial grooves cut in the internal surface of the heat pipe container (Fig. 4.5c) is another widely used wick construction. In this case, there is a low thermal resistance in the transverse cross section of the wick. It is difficult, however, to control the pore size in order to provide the necessary capillary pressure and fluid flow.

The construction of composite wicks have one general characteristic, in particular, the necessary capillary pressure in them is provided by structural elements designed solely for this purpose and fluid flow is secured by other components that have a lower hydraulic resistance.

The heat pipe container. The purpose of the heat pipe container is to isolate the working fluid from the surrounding medium. Therefore, the container must be sealed, withstand the pressure differential between its internal cavity and the surrounding medium, and also transfer heat to the working fluid and remove heat from it.

The following factors determine the choice of container material:

a. Compatibility with the working fluid and the surrounding medium;

b. Fabricability including weldability, simplicity of mechanical treatment, plasticity;

c. Porosity;

d. Capability of being wetted by the working fluid.

Most of these characteristics do not require special explanation. A high ratio of endurance strength to density is very important when there is a restriction on the weight of the heat exchangers. The absence of pores in the material prevents diffusion of gases into the heat pipe. A high thermal conductivity promotes a reduction in the temperature gradient between the heat source and the wick.

a) Screen type
b) Sintered porous metal type
c) Grooved type
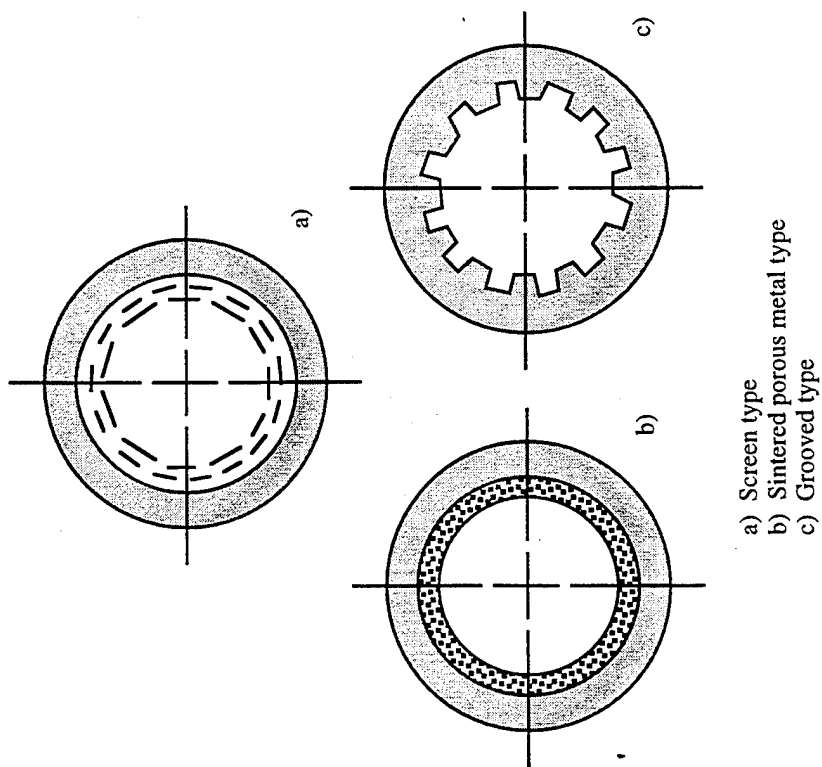
Fig. 4.5 Heat pipe wick designs.

159

In conclusion, we will provide some data on the specific heat flux transferred in the axial and radial directions .

The axial flow density in heat pipes with lithium as the working fluid in long term operation is about 15 kW/cm². The radial heat fluxes in the evaporation and condensation regions of heat pipes with the working fluids Rb-Mo, Li-Mo can reach 200-250 W/cm² at temperatures of about 1000-1200 K.

A possible design of a space radiator panel with heat pipes is shown in Fig. 4.6. The evaporator portion of the heat pipe is inserted in the coolant loop channel. A very important advantage of such panels over panels with the usual working fluids is the possibility of heat pipe redundancy and, as a result, a low probability of panel failure.

4.2. Weight and Size Characteristics of Heat Radiating Fins.

Let's examine a fin (Fig. 4.2) of constant thickness δ, the base of which is attached to the object being cooled (the heat removal surface of the cooled loop of a heat converter, a tubular channel with the radiator panel coolant, etc).

The heat is transferred by thermal conductance from the base of the fin to its periphery while the fin is radiating heat from its top and bottom sides.

We will make the following assumptions:

1. The temperature at the hot base of the fin T_0 is constant with time.

2. The heat radiated from the vertical free sides of the fin is negligible.

3. The emissivity of the fin surface ε_f and the thermal conductivity of its material k do not depend on temperature.

Let's isolate an elementary volume $\delta dHdL$ inside the fin and perform a heat balance on this volume. According to Fourier's law of heat conductance, the change in heat flux during passage through the shaded sides is

$$dq_1^{"} - dq_2^{"} = k\delta\left[\left(\frac{dT}{dH}\right)_1 - \left(\frac{dT}{dH}\right)_2\right]dl = k\delta\frac{d^2T}{dH^2}dHdl$$

In a steady regime, this thermal power is radiated by the outside faces of the elementary volume:

$$dq_1^{"} - dq_2^{"} = 2\varepsilon\sigma T^4 dHdl$$

By equating the right-hand sides of these two relationships, we obtain

$$\delta\frac{d^2T}{dH^2} = \frac{2\varepsilon\sigma T^4}{k}$$

Heat Pipe/Fin Assembly

Liquid Coolant Channel

Heat Pipe Evaporator

Liquid Coolant Channel
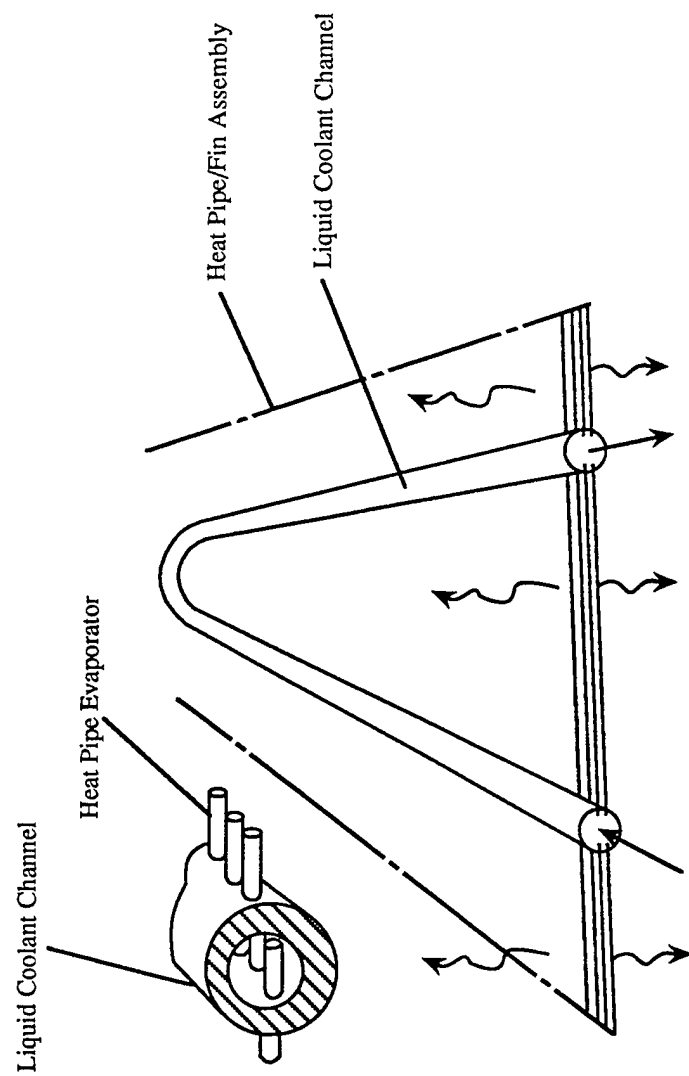
Fig. 4.6 Possible radiator design incorporating heat pipes and fins.

161

By introducing the dimensionless parameters $H^* = H/H_o$, $T^* = T/T_o$, the latter equation becomes

$$\frac{d^2 T^*}{dH^{*2}} = cT^{*4} \qquad . \qquad (4.11)$$

The term $c = \dfrac{2\varepsilon\sigma T^3 H^2}{k\delta}$ is called the fin conductance parameter.

This second order nonlinear differential equation determines the change in temperature along the fin height for a given fin conductance. This quadratic equation cannot be integrated, and it will be necessary to employ appropriate computational means to solve it.

The thermal power radiated by a fin of length dL is

$$dq'' = 2\varepsilon\sigma T_o^4 H dL \int_0^1 T^{*4} dH^* \qquad . \qquad (4.12)$$

The dimensionless integral $q_f =. \int_0^1 T^{*4} dH^*$ is called the fin effectiveness. It evaluates the decrease in radiated thermal power due to the temperature drop from the base to the end of the fin.

Fig. 4.7 shows q_f as a function of c making it possible for given values of ε, k, δ, ρ and q'' to easily determine the required radiating fin surface area, HL.

Let's turn to an evaluation of the fin specific weight, M_{sp}. The weight of a fin of length dL is

$$dM_{sp} = \rho H \delta dL \qquad .$$

By substituting for δ and H the expressions in equations (4.4) and (4.12), we obtain

$$M_{sp} = \frac{\rho\delta}{2\varepsilon\sigma T_o^4 q_f} \qquad . \qquad (4.13)$$

Obviously, there must be some optimum value of the fin thickness δ_{opt} which corresponds to minimum specific weight. In fact, as δ increases, the numerator in the equation for M_f will increase linearly. However, the denominator will also increase (converges to 1 with increasing q_f). In order to determine the numerical value of δ_{opt}, we rewrite the equation (4.13), taking the value of the fin conductance parameter c into account, in the form

$$M_{sp} = \frac{\rho \dfrac{dq''}{dL}}{4k\varepsilon^2\sigma^2 T_o^{9} c q_f^3} \qquad .$$
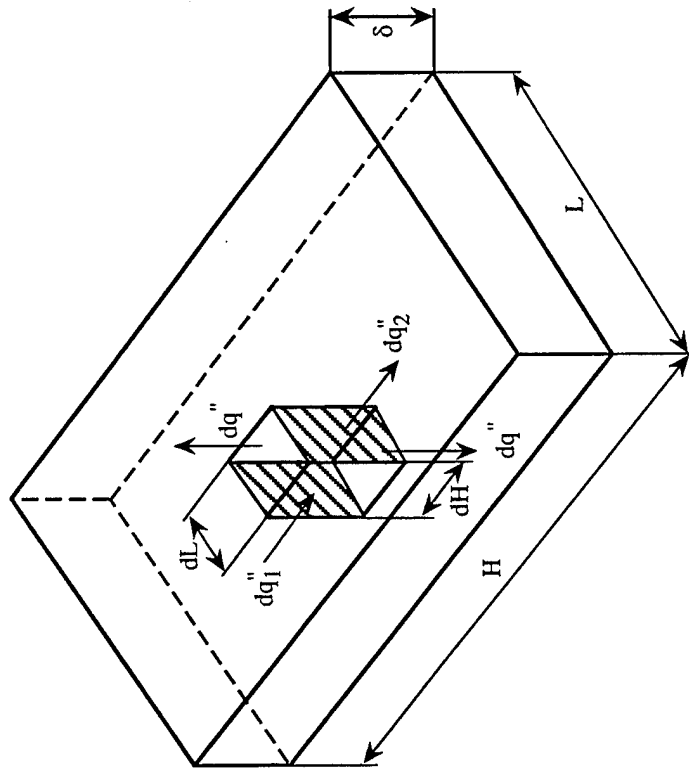
Fig. 4.7 Finite element used to analyze radiator fin performance.

For given values of q_f, k, ε, T_o, and $d(q'')/dL$ (the thermal power which is removed per unit length of the fin and which can be given in the calculations), the minimum specific fin weight corresponds with the maximum of the product cq_f and is easily determined graphically using Fig. 4.8.

By further writing the expression for the fin thickness using equations (4.11) and (4.12), we obtain

$$\delta = \frac{\rho\left(\dfrac{dq''}{dL}\right)^2}{2\varepsilon\sigma T_o^5 kcq_f^2} \qquad . \tag{4.14}$$

Calculations performed using this equation show that the minimum fin specific weight, δ, occurs with very thin fins, only fractions of a millimeter thick. This causes fabrication problems and is unacceptable where fin strength and stiffness are required. In such situations, one must choose a value of $c < c_{opt}$.

Some deviation from c_{opt} by a 30-40% decrease is generally advantageous because the fin specific weight will increase by only 2-3% and the fin geometry will become noticeably more favorable from a structural standpoint.

4.3. Required Surface Area of Tubular Finned Space Radiators and Influencing Factors.

Let's begin by introducing some basic assumptions. Due to the mutual radiation between channels with external diameter D_0 and fins on flat panels (Fig. 4.3c), one can assume that the effective radiating surface is the projection of a panel in the fin plane. Due to this, the elementary thermal power radiated by a panel section of width H and length dL can be given as

$$dq = 2(D_0 q_c + 2Hq_f)dL \tag{4.15}$$

As a second assumption, we will assume that the channel wall temperature T_c is equal to the temperature at the base of the fin, T_{of}. Next, we will assume that the emissivity of the surface of the channel and the fin are identical:

$$\varepsilon_c = \varepsilon_f = \varepsilon \qquad .$$

With these assumptions, equation (4.15) becomes:

$$dQ = 2\varepsilon\sigma T^4 BvdL \tag{4.16}$$

where
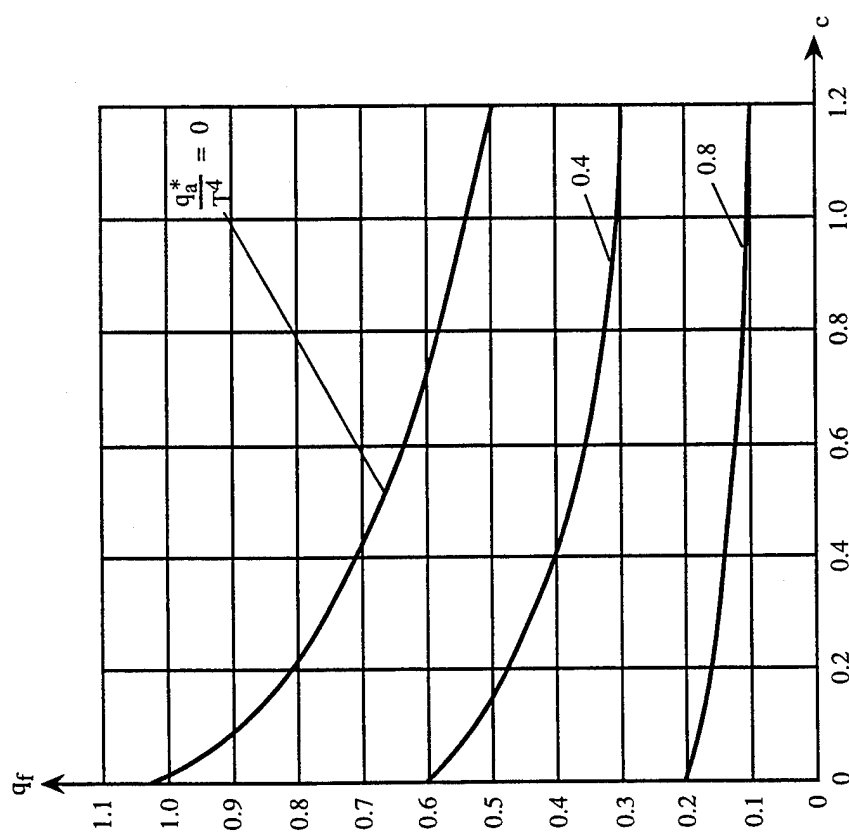
Fig. 4.8 Fin effectiveness as a function of fin conductance parameter. This graph can be used to caculate radiator area requirements, accounting for the temperature drop in the fins.

165

$$\nu = \frac{1 + \dfrac{2Hq_f}{D_o}}{1 + \dfrac{2H}{D_o}} \quad ; B = D_o + 2H \qquad .$$

The relative value ν is the fin factor. It can be seen that $\nu < 1$. With $\nu = 1$, the elementary section BdL (Fig. 4.3a) would radiate the maximum possible thermal power for the given conditions ($q_a'' = 0$) like a plate with a uniform channel wall temperature T_c. We observe that this case is satisfied when $q_f = 1$ or $H_f = 0$.

The thermal power given up by the coolant to an elementary section dL is

$$d\dot{Q}_{cool} = -\bar{c}_p \dot{M} dT_{cool} \qquad (4.17)$$

where T_{cool} is the instantaneous temperature of the coolant; $\bar{c}_p$ is the average heat capacity of the coolant.

The heat flow from the coolant to the channel wall is determined by the temperature gradient $T_{cool} - T_w$:

$$dQ = h\pi D_i (T_{cool} - T_w) dL \qquad (4.18)$$

where D_i is the internal diameter of the tube channel, and h is Newton's convection cooling coefficient.

In a steady state thermal regime, equality exists between the thermal power carried by the coolant and the power radiated by an elementary section of length. Thus for a given fin and tube channel geometry one can establish a relationship between T_{cool} and T_w:

$$2\varepsilon\sigma T_w^4 B\nu = h\pi D_i (T_{cool} - T_w) \qquad (4.19)$$

The direct use of equation (4.19) is difficult because ν depends on T_w, h and k and also on the flow parameters, the Reynolds, Nusselt and Prandtl numbers. The latter are, in turn, complex functions of temperature.

In fact, the task is simplified without any significant error by assuming that the ratio $\varphi = T_w/T_{coolant}$ remains unchanged along the length dL and is evaluated using the average temperature of the coolant $\bar{T}_{cool} = 0.5(T_{cool,in} + T_{cool,out})$. In this case, we obtain from equation (4.19)

$$\frac{1-\varphi}{\varphi^4} = \frac{2\varepsilon\sigma \bar{T}_{cool}^3 \nu B}{h\pi D_i} \qquad (4.20)$$

where h, ν are the average coefficients of convection heat transfer and fin conduction.

Equation (4.20) is simple to solve for φ by using two or three approximations.

166

The method described is used with gas coolants which have comparatively low heat transfer coefficients ν and, consequently, a substantial difference between T_W and T_{cool}. With liquid metal coolants and condensing vapor the heat transfer coefficient will exceed 10^3 W/(m²K). Therefore, φ is close to unity and it is permissible to assume $T_W = T_{cool}$.

If we equate the right side of equations (4.16) and (4.17) and separate the variables, we obtain

$$dL = \frac{\bar{c}_p \dot{M}}{2\varepsilon\sigma B\nu} \frac{dT_{cool}}{T_{cool}^4}$$ (4.21)

In examining the right side of this equation, it should be kept in mind that the fin factor ν also depends on T_{cool}. The integral of this function is complex and inconvenient for analysis. In engineering calculations, therefore, some average value of ν at the temperature $\overline{T}_{cool}$ is assumed.

Let's integrate equation (4.21) over the limits from the tube channel inlet to its exit, taking into account that

$$\dot{Q}_{cool} = \bar{c}_p \dot{M}(T_{cool,out} - T_{cool,in})$$ (4.22)

As a result, we obtain

$$L = \frac{q\nu_t}{2\varepsilon\sigma\nu BT_{cool}^4}$$ (4.23)

where

$$\nu_t = \frac{\left(\dfrac{T_{cool,in}}{T_{cool,out}}\right)^3 - 1}{3\left(1 - \dfrac{T_{cool,out}}{T_{cool,in}}\right)}$$

The factor ν_t determines the increase in length of the radiator section L due to the temperature drop in the coolant from the inlet to the outlet cross section.

The product BL is the area of the radiator section (see Fig. 4.3c) and q is the thermal power radiated by this section. Since all radiator sections operate under the same conditions, the specific radiator area is

$$A^* = \frac{A}{\dot{Q}} = \frac{1}{q''}$$ (4.24)

From equation (4.23) we have

167

$$A^* = \frac{BL}{\dot{Q}} = \frac{\nu_T}{2\varepsilon\sigma\nu T_{cool,in}^4} \qquad (4.25)$$

The required surface area of the tube-fin space radiator is found from a known value of BL/q and a given thermal power $\dot{Q}$. The specific radiator area is a minimum and equal to the specific area of a plate at a constant surface temperature $T_{cool,in}$ with $\nu = \nu_t = 1$. In the general case, $\nu < 1$, and $\nu_t > 1$. Reducing the difference between the two is possible by decreasing the difference $T_{cool,in} - T_{cool,out}$, which, in turn, is attained by increasing the coolant flow rate. This, naturally, reduces the required radiator surface area, but at the same time the power to pump the liquid metal coolant will increase and the radiator weight will increase. In gas turbine power plants that operate on the Brayton cycle, the ratio $T_{cool,in}/T_{cool,out}$ is detemined by the cycle parameters. This ratio is usually small (no more than 0.5-0.6), which is one of the reasons for the large specific radiator area of such power plants.

As we have noted, the fin factor ν is always less than unity. For an optimum fin height, H_{opt} (this concept is discussed below), the factor ν is in the range 0.7-0.8.

Let's turn to an analysis of another important characteristic of the fin-tube space radiator, its specific weight. To this end, we present the expression for this characteristic in the form

$$M_{sp} = \frac{M}{q''} = \frac{\pi D_o \delta_w \varphi + 2H\delta\varphi}{2\varepsilon\sigma T_o^4 B\nu} \qquad (4.26)$$

where δ_w is the channel wall thickness.

Even a qualitative analysis of equation (4.26) shows that there is an optimum value of δ and H which correspond to the minimum specific weight of the radiator panel. In fact, with increases in the height and thickness of the fin, the numerator in equation (4.26) will increase linearly. It is also true, however, that the numerator will change in a different way. Thus, with H = const, the numerator will increase and converge to some limit at $\nu \to 1$. In another case with δ = const, the numerator will increase at first (linear increase in the parameter B, but the effectiveness parameter q_f will decrease insignificantly, at first). The numerator then begins to decrease due to the predominating decrease in q_f.

A joint analysis of the influence of geometric characteristics of the space radiator on specific radiated power and weight shows that it is impossible to satisfy the conditions q''_{max} and $M_{sp,min}$ simultaneously. The solution is a compromise depending on the specific purpose of the space radiator in question. The following numerical values are usually assumed in practice: D_o = 4 to 8 mm, δ = 0.8 to 12 mm, H = 0.6 to 0.8 mm, H = 2 to 4 cm.

In conclusion, let's briefly discuss certain aspects in determining the geometric parameters of a space radiator. The radiation of a given thermal power with given coolant inlet and exit temperatures can be accomplished using radiators with different geometries. The design of possible variants is easily begun by assigning different values of D_o and D_i. The corresponding combinations of the fin parameters H and δ are then selected. An

additional variable can be either the number of sections n_s or the panel length. These are related through the obvious relationship,

$$A = (D_o + 2H) n_s L$$

For each of the combinations of D_O and n_s considered, the flow velocity of the coolant is found,

$$\overline{v} = \frac{4M}{\pi D_i^2 \rho n_s} = \frac{4\dot{Q}}{\pi \overline{C}(T_{cool,in} - T_{cool,out})D_i^2 \rho n_s}$$

from which one can determine the critical flow parameters and perform hydraulic and thermal design of the channels.

4.4. Some Characteristics of Heat rejection at Low Cooling Temperatures.

As we have noted, at comparatively low (less than 500 K) cooling temperatures, heat fluxes from the surrounding medium must be considered, especially if cooling to room temperature, i.e. to 300-310 K, is required. Moreover, under such conditions heat rejection is impossible without taking special steps. Cooling can be accomplished in two ways: by increasing the radiating surface temperature through the use of refrigeration (heat pump) or by absorption (not by radiation) of heat by some substance due to its heat capacity, latent heat of phase transitions and endothermic chemical reactions. The first method requires the consumption of power, and the second a reserve of heat absorbing substances. For this reason, the second technique cannot be used in long term spacecraft operation where heat is liberated constantly over time. However, maximum heat liberation occurs, as a rule, over short time periods. Heat absorption or the discharge of an appropriate refrigerant is, therefore, positively of practical interest. Three simple heat rejection techniques merit attention: radiation, where all the heat is rejected by radiation (Fig. 4.9a); ejection of a working fluid that has been heated by cooling the component in question (Fig. 4.9b); and, finally, a combination of these (Fig.4.9c).

In comparing these methods, we will write an expression for weight in rejecting heat by the first two approaches:

$$M_{rad} = M_{ltr}'' \left(\frac{A}{\dot{Q}}\right)_{ltr} \dot{Q} \quad ; \quad M_{vent} = Q c_{vent} \tau \ . \tag{4.28}$$

where M_{ltr}'' is the mass per unit area of panels and tubes of the low temperature radiator; $(A/Q)_{ltr}$ is the relative low temperature radiator surface area with the influence of the surrounding media parameter Q_{abs} taken into account, Q is the thermal power rejected at the low temperature of the object being cooled; c_{vent} is the mass divided by thermal energy content (kg/kWhr) of vented fluid; and τ is the total operating time of the thermal load.

Depending on the values of the indicated parameters, either the first or the second method can result in minimum weight. The time threshold, at which it is advisable to

Fig. 4.9 Heat rejection schemes for spacecraft thermal systems.
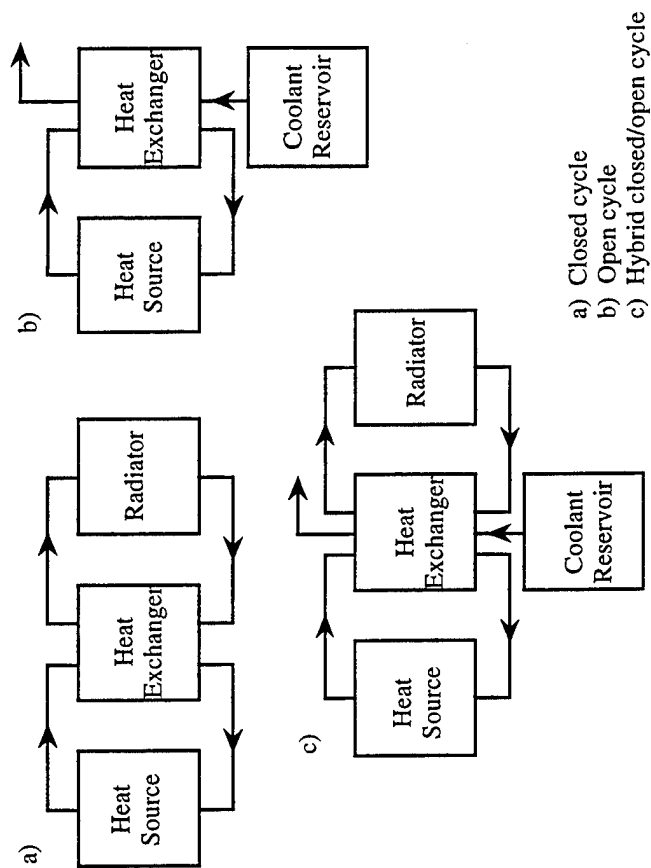
a) Closed cycle
b) Open cycle
c) Hybrid closed/open cycle

170

select a given design approach, can be determined from the condition $M_{rad} = M_{vent}$. Hence, it follows that

$$\tau = \left(\frac{A}{\dot{Q}}\right)_{ltr} \frac{M_{ltr}^{"}}{c_{vent}} \tag{4.29}$$

As is evident, the time threshold does not depend on the absolute magnitude of the power rejected, but is determined only by the parameters $(A/\dot{Q})_{ltr}$, $M_{ltr}^{"}$ and c_{vent}. Let's estimate the numerical value of τ. The following parameters are given:

$$\left(\frac{A}{q}\right)_{ltr} = 10 \frac{m^2}{kW}; \quad M_{ltr}^{"} = 5 \frac{kg}{m^2}; \quad c_{vent} = 0.5 \frac{kg}{kW \cdot hr} \quad .$$

In this case, the time threshold is 100 hours. Naturally, such a spacecraft operating period is of no practical value. For this reason, the approach using working fluid (evaporator) ejection in pure form is not used. However, in existing and, for the most part, in future spacecraft there is no clear definition of constant heat liberation with time.

In the general case, the thermal power liberated during one orbit of a spacecraft around the earth will change according to a prescribed program. We'll take a look at one of the simplest programs (Fig. 4.10): $t = n\tau'$. τ' is the time of maximum heat liberation during one orbital period T; and n is the number of orbits of the spacecraft. We'll assume that the constant liberated thermal power q is rejected by radiation, and the excess (q_{max} - q) by heating and ejection of a working fluid. The appropriateness of such a combined method (Fig. 4.9c) will, as before, be evaluated for the time threshold τ_0. However, this does not now represent the total operating time of the spacecraft, but only the duration of maximum heat liberation. Let t' be 5% of the orbit period T. Then, in calculating the total time of operation using the previously assumed initial data, we obtain $\tau_0 = \tau/0.05 = 100/0.5 = 2000$ hours $\cong$ 83 days. This is significant, and, consequently, such a combined method may appear very reasonable.

In conclusion, we will point out a method for increasing the heat rejection effectiveness at low cooling temperatures. This approach uses thermal energy storage. This involves the absorption of excess heat during time period (by, let's say, melting of a suitable thermal storage substance) and the transfer of absorbed heat by a working fluid circulating through the radiator during the time period . In this case, the low temperature radiator will continuously radiate some average constant power and, thus, the weight of the heat rejection equipment will be less in comparison with that required during liberation of the maximum power.

4.5. Construction of Space Radiators and Liquid Metal Loop Components.

4.5.1. Structural Shapes of Space Radiators and Their Components.

The structural composition of the space radiator has a significant influence on its size and weight, which we need to minimize. We know that it is impossible to satisfy both

171

conditions simultaneously. In this case, particularly when a large quantity of heat has to be rejected and the dimensions of the space radiator become correspondingly large, we must also consider launch vehicle capability. This can result in a need for a space radiator with a shape that can be altered. A space radiator with alterable or nonalterable geometries can have different kinds of radiating surfaces. Some of them are shown in Fig. 4.10. With identical temperatures and rejected thermal power, the designs shown in Fig. 4.11 have the following ratios, $L_1 : L_2 : L_3 = 1:1$, $1:1.5$, and the corresponding mass ratios of the space radiators are 2:1, 4:1. Thus, the most compact but also the heaviest, is a space radiator with a closed conical radiation surface. However, its obvious advantage is that many components of the nuclear power plant can be enclosed in it. This led to the practical application of such a design in existing space hardware (the nuclear power plant "Topaz" series with thermoelectric converters). As the generated electrical power level increases, difficulties arise in mating the nuclear power plant with the launch vehicle. This situation compels the development of space radiators with alterable geometries. By the way, such space radiators are very promising for nuclear power plants that generate burst electrical power for certain short duration periods. The configuration of these space radiators is changed in such a manner that during orbit insertion (during the constant power regime of a burst power nuclear power plant) it will be extremely compact. After orbit insertion of the spacecraft (or in the burst power regime), the space radiator is deployed (unfolded) into its operational state where it can radiate the maximum thermal power. There are different mechanisms for altering the shape of the space radiator. Thus, in the four-vaned space radiator (Fig. 4.11b), each vane, consisting of several panels, is folded into a "bellows" in the launch mode. There are flexible sections at the locations where the tubing with the working fluid and the panels are connected. Such a compact space radiator design results in a multiple decrease in radiator length, but the large number of flexible tubes and hinged joints show up in the weight of the assembly.

One promising variant of a space radiator for very high power (tens of Mw) nuclear power plant is the so called droplet space radiator. The principle of operation of such a radiator (a variable geometry variant) is based on the generation in space of an orderly flow of monodispersed coolant droplets (the droplet substance can be very different and its selection is in itself a scientific problem). This flow must be able to assume different forms, in particular, the flat plate form. At some distance from the source, droplet flow develops towards a suitable receptacle. In the path between the source and the receptacle the droplet flow radiates thermal power to surrounding space. Preliminary calculations show such space radiators to be highly efficient. For example, with a rejected thermal power of ~25 MW at an initial temperature 370-380 K and a temperature drop $\Delta T = 70\text{-}80°$, the total droplet weight is only 1 ton, and droplet loss in the rarefied flow does not exceed ~1 g/sec. It is, however, too early to talk about practical applications of "droplet" space radiators.

The application of a telescopically deployed space radiator is possible. Its sections are stored within each other during the launch phase (Fig. 4.12). Such a construction provides a twofold change in the radiator length, but it requires guides for moving the sections, a locking system for securing the sections in their extreme positions, as well as flexible components in the plumbing system to provide free mutual movement of the sections.
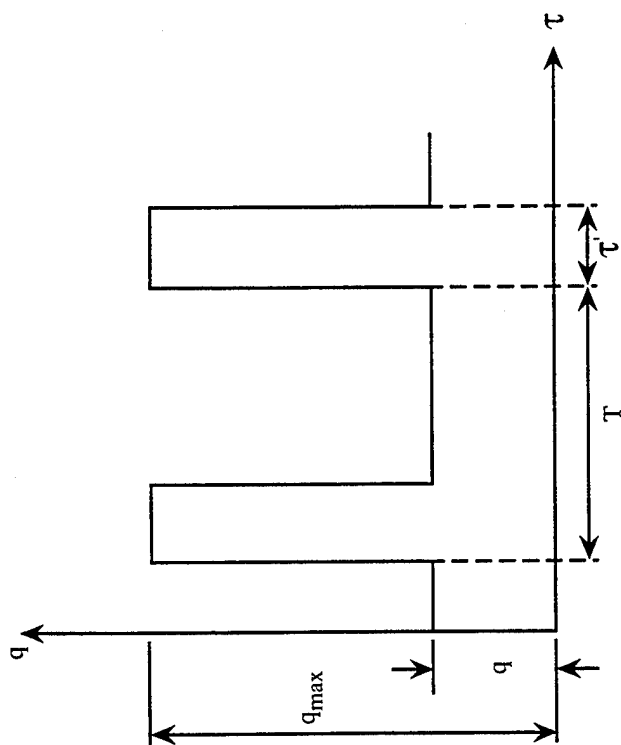
Fig. 4.10 Thermal power load profile, showing a baseline and peak thermal during an orbit.

173

L_1

L_2

L_3

a)

b)

c)

a) Concial type
b) Four-vane type
c) Flat panel type
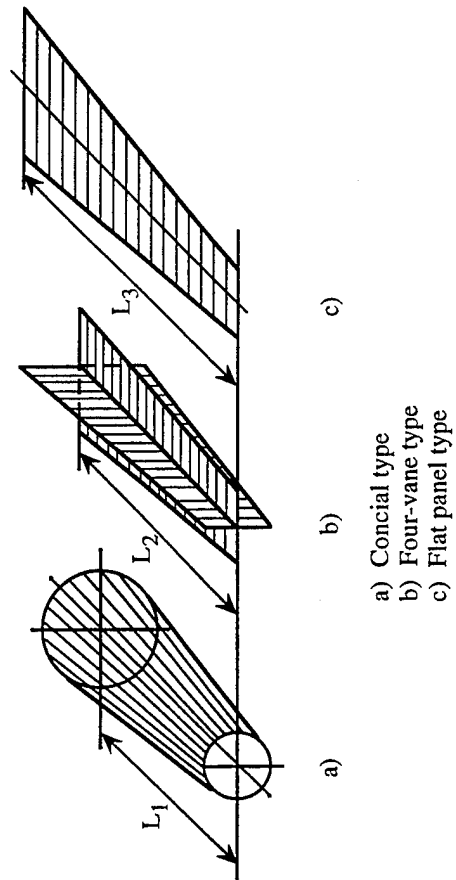
Fig. 4.11 Radiator configurations.

Flexible Pipes

Fixed Radiator Section

Moveable
Section
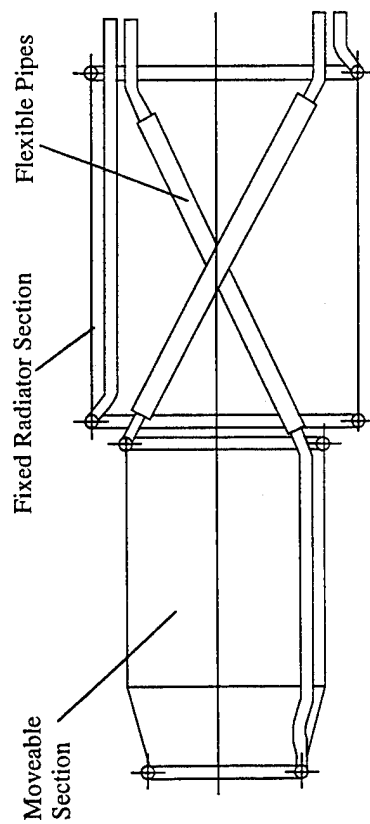
Fig. 4.12 Telescopically deployed radiator, shown in stowed configuration.

175

An approximation of this is provided by using a folded space radiator (Fig. 4.13). Here a decrease in the length of the power plant is achieved by moving the reactor and radiation shield close in with the spacecraft. This results in a favorable contribution to the distribution of spacecraft and launch vehicle mass. Naturally, such a construction has, in addition to its positive side, disadvantages. A fundamental one is the need for a sufficiently powerful drive mechanism and equipment for damping out shocks during the final deployment stage.

Let's turn to the construction of a space radiator and examine the tube-fin radiator, which is most widely used in nuclear power plants.

Such a space radiator consists of one or several sections. Each section is made up (Fig. 4.14) of a radiating panel formed by coolant channels and radiating connectors (fins) as well as inlet and outlet plenums that are directly connected to the source of rejected heat by a plumbing system. In order to increase the flexibility of the radiator panels, they can be connected to a framework.

The construction of the radiator panels differs mainly in the way the fins and coolant channels are joined. A basic requirement on the connection between the coolant channel and the fin is that the joint must have a low thermal resistance. This requirement is satisfied by soldering and diffusion welding.

Fig. 4.15 shows some possible variations in the construction of radiator panels. During joining, a butt seam (Fig. 4.15a) is permitted for control and removal of defects.

The small fin thickness complicates panel fabrication and requires a high joint strength. A joint in which the fin envelops half the coolant channel surface (Fig. 4.15b) is very sensible. The surface area and reliability of the thermal contact between the fin and the channel are increased substantially. In addition, such a fin arrangement reduces the meteorite vulnerability of the channels. Obviously, from the point of view of panels radiating from both sides, it makes sense to attach fins to both sides of the coolant channel (Fig. 4.15c). A disadvantage is that controlling the quality of the welds and eliminating defects present difficulties.

The flat covering fin (Fig. 4.15d) serves as a shield for a significant portion of the coolant channel. This, as will be shown below, decreases the coolant channel vulnerability to meteorite impact significantly. A design with eccentric coolant channels can be used for this purpose (Fig. 4.15e). A design with two covering flat fins should be used with panels that radiate from both sides (Fig. 4.15f). An effective way to shield coolant channels from meteorite impact damage is to use tubular shields which envelop the channels and maintain thermal contact with them and the radiating fins (Fig. 4.15g). Fundamental disadvantages of the shielded channel construction are engineering complications and the reduced radiating effectiveness of the channels.

4.5.2. Choice of Materials for Space Radiator.

In selecting structural materials for space radiator components one must pay attention to such specific operating conditions in space as a hard vacuum and meteors that are capable of disrupting working fluid seals. It should be noted that while these conditions can be considered in the design of many nuclear power plant components, the
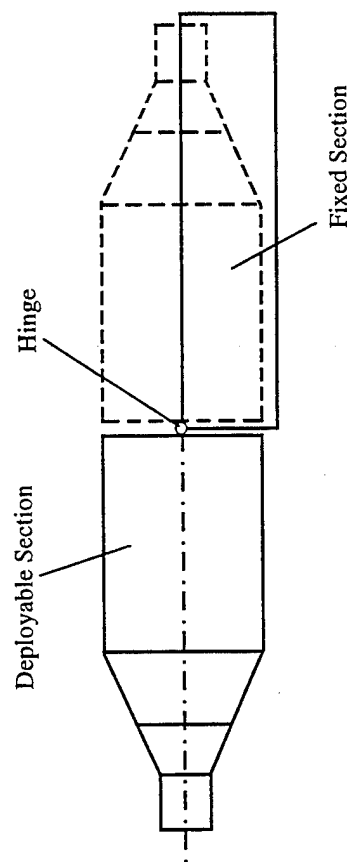
Fig. 4.13 Folding space radiator.

177

a) Profile

b) Axial View

c) Cross Section of
Inlet Plenum
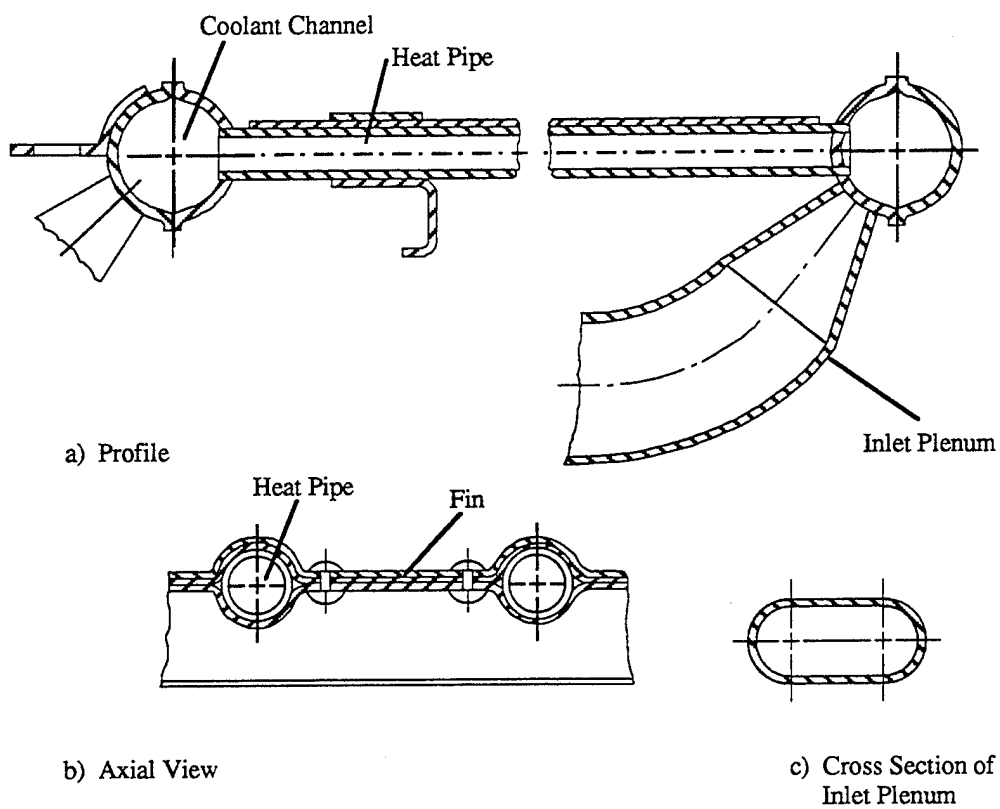
Fig. 4.14 Heat pipe/fin radiator and liquid metal coolant channle configuration.

178

a) Simple butt joint
b) Fin envelopes halt the heat pipe
c) Fins totally enclose the heat pipe
d) Flat fin/micrometeoroid shield
e) Two protective fins for a two-sided radiator
f) Eccentric channel, providing additional shielding
g) Fully enclosed heat pipe
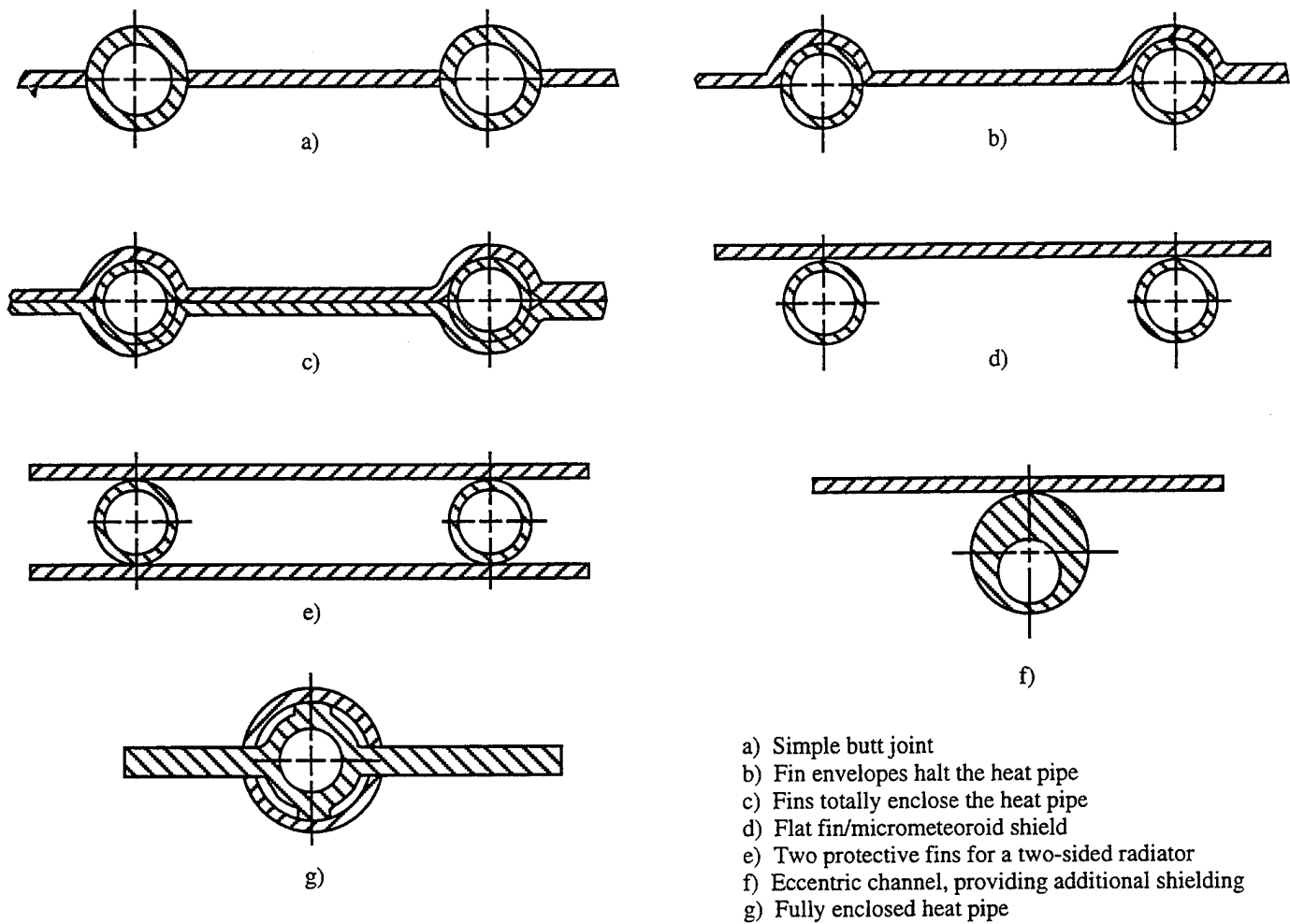
Fig. 4.15 Possible variations of heat pipe/fin designs.

relatively large size of the space radiator makes the problem of selecting materials for it especially acute.

The basic requirements of space radiator materials are the following:

a. The radiating surfaces of the coolant channels and fins must have a high emissivity;

b. The material for the radiator fins must have a high thermal conductivity and a low density, and the coolant channel material must, in addition to these properties, have a high resistance to meteorite penetration;

c. The channel and fin materials must be resistant to heat and vacuum conditions;

d. The channel material must be compatible with the working fluid in the operating regime.

Many materials that basically satisfy these requirements have low surface emissivities. The most reasonable way to increase the emissivity is to deposit a special coating on the radiating surface. In selecting the coating, one must pay attention to its cohesive strength with the base material and also to its stability in a vacuum and ability to withstand meteorite impact.

One characteristic behavior of materials in a vacuum is their more intensive sublimation in comparison with their behavior under normal atmospheric conditions. The stability of materials in a vacuum is characterized by the mass of material lost by sublimation per unit time. The heat and vacuum stability of materials applicable to the fabrication of space radiators is provided by the data in Table 4.4.

Table 4.4 Space Radiator Materials

Material	Melting Point	Temperature of Loss Rate		
		10^{-1} cm/yr	10^{-3} cm/yr	10^{-5} cm/yr
Aluminum	933	1089	953	823
Beryllium	1553	1113	973	893
Copper	1353	1173	1033	903
Molybdenum	2883	2173	1903	1653
Tungsten	3673	2773	2423	2153

A decisive factor in the choice of channel material is its compatibility with the working fluid (coolant). Stainless austenitic steels are usually used in contact with sodium-potassium coolants. Al, Be, or Cu can be used for the fins.

In order to evaluate the resistance of materials to meteorite impact, one must gather information on the velocity of meteor particles, their material densities, and the nature of their distribution as a function of density and mass. Here are the currently available data. The average velocity of a meteorite relative to earth is 30 km/sec. The density of meteorites for calculation purposes is assumed to be 2.3 to 2.8 g/cm^3. The distribution of meteorites in terms of density and mass is estimated by the relationship

$$n = 10^{-14.48} \left(\frac{0.44}{\rho_m} \right)^{1.34} m^{-1.34}$$

where n is the number of meteorites with a mass greater than m that impact per unit time on a unit surface, $m^{-2}sec^{-1}$; ρ_m is the density of the meteorite, g/cm^3; and m is the mass in grams.

The depth of penetration of a meteorite in a material barrier is calculated (in centimeters) from the equation

$$\frac{\Delta}{d} = 0.6 \left(\frac{\rho_m}{\rho_c} \right)^{2/3} \ln \left(1 + \frac{\rho_m^{2/3} \rho_c^{1/3} v_m^2}{4H_B} \right) \qquad . \qquad (4.30)$$

where ρ_c is the density of the channel wall material in g/cm^3; H_B is the Brinell hardness of the wall material in bars; and v_m is the velocity of the meteorite in cm/sec.

The thickness of the unpunctured wall Δm is obtained by increasing the penetration depth by a factor of 1.5-2:

$$\frac{\Delta m}{d} = \left(1.5 \text{ to } 2 \right) \frac{\Delta}{2} \qquad .$$

In order to obtain the wall thickness δ_w (in centimeters) with consideration of the meteorite mass flow distribution and the probability of reliable operation over the time τ (in seconds), the following equation is used:

$$\delta_w = 1.9 \cdot 10^{-4} \frac{\Delta m}{d\rho_m^{2/3}} \left(\frac{F\tau}{1 - p} \right)^{0.25} \qquad (4.31)$$

where F is the surface area exposed to meteorite impact in m^2, and p is the probability of no penetrations.

4.5.3. Some Problems in Meteorite Vulnerability of Space Radiators.

Meteorites that strike space radiator panels can put individual sections of the radiator out of service and disrupt the thermal regime of the nuclear power plant. The latter can be catastrophic. For this reason, meteorite vulnerability of space radiators must be examined intensively. Meteorite impact protection can be achieved in several ways. An obvious approach is to increase the wall thickness of the plumbing that contains the working fluid. Equally obvious is the disadvantage of this approach. A more effective way is to shield the plumbing from the meteorites. The effectiveness of the shield is that it breaks up the meteorite that impacts with it. The meteorite fragments continue toward the channel wall as an expanding cloud. This reduces significantly the penetration by the fragments into the channel wall. Experimental and analytical studies show this method to be very sound.

181

Large space radiators can, in addition to channel shielding, incorporate an effective reserve of separate sections, that is, an excess (above that calculated) number of sections. Naturally, the relevance of such a reserve can only be assessed after a comparison of the weight of the additional sections with the additional weight of other means for increasing space radiator reliability (with respect to meteorite impact).

One of the most promising varieties of sectioned space radiators is one that incorporates heat pipes in its design. Radiating panels of space radiators with heat pipes are similar in design to the tube-fin panels. The difference is that heat pipes are substituted for the coolant channels. In order to increase the thermal effectiveness of the space radiator, the proposal is to replace the radiating fins with an assembly of transverse small diameter heat pipes attached to the longitudinal tubes. In such a design, the transverse heat pipes, together with the radiation of thermal energy, also function as meteorite shields for the longitudinal tubes. In the event a transverse pipe is penetrated by a meteorite, it will continue to radiate the heat conducted to it like a normal fin.

We note in conclusion that the use of heat pipes in a variety of space radiator designs and configurations looks extremely promising.

4.5.4. Liquid Metal Loop Components.

In many of the nuclear power plant designs examined, the basic components are, in a thermal sense, liquid metal loops. They consist of piping, pumps, expansion tanks, oxide traps and other auxiliary equipment.

The piping distribution system is quite extensive and makes up a significant fraction of the power plant weight. Therefore, the selection of reasonable piping sizes is a fundamental design task. The optimum tube diameter equates to the minimum effective weight by which is understood the total weight of the piping and the incremental power plant weight caused by the energy spent in pumping the coolant through the piping system.

The weight of the piping filled with the coolant is calculated from the equation

$$M_t = \pi L r \left(\rho_t \frac{2p}{\sigma} + \rho_p \right) \tag{4.32}$$

where r is the internal radius of the piping; L is its length; ρ_p is the density of the piping material and the coolant; p is the internal pressure in the piping; is the allowable stress in the piping wall.

The incremental power plant weight ΔM_{inc} can be related to the electric power used in pumping the coolant through the piping, q_{el}, through the relationship

$$\Delta M_{inc} = \overline{M}_p q_{el} \tag{4.33}$$

where M_p is the specific weight of the power plant.

By expressing q_{el} through the pressure drop in the piping, the coolant mass flow per second, $\dot{m}$, and the pump efficiency η, equation (4.33) becomes

$$\Delta M_{inc} = M_p \frac{\dot{m}L\lambda}{4\pi^2\rho^2\eta} \left(1 + \frac{2r\Sigma_{mi}}{L\lambda}\right) \qquad (4.34)$$

where λ is the coefficient of friction; E_{mi} is the total piping local loss coefficient.

According to the accepted definition of the effective weight of the piping, the equation is expressed as

$$M_{te} = M_t + \Delta M_{inc} = \pi L r^2 \left(\rho_t + \frac{2\rho}{|\sigma|} + \rho_{th}\right)$$
$$+ \overline{M}_p \frac{\dot{m}L\lambda}{4\pi^2\rho_{th}^2\eta^5} \left(1 + \frac{2r\Sigma_{mi}}{L\lambda}\right) \qquad (4.35)$$

Calculations done using (4.35) show that the optimum coolant flow velocity (Na+K eutectic) in the piping depend little on its mass flow per second. Thus, with changes in mass flow from 1 to 4 kg/sec and with $\eta = 0.3$ and $\overline{M}_p = 0.3$ kg/W, the optimum coolant velocity changes practically linearly from 1.2 to 1.4 m/sec, and with $\overline{M}_p = 0.05$ kg/W and the same value of η, it changes from 1.9 to 2.3 m/sec.

In the design of the piping, proper attention should be paid to problems in allowing for thermal expansion. Curved sections or bellows are considered in solving the thermal expansion problem in the piping system. In order to provide proper sealing, the piping is welded to components in the flow circuit. Individual parts of the piping are butt welded. In order to prevent stress concentrations, it is necessary to avoid welding pipe joints with different wall thicknesses.

Pumps. Electromagnetic conduction pumps are preferable for use in pumping liquid metal coolants through the loops in space power plants with direct conversion of thermal energy into electrical. The principle of operation of such pumps is based on the interaction of an electric current flowing through the liquid metal channel with a magnetic field into which the channel is inserted (Fig. 4.16). The electric current is conducted to the metal through terminals. As a result of the interaction of the current and the magnetic field created by the poles, an electromagnetic force is created which moves the metal through the channel.

Due to their simplicity, conduction pumps are highly reliable. The absence of moving parts eliminates the problem of sealing the flow channel. The low voltage (about 1 V) simplifies the electrical insulation problem at high temperatures and in ionizing reactor radiation.

A disadvantage of the conduction pump is its high current requirement (10^3 - 10^5 A) which requires the use of large cross sectional area terminals as well as the placement of the pump close to the source of electrical power. Conduction pumps have comparatively low efficiencies (15-20%).

Expansion tanks. The density of liquid metal coolants depends in a significant way on temperature. Thus, the density of Na-K eutectic alloy decreases by 20% as the temperature changes from 293 to 973 K.

In order to maintain a constant coolant pressure, special tanks are included in the loop. The volume of these tanks changes as the coolant density changes.
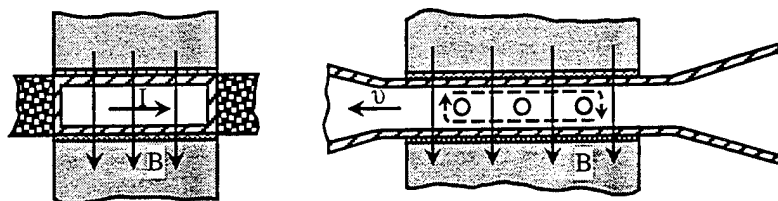
Fig. 4.16 Electromagnetic pump conceptual design.

Constant pressure in the loop is maintained by keeping a constant pressure on the gas supplied to the tanks. In order to separate liquid and gas phases in a zero-g environment, flexible diaphragms or bellows are used.

Oxide traps. The presence of oxides in liquid metal coolants accelerates corrosion of the loop structural materials. So called cold and hot oxide traps are used in removing oxides from the coolant. Cold traps employ the dependence of oxygen (oxides) solubility in metals on temperature. The coolant temperature in the trap is reduced to 350-400 K which causes the oxides to precipitate on a special filler material in the trap.

The operation of the hot trap is based on the formation of compounds of oxygen with materials (getters). These compounds are insoluble in the coolant. Such getter materials include Ti, Zr, I, Mg.

Hot traps are preferred in space power plants because these traps do not require cooling. Consequently, they do not affect the power plant efficiency and do not require additional space radiator surface area. The construction of the hot trap consists of a section of pipe filled with a getter foil. The traps are installed in the hot sections of the loop either in series or in parallel.

Auxiliary equipment. In addition to the components we have considered, auxiliary equipment is also added to the loop. This equipment is directly related to the operation of the loop: fill and drainage valves, heating elements and dummy resistances, temperature and pressure recorders.

Fill valves are needed in order to fill the loop with the coolant. The drainage valves remove the residual inert gas contained in the loop prior to filling. The valves must ensure that the loop is hermetically sealed.

In order to monitor the state of the power plant during its preparation on the ground and during its operation in space, coolant temperature and pressure recorders are needed. Thermocouples are used as temperature recorders. Pressure is measured by manometers in appropriate locations throughout the loop.

5. IONIZING REACTOR RADIATION SHIELDING

5.1. Shielding Equipment and Purpose.

We showed earlier that a basic interaction of neutrons with nuclei is fission of heavy nuclei, which is accompanied by the release of radiation. The most dangerous are neutron fluxes and γ quanta. By interacting with different substances, including biological tissues, radiation can cause atoms within them to ionize and thus destroy their normal functioning.

The following magnitudes of neutron flux and γ quanta are characteristic of space nuclear power plants at the reactor surface: 10^{14} - 10^{16} neutrons/cm²sec and 10^{18} - 10^{20} MeV/cm²sec. These numbers are substantial. They exceed by orders of magnitude the allowable levels not only for humans but also for equipment and instrumentation normally found on a spacecraft. In order to reduce the radiation emissions to allowable levels, a radiation shield is installed around the reactor. The shield material is capable of absorbing neutrons and γ quanta. Since there is virtually no scattering of neutrons and γ radiation in space, unmanned spacecraft will require only limited shielding. Such a shield produces a zone of reduced ionizing reactor radiation levels in a limited space only, which is shaped like a truncated cone. The shape of the shielding block or "shadow" shield is a truncated cone with spherical ends (Fig.5.1). The shielding materials must be chosen for their effectiveness in absorbing both of the above mentioned forms of radiation. Materials for shielding against neutrons must fulfill two functions: fast neutron moderation and subsequent neutron absorption by radiative capture. Lithium hydride moderator and boron carbide or mixtures of boron and aluminum (for radiative capture) are usually used.

Titanium diboride has been proposed as a substitute for B + Al mixtures. The titanium diboride is fabricated in individual briquettes (in Russia, by Scientific Production Organization Red Star, or NPO Krasnaya Zvesda). The briquettes are open-ended cylindrical steel casings filled with a composite titanium diboride material. Its chemical composition is ~38% boron, ~35% titanium, the remainder is copper, nickel and magnesium. The briquettes are placed in a sealed structure operating at a 900 K wall temperature in helium at a pressure not exceeding 3 MPa. Testing has verified the radiation stability of the material at neutron fluence no lower than 10^{20} neutrons/cm².

It should be kept in mind that lithium hydride is unstable at high temperatures. At a temperature of about 900 K, lithium hydride dissociates into hydrogen and lithium. In order to prevent loss of hydrogen, the lithium hydride must be enclosed in a sealed container which is pressurized with helium.

The neutron shield casing (Fig. 5.1) also fulfills a load carrying function. It accepts the loads from the reactor side and transmits them to the structural components of the spacecraft. The shield casing is equipped with appropriate silicon attachments for this purpose.

The shield thickness is designed to attenuate the neutron flux. It is then tested for its ability to attenuate γ radiation.

When the γ radiation flux exceeds the allowable level, a layer of good absorbers of γ quanta are added to the neutron shield. These include such materials as Pb, Mo, W, U and others.

186
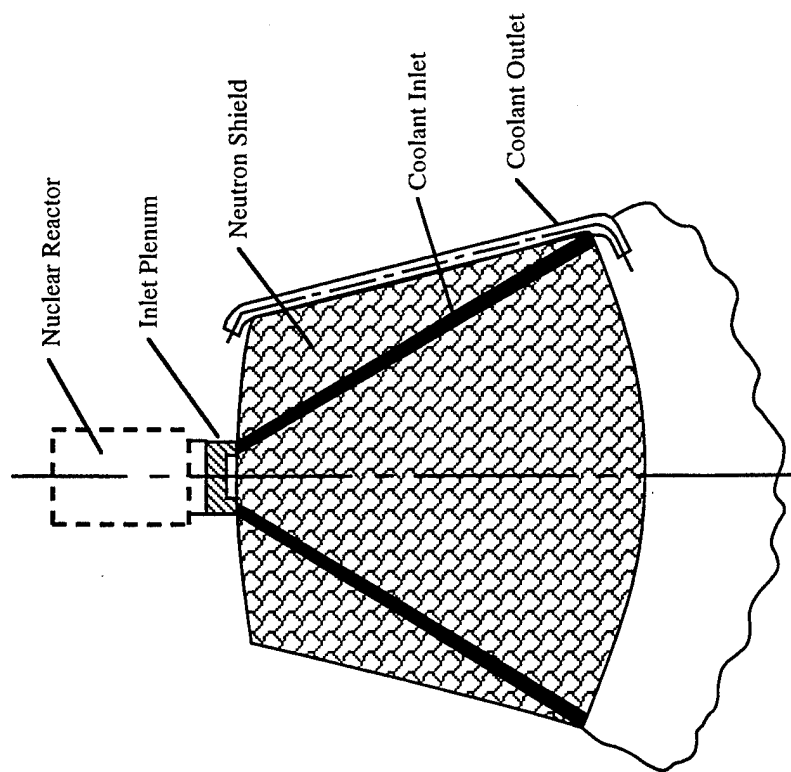
Fig. 5.1 Radiation shadow shield configuration.

187

Heat is generated in the shield during operation of the nuclear power plant. This heat results from the slowing down of neutrons, from their absorption, and also from the absorption of γ quanta. In addition, the shield can absorb thermal energy radiated from the reactor. Shields with relatively small (up to 1-1.5 m) diameters can be cooled by thermal radiation from their container walls. Special coatings with high emissivities and low heat absorption coefficients are deposited on the outer surfaces of the shield in order to enhance thermal radiation. In order to decrease thermal flux from the reactor and the space radiator, the bottom surface of the shield can be equipped with deflectors and vacuum-type thermal insulation.

Biological shields for manned spacecraft (and in the future, lunar bases with nuclear power plants) are designed to prevent the allowable radiation dose rate for humans from being exceeded. The thickness of biological shields is substantially greater than the thickness of shields for unmanned spacecraft. In addition, when the nuclear power plant contains loops with an activated coolant, additional shields are necessary in order to shield the manned compartments from secondary radiation. When the crew has to perform extravehicular activities in space, when docking and departure maneuvers of other spacecraft take place, and with the anticipated use of nuclear reactors in lunar bases, the reactor needs to be shielded on all sides, i.e., with a "4π" shield as opposed to a "shadow" shield.

The entire combination of biological shielding leads in the final analysis to a large mass. The most effective approach to minimizing the shielding mass is to separate the reactor from the objects to be shielded. There are different ways to do this. For example, extension-type trusses and telescopic booms can be used to provide the needed separation.

The basic construction of the "shadow" radiation shield is a sealed container which is filled with lithium hydride, the shield material. The shield is filled with lithium hydride using the casting method. This is done in order to achieve a sufficiently high density of the solid, 730 kg/m^3, and to make sure it is properly packed in the container.

The geometry of the shield and the construction of the container are selected depending on the design layout of the nuclear power plant and the spacecraft. As a rule, the profile of the shield is designed such that all components of the nuclear power plant and the spacecraft are in the shadow of the cone.

Basically, the design of the shield container is dictated by the following factors:

a. The positioning relative to the shield of reactor control drives and their operating modes which determine the presence and geometric arrangement of open passages through the shield;

b. The allowable ionizing radiation level which influences the method of installing liquid metal loop piping and electrical conduits through the shield. They can be located along the surface of the shield, enclosed in special channels in the container shell, or be passed directly through the shield;

c. the load configuration.

The latter factor determines to a significant degree the need for a sharp increase in the strength of the radiation shield. This can be achieved by using the monolithic lithium hydride as the load carrying component of the structure. The structural components of the container that transmit the forces from the reactor to the nuclear power plant components that adjoin the shield should be located in the monolithic lithium hydride. Such a construction allows a substantial increase in the strength of the radiation shield with a concomitant reduction in its mass.

In this case, the container shell serves only as a seal and can be made quite thin, about 1×10^{-3} m. The use of a thin-walled shell makes it possible to impart a complex configuration to the shield, in particular, to install passages for the liquid metal coolant and electrical conduits in the conical shell. The components that carry the load and distribute it through the monolithic lithium hydride can have different designs. Of interest in this regard are channels that penetrate the shield such as those intended to house liquid metal coolant piping. In this case, however, a problem arises concerning allowances for thermal expansion of the channels. Experience in the fabrication of radiation shields has shown that the method of filling the container with lithium hydride plays an enormous role. It is decisive in many situations and determines to a significant degree the design of the shield. As has already been mentioned, the shield is filled with lithium hydride using the casting method. An initially heated container is filled with molten lithium hydride which is followed by directional crystallization and filling of shrinkage cavities. The complexities that arise in this process are related to the extremely unsatisfactory casting properties of lithium hydride. In particular, these are the low thermal conductivity, high heat capacity and significant shrinkage during crystallization and cooling. As a result, cracks, shrinkage cavities, and voids form in the casting and deviations in the casting profile from the geometry of the radiation shield container can also occur. All of these factors have a negative effect on the shield characteristics, which is explicit in the increased portion of unabsorbed neutrons that pass through the cracks in the shield. Moreover, the separation of the monolithic lithium hydride from the container shell gives rise to secondary neutron radiation sources in the shield. These sites in the container shell are visible to both the reactor and the object being shielded. This effect is seen especially in shields where the shell is the load component of the container. This fact provides additional support for employing a design where the lithium hydride incorporates load carrying components and the shell serves only as a seal.

Another factor that deteriorates the shield characteristics and which results from the casting properties of lithium hydride is that loads imparted by the monolithic lithium hydride to the container structure causes it to deform. This pertains especially to channels designed to accommodate reactor control components that pass straight through the shield. The attention paid to these components is dictated by the need to insure a minimum clearance between the control rods and the channels in the shield. An adverse situation arises when a dose of unattenuated radiation passes through the annular clearance to the object being shielded. One method to prevent channel deformation is to provide supplementary bracing between the channels, however, this complicates the design and increases the mass of the shield.

At the present time, a number of radiation shields have been designed and fabricated that differ from each other in design and container geometry. All of these, as

can be seen from the design in Fig. 5.1, are truncated cones with the dimension $l/d = 0.25$-1, where l is the thickness; d is the average shield diameter, and volume $V = (0.4\text{-}3.2) \times 10^{-1}$ m³. They differ in methods of loading and in the methods by which reactor control devices, liquid metal plumbing, etc. are passed through the shield. Radiation shield tests have substantiated that they are highly effective under operational conditions.

Another problem, which requires study in future radiation shield development, is availability of nondestructive inspection methods. These would allow a high degree of accuracy and utility in quality assessments of fabricated shields. A particularly stringent requirement is verification of the monolithic lithium hydride structure and the amount of separation from the container shell. The first parameter characterizes the ability of the monolithic lithium hydride to attenuate ionizing radiation, the second parameter determines the geometry of the shadow shielded zone.

From a technological standpoint, the most acceptable method for verifying casting uniformity is by x-rays. X-ray attenuation will provide needed insight to the quality of monolithic lithium hydride.

5.2. The Nuclear Reactor as a Source of Neutron and γ Radiation.

Let us first introduce some simplifying assumptions.

First, the usual cylindrical reactor is replaced with a spherical reactor with the same volume ($V_{cyl} = V_{sph}$) and with reflectors taken into account.

Second, we will assume that 1 kW of reactor thermal power corresponds to ~3.1 $\times$ 10^{13} acts of fission in the core per second. By keeping in mind that each act of fission generates an average 2.47 fast neutrons, we obtain that 1 kW of reactor thermal power will result in an average of 7.7 $\times$ 10^{13} fast neutrons per second.

Third, we will assume that the entire γ radiation spectrum in the energy range from ~0.25 to 1 MeV derives from an average of five γ quanta with an average energy of ~2.5 MeV per γ quantum. Thus, each fission of nuclear fuel (for example, uranium-235) is accompanied by a total γ radiation yield of ~12.5 MeV.

As we have observed previously, the probability of avoiding neutron leakage during moderation is determined by e^{-B^2t}. Consequently, the relative leakage of fast neutrons from the core confines is 1- $e^{-B^2\tau}$ of the total number of neutrons generated. Thus, the fast neutron flux at the surface of an equivalent spherical reactor (A_{sph}) will equal

$$\phi_o = \frac{7.7 \times 10^{13} \dot{Q}_t}{A_{sph}} \left(1 - e^{-B^2\tau} \right) \quad , \tag{5.1}$$

where $\dot{Q}_t$ is the reactor thermal power in kilowatts.

The intensity of γ radiation at the surface of the spherical reactor at point B (Fig. 5.2) from an elementary spherical volume segment dV is determined from the relationship

$$dJ_o = \frac{dE}{4\pi r^2} e^{-\mu r} \quad , \tag{5.2}$$

190
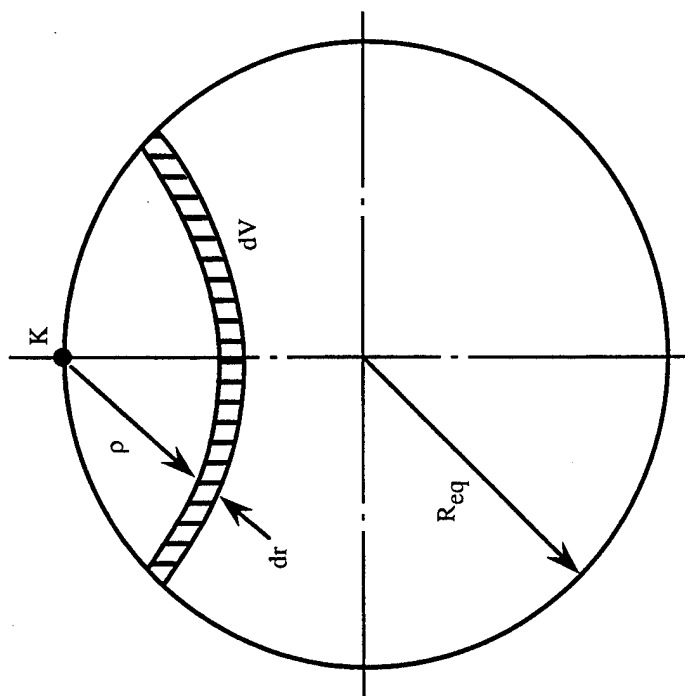
Fig. 5.2 Geometrical construction for calculating gamma radiation intensity in the core.

where $dE = i_\gamma dV$ is the average γ radiation energy per second from the elementary volume dV; $i_\gamma = (38.75 \times 10^{13} \dot{Q}_t)/V_{eq}$, taking the third assumption into account, is the average volumetric γ radiation; μ_Σ is the total linear attenuation coefficient of all materials in the core, with the assumption that $\mu_\Sigma = $ const.

If we take into account that an elementary spherical volume segment is equal to

$$dV = 2\pi r^2 \left(1 - \frac{r}{2R_{eq}} \right) dr \quad , \tag{5.3}$$

equation (5.2) becomes

$$dJ_0 = \frac{i\gamma}{2} \left(1 - \frac{r}{2R_{eq}} \right) e^{-\mu_\Sigma r} dr \tag{5.4}$$

The intensity of γ radiation at point B from the entire core volume is expressed by the relationship

$$J_0 = \int_0^{2R_{eq}} dJ_0 = \int_0^{2R_{eq}} \frac{i_\gamma}{2} \left(1 - \frac{r}{2R_{eq}} \right) e^{-\mu r} dr = \frac{i_\gamma}{2\mu_\Sigma} \left[1 - \frac{1}{2\mu_\Sigma R_{eq}} \left(1 - e^{-2\mu_\Sigma R_{eq}} \right) \right] . \tag{5.5}$$

If we take into account that the average volumetric γ radiation is

$$i_\gamma = \frac{38.75 \times 10^{13} \dot{Q}_t}{\frac{4}{3} \pi R_{eq}^3} \quad , $$

the last equation finally becomes

$$J_0 = \frac{14.53 \times 10^{13} \dot{Q}_t}{2\mu_\Sigma R_{eq}^3} \left[1 - \frac{1}{2\mu_\Sigma R_{eq}} \left(1 - e^{-2\mu_\Sigma R_{eq}} \right) \right] \quad . \tag{5.6}$$

Before proceeding to a step-by-step discussion of shield design, we will take a brief look at the mechanism of γ radiation and neutron flux attenuation.

5.3. Mechanism of γ Radiation and Neutron Flux Attenuation in Shielding Materials

When γ quanta interact with shield materials, the known effects of absorption and scattering of γ quanta and the formation of electron-positron pairs are observed. The end result of these effects is a reduction in γ radiation intensity. This phenomenon is quantitatively described by the equation

$$J = J_0 e^{-\mu x} \quad , \tag{5.7}$$

where I_0 is the γ radiation intensity before the initial shield layer; x is the thickness of this layer; and μ is the linear γ quanta attenuation factor in a layer of thickness x.

When there are several shielding layers, the net γ radiation intensity after the last layer will be

$$J = J_0 e^{-\mu_1 x_1} e^{-\mu_2 x_2} \dots e^{-\mu_n x_n} \tag{5.8}$$

where μ_n, x_n are the linear γ quanta attenuation factor and the thickness of the last layer, respectively.

Equation (5.8) holds true for "narrow beams" of γ quanta which are absorbed during any interaction with a substance.

With "broad beam" γ radiation, characteristic of space power plant nuclear reactors, the shielded object is reached not only by "narrow beams" but also by a portion of γ quanta that have been scattered. This situation accounted for by introducing the factor $B_e > 1$ in equation (5.8), the energy build-up factor. This factor depends on the energy of the γ quanta, the shielding material and its thickness, and on the mutual arrangement of the reactor and the object being shielded. Numerical values of the factor B_e as well as of the linear attenuation factor μ are given in appropriate reference books.

The mechanism of neutron interaction with substances during moderation was examined earlier (2.3). The attenuation of "narrow beam" monoenergetic neutrons is described by a relationship similar to (5.7),

$$\phi = \phi_0 e^{-\Sigma_t x} \quad , \tag{5.9}$$

where ϕ_0 is the neutron flux density before the shield layer; x is the layer thickness; Σ_t is the total macroscopic absorption cross section of the given layer material.

A method called the "exposure cross section" method is widely used in engineering calculations of shielding. This method supposes that the fundamental penetrating component of neutron radiation is fast neutrons. The shielding is designed based on their attenuation and absorption.

As far as thermal neutrons are concerned, it is assumed that they are absorbed by a comparatively thin shield layer. The attenuation and absorption of fast neutrons is described by the relationship

$$\phi = \phi_0 \exp\left(-\Sigma_g x\right) \tag{5.10}$$

where Σ_g is the macroscopic "exposure" cross section, which depends on the characteristics of the shield material. Numerical values are given in appropriate reference books.

5.4. Shield design.

The shield design problem involves a determination of the combination of shield layers and materials that will reduce the total neutron flux and γ radiation past the last shield layer to an established allowable norm and with a shield mass and size that is acceptable. Proposed designs differ in shield thickness and in the shield layer materials. Thus, the shield design problem involves a typical optimization of many variables within given limits which is accomplished in the following sequence.

Neutron flux attenuation is evaluated first. Let's examine a neutron flux emanating from an elementary core surface area dA and which passes into an external medium in the neighborhood of point A (Fig. 5.3). This flux is determined by the following relationship

$$d\phi_a = \frac{\phi_o dA}{2\pi r_a^2}\left[e^{-\Sigma_{g1}r_1}e^{-\Sigma_{g2}r_2}....e^{-\Sigma_{gn}r_n}\right] \qquad , \qquad (5.11)$$

where r_a is the distance between the surface element dA and point A, which is determined by the mutual arrangement of the shield and the object being shielded; Σ_{g1} is the exposure cross section of the i-th shield layer of thickness r_i.

If we take into account that $dA = 2\pi R_{eq}\sin\varphi d\varphi$, and also make the simplifying assumptions of the approximate equalities $r_a = L$, $r_i = x_i$, the neutron flux from the core surface area dA incident at point A after neutron attenuation by the shield will derive from the relationship

$$\phi_a = \phi_o \frac{R_{eq}^2}{L^2}\left[e^{-\Sigma_{g1}r_1}e^{-\Sigma_{g2}r_2}....e^{-\Sigma_{gn}r_n}\right]\cdot\int_0^{\varphi_o}\sin\varphi d\varphi$$

$$= \phi_o \frac{R_{eq}^2}{L^2}\left[e^{-\Sigma_{g1}r_1}e^{-\Sigma_{g2}r_2}....e^{-\Sigma_{gn}r_n}\right](1-\cos\varphi_o)$$

Since $\cos\varphi_o = R_{eq}/L$, the equation becomes

$$\phi_a = \phi_o \frac{R_{eq}^2}{L^2}\left(1-\frac{R_{eq}}{L}\right)\left[e^{-\Sigma_{g1}r_1}e^{-\Sigma_{g2}r_2}....e^{-\Sigma_{gn}r_n}\right] \qquad (5.12)$$

In a similar fashion, one can obtain the expression for the γ radiation intensity at point A,

$$J_a = B_e J_o \frac{R_{eq}^2}{L^2}\left(1-\frac{R_{eq}}{L}\right)\left[e^{-\Sigma_{g1}r_1}e^{-\Sigma_{g2}r_2}....e^{-\Sigma_{gn}r_n}\right] \qquad . \qquad (5.13)$$

194
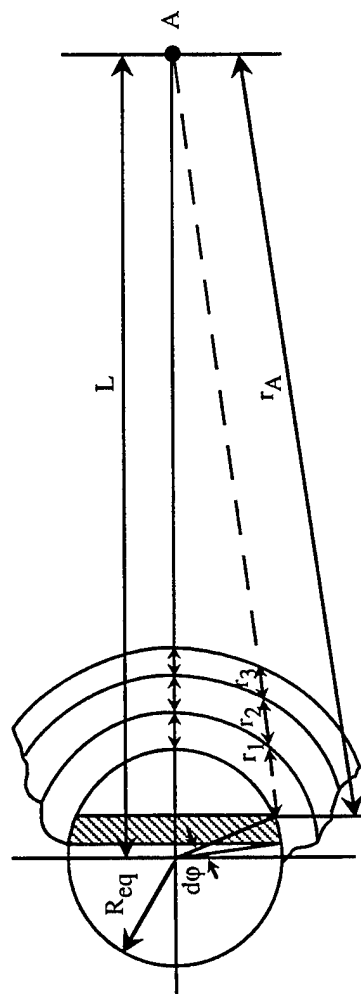
Fig. 5.3 Geometry for radiation shielding calculations.

195

It should be noted that in determining the γ radiation intensity after the last shield layer attention must be paid to secondary γ radiation. This results from radiative neutron capture by the shield material and by γ radiation from loop components that contain a liquid metal coolant activated in the core.

The neutron flux and γ radiation obtained at point A is compared with the allowable level. If necessary, the calculations are repeated for other combinations of thickness and shield layer material and with an increased distance L (if this, of course, is permitted by the nuclear power plant assembly layout on the spacecraft). The purpose of the optimization routine is, as we stated above, to minimize shield mass and size.

5.5. Design of the Shield Assembly for Strength.

As we have stated, the shield assembly is a welded, sealed thin-walled structure consisting of a conical and two spherical jackets or cans (Fig. 5.4). The sealed construction serves to contain the hydrogen that is liberated by dissociation of the lithium hydride. The liberation of hydrogen in the shield during reactor operation causes an increase in positive pressure inside the structure. This requires that cans 1 and 3 be designed for strength and can 2 for rigidity. The design of the shield must also account for heating of the shield components, i.e., the influence of heating on the strength characteristics of the materials. In addition, the nuclear reactor and shield assembly must be subjected to ground tests. An external positive pressure acts on the assembly cans during testing. Consequently, in designing the shield assembly one must verify the rigidity of all cans in the assembly.

We will not discuss methods for obtaining the mathematical relationships for determining critical loads. Instead, we will present the final equations.

The critical positive external pressure acting on a conical can is

$$p_{cr} = 0.92 k_p E \frac{\delta}{L} \left(\frac{\delta}{\bar{r}} \right)^{3/2}$$

Here, the average radius $\bar{r}$ and the factor k_p, which characterize the influence of conicity, are calculated from the formula $k_p = 1 + 0.6 \, r_k$ and $\bar{r} = \dfrac{r_1 + r_2}{2 \cos \gamma}$, where $r_k = 1 - r_1/r_2$.

For a spherical can of radius R and thickness δ,

$$p_{cr} = \frac{2E}{\sqrt{3(1 - \mu^2)}} \left(\frac{\delta}{R} \right)^2$$

The critical pressure computed from the equations must exceed the effective stress during testing by the amount of the safety factor.

196
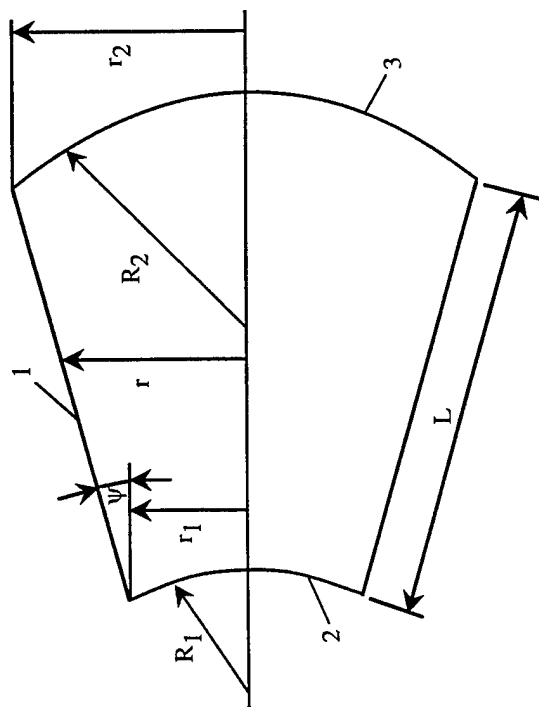
Fig. 5.4 Neutron shield geometry.

The determination of the effective stress usually employs relationships from the "no moment" (momentless) theory. Accordingly, the circumferential (σ_α) and longitudinal (σ_θ) stresses are computed from the following equations:

$$\sigma_\alpha = \frac{pr}{\delta \cos\gamma} \quad ; \quad \sigma_\theta = \frac{pr}{2\delta \cos\gamma}\left(1 - \frac{r_1^2}{r}\right)$$

and for a spherical can,

$$\sigma_\alpha = \sigma_\theta = \frac{pR}{2\delta} \quad .$$

In the operating regime the membrane forces σ_α and σ_θ for cans 1 and 3 are also computed from these relationships and are compared with the endurance limit. The effective stress in can 2 is compared with the critical stress, which is found by taking the modulus of elasticity of the material at the operating temperature into account.

6. THERMOELECTRIC CONVERTERS

6.1. Physical Fundamentals of the Working Process and Schematic of the Thermoelement.

Earlier and in a general way we elaborated on the principles of developing an emf in different direct converters of primary energy into electrical. In this and subsequent chapters we will discuss energy (basically, thermal) conversion processes in greater detail. In keeping with the purpose of this book, this discussion begins with thermoelectric converters.

The principle of operation of thermoelectric converters of heat (TEC) is based on three thermoelectric phenomena known as the Seebeck, Peltier and Thompson effects. We will briefly examine these phenomena in one-dimensional representations of isotropic conductors.

The Seebeck effect. When there is a temperature gradient in a conductor, the concentration and average energy of the electrical charges will change and they will diffuse from regions of higher temperature to regions of lower temperature. This process will continue until equilibrium is established due to the effect of the electrical field that is created. The higher the temperature gradient, the higher the difference in charge concentration between opposite ends of the conductor when equilibrium is reached.

In dissimilar metal conductors that make up a diode, the electrical charges that diffuse are of the same sign, electrons. But their concentration gradient and degree of diffusion in these conductors differ. Therefore, across the ends of an open circuit of a simple thermocouple consisting of conductors 1 and 2 in the diode (Fig. 6.1), a potential difference appears, the so called thermal emf, which is proportional, other conditions being equal, to the temperature drop. However, the thermal emf of the conductors is extremely small, no more than $(2-4) \times 10^{-5}$ V/K. Such an emf is of no practical value in the design of power plants. Such thermocouples are used mainly in measurement technology.

The circuit must consist of two semiconductors, one of which possesses electron conductors (n) and the other hole conductors (p). In the first, electrons diffuse to the cold junction, and "holes" diffuse in the second. This is one of the reasons for the increase in thermal emf because the potential ends of the circuit acquire different signs. Thus, p-n type semiconductor materials typically have a thermal emf of $\sim(4-6) \times 10^{-4}$ V/K.

Quantitatively, the phenomenon is described is follows. Let the temperature difference dT between the junctions of a simple thermocouple be infinitely small. Then

$$dE_{1,2} = \alpha_{1,2}dT \qquad , \qquad (6.1)$$

where E is the thermal emf; and $\alpha_{1,2}$ is the differential thermal emf factor of conductors 1 and 2. This factor depends not only on the individual properties of the semiconductors but also on temperature. If the temperature difference between the junctions is finite, then the thermal emf will also acquire a finite value:
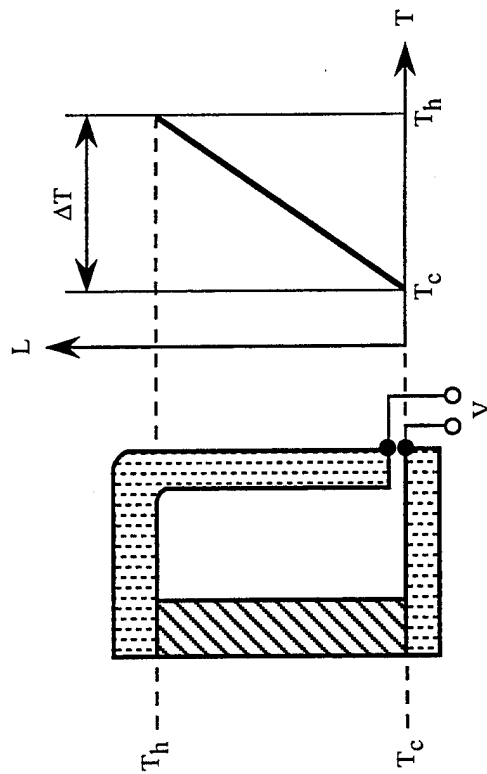
Fig. 6.1 Idealized thermoelectric element schematic.

$$E_{1,2} = \int_{T_c}^{T_h} \alpha_{1,2} dT = \overline{\alpha}_{1,2}(T_h - T_c) \qquad (6.2)$$

where $\overline{\alpha}_{1,2}$ is the average differential thermal emf factor in the range T_h - T_c (the temperatures of the hot and cold junctions) determined from the equation

$$\overline{\alpha}_{1,2} = \frac{\int_{T_c}^{T_h} \alpha_{1,2} dT}{T_h - T_c} \qquad . \qquad (6.3)$$

The Peltier Effect. During the flow of an electrical current in a circuit consisting of two or several dissimilar conductors in series, heat (Peltier heating) is generated or absorbed at the junctions depending on the direction of the current and on the properties of the individual conductors.

The Peltier effect is explained by the fact that in dissimilar conductors the current carrier (electron) distributions differ depending on energy. During the passage of an electric current through a conductor junction and during the transfer of charges from one conductor to another, a charge redistribution occurs depending on energy. If the average energy of the charges decreases, then the excess energy is converted into heat. If, on the other hand, the average energy increases, then excess energy is taken from the surroundings and heat absorption occurs.

It follows that the liberated or absorbed heat must be proportional to the number of charges transferred per unit time, that is, to the current strength. In fact, there is a relationship which is in very good agreement with experimental data:

$$\dot{Q}_P = P_{1,2}I \qquad , \qquad (6.4)$$

where $P_{1,2}$ is the Peltier factor which depends on the specific properties of conductors 1 and 2 and on the junction temperature; $\dot{Q}_P$ is the absorbed or liberated thermal power.

The Peltier effect is many times stronger in p-n type semiconductors than in metals. This is caused by the substantial change in energy of oppositely charged charge carriers (electrons and "holes") as they transition through the junction during the passage of the current. Let's assume that a current flows through a p-type material to an n-type material. The "holes" travel in the same direction, the electrons in the opposite direction. After passing through the junction, the "holes" and the electrons recombine in both materials which, as is well known, is accompanied by the liberation of energy. During the flow of current from an n-type material to an p-type material, the direction of the "holes" and the electrons reverses. In the junction, a deficiency of electrons occurs in the n-type material, and in the p-type material there is a deficiency of "holes." Compensation takes place by a transition of electrons in both materials from the valence band to the conductivity band with the formation of new electron-hole pairs which diffuse through the junction toward each other.

The transition of electrons from the valence band to the conductivity band requires the expenditure of energy. This is absorbed from the surroundings as heat. The sign of Peltier heat (absorption or liberation) at the junction point of any two conductors, either metals or semiconductors, is related to the Seebeck effect in a circuit made up of these materials.

If the circuit in Fig. 6.1 is closed, then a current will develop in any direction, but Peltier heat will always be absorbed at the hot junction and liberated at the cold junction.

The Thompson Effect. When a current passes through a conductor with a temperature gradient in it, heat (Thompson heat) is liberated or absorbed in it. It is not entirely related to joule heating, which, of course, is always generated by an ohmic resistance different from zero.

Thompson heat is caused by the Peltier effect, i.e., by a change in the average energy of the diffusing charge carriers during transitions into regions of lower or higher temperatures.

The quantity of heat liberated or absorbed per unit time in finite length conductors is

$$d\dot{Q}_{Thm} = \tau_1 I \frac{dT}{dx} dx = \tau_1 I dT \tag{6.5}$$

where τ_1 is the Thompson factor which depends on the temperature and specific properties of the conductors.

Physically, the essence of the Thompson effect is its close interrelationship with the Seebeck and Peltier effects. All three effects are reversible. They manifest themselves simultaneously if the thermocouple circuit in Fig. 6.1 is closed. In addition, two irreversible processes also take place: joule heating and heat transfer from the hot junction to the cold junction by thermal conductance.

In establishing a quantitative relationship between the three reversible thermoelectric effects, Thompson used the first and second laws of thermodynamics without accounting for irreversible processes. By solving these equations simultaneously, Thompson obtained the desired interrelationship in the form $P_{1,2} = \alpha_{1,2} T$, where the factors $P_{1,2}$ and $\alpha_{1,2}$ correlate with the given temperature, T.

In evaluating the magnitude of the thermal emf, we will mention the following.

If conductors 1 and 2 have the same conductivity, for example, electron conductivity, then the absolute thermal emf factors of the thermocouple in Fig. 6.1 have the same sign and their mean differential thermal emfs are determined by the difference in the absolute values: $\bar{\alpha}_{1,2} = |\bar{\alpha}_1| - |\bar{\alpha}_2|$.

If the materials of branches 1 and 2 are p and n type semiconductors, respectively, then the absolute thermal emf factors are of opposite sign and the mean differential thermal emf factor is determined by the sum of the absolute values: $\bar{\alpha}_{n,p} = |\bar{\alpha}_n| - |\bar{\alpha}_p|$.

This situation, as has already been noted, is one of the reasons for the higher thermal emf of semiconductor thermocouples in comparison with metallic thermocouples. Another, and more significant, reason is that the thermal emf of any single semiconductor is on the average 10-20 times higher than of a metal conductor.

If the open ends of a thermocouple is connected to an external load with a resistance R_L, a current will then flow through the circuit. Thermal power, I^2R_L, will be produced at the load. A generator is created in which thermal energy is converted directly into electrical energy. In order to maintain a given temperature of the hot and cold junctions during operation of the generator, heat must be supplied continuously to the hot junction and removed from the cold junction. The supplied heat is absorbed in the hot junction as Peltier heat, and, in addition, transferred by thermal conductance to the cold junction. The heat removed is that accumulated from Peltier heat liberated at the cold junction and heat transferred by thermal conductance from the hot junction. A heat balance on the junctions should also take into account Thompson and joule heating produced in the conductors. The schematic of an actual thermoelement comprising a basic TEC differs from the simple one shown in Fig. 6.1. First of all, it does not use conductors but semiconductors of p and n type materials. In addition, it is advisable not to make the junctions directly as in Fig. 6.1, but through intermediate metallic conductors, electrical connectors, as is shown in Fig. 6.2, a schematic of an actual thermoelement. The increase in internal resistance of the thermoelement due to the electrical connectors is negligibly small because the electrical conductivity of these plates is 2-3 times higher than that of the semiconductors which make up the thermoelement. The joints between the metals and the semiconductors can also be made with relatively low electrical resistances.

A layer of electrical insulation must be placed between devices for adding and removing heat and the electrical connectors. Therefore, the temperature of the heat source, T_{hs}, will of necessity exceed the hot junction temperature, T_h, and the temperature of the cooling device, T_{cd}, will be lower than the cold junction temperature, T_c. The temperature drop between the heat source and the cooling device ($T_{hs} - T_{cd}$), which determines the external temperature regime of the power plant as a whole, is greater than the temperature drop in the thermoelement: $\Delta T_{tot} = T_{hs} - T_{cd} > \Delta T = T_h - T_c$.

6.2. Volt-Ampere Characteristics and Power of a Thermoelement.

Let's examine the steady-state operating mode of the thermoelement. In Ohm's law for a closed circuit, $I = \dfrac{E - V}{r} = \dfrac{E}{R + r}$, the electromotive force E is determined from the relationship (6.2), and the internal resistance of the thermoelement r for given temperature conditions remains constant. Therefore, the current I as a function of voltage V, which is the volt-ampere characteristic of the thermoelement, is a linear function (Fig. 6.3). As the load resistance R changes from zero (short circuit) to infinity (open circuit), the current,

$$I = \frac{E}{R + r} \qquad (6.6)$$

changes from a maximum (I_{sc}) to zero, and the voltage $V = IR$ changes correspondingly from zero to E.
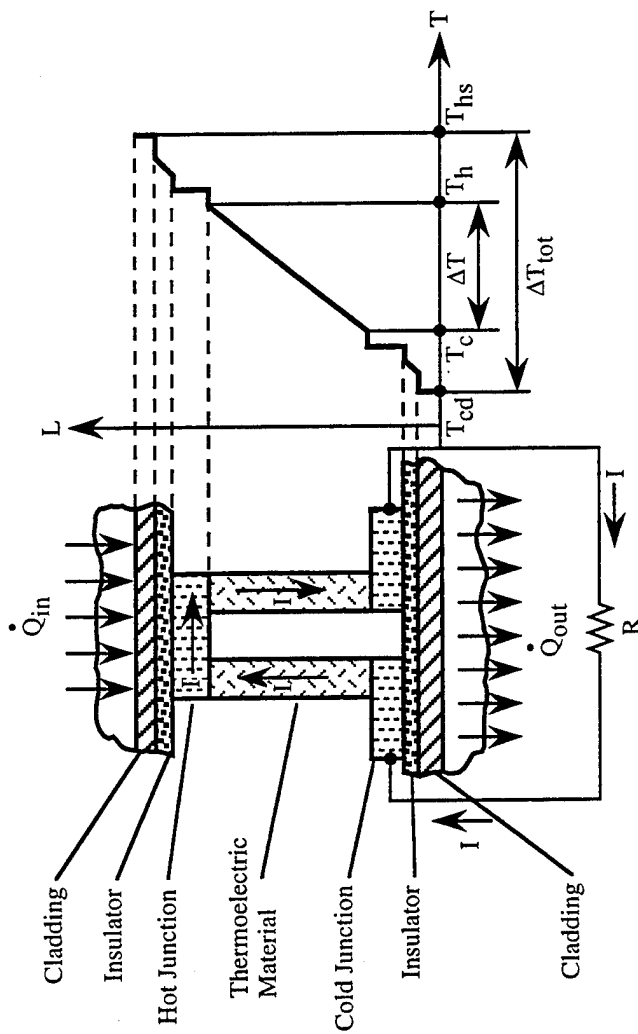
Fig. 6.2 TEC temperature profile. Temperature drops occur not only in the thermoelectric materials, but also in toher materal layers.
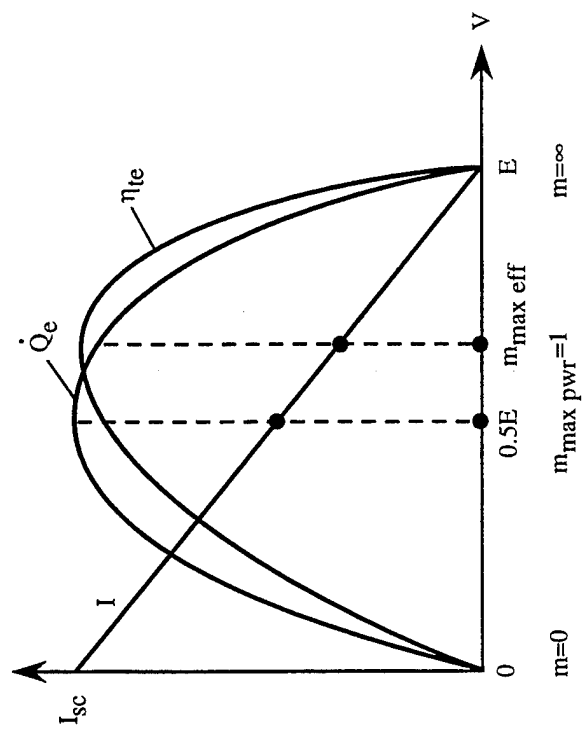
Fig. 6.3 Electric power, efficiency and current versus output voltage of a thermoelectric converter.

As is evident in Fig. 6.3, the shape of the volt ampere characteristic depends on the internal resistance r for a given E. In the ideal case (r=0), the volt ampere characteristic would become a straight line, E = const, parallel to the ordinate axis.

By using the relationship in (6.2), equation (6.6) can be written in the following form:

$$I = \frac{\overline{\alpha}_{n,p}\Delta T}{r(1+m)} \qquad , \qquad (6.7)$$

where $\Delta T = T_h - T_c$; and $m = R/r$ is the relative resistance of the external circuit.

Hence, the load voltage is

$$V = \frac{\overline{\alpha}_{n,p}\Delta T_m}{1+m} \qquad . \qquad (6.8)$$

The power produced at the load

$$\dot{Q}_e = I^2 R = \frac{E^2}{r}\frac{m}{(1+m)^2} \qquad . \qquad (6.9)$$

reaches a maximum at r = R, i.e., at m = 1. $\dot{Q}_e$ as a function of V (Fig. 6.3) is a quadratic parabola:

$$\dot{Q}_e = VI = V\frac{E-V}{r} \qquad .$$

It is not difficult to see that the maximum $\dot{Q}_e$ is reached when V = 0.5E. Taking the relationship in (6.2) into account, equation (6.9) becomes

$$\dot{Q}_e = \frac{\left(\overline{\alpha}_{n,p}\Delta T\right)^2 m}{r(1+m)^2} \qquad . \qquad (6.10)$$

The effectiveness of the thermoelement is usually not evaluated in absolute but in relative terms. Such characteristics are: the current density J"; the power density

$$\dot{Q}_e^{\,"} = \frac{\dot{Q}_e}{A_{n,p}}$$

where $A_{n,p}$ is the total cross sectional area of both branches of the thermoelement; the volumetric power

$$\dot{Q}_e''' = \frac{\dot{Q}_e}{V_{n,p}}$$

where $V_{n,p}$ is the total volume of the thermoelement branches; and the power to mass ratio

$$\dot{Q}_{e,spec} = \frac{\dot{Q}_e}{m_{te}}$$

where m_{te} is the mass of the thermoelement branches.

In order to obtain an approximate evaluation of these parameters we will assume that the branches of the thermoelement have equal cross sectional areas, $A_n = A_p = 0.5A_{n,p}$, and equal electrical conductivity and density. In addition, we will neglect the ohmic resistance of the electrical connectors and junctions. For these conditions, the internal resistance of the thermoelement is $r = \dfrac{2L}{\bar{\sigma}A_b}$, where L is the length of the branches, $\bar{\sigma}$ is the average electrical conductivity of the material of the branches in the temperature range $T_h - T_c$; $A_b = 0.5A_{n,p}$ is the cross sectional area of each branches. If we substitute these expressions in equations (6.7) and (6.10), we obtain

$$J'' = \frac{I}{A_b} = \frac{\bar{\alpha}_{n,p}\bar{\sigma}\Delta T}{2L(1+m)} \qquad ; \qquad (6.11)$$

$$\dot{Q}_e'' = \frac{\dot{Q}_e}{2A_b} = \frac{\left(\bar{\alpha}_{n,p}\Delta T\right)^2 \bar{\sigma}m}{4L(1+m)^2} \qquad ; \qquad (6.12)$$

$$\dot{Q}_e''' = \frac{\dot{Q}_e}{2A_b L} = \frac{\left(\bar{\alpha}_{n,p}\Delta T\right)^2 \bar{\sigma}m}{4L^2(1+m)^2} \qquad ; \qquad (6.13)$$

$$\dot{Q}_{e,spec} = \frac{\dot{Q}_e}{2\rho A_b L} = \frac{\left(\bar{\alpha}_{n,p}\Delta T\right)^2 \bar{\sigma}m}{4\rho L^2(1+m)^2} \qquad . \qquad (6.14)$$

As is evident, all the parameters presented will increase as $\bar{\alpha}_{n,p}$, $\bar{\sigma}$ and ΔT increase and as L decreases. Hence, it would seem that an unlimited decrease in the length of the branches L is prudent. However, for a given $\Delta T_{tot} = T_h - T_c$ (see Fig. 6.2), as L decreases ΔT will also decrease. Therefore, in choosing L it is necessary to take all these factors into account. In existing designs, L falls in the range 1-3 cm, and typical thermoelement parameters are: $V = 0.05$-0.07 V; $J'' = 5$-10 A/cm²; $\dot{Q}_e'' = 0.1$-0.4 W/cm²; $\dot{Q}_e''' = 0.05$-0.2 W/cm³; $\dot{Q}_{e,spec} = 30$ W/kg.

6.3. Thermoelement Efficiency.

By definition, the efficiency of any converter of thermal energy into electrical is the ratio of the electrical power consumed by an external load to the input thermal power. The efficiency of the thermoelement we are looking at is $\eta_{te} = \dfrac{\dot{Q}_e}{\dot{Q}_t}$. The following assumptions are used in deriving the equation for efficiency:

1. The ohmic resistance of the electrical connectors and junctions is negligibly small and they produce no joule heat.

2. The side surfaces of the branches are fully insulated, and the input and removal of heat is done only through the contact surfaces of the branches with the electrical connectors.

3. Heat from the heat source can be transferred only by thermal conductance through the branch materials.

These assumptions model reality quite well and do not introduce any significant error in the analysis of efficiency. According to the second assumption, Thompson heat and joule heat is transferred by thermal conductance to the junctions.

It can be shown that the total Peltier and Thompson heat absorbed by the hot junction is in practice equal to only Peltier heat if the factor $P_{n,p}$ is not determined by the differential thermal emf factor $\alpha_{n,p}$ at the temperature T_h, but by the average differential thermal emf factor $\bar{\alpha}_{n,p}$ in the temperature range $T_h - T_c$:

$$\dot{Q}_{Pel-Thom} = \bar{\alpha}_{n,p} I T_h \quad . \tag{6.15}$$

In addition, two irreversible thermal processes occur in thermocouples: heat transfer from the hot junctions to the cold junctions by thermal conduction,

$$\dot{Q}_{cond} = K(T_h - T_c) \quad ,$$

where K is the thermal conductance; and joule heating in the branches,

$$\dot{Q}_j = I^2 R \quad .$$

It will be assumed that joule heating is equally divided between the branches. This agrees with reality when the thermal conductivity and the electrical conductivity are constant along the branches. Consequently, a thermal power $\dot{Q}_t = 0.5 I^2 R$ is produced at the hot junctions.

In the steady-state thermal regime, the input thermal power from an external source is

$$\dot{Q}_i = K(T_h - T_c) + \bar{\alpha}_{n,p} I T_h - 0.5 I^2 R.$$

By substituting this expression and equation (6.10) in the basic expression for efficiency and by using equation (6.7), we obtain after some simple transformations

$$\eta_{te} = \frac{\Delta T}{T_h} \frac{m}{\dfrac{Kr(1+m)^2}{\bar{\alpha}_{n,p}^2 T_h} + m + 1 - 0.5 \dfrac{\Delta T}{T_h}} \qquad . \tag{6.16}$$

It is apparent that the efficiency of a thermoelement is the product of the Carnot cycle efficiency of a heat engine operating in the temperature range T_h - T_c, i.e.,

$$\eta_{Carnot} = \frac{\Delta T}{T_h} = 1 - \frac{T_c}{T_h}$$

and some factor $\eta_{n,p}$,

$$\eta_{n,p} = \frac{m}{\dfrac{Kr(1+m)^2}{\bar{\alpha}_{n,p}^2} + m + 1 - 0.5 \dfrac{\Delta T}{T_h}} \tag{6.17}$$

This factor depends on the properties of the thermoelement branches (K, r, $\alpha_{n,p}$), the temperature conditions (ΔT, T_h), and the operating regime determined by the operating point on the thermoelement volt ampere characteristic.

The factor $\eta_{n,p}$ reflects the influence of irreversible processes, thermal conductance and joule heating. Indeed, if it is assumed that these processes do not take place (K = r = 0), then it is easy to ascertain that $\eta_{n,p} = 1$ and $\eta_{te} = \eta_k$.

All parameters that characterize the properties of both branches can be combined into a quantity

$$\bar{Z}_{n,p} = \frac{\bar{\alpha}_{n,p}^2}{kr} \qquad , \tag{6.18}$$

which is measured in degrees Kelvin to the minus first power (K^{-1}) and which pertains to the same temperature interval T_h - T_c in which these parameters are determined.

$\bar{Z}_{n,p}$ is called the average figure of merit of the thermoelement. It is an important characteristic of the efficiency of any thermoelectric device. By using it, we can rewrite equation (6.16) in the following form:

$$\eta_{te} = \left(\frac{\Delta T}{T_h}\right)\left\{\frac{m}{\dfrac{(1+m)^2}{\overline{Z}_{n,p}T_h} + m + 1 - 0.5\dfrac{\Delta T}{T_h}}\right\} \qquad (6.19)$$

The larger $\overline{Z}_{n,p}$ is, other conditions being equal, the higher the efficiency of the thermoelement.

Obviously, in order to obtain the maximum average figure of merit the cross section of the thermoelement branches must be chosen such that the product KR is a minimum. Let's write the equations for K and R:

$$K = K_n + K_p = \frac{\overline{k}_n A_n}{L_n} + \frac{\overline{k}_p A_p}{L_p} \quad ; \quad R = R_n + R_p = \frac{L_n}{A_n \overline{\sigma}_n} + \frac{L_p}{A_p \overline{\sigma}_p}$$

,

where $\overline{k}_n$ and $\overline{k}_p$ are the average thermal conductivities in the temperature range T_h - T_c.

From manufacturing considerations, the length of the branches should be the same $(L_n = L_p)$, therefore

$$KR = \left(\overline{k}_n + \overline{k}_p \frac{A_p}{A_n}\right)\left(\frac{1}{\overline{\sigma}_n} + \frac{1}{\overline{\sigma}_p}\frac{A_n}{A_p}\right)$$

If we assume that the properties of the branch materials are known, we find from the equation

$$\frac{\partial(KR)}{\partial\left(\dfrac{A_n}{A_p}\right)} = 0$$

the condition which the cross-sectional area of the branches should satisfy:

$$\frac{A_p}{A_n} = \sqrt{\frac{\overline{k}_n \overline{\sigma}_n}{\overline{k}_p \overline{\sigma}_p}} \qquad (6.20)$$

In observing this condition, equation (6.18) becomes

$$\overline{Z}_{n,p} = \frac{\overline{\alpha}_{n,p}^2}{\sqrt{\overline{k}_n/\overline{\sigma}_n} + \sqrt{\overline{k}_p/\overline{\sigma}_p}} \qquad . \qquad (6.21)$$

Reference books on thermoelectric materials list the average figure of merit for given materials, in our case, for n- and p-type semiconductors:

$$\overline{Z}_n = \frac{\overline{\sigma}_n \overline{\alpha}_n^2}{\overline{k}_n} \quad , \quad \text{and} \quad \overline{Z}_p = \frac{\overline{\sigma}_p \overline{\alpha}_p^2}{\overline{k}_p} \qquad (6.22)$$

If the parameters of the materials α, λ, and σ are not averaged over the temperature range T_h - T_c, but are determined for a certain temperature, then

$$Z_n = \frac{\sigma_n \alpha_n^2}{k_n} \quad , \quad \text{and} \quad Z_p = \frac{\sigma_p \alpha_p^2}{k_p} \qquad (6.23)$$

are the figures of merit at the given temperature.

Thus, the criterion for selecting semiconductor materials that will result in maximum thermoelement efficiency is the figure of merit. The figure of merit depends on three different properties of the material: thermal conductivity, electrical conductivity and thermal emf.

Another factor that influences thermoelement efficiency is the temperature regime (T_h and T_c). It follows from equation (6.19), other conditions being equal, that the efficiency will increase as T_h increases and as T_c decreases. However, one cannot be limited to such a simple examination of the isolated influence of T_h and T_c on η_{te}. An increase in T_h or a reduction in T_c to a level higher or lower than a certain value can lead to a significant reduction in $\overline{Z}_{n,p}$. Instead of an anticipated increase in efficiency, it may be reduced instead. In the end, an evaluation of the influence of T_h and T_c on η_{te} is possible only by knowing $Z_{n,p}$ as a function of T for specific thermoelectric materials.

Finally, the last factor that according to equation (6.19) influences η_{te} is the relative external circuit resistance m. We find from the equation

$$\frac{\partial \eta_{te}}{\partial m} = 0$$

the optimum value of m that corresponds to the maximum efficiency:

$$m_{maxeff} = \sqrt{1 + \overline{Z}_{n,p} \overline{T}} \qquad , \qquad (6.24)$$

where $\overline{T} = \dfrac{T_h + T_c}{2}$.

Typically, $m_{max\ eff} > 1$ and depends on the temperature conditions and on $\overline{Z}_{n,p}$, while $m_{max\ pwr}$ always equals unity. $\overline{Z}_{n,p} = (0.6\text{-}1.4) \times 10^{-3}$ K^{-1} for existing thermoelectric materials. At $T_h = 1000\text{-}1100$ K and $T_c = 600\text{-}700$ K, the optimum resistance $m_{opt} = 1.2\text{-}1.5$, i.e., it exceeds $m_{max\ pwr}$. The maxima of η_{te} and Q_e for m do not agree with each other (see Fig. 6.3). Let's discuss this in more detail. To the left, the

maximum power is reached as the efficiency is decreasing. To the right, the numerator in the equation for the slope of the efficiency changes insignificantly. At the same time, the denominator, i.e., the input thermal power, decreases (the influence of the last two terms in the expression for Q_t) which leads to an increase in efficiency. This continues until the reduction in Q_t does not compensate for the sharp drop in useful electrical power Q_e. Thus, the maximum efficiency on the volt ampere characteristic is located to the right of the maximum power. Such a situation is characteristic of any (except photoelectric) direct converters of primary energy. At the same time, the range of operating points on the volt ampere characteristic in the indicated range permits one to solve important problems in selecting the design regime for a given converter.

If we solve equations (6.19) and (6.21) simultaneously, we obtain

$$\eta_{te\,max} = \frac{\Delta T}{T_h} \frac{m_{max\,eff} - 1}{m_{max\,eff} + \frac{T_c}{T_h}} = \frac{\Delta T}{T_h} \frac{\sqrt{1 + \overline{Z}_{n,p}\overline{T}} - 1}{\sqrt{1 + \overline{Z}_{n,p}\overline{T}} + \frac{T_c}{T_h}} \qquad . \qquad (6.25)$$

Here, as well as in equations (6.16) and (6.19), there is the product of the Carnot cycle efficiency and the factor $\eta_{n,p}$,

$$\eta_{n,p} = \frac{\sqrt{1 + \overline{Z}_{n,p}\overline{T}} - 1}{\sqrt{1 + \overline{Z}_{n,p}\overline{T}} + \frac{T_c}{T_h}} \qquad , \qquad (6.26)$$

which reflects the influence of irreversible processes.

In order to increase efficiency, it is important not just to have a high figure of merit, but also a large product $\overline{Z}_{n,p}\overline{T}$.

The advantage in space nuclear power plants of materials that have approximately the same $\overline{Z}_{n,p}\overline{T}$ is a higher T_h and T_c. An increase in T_c will decrease the required radiator surface area. The product $\overline{Z}_{n,p}\overline{T}$ as well as the product $\overline{Z}_{n,p}T$ for a certain material at a given temperature is sometimes called the Ioffe criterion or the figure of merit criterion. The following parameters are typical of thermocouples for space nuclear power plants: $\overline{Z}_{n,p}\overline{T} = 0.8$ to 1.0; $T_c/T_h = 0.65$ to 0.7. The efficiency η_{te} is 5-7% in this case. This is a comparatively low efficiency considering that in a thermoelectric generator consisting of several thermoelements there are additional losses that reduce the efficiency. The main reason for the low efficiency is the irreversible processes. These are estimated by the factor $\eta_{n,p}$, which is about 20% for the parameters indicated above. In other words, the efficiency of a thermoelement is about five times less than the corresponding Carnot cycle efficiency.

The most effective way of increasing the efficiency of a thermoelement is to increase the $\overline{Z}_{n,p}\overline{T}$ criterion. That's because a reduction in T_c is limited by the radiator dimensions. In addition, there are a number of design and manufacturing measures. We will point out some of them.

1. Nonuniform distribution of impurities along the height of the thermoelement branches. It has been established experimentally that in order to increase $\overline{Z}_{n,p}$ and $\overline{Z}_{n,p}\overline{T}$ of n and p-type branches, it is recommended that the concentration of impurities be reduced from the hot to the cold junction. This, as a rule, is valid for any thermoelectric material.

2. Cascading the branches. Since the maximum figure of merit for different materials correspond to different temperatures, it is recommended that each branch of the thermoelement be made of several materials connected in series. Such branches are called cascaded branches. In reality, however, additional losses associated with thermal and electrical resistances of the junctions must be accounted for. These losses will increase with an increasing number of cascades, but the increase in the figure of merit will be much less obvious. Therefore, it is doubtful that more than two or three cascades in thermocouples with a finite temperature drop $T_h - T_c$ should be used in thermoelectric converters for nuclear space power plants. For example, during operation in the 800-1300 K temperature range with two cascades a figure of merit $\overline{Z}_{n,p}\overline{T} = 1.3$-$1.4$ is successfully obtained. The efficiency of such a cascaded thermoelement compared with a single cascade thermoelement increases by about 30-40%.

3. Profiling the branches. The maximum efficiency of a thermoelement, as shown in Fig. 6.3, is obtained for a fully defined relative external load $m_{max\ eff} = R/\overline{r}$ as determined by equation (6.24). In addition, any infinitely small segment of a branch dL can be viewed as a simple thermoelement connected in series in a circuit of similar thermocouples. Of course, a condition can be set up such that not only the branch but also the elementary generator made up of several thermocouples has a maximum efficiency. An infinitely small load befitting any simple thermoelement ought to be optimum and satisfy an equation like (6.24) in which instantaneous values instead of average values of $\overline{Z}_{n,p}$, and $\overline{T}$, should be substituted. The current in all sections is the same: $I = J''A_b$.

From this condition, the change in cross sectional area of the branches as a function of T and L is found, which will satisfy the equalities $m_{max\ eff} = \sqrt{1 + ZT}$, and

$$A_b = \frac{I\left(1 + \sqrt{1 + ZT}\right)}{\sigma\alpha \dfrac{dT}{dL}}$$

Calculations show that profiled branches can increase the efficiency of a thermoelement by 10-15%.

6.4. Design of Thermoelectric Converters.

The preceding relationships, conclusions and quantitative characteristics pertain to a single ideal thermoelement. In an actual thermoelectric converter which consists of hundreds and thousands of series-parallel connected individual thermoelements that

213

operate under far from identical conditions, there are a number of additional losses that reduce its output characteristics.

All kinds of losses (additional) can be subdivided into thermal and electrical losses. Thermal losses include the following: losses of a portion of the supplied heat by conductance through the side faces of the branches, the connectors and through the insulation between the thermoelements; temperature drops in the multilayer walls (Fig. 6.2); and losses related to the lack of isothermal heat supply and heat removal surfaces.

Sources of electrical losses are ohmic resistances of the electrical connectors, junctions and terminals (series resistances). The expenditure of electrical power on its internal needs by a nuclear power plant is also a loss in output electrical power.

Let's examine the influence of these losses on the basic output parameters of a thermoelectric converter.

1. When thermal conductance losses are taken into account, the power of the heat source must equal $\dot{Q}_i + \Delta \dot{Q}_i$. Therefore, the converter efficiency, other conditions being equal, is reduced by the proportionality factor

$$\eta_{cond} = \frac{\dot{Q}_i}{\dot{Q}_i + \Delta Q_t} \qquad (6.27)$$

For a given thermal power this factor characterizes the relative reduction in electrical power and equals 0.92-0.96.

2. Losses associated with temperature gradients in multilayer walls depend on the thickness of the conductor plates and the insulator layer (see Fig. 6.2), the length of the branches, etc. As δ_{con} and δ_{ins} decrease, the temperature gradients decrease, but the electrical losses will increase. This relationship is quite complex. Rigorous calculations must, in addition to the thermal resistance of multilayer walls, account for volume joule heating in the electrical connectors and heat liberated in the junctions. Calculations show that for combinations of δ_{con}, δ_{ins}, and L close to optimum, the heat transfer coefficient for multilayer walls is about (6 to 8) x 10^3 W/(m²·K). Hence, it is easy to show that the temperature gradient is 15-20 °C.

3. As a result of losses associated with lack of isothermal heat supply and heat removal surfaces, the total power of the individual thermoelements will be less than the product of the power of an ideal thermoelement under the best temperature conditions and the number of thermoelements, i.e.,

$$\sum_{i=1}^{n} \dot{Q}_{ei} < n\dot{Q}_{e,ideal}.$$

The greater the total number of individual thermoelements connected in a series-parallel circuit, the higher the heat losses associated with the lack of isothermal heat addition and

removal. This kind of heat loss is easily estimated by a factor which accounts for nonisothermal heat addition and removal:

$$\eta_{nonisothermal} = \left\{ \frac{\sum\limits_{i=1}^{n} \dot{Q}_{ei}}{n\dot{Q}_{e,ideal}} \right\} . \qquad (6.28)$$

In the most widely used double-loop designs of thermoelectric nuclear power plants, this factor will increase as the flow of liquid metal coolant increases because the temperature gradient at the inlet and outlet of the thermoelectric converter will decrease. However, the pumping power consumption will increase. Therefore, one of the conditions for choosing an optimum flow rate is to maximize the output power. Calculations show that for this condition $\eta_{nonisothermal} = 0.95\text{-}0.98$.

4. In order to evaluate the electrical losses, we will use the simplification that the additional parallel loads (for example, insulation) are at the output voltage V and that the entire generated current in the thermoelectric converter passes through the additional series loads. The useful electrical power will then be less than the thermoelement power determined by equation (6.9) and equation (6.10). The additional load factor can be used in estimating the reduction in useful electrical power,

$$\eta_{load} = \frac{1}{\left(1 + \dfrac{\Delta V}{V}\right)\left(1 + \dfrac{R_L}{R_{par}}\right)} , \qquad (6.29)$$

where R_L is the resistance of the external load; R_{par} is the resistance of the parallel loads; ΔV is the voltage drops in the additional in-series loads.

The efficiency of the thermoelement should be reduced in a similar fashion. The factor η_{load} turns out to equal to about 0.96 to 0.97.

5. Electrical power consumption by internal needs in the electrical power plant (pumps, automatic equipment, etc.) is estimated by the factor

$$\eta_{int} = 1 - \frac{\dot{Q}_{e,int}}{\dot{Q}_e} . \qquad (6.30)$$

which, depending on the design of the power plant and its output power, can vary over a wide range, 0.75-0.9.

Design calculation sequence. The following input data are usually used in design calculations:

a. the required electrical power $\dot{Q}_e$ and the design output voltage V;

b. The thermoelectric converter temperature conditions, i.e., the inlet and outlet coolant temperature;

c. The geometric (see Fig. 6.2), the thermophysical and thermoelectric characteristics of the thermoelements, which depend on temperature.

An ideal thermoelement is adopted in the design calculations. Its characteristics are determined using the average parameters

$$\overline{T}_{hs} = 0.5\left(T_{hs,in} + T_{hs,out}\right) \quad ; \quad \overline{T}_{cd} = 0.5\left(T_{cd,in} + T_{cd,out}\right) \quad ;$$

i.e., the temperature of the heat source and cooling device is assumed to be adequately specified by averages of their inlet and outlet temperatures.

The thermophysical and thermoelectric properties of the thermoelement branches can be averaged using the trapezoidal method, which allows one to obtain the simple equation

$$X_i = \frac{1}{m}\left[0.5x(T_{cd}) + x(T_1) + \ldots x(T_{m-1}) + 0.5x(T_{hs})\right]$$

where $x(T_i)$ are the values of the average parameter at the temperature T_i; m is the number of different segments into which the temperature interval $T_{hs} - T_{cd}$ is divided and in which the given change in the parameter being considered is assumed.

The calculations are continued in this sequence:

1. From the average parameters obtained for each thermoelement branch, the parameters for the branches as a whole are determined:

$$\bar{\alpha}_{n,p} = \bar{\alpha}_n + \bar{\alpha}_p \quad ; \quad \bar{k}_{n,p} = \frac{\bar{k}_n}{1 + \dfrac{A_p}{A_n}} + \frac{\bar{k}_p}{1 + \dfrac{A_n}{A_p}} \quad ; \frac{A_p}{A_n} = \sqrt{\frac{\bar{k}_n \sigma_n}{\bar{k}_p \bar{\sigma}_p}}$$

2. The electrical resistance of the thermoelement branches is calculated with respect to A_n:

$$\bar{r}_{n,p} = \frac{1}{3}\bar{r}_{hs}\frac{\left(w_n + w_p\right)w_n}{w_{hs}L} + \frac{1}{2}\left(\bar{r}_n + \bar{r}_p\frac{A_n}{A_p}\right)$$

where w_n, w_p are the widths of the branch columns.

216

3. The average figure of merit for the thermoelement is calculated,

$$\overline{Z}_{n,p} = \frac{\overline{\alpha}^2_{n,p}}{2\overline{k}_{n,p}\overline{r}_{n,p}\left(1 + \dfrac{A_p}{A_n}\right)}$$

4. By taking into account the loss in temperature in the multilayer walls (ΔT = 15-20 °C), as was discussed above, the junction temperatures T_h and T_c of the thermoelement are determined:

$$T_h = \overline{T}_{hs} - \Delta T \quad ; \qquad T_c = \overline{T}_{cd} + \Delta T$$

5. The value of m at the maximum efficiency of the thermoelement is determined, $m_{max\ eff}$ (the design point on the volt-ampere characteristic).

6. The efficiency, electrical power and voltage of the thermoelement (η_{te}, Q_e, V) are computed from equations (6.25), (6.10) and (6.8).

7. The efficiency of the thermoelectric converter is computed taking into account all losses. The net electrical power of an actual thermoelectric converter is also computed.

$$\eta_{conv} = \eta_{te}\,\eta_{nonisothermal}\,\eta_{load}\,\eta_{cond}\,\eta_{int} \qquad \text{(6.31)}$$

$$\dot{Q}_e = n\dot{Q}_{te}\,\eta_{nonisothermal}\,\eta_{load}\,\eta_{cond}\,\eta_{int}. \qquad \text{(6.32)}$$

As a rule, the total losses are 30 - 40% and $\eta_{conv} = (0.6 - 0.8)\eta_{te}$.

8. The required number of thermoelements n for a given electrical power output and the number of thermoelements connected in series are determined:

$$n = \frac{\dot{Q}_e}{\dot{Q}_{te}}\;\frac{1}{\eta_{cond}\,\eta_{nonisothermal}\,\eta_{load}\,\eta_{int}}$$

9. The size and mass of the thermoelectric converter is determined from the known specific mass parameters of the thermoelectric converter elements.

a) N-type SiGe

b) P-type SiGe
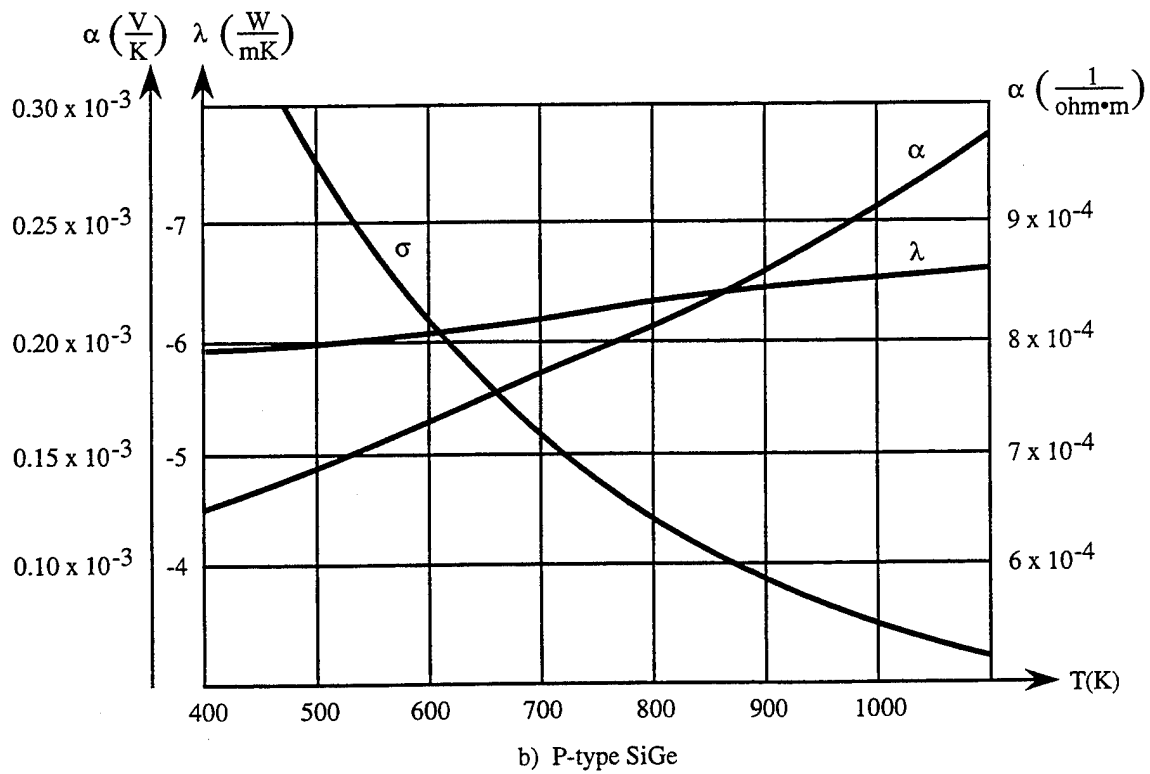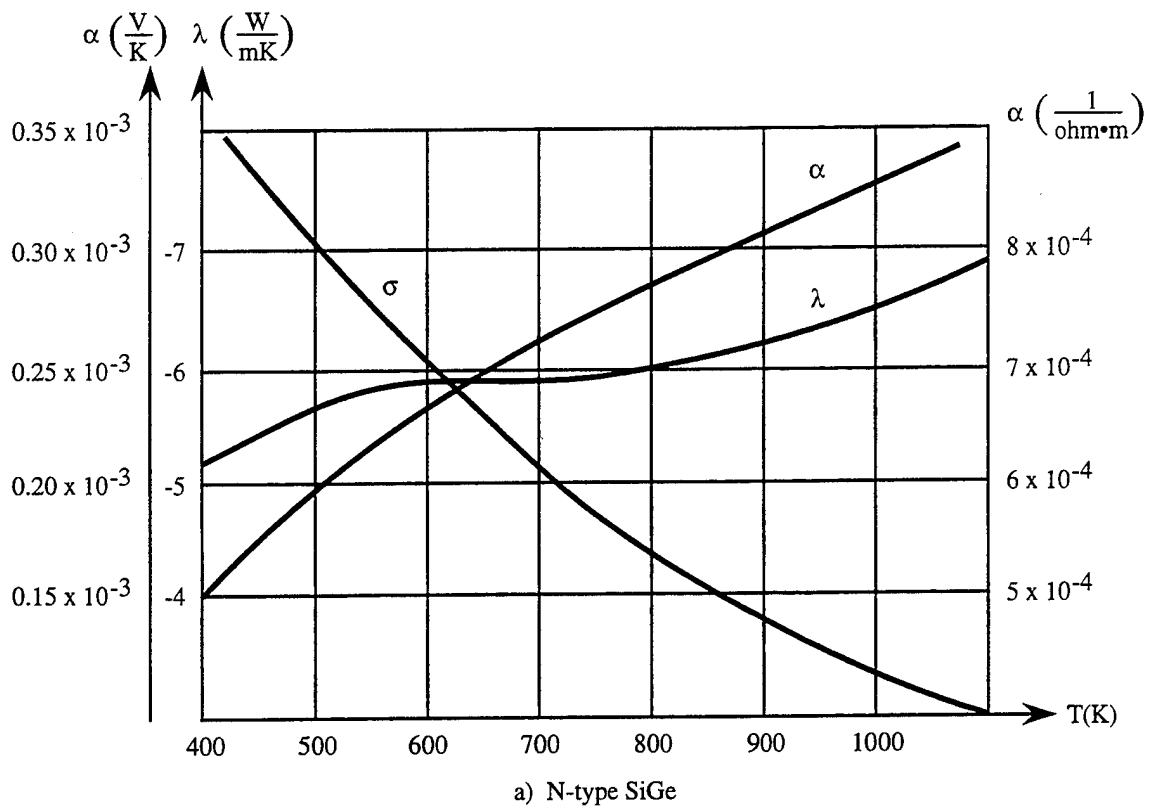
Fig. 6.4 Approximate material characteristics of SiGe.

7. THERMIONIC CONVERTERS AND POWER PLANTS

7.1. Equipment and Principles of Operation of Thermionic Converters.

The principle of operation and especially the working processes of thermionic converters differ significantly from thermoelectric converters in complexity and in the diverse and conflicting influences of different factors on their output characteristics and parameters. For this reason, the material in this chapter is separated into three consecutive stages. Initially, we will discuss simple schematics and models of thermionic converters with plane electrodes. Using these, we will explain the essence and physical fundamentals of simple thermionic conversion of heat into useful work by comparing it with an ordinary heat engine that fulfills the same function. In the second stage, we will examine in more detail the fundamental parameters that portray the effectiveness of thermionic converters and analyze the influence of basic working process parameters. For these purposes, we need to select a thermionic converter operating mode such that its description will be easily understood without doing a disservice to the thoroughness of relevant relationships. In conclusion, in the third stage we will discuss briefly the attributes of thermionic converters that operate in modes of greatest practical importance and evaluate the output parameters of power plants with thermionic converters as a whole.

With that said, let's begin with the first stage. Generally speaking, the principle of operation of the thermionic converter is based on the well known phenomenon of thermionic emission, i.e., the emission of electrons from a metal surface that is heated to a certain temperature. In principle, the emission of electrons from the surface of one or another metal can be caused by different reasons: illumination (photoemission), radiation by electromagnetic fluxes at certain wave lengths (radioelectronic emission) and, finally, by the supply of heat (thermionic emission). Thermionics is, however, of the greatest practical importance in space power and the subsequent sections will be devoted to this topic.

Let's look at a metal surface in a vacuum (Fig. 7.1). Under certain conditions (in this case, an increase in temperature) electrons are capable of boiling off the metal surface, i.e., they will "tear away" from the crystal lattice of atoms that make up the structure of the given metal. However, in doing this the electrons have to overcome a certain potential barrier which is created by a "mirror reflection" electric force field. This force acts between the emitted electrons and the positive charges induced by them on the "stripped" atoms in the crystal lattice of the metal. The electrostatic force of attraction between the positively charged "stripped" atoms and the emitted electrons tries to turn them back. This force can be calculated from Coulomb's law which states that this force is proportional to the square of the distance between the given electrons and the induced positive charges in the metal. Coulomb's law applies only to distances that equate to the size of the atom, that is, on the order of 10^{-8} cm. In order to simplify the discussion of the electron emission process, we will assume that as the electron leaves the metal the "mirror reflection" force is applied instantaneously, that is to say, the potential energy of the electrons changes abruptly. As a result, an electron gas "film" develops above the metal surface. In addition to leaving positive charges inside the metal, the electron "film" forms a thin double layer. The thickness of this layer, which is like a thin flat capacitor, is on the order of interatomic
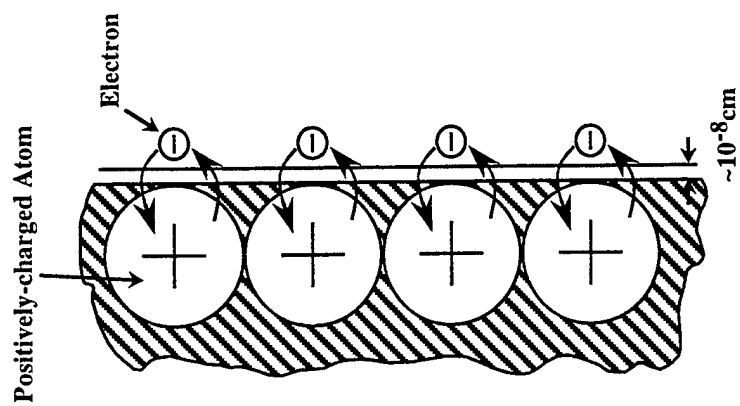
Fig. 7.1 Illustration of electron motion with respect to a heated metal surface adjacent to a vacuum.

distances, and the potential difference in the electrical field is on the order of units of volts. The potential difference in the electrical field of the double layer is called the surface potential barrier of the metal, φ. During the emission of an electron from a metal in a vacuum, the electron energy can equal or exceed the product $e\varphi$. This is called the work function.

According to Fermi-Dirac statistics, as the metal temperature increases the probability increases of finding free electrons with energies that exceed the Fermi level (the maximum energy of electrons at absolute zero). Therefore, the magnitude of φ is read from the Fermi level and it depends, basically, on the chemical nature of the metal, its surface state and structure (Table 7.1).

Table 7.1 Thermionic Work Functions

Material	φ, V
W	4.53
Mo	4.2
Ta	4.2
Pt	4.0
Ni	4.1
Cs	1.81
Cs on W	1.4 to 1.81
Ba	2.2
Cs + O	1.15 to 1.32

The emission of electrons results in an amount of charge emitted from a unit surface area per unit time. This is referred to as the emission current density J''. When there is no barrier in the path of the electron travel in a vacuum, this current density is determined from the Richardson-Dushman equation and is called the saturation current:

$$J''_s = AT^2 \exp\left(\frac{-e\varphi}{kT}\right) \quad , \tag{7.1}$$

where A is the emission constant which is approximately the same for all metals and is equal to 120 A/cm^{2}K^2; and k $= 8.62 \times 10^{-5}$ eV/K is the Boltzmann constant.

Equation (7.1) shows that the saturation current depends strongly on temperature and the work function. Practical emission current values are attained only at temperatures above ~1000 K.

The electrons that escape beyond the limits of the double layer form a negatively charged cloud. This space charge in a vacuum is a maximum at a distance from the surface on the order of 10^{-3} - 10^{-4} cm. In order to overcome this additional so-called space potential barrier δ, the electrons must have an excess of directional kinetic energy. Analogously with (7.1), the emission current density will in this case equal

$$J'' = AT^2 \exp\left[\frac{-e(\varphi + \delta)}{kT}\right] = J_s'' \exp\left(\frac{-e\varphi}{kT}\right) \qquad (7.2)$$

As can be seen, the saturation current density is reached when the space barrier is eliminated in some way.

Let us consider a simple schematic of a thermionic converter consisting of two metallic electrodes: a cathode and an anode (Fig. 7.2) which are connected to each other through an external circuit with a load R_L. The cathode is also referred to as the *emitter* and the anode is called the *collector*. This figure also shows the potential diagram for a simple thermionic converter, i.e. the potential energy distribution of the electrons in the interelectrode gap with account taken of the electron work functions of the emitter and collector (φ_e, φ_c) calculated from the Fermi level, respectively.

Thermal power, $\dot{Q}_t$, must be supplied continuously in order to maintain a given high emitter temperature, T_e. This heat compensates for the energy carried away by the emitted electrons (electron cooling) and also for the heat loss by radiation from the emitter to the collector and thermal conductance across the gap between them. As the electrons "condense" on the collector they give it their kinetic energy and in "dropping down" to the collector Fermi level, the electron potential energy decreases to the collector work function, φ_c. This portion of the electron energy is liberated as heat in the collector. This heat must constantly be removed by maintaining the collector at a temperature, T_c, lower than the emitter temperature. If the emitter work function is greater than the collector work function ($\varphi_e > \varphi_c$), then upon "condensing" on the collector the electrons will have a surplus of energy, $e(\varphi_e - \varphi_c)$, where $\varphi_e - \varphi_c$ is the contact potential difference. Thus, the electrons are free to return to the emitter through the external circuit and perform useful work in the external load, R_L.

In summing up the above discussion, one can draw the obvious conclusion that the thermionic converter is a typical heat engine to which heat (Q_1) is supplied from without at a high temperature, T_e, and from which a portion of this heat (Q_2) is removed to the surrounding medium at a much lower temperature, T_c. The working fluid in this heat engine is the electron gas and the potential diagram shown in Fig. 7.2 is essentially a cycle diagram of the conversion of thermal energy into electrical. In continuing the discussion of this analogy, one can add the following. Let's take as an example a simple steam engine. In order to produce steam in this engine, it is necessary to heat its working fluid (let's say, water) to a certain temperature (the boiling point) in order to overcome the liquid surface tension force. Analogously, in the thermionic converter the emitter must be heated to a certain temperature sufficient for the electrons (the thermionic converter working fluid) to overcome the surface potential barrier. The hot steam, upon condensing in the cold component (analogously, the collector of the thermionic converter which is at a much lower temperature than the emitter) into a liquid, will possess excess potential energy compared to its initial state. This excess can be put to useful work in, for example, a hydraulic turbine. Analogously, the excess energy of the electrons can perform useful work in an external load as the electrons return to the emitter from the collector.

Of course, this is a rough analogy between the thermionic converter and a heat engine. It reflects, however, the profound relationship between different converters of heat
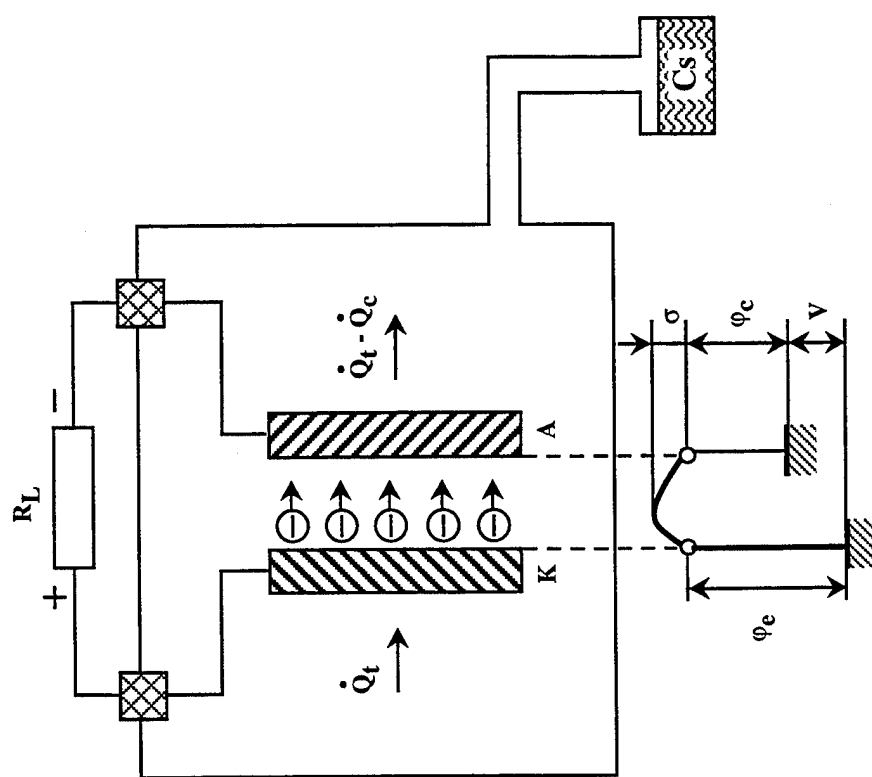
Fig. 7.2 Motive diagram, energy balance and simple circuit of a thermionic energy converter.

into useful work that dictates obligatory temperature differences in the heat supply and heat removal regions.

Let's continue our discussion of the first stage. Let's return to the schematic of the thermionic converter shown in Fig. 7.2. As we have stated, in traveling from the emitter to the collector the electrons create in the interelectrode gap (IG) a negative space charge called the space barrier, ψ. In order to overcome this barrier, the electrons must be given additional kinetic energy by heating the emitter. The amount of this energy is so great that the use of such a thermionic converter as a source of electrical energy would be impractical. Hence, it is necessary to eliminate this space barrier (or just reduce it to an acceptable value). This problem was successfully resolved by introducing an easily ionized gas in the interelectrode gap. Cesium is most convenient for this purpose. Its positive ions compensate the charge from of negative electrons.

Cesium ionization methods and different distributions of cesium vapor in the interelectrode gap make it possible to achieve different thermionic converter operating modes.

7.2. Classifications of Thermionic Converters and their Operating Modes.

The fundamental classification indicators of the thermionic converter are the composition and properties of the interelectrode medium. If a hard vacuum is maintained in the interelectrode gap, then such a converter is called a vacuum converter. Vacuum Thermionic converters are of practical interest only with interelectrode gaps that are thousandths of a millimeter in width. It is extremely difficult to produce and maintain such gaps in high temperature thermionic converters. In addition, there is always the danger of arcing and the high rate of emitter material vaporization will limit the life of the thermionic converter. All of this make such converters of little practical value.

Thermionic converters with gaps on the order of tenths of millimeters possess significantly higher power characteristics and are much more practical to manufacture. The interelectrode gaps of these thermionic converters are filled with the vapor of an easily ionized substance. The positively charged ions that form neutralize the electron space charge, which allows a significant increase in the emission current density. Among the most widely used media for this purpose are easily-ionized cesium ions (the first ionization potential, $E_i = 3.89$ v). Such thermionic converters are called gas-filled or plasma converters. The method of ionization sets the following plasma converters apart.

1. *Converters with volume ionization by electron collisions in an auxiliary discharge.* The latter is created between the emitter and a third auxiliary electrode which is supplied with a positive (attractive) voltage from an external source of emf. At the present time, these thermionic converters have not found any practical applications for a variety of reasons, including complexity and the cost of the additional energy required for the auxiliary electrode.

2. *Converters with surface or contact ionization at the emitter.* Contact ionization occurs when a neutral atom collides with a hot metal surface. As a result of the collision, the atom can give up one electron and be reflected as an ion. The probability of

this process (the degree of ionization, $\beta_i = n_i/n_a$, is the ratio of the number of reflected ions to the number of neutral atoms colliding with the emitter) is described by the Saha-Langmuir equation. For alkali metal atoms, this equation is

$$\beta_i = \left[1 + 2\exp\left(\frac{e(E_i - \varphi)}{kT}\right)\right]$$

(7.3)

As can be seen, the degree of ionization increases as the ionization potential decreases and as the work function of the metal increases. The influence of temperature is ambiguous: as T increases with $E_i > \varphi$ the degree of ionization increases, but it decreases with $E_i < \varphi$. With $E_i > \varphi$ the probability of ionization is low and neutral atoms predominate in the plasma flow. The *compensation parameter* α is used to describe the characteristics of the plasma state in the interelectrode gap. It is equal to the ratio of the ion concentration and the electron concentration: $\alpha = n_i/n_e$. If $\alpha = 1$, that is $n_e = n_i$, then the plasma is near neutral. When $\alpha > 1$ there is a surplus of ions and the mode is called overcompensated, and when $\alpha < 1$ ($n_e > n_i$), the mode is undercompensated.

Cesium has the lowest ionization potential among the chemical elements (with the exception of francium, which is rarely encountered in nature). Therefore, the interelectrode gap is filled, as a rule, with cesium vapor, sometimes with the addition of other elements (for example, barium). For this purpose, the electrode vacuum cavity is connected to a reservoir that contains liquid cesium (Fig. 7.2). The required cesium vapor pressure is provided by maintaining the liquid cesium in the reservoir at a specific temperature. The cesium atoms in the interelectrode gap are subjected also to thermal ionization. However, at practical emitter temperatures (no higher than 2200-2300 K) the contact ionization contribution can be considered to be negligibly small. The role of cesium in the interelectrode gap is not limited to neutralization of the space charge. A no less important property of cesium is its low work function. By adsorbing on the electrode surfaces of refractory metals, cesium reduces their work functions which increases the emission current sharply. This factor leads to an increase in the contact potential difference for a given cesium atom concentration, which is determined by the cesium reservoir temperature, and the degree of cesium adsorption. Consequently, the electrode work functions depend on the electrode temperatures. As the electrode temperature increases, the probability of adsorption falls off, and φ increases approaching a value that relates to the purity of the metal. Therefore, as T changes in equation (7.3), φ changes simultaneously. This results in that β_i as a function of T is not monotonic, it has a maximum. Preservation of a high degree of cesium adsorption on emitter surfaces heated to high temperatures is possible by increasing the cesium vapor pressure in the interelectrode gap. This permits control of the thermionic converter electrode work function. The work function of tungsten electrodes in cesium vapor can be varied from 4.53 eV (polycrystalline tungsten) to 1.4 eV, that of a metal coated tungsten surface and cesium (Fig. 7.1). Decreasing the emitter work function initially leads to a significant increase in current density and specific thermionic converter power. In accordance with equation (7.3), the degree of atom ionization at the electrode surface will decrease at the same time. This causes a negative space barrier to appear (undercompensated mode) which limits the

emitter current. Therefore, there exists some optimum emitter work function at which the thermionic converter power will reach a maximum. Depending on the size of the interelectrode gap L and the cesium atom concentration, different combinations of gap sizes and mean free path lengths of electrons, λ_e, are possible. Usually, two significantly different operating modes of plasma thermionic converters with surface ionization are considered:

    a. The Knudsen or near-vacuum mode, when $\lambda_e \gg L$;

    b. The diffusion mode, when $\lambda_e \ll L$.

In the Knudsen mode the electrons and ions travel in the interelectrode gap with few collisions. Losses due to electron scattering and plasma formation in the gap between the emitter and the collector are minimal.

Reducing the work function and increasing the electrode emission current by cesium atom adsorption on the emitter requires increasing the cesium vapor pressure in the gap, p_{Cs}. Increasing p_{Cs} is necessary in order that the ion concentration in the gap be increased in order to compensate the space charge, especially at a low φ_c when the degree of surface ionization β_i is small and the emitter current is comparatively high. Increasing p_{Cs} results in the inequality $\lambda_e < L$. The electrons, ions and atoms along the free path experience different kinds of interactions. Electron migration from the emitter to the collector is accomplished by diffusion. Therefore, this thermionic converter operating mode is called the diffusion mode.

    3. Converters with volume ionization in a low voltage discharge. In some situations, which are determined by the electrode work function, the plasma pressure, the size of the interelectrode gap and the emitter temperature, a stable arc will form and be sustained in the gap. This attests to the existence of volume ionization. Such a thermionic converter operating mode is called the arc mode. It usually comes about in a comparatively dense plasma. The thermionic converter transitions from the diffusion mode to the arc mode. It is understood that surface ionization is maintained together with volume ionization, but the role of surface ionization becomes superficial. This important circumstance permits lowering the emitter work function without running the danger of simultaneously reducing the degree of ionization, β_i. It is true that the cesium vapor pressure is several mm Hg in this case, but the emitter emission current increases rapidly. There are also other reasons for increases in current density, and we will discuss them below. As a result of the growth in current density, despite some decrease in load voltage, the thermionic converter power turns out to be very significant. For this reason arc mode converters have been widely used (for example, in the Topaz power plant).

7.3. Thermionic Converter Characteristics.

One of the features of the thermionic converter as a subject of multiparameter analysis is the conflicting influence of many factors on its output characteristics: specific parameters, power, efficiency, and others. Likewise, we referred above to the influence of

emitter temperature on the degree of ionization, and, consequently, also on the emission current and the relationship that emanates from it. To this pertain also the influence of the interelectrode gap, the emitter and collector work functions, etc. We will return later to this problem in discussing the thermionic converter volt-ampere curves (IV curves), its power, etc.

The most characteristic example that illustrates the thermionic converter features under consideration is an analysis of the influence of cesium plasma parameters on the electrode emission properties and the converter operating modes.

The degree to which the surface of a pure metal is coated by cesium, θ, is determined by the dynamic equilibrium between the quantity of precipitating and evaporating cesium atoms (or ions). An approximate dependence of cesiated work function φ' on φ and θ for a pure metal is described by the equation

$$\varphi' = \theta\varphi_{Cs} + (1-\theta)\varphi \qquad (7.4)$$

where φ_{Cs} is the surface potential barrier of cesium.

In turn, θ depends on φ, the surface temperature T and the cesium vapor pressure p_{Cs} or the effective cesium reservoir temperature, T_{Cs}. As a result, φ' turns out to be a function of these values as well (Fig. 7.3).

From Fig. 7.3 it follows that φ' is reduced as T decreases and as T_{Cs} increases. In some intervals of change in the ratio T/T_{Cs}, the greater the work function of the pure surface, φ, the lower it becomes as a result of coating by cesium. This is caused by the increase in the energy of cesium adsorption as φ increases.

The influence of cesium adsorption on φ' leads, naturally, to a change in the saturation current density J_s'' in accordance with equation (7.1). J_s'' as a function of T_{Cs} and T for tungsten is illustrated graphically by a family of so-called S-shaped curves, which were obtained first by Taylor and Langmuir (Fig. 7.4). Let's select one of the curves, T_{Cs} = const. At very high temperatures (that is, the left part of the S-shaped curve), the surface is free of cesium and the curve intersects the line for pure metal. Traveling on the curve from left to right, partial adsorption of cesium begins and the current density diminishes but at a slower rate than for the constant work function lines. Then the influence of φ becomes more important, despite a reduction in temperature, the current density increases to some maximum value. Thereafter, as the surface is almost completely coated with a cesium layer, a reduction in J_s'' begins. With a sufficiently thick layer of cesium the work function and the saturation current will approach some minimum value. Surprisingly, the work function can be lower than that for pure cesium. This is because a thin layer of cesium results in a dipole layer being formed. That is, the cesium valence electron tends to be attracted to the metal, with the result that the potential at the surface is correspondingly more positive. This results in the work function being lowered by a few tenths of an electron volt.

Taylor-Langmuir S-shaped curves are available for many different metals in Cs and Ba vapor.

Table 7.2 summarizes data for T_{Cs}, λ_e, φ_e and β_i with the interelectrode gap fixed at L = 0.1 mm. As can be seen, with a gap not exceeding 0.1 mm, the near vacuum mode
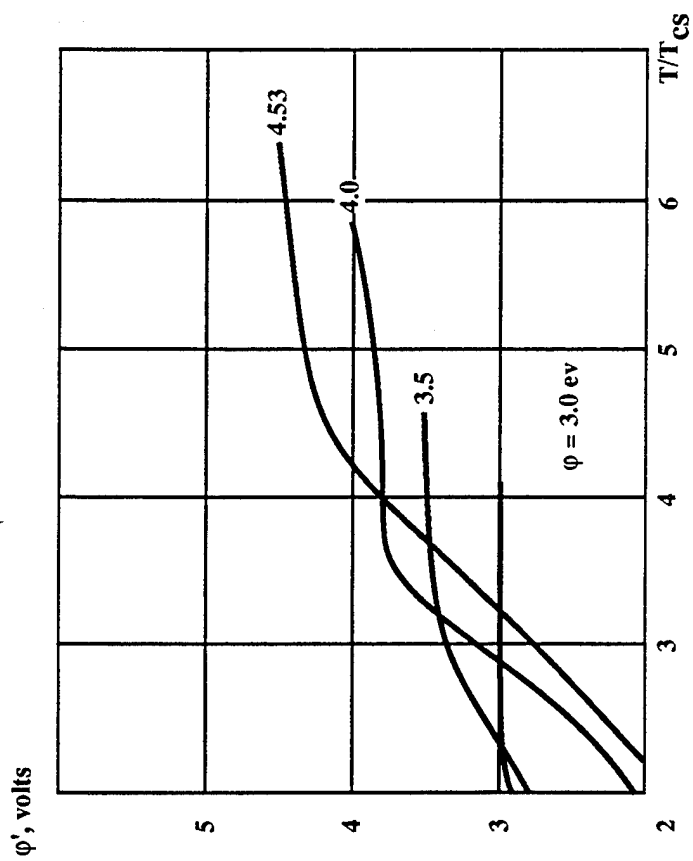
Fig. 7.3 Effective work function, φ, as a function of temperature ratio of the surface and cesium temperature.

228
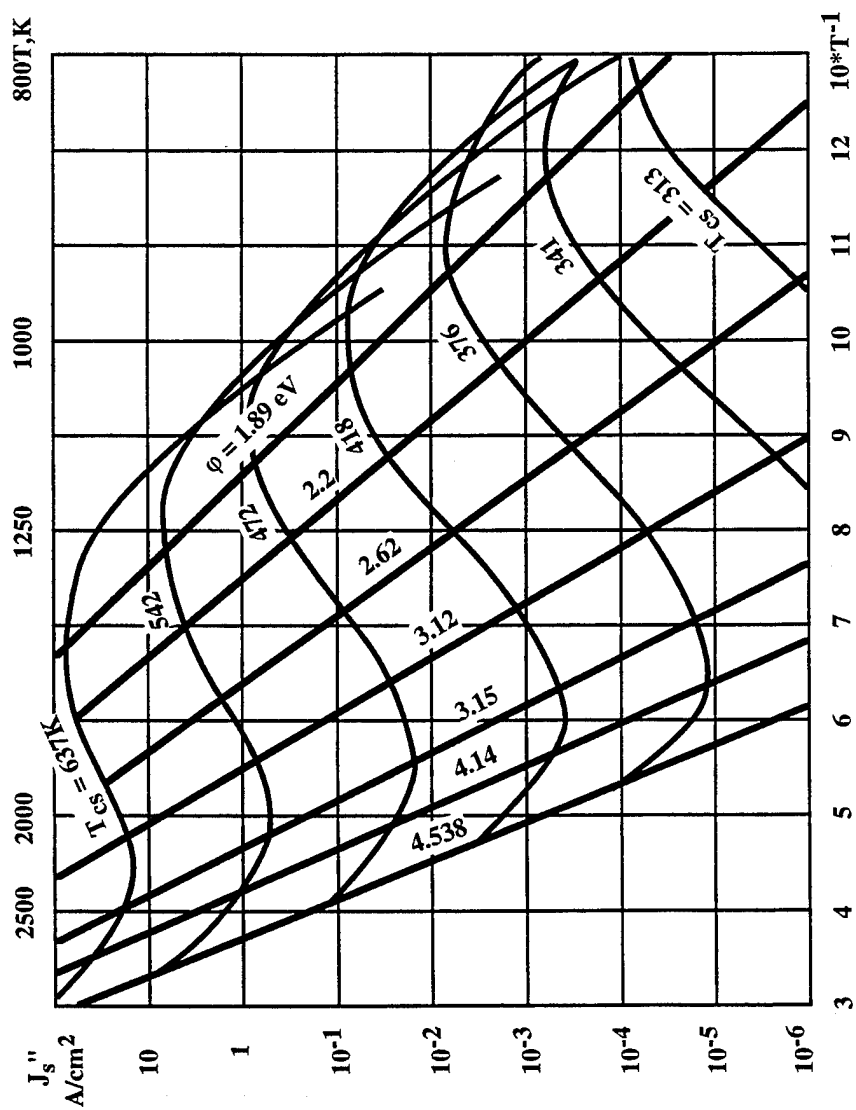
Fig. 7.4 Taylor-Langmuir curves, showing saturation current density dependence on inverse temperature. Cesium reservoir temperature and work function are used as parameters.

can be assured only with $\varphi = 4$ V. In this situation, the output parameters of the thermionic converter in terms of current and power turn out to be so low that the converter is of no practical interest.

Generally speaking, complex analysis is required to deduce the output characteristics of the thermionic converter in any of its operating modes.

Table 7.2 Properties of Tungsten

φ, V	Cesiated W			For α = 1		
	T_{Cs}, K	p_{Cs}, mm Hg	$\overline{\lambda}_e$, mm	β_i	p_{Cs}, mm Hg	$\overline{\lambda}_e$, mm
4	480	0.1	1.8×10^{-1}	0.485	5.8×10^{-6}	100
3.5	540	0.7	3.2×10^{-2}	0.0498	9.8×10^{-4}	2.2
3	610	4.2	6.0×10^{-3}	2.87×10^{-3}	0.30	6.5×10^{-2}
2.5	700	24.0	1.0×10^{-3}	1.58×10^{-4}	97.3	2.1×10^{-4}

7.4. Current-Voltage Curves, Power and Efficiency of the Thermionic Converter in the Knudsen Mode.

Investigation of thermionic converter output characteristics, particularly in the diffusion and arc modes, is quite complicated. This is due to the large number of interrelated processes that proceed simultaneously in the low temperature plasma volume, in the near electrode layers, and on the electrode surfaces: emission, adsorption, different kinds of scatter, ionization and recombination, etc.

The task of investigating the thermionic converter characteristics is greatly simplified when the thermionic converter operates in the Knudsen (quasi-vacuum, "collisionless") mode. As we have noted, this mode can be overcompensated, undercompensated or fully compensated depending on the value of the parameter α. The last of these is of interest to us. This is the mode in which the space barrier does not exist. For this purpose, let's consider the negative space charge compensation case.

The ion and electron concentration ratios in modes without volume ionization are determined by the relationships

$$\alpha = \frac{n_i}{n_e} = \frac{J_i^{"}}{J_e^{"}} \frac{\overline{v}_e}{\overline{v}_i} \qquad ,$$

where $J_i^{"}$, $J_e^{"}$ are the ion and electron current densities; and $\overline{v}_i$, $\overline{v}_e$ are the average ion and electron velocities in the direction normal to the electrodes.

Upon contact with the emitter surface, the ions acquire the same temperature, T_e, as the electrons, that is,

$$\overline{v}_i \sqrt{m_i} = \overline{v}_e \sqrt{m_e} \qquad .$$

Hence,

$$\alpha = \frac{J_i^{"}}{J_e^{"}} \sqrt{\frac{m_i}{m_e}}$$

In order to secure a fully compensated mode ($\alpha = 1$), with the mass of the ions and electrons taken into account (m_i and m_e) one must obtain a ratio of the required electron and ion currents $J_i^{"}/J_e^{"} \approx 500$;, that is, one ion must compensate the charge of about 500 electrons. An analogy can be made with a railroad station lamp that illuminates the railcar windows of a fast moving train. It is easy to visualize that one lamp can illuminate hundreds of windows and that this number will be greater the faster the train travels.

For a nearly-collisionless plasma in the gap, the cesium vapor pressure should not exceed 10^{-2} to 10^{-4} kPa.

The properties of the near vacuum mode permit a mathematical description of the processes that take place in the thermionic converter interelectrode gap in this mode. Let's examine the electric potential distribution in the internal and external circuits of the converter. Three characteristics are drawn by way of potential diagrams in Fig. 7.5 that identify the potential differences at the emitter and collector (the voltage in the external circuit V). The increase in negative potential is plotted upwards from the emitter Fermi level.

The basic component of V is the voltage drop at the load, V_L. To this should be added the voltage drop in the electrodes (V_E) and in the external electrical leads (V_{lead}) as well as the Seebeck emf which arises in the external circuit due to the temperature drop at its ends:

$$V = V_L + V_E + V_{leads} + \bar{\alpha}(T_e - T_c)$$

The Seebeck emf effect acts to increase the external circuit resistance. However, this effect can be neglected because for metals, as we noted earlier, the average absolute thermal emf factor is small. In addition, we will neglect the voltage drop in the electrodes and in the conductors and we will consider only the voltage drop across the load.

Using the thermionic converter model under consideration, we will examine the emission current from the emitter and collector separately. In doing this, it is convenient to isolate two parts that characterize the load voltage:

1) For $V \le \varphi_e - \varphi_c$ (Fig. 7.5 a,b),

$$J_e^{"} = J_{es}^{"} = AT_e^2 \exp\left(-\frac{e\varphi_e}{kT_e}\right) \quad ,$$

(7.5)

$$J_c^{"} = AT_c^2 \exp\left(-\frac{e(\varphi_c - V)}{kT_c}\right) = J_{cs}^{"} \exp\left(-\frac{e(\varphi_e - \varphi_c - V)}{kT_c}\right)$$

2) For $V > \varphi_e - \varphi_c$ (Fig. 7.5c),
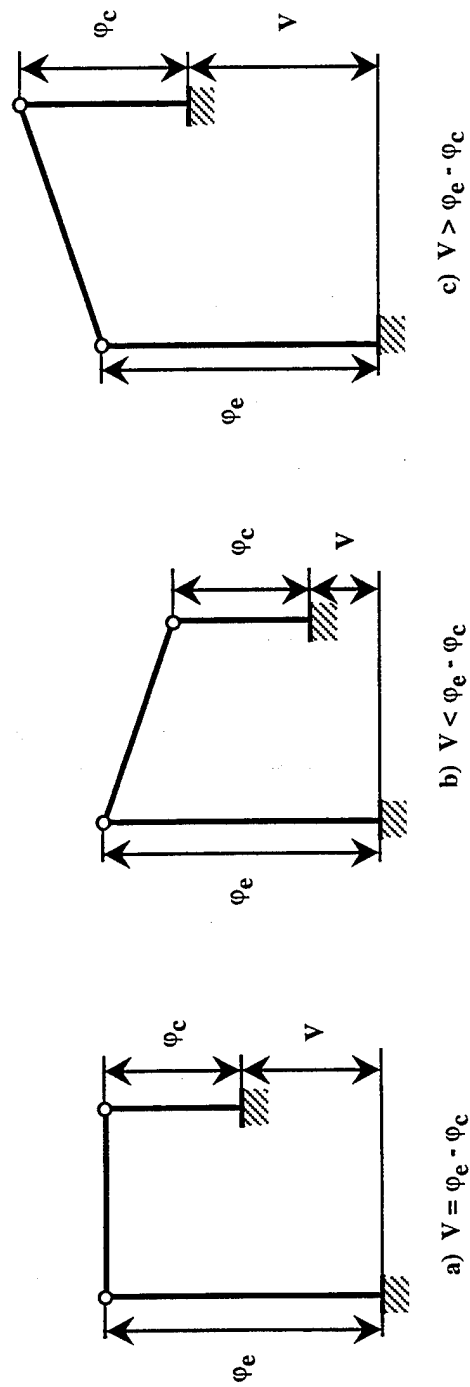
Fig. 7.5 Potential diagrams for quasi-vacuum converters.

a) $V = \varphi_e - \varphi_c$

b) $V < \varphi_e - \varphi_c$

c) $V > \varphi_e - \varphi_c$

232

$$J_e'' = AT_e^2 \exp\left(-\frac{e\varphi_c + V}{kT_e}\right) = J_{es}'' \exp\left(-\frac{e(\varphi_c - \varphi_e + V)}{kT_c}\right) \qquad ,$$

(7.6)

$$J_c'' = J_{cs}'' AT_c^2 \exp\left(-\frac{e\varphi_c}{kT_c}\right)$$

The resulting current density is equal to the difference in emitter and collector currents

$$J'' = J_e'' - J_c''$$

(7.7)

The ion current in the interelectrode gap is not taken into account in these equations because, as we have noted, with $\alpha = 1$ it is small.

Equations 7.5 - 7.7 describe the current-voltage (IV) curves of the near vacuum converter for known values of φ_e, φ_c, T_e and T_c (Fig. 7.6). As can be seen, there are two portions of the curve with a boundary at the voltage $V = \varphi_e$, φ_c. To the left of the boundary the potential distribution corresponds to that in Fig. 7.5b. In this case, all electrons emitted by the emitter are accelerated and reach the collector, and those emitted by the collector are partially retarded by the electrical field established between the emitter and the collector. The only electrons that reach the emitter surface are those with energies sufficient to overcome the retarding electrical field. To the right of the boundary the current direction reverses. The resulting emission current, which is the difference between the emitter and collector currents, is shown in Fig. 7.6.

Let's evaluate the influence of φ_e and φ_c on the shape of the IV curve by considering these parameters as independent variables and by assuming that the converter temperature regime remains unchanged. Let's examine both cases indicated above:

a) φ_c = const, φ_e = var;

b) φ_e = const, φ_c = var.

Let's assume that in the first case the reverse collector current is negligibly small, i.e. $J_{es}'' \gg J_{cs}''$ and, consequently,

$$\varphi_c > \frac{T_c}{T_e}\left(\varphi_e + \frac{2kT_e}{e}\ln\left(\frac{T_c}{T_e}\right)\right) \qquad .$$

Thus, as a first approximation one can consider only the emitter current density, J_e''. With incremental changes in T_e we obtain a family of IV curves for different saturation currents (Fig. 7.7).
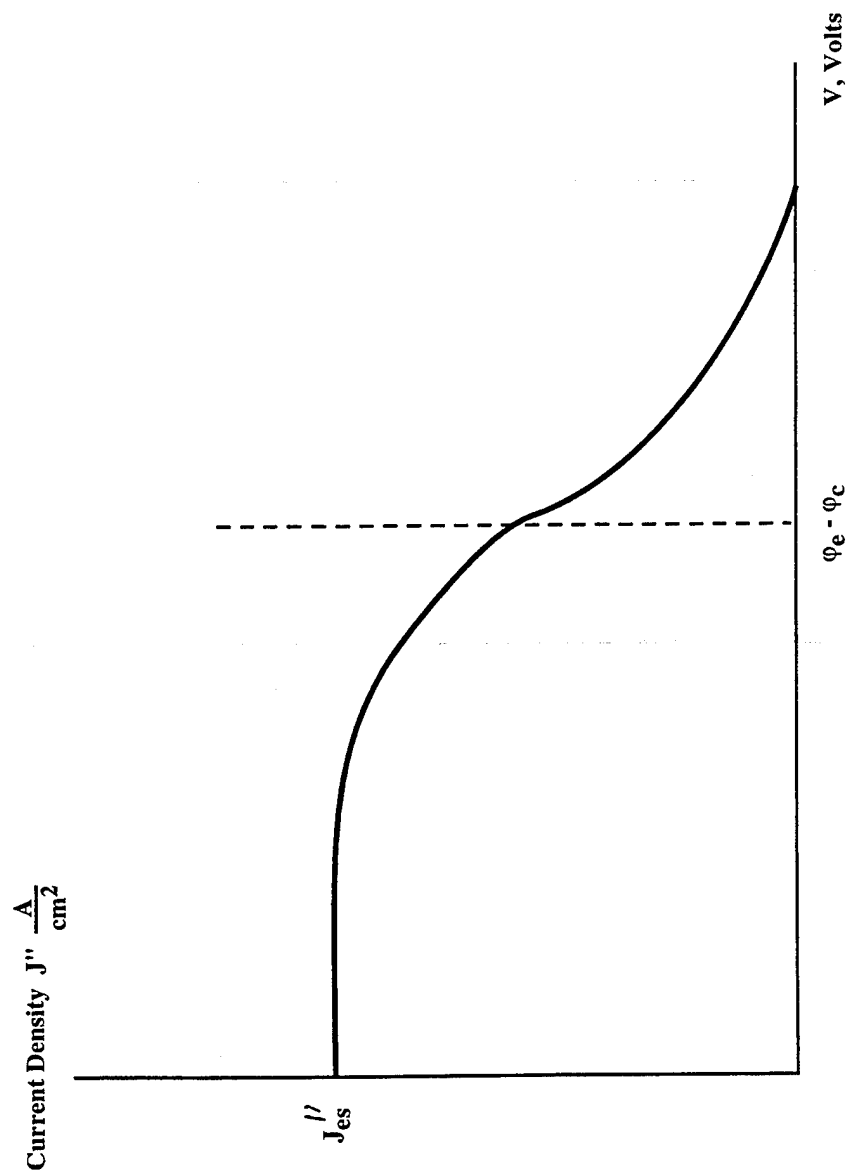
Fig. 7.6 Approximate I - V characteristics for a quasi-vacuum thermionic.

234

In regions of low and average load voltages the current density increases with decreasing φ_c. But at very low current densities in modes close to open circuit (V_{oc}), the picture reverses. Here the deciding role begins to be played by an increase in reverse collector current which increases as φ_c decreases. The open circuit voltage, which can be determined by equating the right sides of equations (7.5) and (7.6), will equal

$$V_{oc} = \varphi_c\left(\frac{T_e}{T_c} - 1\right) + 2\frac{kT_e}{e}\ln\left(\frac{T_e}{T_c}\right) \tag{7.8}$$

and it will begin to drop as φ_c decreases (Fig. 7.7). The mode, however, close to V_{oc} is of no practical value because of the very low current density. Therefore, it should be kept in mind that decreasing φ_c is advisable in maintaining condition (7.8). When φ_c has decreased to some value $\varphi_{c\,min}$ at which $J_{es}'' = J_{cs}''$, the above indicated inequality leads to the equation

$$\varphi_{c\,min} = \frac{T_c}{T_e}\left(\varphi_\kappa + \frac{2kT_e}{e}\ln\frac{T_c}{T_e}\right) \quad . \tag{7.9}$$

The limiting voltage becomes the open circuit voltage, $V_{oc} = \varphi_e - \varphi_{c\,min}$, and only one portion of the IV curve remains.

Thus, one can arrive at the following conclusions regarding the desired φ_e and φ_c from the point of view of their influence on the shape of the IV curve:

1. With φ_c = const it is advantageous to reduce φ_e to $\varphi_e = \varphi_c$.

2. With φ_e = const it is advantageous to reduce φ_c to $\varphi_{c\,min}$ as determined from equation (7.9).

The specific power (the ratio of converter power to the emitter surface area) is determined from the expression $\dot{Q}_e'' = J''V$ (Fig. 7.6). This relationship has a maximum at $V = \varphi_e - \varphi_c$. At the short circuit and open circuit points (j = 0, $V = V_{oc}$) the specific power is equal to zero.

In order to provide the necessary ion current in converters with cesium vapor, a low Cs pressure (fractions of mm of Hg) in the interelectrode gap is sufficient. However, at such a pressure the degree of cesium adsorption on the emitter surface is low and insufficient to obtain a current density of practical value. Increasing the cesium pressure leads to collision processes that result in additional current losses.

In order to maintain a near vacuum mode and decrease the emitter work function at the same time, a binary cesium-barium vapor can be used (Cs + Ba). Barium has a much higher heat of adsorption. Therefore, a stable surface coating is obtained at low pressures. In addition, barium atoms have a small electron scattering cross section. This circumstance allows regulation of the emitter work function independently of the cesium
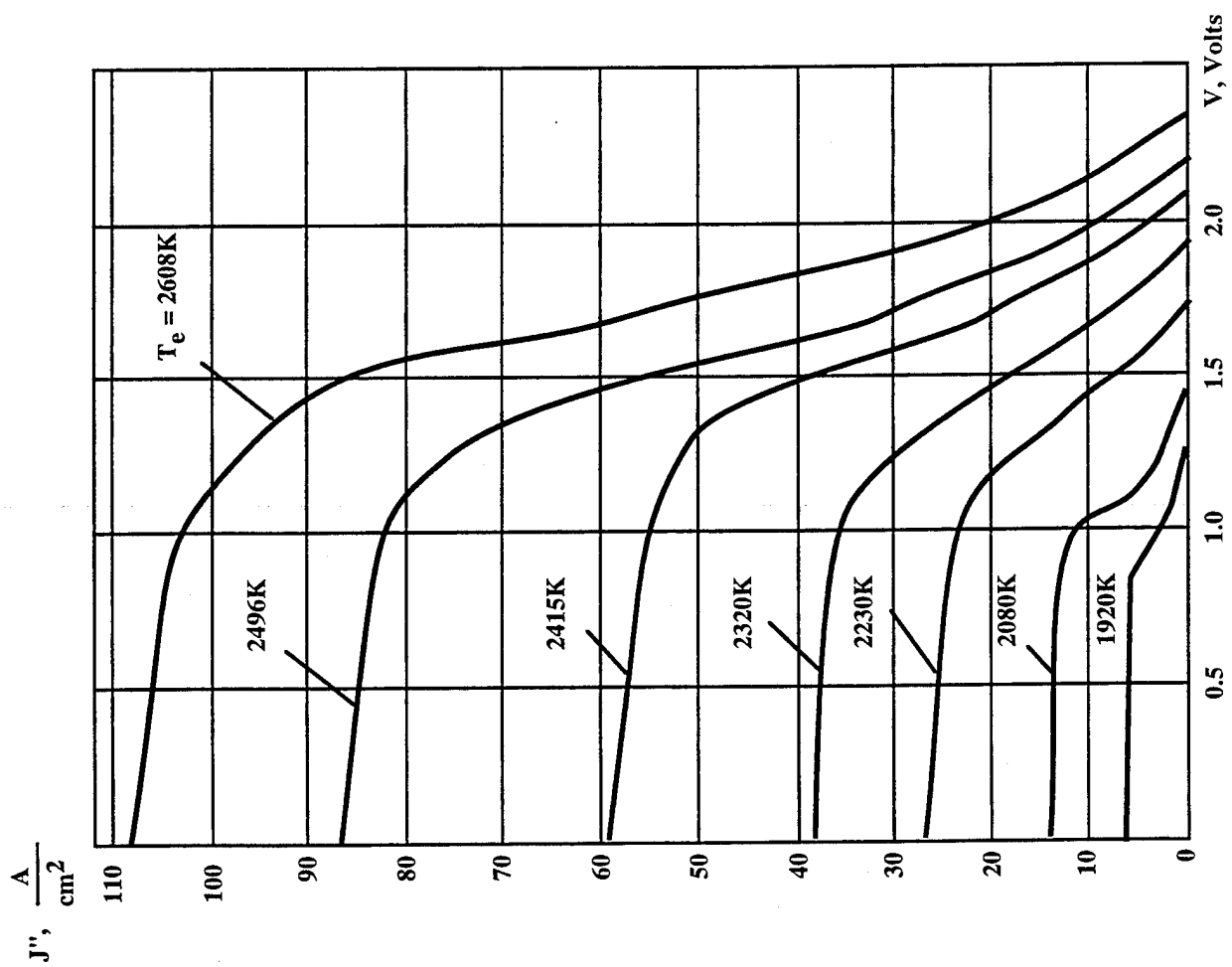
Fig. 7.7 Current density versus voltage characteristics for various emitter temperatures.

236
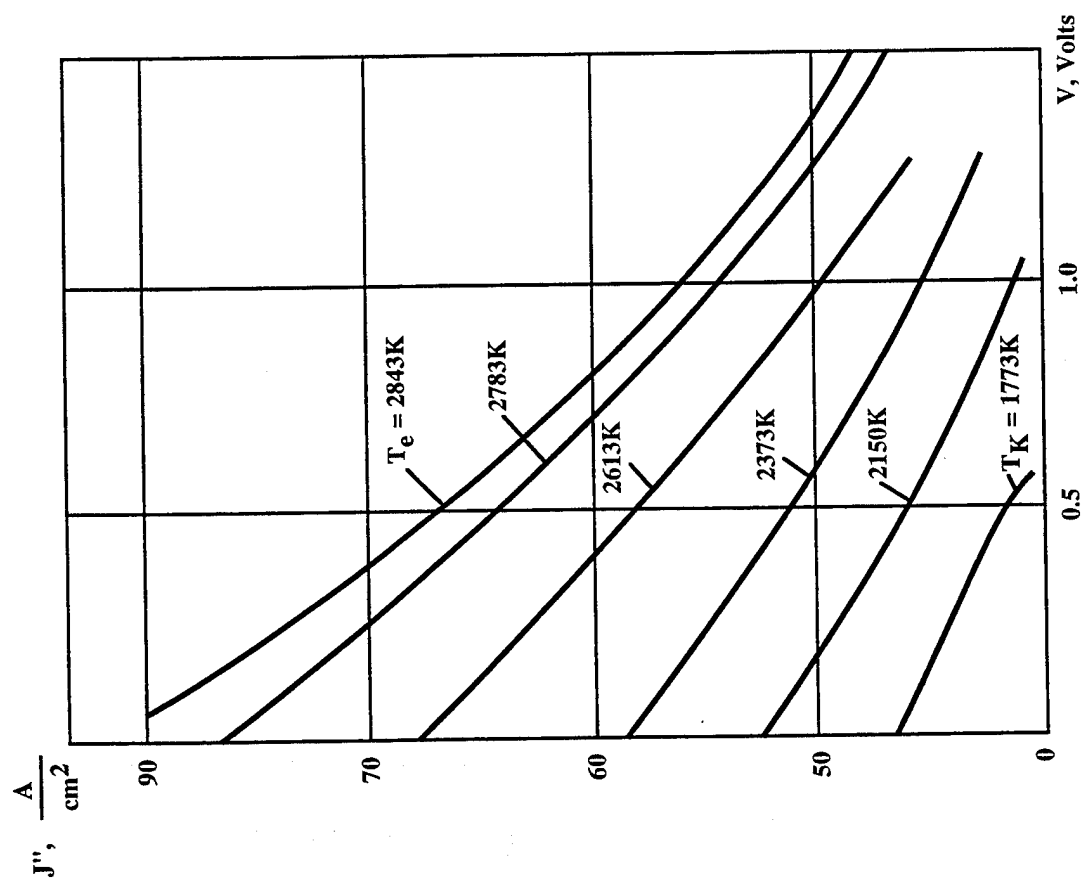
Fig. 7.8 Cesium-barium converter characteristics for various emitter temperatures.

The chart axes and labels:

- Vertical axis: J'', $\dfrac{A}{cm^2}$ with values 90, 70, 60, 50, 0
- Horizontal axis: V, Volts with values 0.5, 1.0

Curve labels:
- $T_e = 2843K$
- $2783K$
- $2613K$
- $2373K$
- $2150K$
- $T_K = 1773K$

237

pressure by changing the partial pressure of barium. The converter power characteristics are improved substantially by optimizing the emitter work function.

Fig. 7.9 shows experimental current-voltage curves which were obtained by optimizing the partial pressures of barium and cesium.

The high heat of adsorption of barium leads to its condensation on the collector surface. Therefore, a feature of cesium-barium converters is an elevated collector work function, ~2.2 eV, compared with cesium converters (1.4 - 1.7 eV). This allows an increase in collector temperature by 200-300° without a significant increase in the reverse collector current. Increasing the collector temperature has a benefit in that the space radiator surface area is reduced. On the other hand, high collector work function results in decreased output voltage.

One can assume that the maximum value of emitter work function in the Knudsen mode with cesium-barium vapor corresponds to φ_e = 3.0 - 3.1 V. For correspondingly low values of φ_c on the order of 3.0 - 2.8 V, these parameters with T_e > 2000 K are: J" = 6 to 10 A/cm², $Q_e^{"}$ = 5 to 8 W/cm².

One can also develop emitters with work functions that are close to optimum (approximately 3 eV) and then the requirement for barium additive falls off. Such refractory materials, however, do not exist in nature. Scientific research is needed in order to develop them.

Another approach to improving the characteristics of the near vacuum converter is to use multiple cavity emitters. The emitter is pitted (uniformly over the emitter surface) with cavities that are significantly smaller in size than the interelectrode gap.

The current density and the specific power of the near vacuum thermionic converter as a function of the work function have a maximum for the condition (α = 1). At low (~1300 K) and medium (~2000 K) emitter temperatures the relationship (α = 1) is satisfied while the plasma concentration in the interelectrode gap (and this means also the current flow) is insufficient to provide the specific power required for space power plants. The low value of $\dot{Q}_e^{"}$ is explained by the low intensity of surface ionization at such temperatures.

The efficiency of a thermionic converter in the near vacuum mode. This important characteristic of any energy converter is in this case determined by the ratio of the specific electrical power, $\dot{Q}_e^{"}$, to the specific thermal power supplied, $\dot{Q}_t^{"}$. Since $\dot{Q}_e^{"}$ is determined by the thermionic converter current-voltage characteristics, we will discuss in more detail the specific thermal power, $\dot{Q}_t^{"}$, and isolate its basic components:

1. The energy carried away by the electrons emitted by the emitter, $\dot{Q}_{ecool}^{"}$, (electron cooling) comprises potential and kinetic energy. In addition, the electrons emitted by the collector, and which strike the emitter, impart to it an energy, $\dot{Q}_{ccool}^{"}$. The resulting thermal power associated with electron cooling of the emitter is equal to

$$\dot{Q}_{el\,cool}^{"} = \dot{Q}_{ecool}^{"} - \dot{Q}_{ccool}^{"} = J_e^{"}\left(\varphi_e + \frac{2kT_e}{e}\right) - J_c^{"}\left(\varphi_e + \frac{2kT_c}{e}\right) \quad . \tag{7.10}$$

238
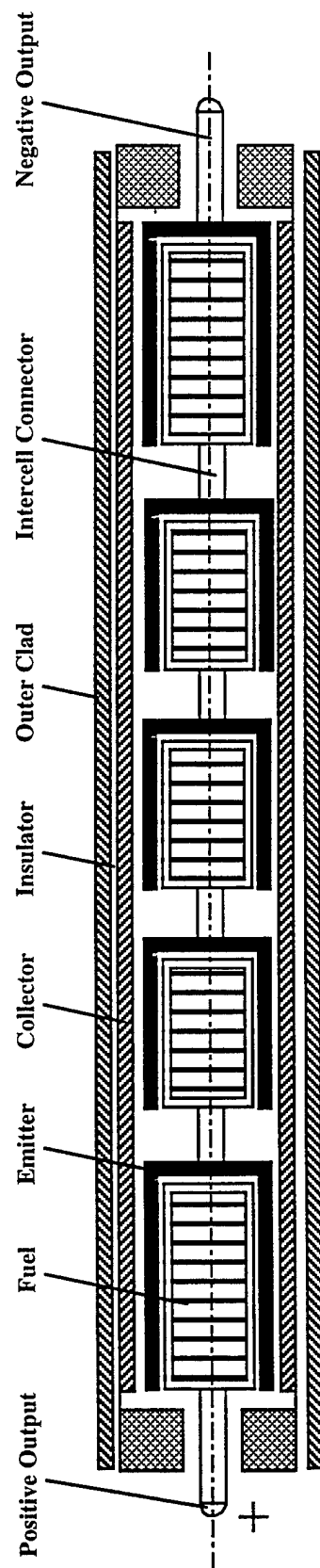
Fig. 7.9 Schematic drawing of a multicell thermionic fuel element.

Positive Output

Fuel   Emitter   Collector   Insulator   Outer Clad   Intercell Connector   Negative Output

239

2. The thermal power transferred from the emitter to the collector due to mutual radiation heat transfer is

$$\dot{Q}''_{rad} = \varepsilon_{eq}\sigma\left(T_e^4 - T_c^4\right) \qquad \text{.} \qquad (7.11)$$

where

$$\varepsilon_{eq} = \left[\frac{1}{\varepsilon_e} + \frac{1}{\varepsilon_c} - 1\right]^{-}$$

is the equivalent emissivity.

3. The thermal power transferred from the emitter to the collector due to the thermal conductivity of the plasma in the interelectrode gap is

$$\dot{Q}''_{cond} = k_{plasma}\left(T_e - T_c\right) \qquad \text{.} \qquad (7.12)$$

where k_{plasma} is the heat transfer coefficient in the plasma.

However, due to the highly rarefied plasma, this component can be neglected.

Thus, without taking into account some additional losses, the efficiency of a single thermionic converter is determined by the expression

$$\eta_e = \frac{J''V}{J''_e\left(\varphi_e + \dfrac{2kT_e}{e}\right) - J''_c\left(\varphi_e + \dfrac{2kT_c}{e}\right) + \varepsilon_{eq}\sigma\left(T_e^4 - T_c^4\right)} \qquad \text{.} \qquad (7.13)$$

Let's evaluate the maximum efficiency of an ideal thermionic converter in the mode under consideration. For this purpose, let's neglect irreversible losses, in particular, electron kinetic energy and mutual radiation between the emitter and the collector, i.e., $2kT_c = 2kT_a = 0$, $\dot{Q}''_{rad} = 0$. In this case, the thermionic converter efficiency will equal

$$\eta_{max} = \frac{J''V}{\varphi_e\left(J''_e - J''_c\right)} = \frac{V}{\varphi_e} \qquad \text{.} \qquad (7.14)$$

In the absence of losses in the interelectrode gap, the maximum electrical power will correspond to a voltage equal to the contact potential difference, $V = \varphi_e - \varphi_c$. In this case,

$$\eta_{max} = 1 - \frac{\varphi_c}{\varphi_e} \qquad \text{.} \qquad (7.15)$$

240

It can be shown that the maximum thermionic converter efficiency corresponds to the condition

$$\frac{\varphi_e}{T_e} = \frac{\varphi_c}{T_c}$$

Thus,

$$\eta_{max} = 1 - \frac{T_e}{T_c} = \eta_{Carnot}$$

This conclusion is analogous to the maximum efficiency of a thermionic converter, which, as follows from (6), in the absence of irreversible losses also equals the ideal Carnot cycle efficiency.

For all kinds of direct converters of heat that have diminishing current-voltage curves, the maximum efficiency corresponds to a voltage $V_{max\ \eta}$ that is higher than the voltage, $V_{max\ P}$, that yields the maximum power (Fig. 7.6). This holds true also for the thermionic converter. In fact, the maximum specific power level, by virtue of its slope (the numerator in the efficiency equation (7.13)), changes insignificantly. At the same time, due to a decrease in current density, the denominator in this equation decreases which results in a growth in efficiency. Later, despite the decrease in the denominator, the efficiency begins to diminish due to a sudden fall in specific power.

The optimum operating mode of a converter, as always, is determined by a compromise between power and efficiency.

7.5. The Thermionic Converter Diffusion Mode and Arc Mode.

At significant cesium or cesium-barium plasma pressures the flow of the carrier current in the interelectrode gap becomes diffusive in nature. In this event, one can define three characteristic regions in the gap: two thin near electrode layers and a near neutral plasma region between them. The thickness of the near electrode layers is on the order of the Debye radius, which falls in the 10^{-4} - 10^{-5} cm range for characteristic plasma densities. In the near electrode layers, frequently called the Langmuir layers, potential drops arise in the overcompensated and undercompensated modes which provide for near neutralization of the plasma region. Thus, with $\alpha < 1$ the negative potential drop close to the emitter reflects the electron flow back to the emitter and the ions reflected by the emitter are pulled by the electrical field into the plasma. The plasma potential near the emitter causes a lower emitter surface potential. In the overcompensated modes ($\alpha > 1$), the reverse situation occurs. With full compensation ($\alpha = 1$), there is no change in the Langmuir layer potential.

The potential distribution in the gap depends on the voltage drop in the external circuit. The electron and ion current densities and the thermionic converter current-voltage curves in the diffusion mode is determined basically by the motion of the charges in the near neutral region. This motion is effected by the electrical field $d\varphi/dx$ (at any instant of time in the direction of an axis normal to the electrode surfaces) and by the concentration gradients (diffusion currents) of electrons (dn_e/dx) and ions (dn_i/dx). In the

open circuit mode, the electrical field compensates the electron diffusion current and J''_{elec} = 0. As the voltage decreases, the retarding influence of the electrical field begins to weaken. It then changes sign ($-d\varphi/dx$) and the electron current increases continuously. This situation is maintained until the electrical field reaches a value at which the ion current in the direction of the collector by diffusion (dn_i/dx) becomes equal to the reverse ion current by the field ($-d\varphi/dx$). With a further decrease in V down to V = 0 (the short circuit mode), neither the electrical field strength in the near neutral region nor the electrical current will change.

The current-voltage curves of a diffusion mode thermionic converter look like the current-voltage curves of the near vacuum thermionic converter in a qualitative sense. However, the output characteristics of the diffusion mode thermionic converter turn out to be low. Thus, with T_e = 1700 to 1800 K and an optimum cesium pressure (1- 2 mm Hg), the maximum power density is reached at an output voltage V = 0.6 - 0.8 V and is 1.5 - 2 W/cm². For this reason, this mode is virtually unused in practical thermionic converter designs. Nevertheless, the diffusion mode possesses certain advantages that have to do with the small influence of the size of the interelectrode gap, especially at high values of T_c. To this should be added also the influence of the transverse magnetic field, which is substantially less than it is in the near vacuum thermionic converter. Thus, the size of the gap at T_c = 1800 K can be 0.1 - 1.0 mm but the magnetic field will reduce the power by just ~4-8%.

The arc mode. At some emitter temperatures, cesium pressures in the interelectrode gap, and at certain load voltages, electron-atom collisions begin to play a positive role. This leads to the development of volume ionization and the onset of a low voltage arc. This phenomenon, which arises directly from the diffusion mode, is accompanied by a sharp increase in current by about one magnitude. The maximum power in operating modes (V = 0.8 to 1.0 V) increases substantially as well and at T_e ~ 2000 K, it can reach 20 to 25 W/cm².

Together with this external manifestation of volume ionization, all plasma parameters in the gap will also change substantially: the electron, ion, and atom concentrations, their temperatures, and the nature of change in the potential φ. Surface ionization ceases to play a decisive role in supplying ions to the plasma. The volume plasma generation results in the plasma potential in the middle of the gap being below the potentials at the electrode surfaces and an electron potential well forms. Ions, on the other hand, are driven from the plasma to the electrodes. A reduction in φ_c (in order to increase the emission current) under these conditions does not result in an increase in the space potential barrier and a decrease in the compensation parameter α, such as is the case in the diffusion and near vacuum modes with single component gap media. In other words, it is as though the tie between φ_c and α is broken in the arc mode, while this basically prevented the current density from increasing in the diffusion and Knudsen modes.

In order that inelastic collisions of electrons with atoms will result in ionization of the latter from the basic (unexcited) state, the electron energy should be at least below the first ionization potential. At any point in the gap the electron energy is made up of thermal energy having, basically, a Maxwellian distribution, and directional energy which

242

is acquired as a result of two factors: acceleration in the electrical field $d\varphi/dx$ and diffusion as a result of the concentration gradient dn_e/dx.

Of the enumerated energy components of electrons, of greatest significance in the diffusion mode is the energy which is acquired in the electrical field. But even this energy is substantially below the energy of the first ionization potential of cesium ($E_i = 3.89$ V).

Under these conditions, the most likely process is gradual ionization. Together with the formation of ions, a reverse process occurs - their recombination. The combined effect of ionization and recombination determines basically the electron and ion currents and the potential distribution in the arc mode.

Let's examine the nature of the onset and quenching of arcs beginning with different states in the pre-arc diffusion mode. Differences in these transitions are determined by external conditions: T_e, p_{Cs} and L, the principal one being the emitter temperature, T_e.

Let's suppose that the emitter in the initial diffusion mode is at a comparatively low temperature (T_e 1600 - 1700 K). Due to the high degree of cesium adsorption, the emitter work function is low. This results in a low surface ionization and the mode is undercompensated ($\alpha < 1$). As can be seen, the largest accelerating potential for the electrons occurs in the collector plasma sheath region ($\Delta\varphi + \delta_c$).

The accelerating collector plasma sheath potential drop $\Delta\varphi$ can be made somewhat larger (by using an external voltage, $V < 0$) so that the electrons can accumulate sufficient energy to initiate intensive ionization.

The initiation of ionization is visually observed as a glow in the collector plasma sheath region. The ions that form diffuse by the field effect through the plasma to the emitter side because their removal at the collector is prevented by the precollector barrier. The positive volume potential grows, the electron concentration and energy increase, ion generation begins in the volume and the glow region propagates through the entire gap.

Upon arc ignition, the potential distribution changes abruptly, the operating mode goes from the undercompensated diffusion mode to the strongly overcompensated arc mode, and the current density increases by several factors. We note that theoretical analysis of the transition process indicates the existence of a negative resistance region, which is caused by an increase in the electrical conductivity of the gap as intensive volume ionization begins.

In the developed arc mode, the accelerating electron potential drop in the emitter plasma sheath layer is ~0.8 to 1.2 V, the maximum potential in the center region of the gap is ~0.2 to 0.4 V, and the negative potential difference in the collector plasma sheath is ~0.1 to 0.3 V. Ion generation is accomplished, basically, by two means. First, nonequilibrium ionization takes place in the emitter plasma sheath region where electron acceleration by the electrical field occurs almost without collisions. Second, gradual ionization in thermal equilibrium occurs in the plasma volume. The rate of this process is proportional to $\exp(-E_i/T_{elec})$, with T_{elec} usually ~2300 - 2800 K. The ratio of the nonequilibrium and thermal ionization rates falls in the range 0.3-3, that is, the effects of these processes are comparable.

The reasons why the current density exceeds the Richardson value in the developed arc mode are due to the emitter plasma sheath potential drop which gives rise to the Schottky effect, an increase in the ion current at the emitter, and a decrease in the

return of electrons from the plasma to the emitter. The Schottky effect increases the current density by about 30%. In emitters where the grain orientations in the crystal lattice differ with different work functions, the influence of the Schottky effect increases in low work function areas (referred to as the "anomalous Schottky effect"). The maximum ion current contribution is also ~30%.

If, after arc ignition, the load voltage is increased to some value in the range

$$V = V_{ig} - V_{ext}$$

then the volume ionization mechanism will not be disrupted. A characteristic of the arc mode is that the potential distribution is maintained in a qualitative sense and the arc continues to burn in the region of positive load voltage. With an increasing voltage, the current density drops continuously without saturation plateaus as has been observed in the near vacuum and diffusion modes.

At some positive voltage V_{ext} the arc extinguishes and the potential diagram returns to the initial shape that corresponds to the pre-arc diffusion mode. As is apparent, a unique hysteresis in the current-voltage curve takes place, which is caused by the coupling-hysteresis effect in restructuring the potential diagram with voltage changes in different directions.

At emitter temperatures in the 1800 - 2000 K range, the nature of the onset of the arc mode changes qualitatively. Here, the initial diffusion mode is overcompensated ($\alpha >$ 1) due to low cesium adsorption and a high emitter work function which result in a high degree of surface ionization. The electrons are accelerated in the extended field in the emitter plasma sheath region and, in addition, in the volume field.

Ionization begins in the emitter plasma sheath region. However, a sudden restructuring of the potential diagram does not take place. As the load voltage decreases due to the strengthening ionization, the potential in the volume increases (an electron potential well is formed). The potential distribution in the gap assumes a shape that is characteristic of the arc mode.

On the current-voltage curve the transition to the arc mode is observed as a break at some voltage V_{arc} up to the saturation current point in the diffusion mode.

At $V < V_{arc}$ the operating mode corresponds to the developed arc mode. Extinguishing the beam, like ignition, takes place smoothly without hysteresis in the current-voltage curve.

At emitter temperatures $T_e > 2000$ K the energy of the emitted electrons becomes so high that gradual ionization in the emitter region and in the plasma volume proceeds through all operating voltages from the open circuit to the short circuit mode. Therefore, at very high emitter temperatures the thermionic converter will operate only in the arc mode and the current-voltage curve does not have any discontinuities. As the voltage diminishes, the current density increases rapidly and monotonically.

Calculation of the plasma parameters in the interelectrode gap (particle concentration, potential, electron temperature) and the current-voltage curve is done by solving a system of differential equations for the transport (motion) of electrons and ions through the plasma, and by taking into account electron-ion collisions because of the significant ion and electron concentrations, especially at high current densities. Unlike the

diffusion mode, the electron and ion currents do not remain constant due to the ionization and recombination processes that take place in the plasma volume. Therefore, one must add the equation of conservation particle numbers (the continuity equation) to the transport equations for the electron and ion currents and the electron energy flow. These equations can be solved on a computer using preelectrode layer boundary conditions.

A number of studies are currently available that are devoted to the calculation of current-voltage curves in the arc mode. Calculated data generally agree quite satisfactorily with experimental data. However, in engineering practice results of theoretical analyses are used in the design of thermionic power units, as a rule, in the preliminary selection of parameters. The input data used in the design of power plants are usually experimentally obtained current-voltage curves.

7.6. Design of Thermionic Converters Taking Different Losses into Account.

We pointed out earlier the different energy losses in the interelectrode gap (the space barrier, collisions between electrons, atoms and ions, heat transfer from the emitter to the collector, etc.). However, in actual thermionic converter designs with thermionic fuel elements (TFEs) inserted in the reactor core there are additional losses. In order to evaluate them, let's turn to the design of one of the thermionic cells from which a multielement TFE is made. The following kinds of losses are characteristic of this design:

1. Flow of heat from the emitter to the collector through the electrical connectors. In addition to direct loss of nuclear reactor heat, this results also in nonisothermal electrodes, in particular, the portion of the emitter where the connection is made becomes cooler than the remainder of the emitter, and the collector part near the connector becomes overheated. Since the optimum cesium vapor pressure in the interelectrode gap (IEG) depends significantly on the electrode temperatures, the indicated nonisothermal conditions make it impossible to provide optimum conditions for all portions of the TFE.

2. A significant kind of loss is from joule losses by current flow in the emitters, collectors, and electrical connectors that make up the TFE. In order to ensure reactor criticality and to satisfy requirements for minimum size and weight, the volume of nonfissioning materials in the core should be kept at the lowest possible minimum. Therefore, the TFE electrodes are made relatively thin with a thickness of about 0.5 mm. As a result, electrical energy losses during current flow become significant. In addition, current flow in thin electrodes results in a voltage drop along the length of the electrodes. This shows up in differences in the operating modes of individual sections of the TFE. This variation in electrode potential make it impossible to provide an optimum operating point on the IV curve at the same time for all parts of the TFE electrodes.

3. Losses associated with current losses through the collector insulation to the support tube into which the TFE is inserted. However, the fraction of this loss is comparatively small and substantially less in comparison with the losses mentioned above.

245

Let's calculate these losses. The flow of heat from the emitter to the collector can be determined from the equation

$$\dot{Q}_{lead} = A_{lead} \frac{k_{lead}}{L_{lead}}(T_e - T_c) \qquad (7.16)$$

where A_{ec} is the connector cross-sectional area; L_{lead} is the connector length; k_{lead} is the lead thermal conductivity; T_e and T_c are the emitter and collector temperatures, respectively, at the connection points.

In actual designs, the thermal loss through the leads is 5-15% of the TFE thermal power.

In order to obtain a rough estimate of ohmic losses in the emitter, collector and the electrical connectors, one can assume a constant current along the height of the electrodes, $J'' = const$, and the energy losses through the collector insulation can be neglected. In this case, the expressions for the indicated losses become

$$\dot{Q}_{loss,e} = \frac{2\pi r_e \rho_e L^3}{3\delta_e}(J'')^2 \quad ; \quad \dot{Q}_{loss,c} = \frac{2\pi r_c \rho_c L^3}{3\delta_c}(J'')^2 \quad ;$$

$$\dot{Q}_{loss,lead} = \frac{4\pi r_e^2 \rho_{lead} L_{lead} L^2}{A_{lead}}(J'')^2$$

where r_e and r_c are the outer radii of the emitter and collector, respectively; L is their length; ρ_e and ρ_c are the electrical resistivity of emitter and collector; and δ_e and δ_c are the thickness of the collector.

From the stated relationships it follows that ohmic losses depend on the geometric dimensions of the TFE. In order to decrease these losses, one must decrease the length and radius of the electrodes and increase their thickness. However, from the standpoint of thermal losses, decreasing the electrode length leads to an increase in the heat loss fraction through the connectors and to a significantly greater nonisothermal condition and, consequently, to a reduction in the generated power. Increasing the electrode thickness contributes additional nonfissioning material to the core and this worsens the neutron-physics characteristics of the reactor. The cross section of the electrical connectors exerts also a conflicting influence on the properties of the TFE. An increase in this cross section leads, on the one hand, to a decrease in ohmic loss in the connector, and, on the other hand, to an increase in the portion of heat that flows from the emitter to the collector and to an increase in nonisothermal electrode conditions. With this in mind, the real problem is to optimize the geometric and thermophysical parameters of the TFE. Its correct solution requires the use of mathematical models that include equations for the transport of heat and electricity in the components of the TFE design. It also requires equations that describe temperature and potential distributions in the electrodes.

In order to illustrate such models and approaches to their solution, we will discuss the determination of current-voltage curves of thermionic converters operating in the arc mode.

One of the most widely used methods for calculating the current-voltage curves of the thermionic cell and thermionic converter as a whole is based on using experimental data obtained on individual elementary sections of the TFE. These data pertain to the "ideal" TFE (i.e., no ohmic losses). In other words, this has to do with laboratory TCs. Accounting for the additional losses, which are inherent in actual TFE designs, leads to a complex system of nonlinear differential equations with nonlinear boundary conditions. These describe the thermal and electrical processes in an TFE with a cylindrical geometry. Thus, such kinds of losses are considered as joule heating in the emitter, collector, electrical connectors and current leads; heat flow along the spacers, electrical connectors and current leads; operation of individual sections of the TFE at nonoptimum points on their current-voltage curves due to nonuniform heat generation along the length of the emitter.

The above mentioned equation can be written in the form:

$$\pi r_e^2 L \frac{\partial}{\partial r} k \frac{\partial T_e}{\partial r} + \pi r_e^2 L \dot{Q}'''(r) - 2\pi r_e L \varepsilon_{eq} \sigma \left(T_e^4 - T_c^4\right) - 2\pi r_e L J''(T_e, V_e - V_c)\left[\varphi_e(T_e) + 2kT_e\right]$$

$$- \frac{k_{spac}}{d_{spac}} 2\pi r_e L_{spac}(T_e - T_c) + \left\{J - 2\pi r_e \int_x^L J''(T_e, V_e - V_c)dz\right\}^2 R_e(T_e) = 0$$

$$(7.17)$$

where k_{spac} is the thermal conductivity of the spacers (or other physical connectors between emitter and collector such as current leads) , d_{spac} is the thickness of the spacers, and L_{spac} is the sum of the length of the spacers in the z direction.

This equation describes a heat balance on the emitter with the following boundary conditions

$$\left.\frac{\partial T_e}{\partial x}\right|_{x=0} = X_1 \quad ; \quad \left.\frac{\partial T_e}{\partial x}\right|_{x=L} = X_2 \quad , \quad (7.18)$$

where X_1 and X_2 are temperature functions (in the general case, nonlinear taking into account heat transfer between the emitter of the i-th element and collectors and emitters of the (i-1) and (i+1) elements for a TFE with internal electrical connections). One can account for heat transfer between the emitter and current leads in a single-element channel in an analogous manner.

The equation for the collector is written quite simply as T_c = const. This holds true for T_c < 750 °C and an average emitter temperature of T_e 1500 °C because the output current-voltage curves change insignificantly over a wide range of change in T_c.

The equations for the current and potential distributions along the thermionic cell can be written as

$$\frac{\partial}{\partial x}\frac{1}{R_e}\frac{\partial V_e}{\partial x}+2\pi r_e J''\left(T_e, V_e - V_c\right)=0 \quad ;$$

(7.19)

$$\frac{\partial}{\partial x}\frac{1}{R_c}\frac{\partial V_c}{\partial x}+2\pi r_e J''\left(T_e, V_e - V_c\right)=0 \quad ,$$

where R_e, R_a are the electrical resistances of the emitter and the collector, respectively; r_e is the emitter radius, J'' is the current density.

The boundary conditions for the above equations for a thermionic cell with current leads on both ends are:

$$\left.\frac{\partial V_e}{\partial x}\right|_{x=0}=0 \quad ; \quad \left.\frac{\partial V_c}{\partial x}\right|_{x=0}=R_e J \quad ; \quad \left.\frac{\partial V_e}{\partial x}\right|_{x=L}=R_c J \quad ; \quad \left.\frac{\partial V_c}{\partial x}\right|_{x=L}= \quad \text{(7.19a)}$$

or , for an thermionic cell with a current lead on one end only,

$$\left.\frac{\partial V_e}{\partial x}\right|_{x=L}=J R_e \quad ; \quad \left.\frac{\partial V_c}{\partial x}\right|_{x=L}=R_c J \quad ; \quad \left.\frac{\partial V_e}{\partial x}\right|_{x=0}=0 \quad ; \quad \left.\frac{\partial V_c}{\partial x}\right|_{x=L}= \quad . \quad \text{(7.19b)}$$

The solution to the above equations is quite complex, especially in engineering calculations. The problem is simplified significantly if a number of assumptions are made:

a. The ideal arc mode current-voltage curves are assumed to be linear;

b. The emitter is isothermal along its height, i.e., its thermal conductivity is infinitely large.

In this case, the current and potential distribution equations are integrated quite readily. By omitting intermediate transformations, we can show the current-voltage curve of an TFE with a single-sided current lead as:

$$J = \frac{V_{oc} - V}{R_e + R_c}\coth kL$$

(7.21)

where $k = \sqrt{\dfrac{R_e + R_c}{R_o}}$, and the internal resistance of the interelectrode gap per unit length

is equal to $R_o = \dfrac{V_{oc}}{2\pi r_k J''_{sc}}R$. V_{oc} is the open circuit voltage (emf), and J''_{sc} is short circuit current density (coth designates the hyperbolic cotangent function).

For a thermionic cell with two-sided current leads, the equation for the current-voltage curve is:

$$J = \frac{V_{oc} - V}{A(R_e + R_c)} \coth kL \qquad (7.22)$$

where $A = 1 - \dfrac{2a}{(1+a)^2} + \dfrac{2a}{(1+a)^2} \dfrac{1}{\text{cthk}L} + \dfrac{a}{(1+a)} kL \coth kL$,

and a is equal to the ratio R_c/R_e.

The internal thermionic cell resistances written here for the single-sided and double-sided current lead cases are, respectively:

$$R_i = R_o \text{kcthk}L \quad ; \quad R_i = AR_o \text{kcthk}L \qquad . \qquad (7.23)$$

A comparison of these two cases makes it apparent that they agree with each other for A = 1, i.e. $R_a = 0$ or $R_c = 0$, or as $kL \to 0$.

These conditions are characteristic of the multielement power plant, "Topaz-1," in which the length of individual thermionic cells does not exceed 10 cm.

The maximum power obtained from a single thermionic cell is determined from the equation

$$\dot{Q}_{e,max} = \frac{V_{oc}^2}{R_i} \qquad . \qquad (7.24)$$

If it is assumed further that joule losses in the thermionic cell are small (no greater than 5% in actual designs) and that the emitter is isothermal, then it is not difficult to do a heat balance which reduces to an algebraic equation. This equation permits one to determine the heat generation in the TFE that will result in the chosen emitter temperature (for a given current-voltage curve).

In the evaluation of the parameters of a multielement TFE the lengths of individual thermionic cells are chosen from a calculation such that the TFE as a whole produces the maximum electrical power for a given heat generation rate. (In the "Topaz-1" TFE, the optimum number of thermionic cells in the TFE equaled five).

The approximate method presented for calculating current-voltage curves of thermionic converters is sufficiently accurate (at any rate, for the engineering calculations that are characteristic of our book). From comparisons with accurate calculations done on a computer, the deviation does not exceed 10-15%.

7.7. Fundamentals of Reactor-Converter design.

The design of a in-core thermionic reactor is a complex problem that simultaneously accounts for neutron-physics, electrical and thermal processes. The solution to this problem, as a rule, is accomplished by the method of successive approximations. Thus, for example, in the first stage (of approximations) based on the

requirement to obtain a given electrical power output over an established life time, the operating mode of the thermionic converter, the basic temperature regime of the emitter and collector and other parameters are selected. Then, by using the method presented above for calculating the thermionic cell current-voltage curve, one can find the average current density and voltage of a single TFE and also the average power produced by it.

In the succeeding stage, based on a given TFE output power, one can find the total emitter surface area, A_e. Such an average power can, naturally, be obtained from an assembly of n_{cell} cells in an thermionic core with a volume $\pi H_{core} R^2_{core}$. Since the emitter diameter in a TFE falls, as a rule, in the 10-15 mm range, it is not difficult to determine the approximate value of n_{cell}. In such a manner, the geometry of the thermionic core is established as a first approximation. Now one can transition to the first neutron-physics calculations of the thermionic core. These result in improved geometric dimensions of the core, and also knowledge of the temperature and heat generation fields. The latter, naturally, are required in making appropriate adjustments in which the physical and geometrical profiling of the core discussed earlier are used. By following general principles of minimizing electrical losses, efforts are made to increase the output voltage of each thermionic cell (typically, V_o 0.5 volts). Later, the problem of series-parallel connections of the TFES is resolved by summing their current-voltage curves in accordance with the energy liberation fields in the thermionic core obtained above.

The first approximation calculations are then optimized based on certain criteria (minimum weight, a given thermionic operating mode, etc.) taking into account the parameter limitations that to the greatest degree influence the life of the nuclear power plant with TCs.

In the event it is necessary to refine the neutron-physics, thermal and electrical characteristics, similar calculations are repeated in the successive approximation process.

8. NUCLEAR POWER PLANTS WITH MECHANICAL ENERGY CONVERSION

8.1. General Information.

In this section, nuclear power plants with mechanical (machine) converters of thermal energy into electrical and nuclear sources of primary energy are discussed. These include power plants that operate with gases and vapors in the Brayton and Rankine cycles as well as piston engines using the Stirling cycle. They are of interest because their operating processes approximate the ideal Carnot cycle. However, despite the wide use of power plants with mechanical converters of heat in stationary and transport power, to date they have not found practical use in space power.

Space nuclear power, as is well known, has taken the path towards the application of power plants with direct converters (thermoelectric and thermionic) of heat. The following comments are appropriate here. At the end of the 1950's when the development of space nuclear power plants appeared on the agenda, two development paths were taken. The first path (that is, power plants with mechanical converters) was taken in the USA, and the second (with direct converters) began in the then Soviet Union. The simultaneous design and development of both classes of power plants was not undertaken by either government. Experience during the past two decades has shown which path was the most rational. The development of power plants with mechanical converters (mainly, vapor turbines in the even-numbered SNAP series) in the USA did not progress beyond test stand versions and has virtually ceased in recent years. At the same time, power plants with direct converters did not only progress through the test phase in the USSR, but were repeatedly used in space. This has resulted in a broad interest in such power plants in the USA (in particular, with the purchase of the "Topaz-2" power plant).

Let's discuss the fundamental reasons for such a development in space nuclear power. It is appropriate here to discuss the advantages and disadvantages of both classes of power plants. Problems in the theory and design of mechanical converters of heat of different kinds used in transportation, in aviation, and in stationary power plants have been the subject of numerous papers by Russian and foreign scientists. Their practical application for a variety of purposes was widely expanded. For this reason, apparently, their development was given primary preference in the USA for space power. Aside from an adequate state-of-the-art in components and assemblies of mechanical converters, these had a number of positive advantages: the possibility of producing alternating current at any frequency, in principle a much higher efficiency compared with direct converters, and a broader and more easily accomplished range of power control. In addition to that, mechanical converters have some significant disadvantages. The basic ones are:

a. Gyroscopic moments produced by rotating components (turbines, pumps, compressors, electric generators);

b. Difficulties with a number of two-phase flow processes (vapor generation, condensation) in a zero-G environment;

c. The influence of "size" factors (i.e. complications and limitations on high efficiencies in small size power plants);

d. Significant complexity in the development of power plants with a long operating life (multi-loop power plant designs, bearing life, etc.).

Power plants with direct converters of heat do not have these disadvantages. The absence of the "size" factor (in this regard, one should keep in mind that the electrical power initially needed did not exceed units of kW), absolute simplicity in construction, and no rotating components resulted in their preferential development in the USSR. Moreover, power plants with mechanical converters would not be considered.

The reality of the substantial increase in working fluid temperature at turbine inlet that has come about in recent years and the need for power plants with high power outputs (for example, the spacecraft power needs mentioned earlier) have provided new possibilities for the development of such power plants. Among these, in our opinion, gas turbine power plants should be given preference. For this reason, we will concentrate our discussion on them. The following also supports this approach. We are all aware that gas turbine converters - turbojet engines - have received wide use in aviation, particularly in supersonic flight. The development of powerful aviation engines, that is, engines for aerospace vehicles, has been the subject of extensive research and design work in many countries in the world.

In addition, knowledge of the fundamental working processes in power plants operating on the Brayton cycle is needed by any engineer working in the power area. Therefore, the basic content of this section is devoted just to gas turbine power plants.

8.2. Gas Turbine Power Plants.

The simplest thermal schematic of a gas turbine power plant is shown in Fig. 8.1. It includes the following basic components: a heat source (in this case, a nuclear reactor), a turbine which drives an electric generator, a space radiator and a compressor. The thermodynamic cycle of a simple gas turbine power plant in T-S coordinates is shown in Fig. 8.2. The ideal cycle (dashed lines) consists of two constant pressure lines 4_{ad} - 1 and 2_{ad} - 3_{da} and two adiabatic lines 1 - 2_{ad} and 3_{ad} - 4_{ad}. The constant pressure lines represent heating of the working fluid in the reactor and cooling in the radiator, the adiabatic lines reflect expansion in the turbine and compression in the compressor. In an actual cycle (solid lines) the expansion and compression processes proceed along the polytropic lines 1 - 2 and 3 - 4, respectively, and are accompanied by an increase in entropy due to the conversion of work against friction into heat.

The processes of heating 4 - 1 and cooling 2 - 3 in a real cycle is accompanied by losses in total pressure p^* (stagnation pressure). In comparing ideal and real cycles, the following conditions were assumed: point 1 is the gas temperature at turbine inlet, identical working fluid expansion ratios in the turbine ($p_2^* = p_{2ad}^*$) and identical compression ratios in the compressor ($p_4^* = p_{4ad}^*$ and $T_4^* = T_{4ad}^*$).
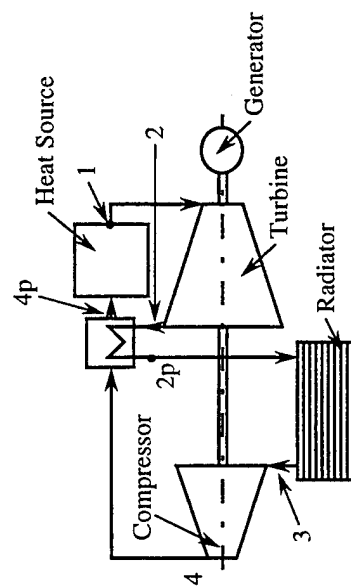
Fig. 8.1 Gas turbine power plant.

253
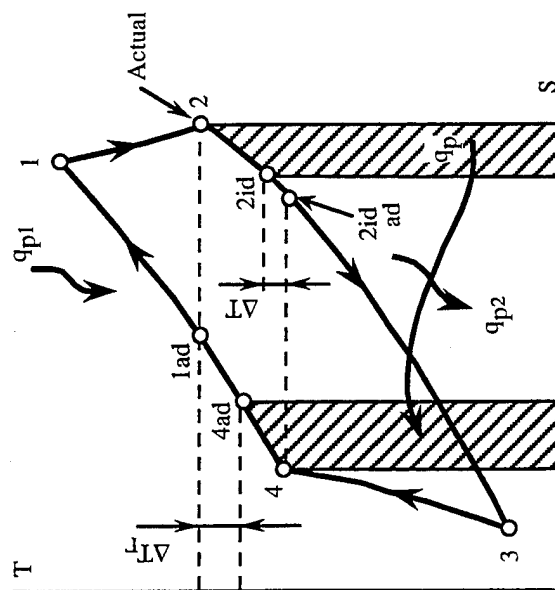
Fig. 8.2 T-S diagram for a gas turbine.

The useful work of a real cycle per kg of working fluid can, based on the conservation of energy equation, be expressed as the difference in turbine and compressor work:

$$Q_{net} = Q_{tur} - Q_{comp} = c_{pg}(T_1 - T_2) + \frac{C_1^2}{2} - \frac{C_2^2}{2} - c_{px}(T_4 - T_3) + \frac{C_4^2}{2} - \frac{C_3^2}{2} \ . \quad (8.1)$$

In order to simplify the subsequent analysis, we will assume a constant heat capacity of the working fluid along the compression and expansion lines ($c_{pc} = c_{ph} = c_p$). We will also examine the working process parameters based on the stagnation parameters:

$$T^* = T + \frac{C^2}{2c_p} \qquad .$$

Thus, we can write

$$Q_{net} = c_p\left(T_1^* - T_2^*\right) - c_p\left(T_4^* - T_3^*\right) \qquad (8.2)$$

The turbine and compressor efficiencies are determined from the following relationships:

$$\eta_{comp}^* = \frac{Q_{comp,ad}}{Q_{comp}} = \frac{T_{4ad}^* - T_3^*}{T_4^* - T_3^*} \quad \text{and} \quad \eta_{turb}^* = \frac{Q_{turb}}{Q_{turb,ad}} = \frac{T_1^* - T_2^*}{T_1^* - T_{2ad}^*} \qquad .$$

The compression ratio in the compressor and the expansion ratio in the turbine are determined from:

$$PR_{comp}^* = \frac{p_4^*}{p_3^*} = \left(\frac{T_4^*}{T_3^*}\right)^{\frac{k}{k-1}} \quad ; \qquad PR_{turb}^* = \frac{p_1^*}{p_2^*} = \left(\frac{T_1^*}{T_2^*}\right)^{\frac{k}{k-1}}$$

The turbine expansion ratio is related to the compressor compression ratio by the simple relationship

$$PR_{turb}^* = PR_{comp}^* \sigma_\Sigma \qquad ,$$

where $\sigma_\Sigma = \sigma_{reac}\sigma_{rad}\sigma_{plumb}$ is the total pressure loss factor which takes into account losses in the individual components of the gas turbine power plant (reactor, radiator, gas plumbing).

The useful electrical power of the gas turbine power plant can now be shown to be

255

$$Q_{el} = \dot{M}\eta_{mech}\eta_{eg}c_pT_1^* \left\{ \left[1 - \frac{1}{\left(PR_{comp}^*\sigma_\Sigma\right)^{\frac{k-1}{k}}} \right]\eta_T^* - \frac{T_3^*}{T_1^*}\left[\left(PR_{comp}^*\right)^{\frac{k-1}{k}} - 1\right]\frac{1}{\eta_{comp}^*} \right\} , \quad (8.3)$$

where $\dot{M}$ is the working fluid mass flow per second; η_{mech} is the mechanical efficiency which accounts for bearing friction, friction in auxiliary component drives, etc.; η_{eg} is the electric generator efficiency. If a turbine RPM reductor coupling is needed, one needs to introduce an appropriate efficiency, η_{red}.

The gas turbine power plant efficiency is equal to the ratio of the useful electrical work to the heat added to 1 kg of working fluid in the reactor, Q:

$$\eta_{gtpp} = \eta_{eg}\frac{Q_{net}}{Q} = \eta_{eg}\frac{Q_{net}}{c_p\left(T_1^* - T_4^*\right)} \quad . \quad\quad (8.4)$$

The temperature at the compressor outlet T_4^* is related to the temperature T_3^* and the compression ratio PR_{comp}^* by the relationship

$$T_4^* = T_3^*\left(\frac{\left(PR_{comp}^*\right)^{\frac{k-1}{k}} - 1}{\eta_{comp}^*} + 1\right) \quad . \quad\quad (8.5)$$

Therefore, for constant value of turbine and compressor efficiencies, power plant efficiency is a function of two independent variables PR_{comp}^* and T_3^*/T_1^*.

The efficiency of an ideal Brayton cycle is given by the following:

$$\eta_{ideal} = 1 - \frac{1}{\left(PR_{comp}^*\right)^{\frac{k-1}{k}}} \quad .$$

In order to determine the specific area of the radiator, the following equation can be used:

$$\frac{A_{rad}}{Q_{el}} = \frac{1}{3\varepsilon\sigma\varphi^4 v_p\left(T_2^*\right)^4} \cdot \frac{1 - \eta_{gtpp}}{\eta_{gtpp}} \cdot \frac{\left(\frac{T_2^*}{T_3^*}\right)^3 - 1}{1 - \frac{T_3^*}{T_2^*}} \quad\quad (8.6)$$

where

$$\varphi = \frac{T_{chan}}{T_{wf}} < 1$$

is the temperature ratio of the radiator channel and the gas heat carrier.

We observe further that the temperature of the working fluid (gas) at the outlet can be expressed in terms of the inlet temperature T_1^*:

$$T_2^* = T_1^* \left\{ 1 - \left[1 - \frac{1}{\left(PR_{comp}^* \sigma_\Sigma \right)^{\frac{k-1}{k}}} \right] \eta_{turb}^* \right\} \qquad (8.7)$$

and therefore, the specific area A_{rad} also is function two these same parameters.

It is difficult to determine analytically the optimum values of the indicated parameters. This problem is solved more easily graphically. The relationship between power plant efficiency and A_{rad}/Q_{el} in the functions PR_{comp}^* and T_3^*/T_1^* is constructed and shown in Fig. 8.2-8.4. As can be seen, the optimum temperature ratio $(T_3^*/T_1^*)_{opt}$ for the condition $(A_{rad}/Q_{el})_{min}$ is significantly less than, let's say, in thermionic power plants and is 0.2-0.3 instead of 0.6-0.7. The reason is that as T_3^* is reduced, the overall turbine power plant efficiency will increase more intensively due to the decrease in compressor work than in other types of power plants. However, the specific radiator area of gas turbine power plants at gas turbine inlet temperatures of $T_1^* \approx 1200$ to 1400 K will be somewhat greater than in, let's say, thermionic power plants. The reason is that the tube wall and fin temperatures of the radiator are lower compared with what they are in power plants that use liquid metal coolants. This is why gas turbine power plants have not been used in spacecraft power systems. The situation will change substantially with the use of turbine blades capable of operating at much higher temperatures, up to 2000-2200 K. In this event, the gas turbine power plant efficiency will increase significantly and the specific radiator area will decrease substantially (see Figs. 8.5-8.6). Hence, we can draw the important conclusion that the gas turbine power plant remains a very viable competitor with nuclear thermionic power plants, especially at high electrical power outputs.

There are a number of ways to increase the power plant efficiency: the application of regenerative cycles and cycles with multistage heat addition and removal. However, all of these complicate the power plant design, which is not desirable in space nuclear power plants. For this reason, we will not discuss these further.

There are a number of power plant projects for spacecraft power systems that have been pursued in the USA. However, project development has not continued and it is premature to talk about practical applications of the power plant.

We note in conclusion that other kinds of mechanical converters, especially vapor turbine power plants, have been investigated in parallel with gas turbine power plants. However, in view of the limited scope and purpose of this book, we will not discuss other kinds of nuclear power plants with mechanical converters of heat.
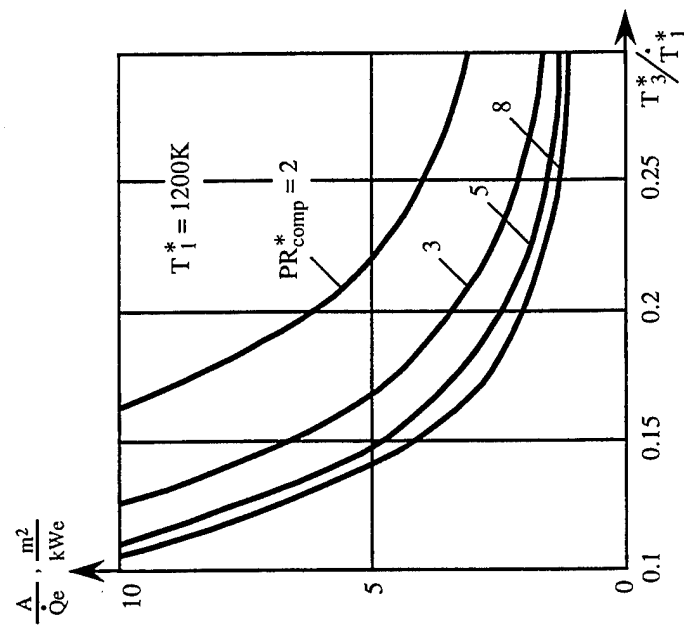
Fig. 8.3 Specific radiator area versus temperature ratio;
$A_{rad}/\dot{Q}_{el}$ vs T_3^*/T_1^* for $T_1^* = 1200K$.
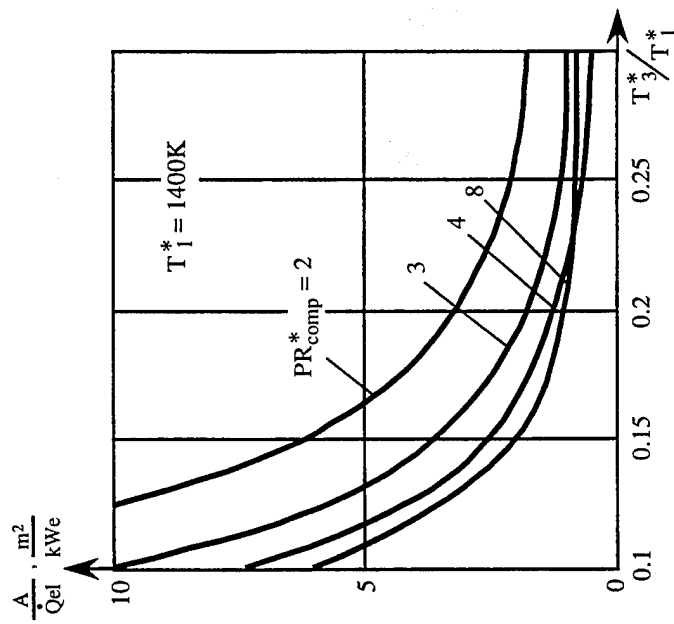
Fig. 8.4 Specific radiator area versus temperature ratio; $A_{rad}/\dot{Q}_{el}$ vs T_3^*/T_1^* for $T_1^* = 1400K$.
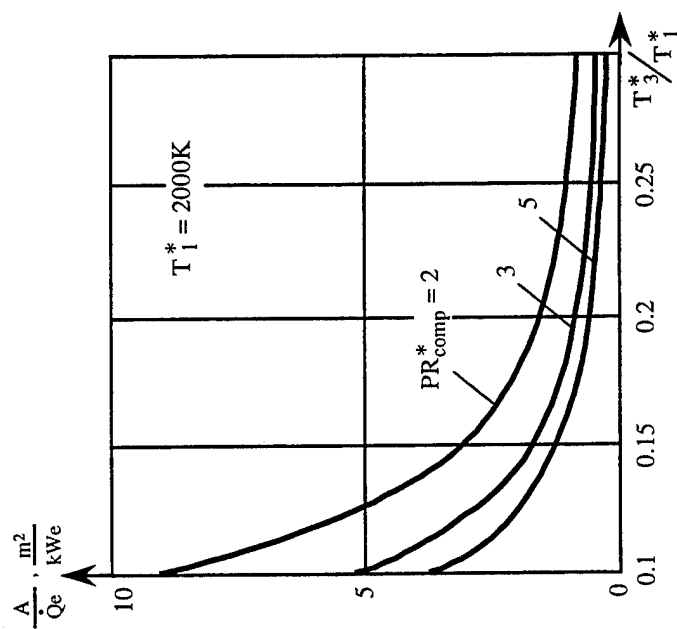
Fig. 8.5 Specific radiator area versus temperature ratio; $A_{rad}/\dot{Q}_{el}$ vs T_3^*/T_1^* for $T_1^* = 2000K$.
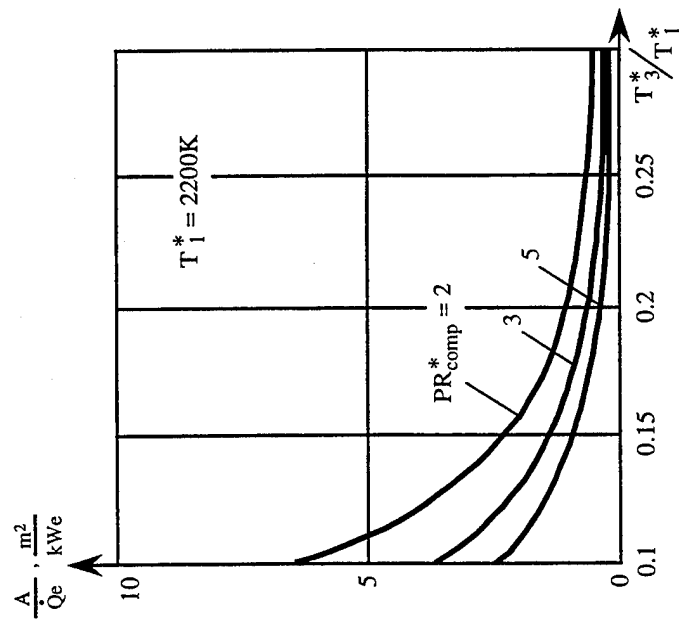
Fig. 8.6 Specific radiator area versus temperature ratio; $A_{rad}/\dot{Q}_{el}$ vs T^*_3/T^*_1 for $T^*_1 = 2200K$.

9. DESIGN OF NUCLEAR POWER PLANTS WITH DIRECT ENERGY CONVERSION (THERMOELECTRIC AND THERMIONIC)

9.1. Fundamental Stages in the Development of Space Nuclear Power Plants and General Principles of Assembly.

Aside from the relationship to the kind of energy conversion used, the development of space nuclear power plants generally includes the following stages:

a. Exploratory scientific research work and generation of technical proposals for the development of space nuclear power plants for specific purposes (it is understood that the conditions that favor the development of systems with nuclear energy sources meet the criteria formulated in 1.3.);

b. Compilation and coordination of technical tasks for competitive designs of the given nuclear power plant;

c. Development of a preliminary design ;

d. Development of a working engineering design (or detailed engineering designs and operating documentation);

e. Full-scale experimental development and fabrication of test specimens of individual components of the nuclear power plant;

f. Test bed testing (on the ground) with simulation of space conditions;

g. Experimental design testing of the nuclear power plant in accordance with state standards;

h. Fabrication and delivery to the customer of series produced models of the given nuclear power plant and initiation of performance testing on appropriate spacecraft in accordance with government standards.

High reliability of the nuclear power plant being designed is assured by thoroughness in completing a multiplicity of associated work in the following directions:

a. Multifaceted theoretical investigations;

b. General testing of models and wide use of statistical data;

c. Mathematical modeling;

262

d. In-depth experimental investigations with simulation of actual conditions and with the use of modern measurement equipment;

e. Strict and continuous satisfaction of engineering, fabrication and management requirements in order to eliminate defects in any nuclear power plant component.

The reliability requirements for the nuclear power plant and its components are incorporated in the technical task and then in the technical documentation for the fabrication of the given nuclear power plant. Reliability during the nuclear power plant development phases is assured and verified based on a common plan covering the entire fabrication process. The achievement and verification of high nuclear power plant reliability is a process that continues through the entire life cycle of the nuclear power plant from the moment of approval of the development technical task to the end of its operational cycle.

9.2. Nuclear Power Plants with Thermoelectric Converters.

The manner of assembling a nuclear power plant with thermoelectric converters is chosen depending on how the heat transfer between the reactor converters and the space radiator is managed. According to the schematic in Fig. 9.1, one can employ thermal conductance and radiation heat transfer, coolant loops (containing liquid metals, gases, vapors), heat pipes, as well as different combinations of these methods and media. Thus, possible designs include designs without coolant fluids in which heat is transferred by conductance only; single-loop designs where heat is transferred by conductance from the reactor to the converters or from the converters to the radiator, and where heat is transferred by circulation of a coolant in a coolant loop. Finally, a possible design is one in which the thermal coupling between the reactor, the thermoelectric converters, and the radiator is accomplished by the circulation of coolant fluids. This is the two-loop design.

Each of these designs have their advantages and disadvantages.

The nuclear power plant design in which heat transfer proceeds directly by thermal conductance is the most compact. The limited surface area on which to place the thermoelements, the relatively low effectiveness of the radiator fins and the large temperature gradient between the center of the reactor core and the external surface of the reflector limits the power of such power plants to hundreds of watts and their specific weight is very high. However, because of the simplicity of this design and because of the special nature of the research task in the early stages of nuclear power plant development, the world's first nuclear thermoelectric power plant, the "Romashka," was developed based on this design. Its power output was limited to about 500 W (Fig. 9.2).

In order to increase the efficiency of heat rejection in space, a preferable design is one in which the radiator is a separate component. The reactor and the thermoelectric converters constitute a single assembly, the reactor-converter, and it is coupled to the radiator through a coolant loop (Fig. 9.3). However, the power output of such a power plant remains low for the previously noted reason that the thermoelements are placed on the reactor surface.

Cooling Radiator

Converter

Radiation Shield
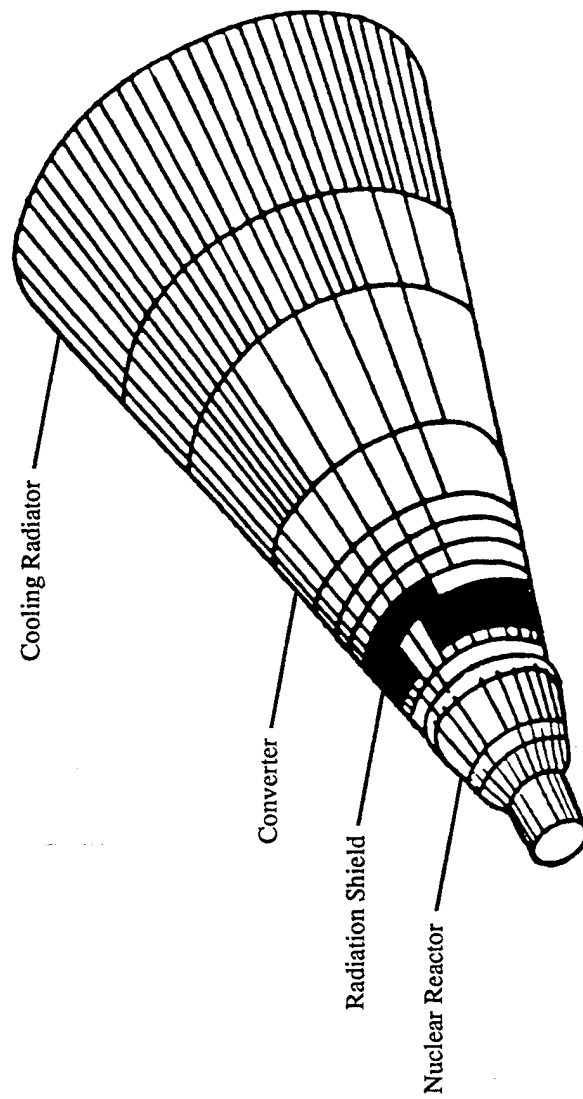
Nuclear Reactor

Fig. 9.1 Illustration of a space nuclear power plant.
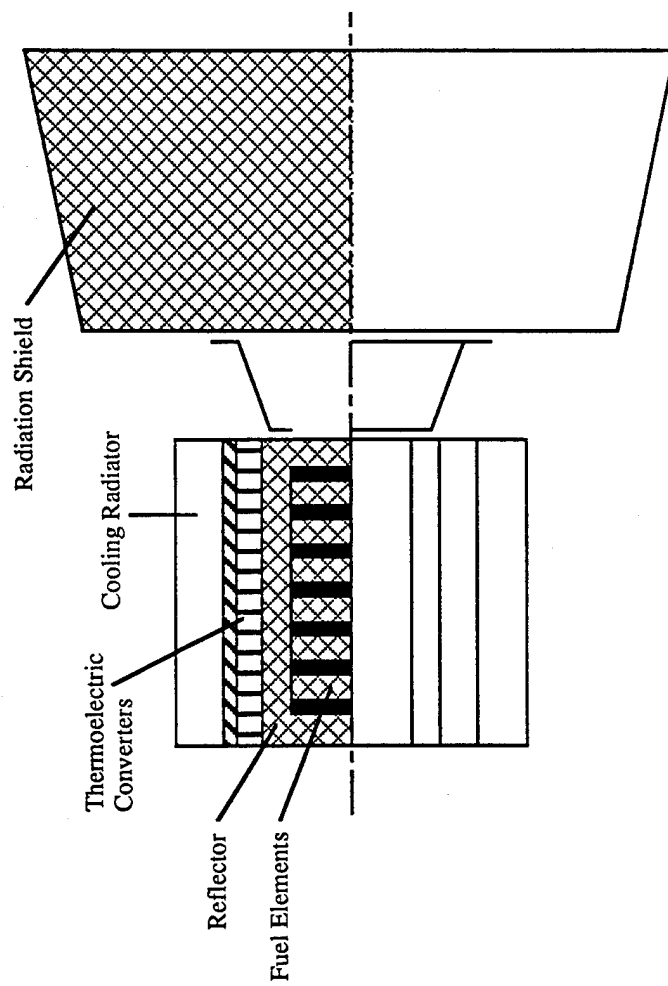
Fig. 9.2 An illustration of a "Romashka"-type nuclear power plant using thermoelectric converters.

Radiation Shield

Cooling Radiator

Thermoelectric Converters

Reflector

Fuel Elements

265
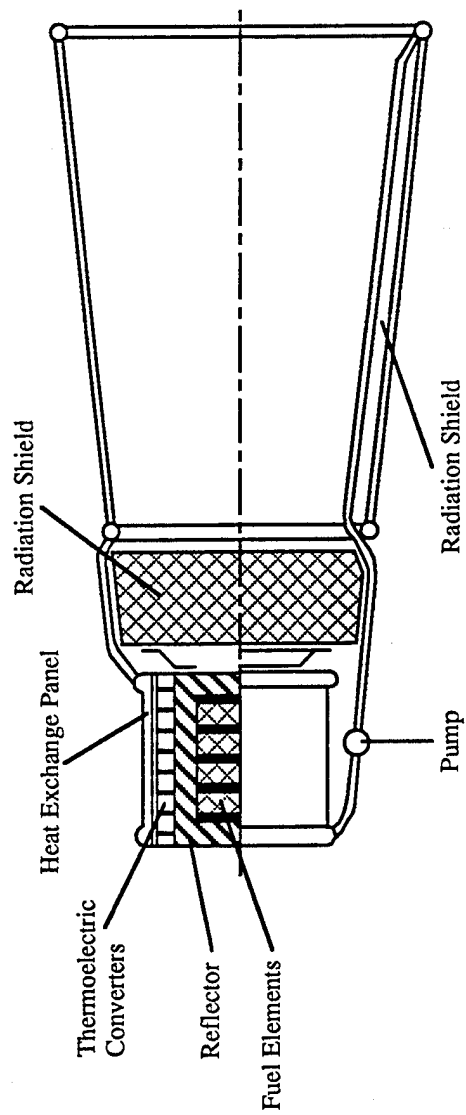
Fig. 9.3 Modified Romashka-type reactor with external coolant loop and radiator.

Radiation Shield

Radiation Shield

Heat Exchange Panel

Thermoelectric Converters

Reflector

Fuel Elements

Pump

Also, the American nuclear power plant, the SNAP-10A, was built using this design and produced 500 W. It was first tested in space in 1965.

In order to eliminate the stated disadvantages, a design can be adopted in which the reactor is a separate component, and the thermoelectric converters and the radiator constitute a single assembly, the radiator-converter. The specific characteristics of such power plants are much improved, but there are disadvantages associated with assembling the components of such a nuclear power plant.

The next step in the development of nuclear power plant and thermoelectric converter assemblies was the two-loop design in which the three basic components are independent and the energy coupling is done by means of coolant loops. Since each component is a separate entity, experimental design work can be done on each component separately. A Russian nuclear power plant was built using this design and it has been used in space repeatedly. The power plant consists of a reactor, a radiation shield, a thermoelectric generator assembly, and a space radiator with a liquid metal loop.

The fast reactor consists of a compact core with an assembly of 37 cylindrical fuel elements with beryllium end reflectors. A uranium-molybdenum alloy is used as the nuclear fuel. The core loading is 30 kg of 90% enriched uranium-235.

The reactor structural material is stainless steel. The reactor design incorporates beryllium side reflectors using rotating drums with approximate dimensions 100 diameter x 255 mm long. The moderator is lithium hydride.

Significant disadvantages of all nuclear power plants that use coolant loops are the real danger of failure due to leakage and the electric power that has to be expended by the electomagnetic pumps in pumping the coolant through the loops.

A design that is free of these disadvantages is one in which the energy coupling between the basic components is accomplished by heat pipes. The use of heat pipes eliminates the expenditure of pumping power. The low working fluid flow rate in the heat pipes reduces the secondary γ radiation beyond the radiation shield. Leakage of a single heat pipe in the reactor or in the radiator will reduce the output characteristics of the nuclear power plant, but will not result in complete failure. One variant of nuclear power plants with heat pipes is a design in which the heat from the reactor heat pipes is transferred to the thermoelements by radiation. Such a design was used in the USA in a nuclear power plant in the SP-100 program with a useful electric power output of up to 100 kW. Since the practical development and application of nuclear power plants with thermoelectric converters resulted in two-loop designs with independent positioning of individual components and in view of the previously mentioned information on reactors and radiators, our main attention will now be devoted to thermoelectric converters.

9.3. Design of Thermoelements and Thermoelectric Converters.

Thermoelements constitute the basis for thermoelectric converters (TECs). Larger units of separate modules and thermopiles are made from single thermoelements. The thermoelement, in turn, consists of two semiconductor branches which are joined by electrical connectors (Fig. 9.4) and separated from the heat conductors by a layer of insulation. The semiconductor branches can be configured differently depending on the thermoelement configuration.
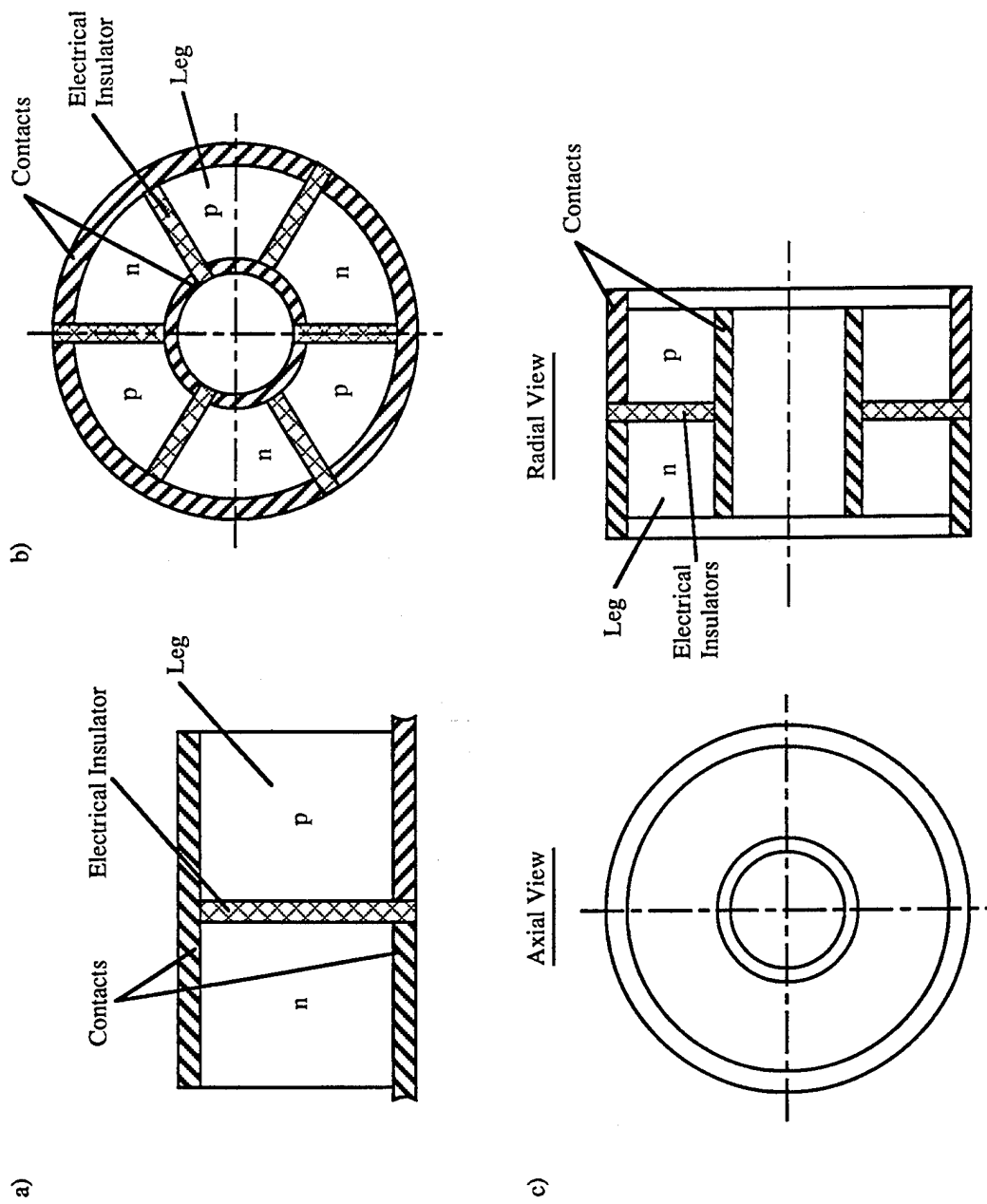
Fig. 9.4 Schematics of thermoelectric converters for a) planar configuration, b) radially segmented configuration, and c) annular configuration in both axial and radial views.

There are planar, annular and segmented thermoelements (Fig. 9.4) which are determined by the shape of their junction surfaces. Planar thermopiles and converters are made from planar thermoelements and cylindrical ones are made from annular and segmented thermoelements. There is a good number of suitable thermoelectric materials available at the present time for use in space nuclear power plants. These are so-called medium and high temperature materials. Some data on the thermoelectric and thermophysical properties of these materials are presented in Table 9.1.

Table 9.1.Thermoelectric Materials.

Material	Additive	Type	Melt Temp	T_h	ΔT	Z, $10^{-3}K^{-1}$	λ W/mK	ρ g/cm^3
PbTe	Br+Pb	n	1195	900	350	1.30	1.7	8.16
PbTe	Na,Ag,K	p	1195	900	350	1.20	1.8	8.16
PbSe	-	n	1360	950	400	1.05	-	8.10
PbTe(75%)+SnTe(25%)	-	n	1183	1000	400	1.15	1.4	7.90
PbS	Cl	n	1387	1000	450	0.80	1.7	·5.90
AgSbTe$_2$	-	p	840	750	250	-	-	6.22
GeTe(95%)+Bi$_2$Te$_3$(5%)	-	p	985	900	300	1.40	2.0	6.28
Si(70%)+Ge(30%)	P,As	n	1603	1200	900	0.65	4.3	3.25
Si(70%)+Ge(30%)	B,Ga	p	1643	1200	900	0.50	4.7	3.25
Si(85%)+Ge(15%)	P,As	n	1643	1300	1000	0.65	5.0	-
Si(85%)+Ge(15%)	B,Ga	p	1643	1300	1000	0.50	5.8	-
GeS	Sr,S	n		1400	1100	0.20	2.1	5.27
InAs(90%)+InP(10%)	-	n	-	1140	840	0.41	0.7	5.58
MnTe	Na	n	1443	1300	600	0.35	-	-

There are several methods for joining the electrical connectors to the semiconductor branches. Among these, the most widely used methods are diffusion welding and soldering. Sometimes a simple method is used, such as clamping the electrical connectors to the ends of the branches.

In addition to the material of the branches, the material and dimensions of the electrical connectors influence significantly the characteristics of the thermoelement. The materials used are copper, silver, nickel, molybdenum, and others. The thickness of the electrical connectors is optimized depending on the thermophysical properties of the branches and connectors and their dimensions and also depending on the converter operating temperature conditions.

As a rule, the branch and connector materials have substantially different coefficients of linear expansion. This results in large thermal stresses that can damage the junction and increase its electrical and thermal resistance, especially during thermal cycling. At the point of contact between the connectors and the semiconductors the connector material can diffuse into the semiconductors. This phenomenon leads to degradation of the thermoelectric characteristics of the semiconductors and may become one of the main reasons for degradation of the output parameters of the thermoelectric converters. In order to eliminate these detrimental factors, special sublayers are introduced between the electrical connectors and the semiconductors during the fabrication process. These sublayers will attenuate thermal stresses and prevent diffusion.

A multilayer connection is sometimes used to achieve the needed effect. Of course, the sublayer material must possess the lowest possible electrical and thermal resistance and have an adequate mechanical strength.

As we noted above, the electrical connection is sometimes done by clamping the electrical bus directly to the branches. Such an electrical connection method will prevent thermal stresses at the junctions and permit the elements to be replaced quickly, however, the junction will have a high thermal resistance and the thermoelement will be larger and heavier.

Electrical insulation is used in order to prevent electrical contact between the thermoelements and the heat conductors. These can be clamped to the hot and cold junctions, or only to the hot or the cold junctions, and also to the thermoelement branches. The most critical function is fulfilled by the electrical insulation on the thermal contact surfaces of the electrical connectors. This insulation layer should have a quite high electrical resistance to assure a minimum loss of electrical energy, and also the lowest possible thermal resistance in order to reduce the temperature drop in the insulation. This situation necessitates the selection of an optimum electrical insulation thickness which depends on the properties of the material used, the operating temperature conditions of the converter and the emf developed by it. BeO and Al_2O_3 are used as thermal contact insulation materials. In order to decrease the thermal contact resistance between the electrical connectors and the electrical insulation layer, the latter is bonded to the connectors by soldering or by diffusion welding.

Thermoelectric converter assemblies. A thermoelectric converter assembly consists of a large number of series-parallel connected thermoelements. Depending on the design configuration of the converter and the method by which it is connected to the reactor (the heat source) and the radiator cooling unit, only the structural shape of the components by which this connection is made will change, while the design of the thermoelements will remain virtually unchanged.

The design of the attachment devices should provide reliable thermal contact between the thermoelements and the heat conductors and free them from thermal deformation. In order to reduce the thermal resistance in the heat conductor-junction section, the thermal contact electrical insulation should be bonded by soldering or diffusion welding to the heat conductor surface. In this attachment, just as in the electrical connection of the thermoelements, the problem of compensating for thermal stresses arises. For this reason, transitional layers are used between the electrical insulation and the heat conductors. These smooth out the differences in the coefficients of linear expansion. Flexible compensators in the electrical connectors are also used. The soldered or diffusion welded contacts are used to attach individual thermoelectric modules that are spaced comparatively far apart and in those situations where the design configuration requires a mechanical connection between the heat conductors and the thermoelements.

The simplest contact from a technological standpoint is that which is made by clamping the thermoelement to the heat transfer surface. The problem of compensating for thermal stresses is eliminated in such structures, however, steps must be taken to reduce the thermal contact resistance. Increasing the clamping force does not eliminate the problem because thermal deformation will distort the shape of the contacting surfaces and will eliminate contact between them over their entire surface area even at high

compression forces. The most effective method for reducing the thermal contact resistance is to use high thermal conductivity plastic materials, powder or liquid fillers, and gases in the contact region. When gases are used, for example, helium, one needs to enclose the thermoelectric converters in sealed cartridges. This method is useful in suppressing sublimation and mass transfer of the semiconductor materials.

Let's examine some design variants of practical interest in space power involving the placement of thermoelements on the surface of a heat source.

In this regard, thermoelectric converters with coolant loops deserve attention. In general, such thermoelectric converters can be constructed using thermoelements with cylindrical or planar configurations. Thermoelectric converter designs based on cylindrical thermoelements are used in radioisotope generators or in stationary nuclear power plants for industrial purposes. The functions of the power components that connect the thermoelements in the pile are performed by coaxially arranged support tubes. These tubes are the hot or cold coolant flow channel components. Ampoules with radioactive isotopes or heat pipes, which serve to supply or remove heat, can be placed in these tubes. The thermoelement junctions are attached to the power tube surfaces through the insulation.

Planar piles, from which the reactor thermoelectric converters are made, consist of several planar thermopiles, which are connected in individual series units, in parallel or in series electrical circuits. The hot and cold junctions of the pile are attached to the flat coolant panels through the electrical thermal contact insulation. The entire assembly is enclosed in a sealed container which is filled with an inert gas in order to suppress sublimation of the semiconductor materials and to enhance thermal contact between the piles and the heat conductors.

Thermoelectric converters with coolant loops have a number of the previously noted disadvantages associated with nonisothermal heat addition and heat removal. These disadvantages are virtually nonexistent in thermoelectric converters using heat pipes. Such a design was incorporated in the thermoelectric nuclear power plant project under the SP-100 program.

10. NUCLEAR POWER PLANTS WITH THERMIONIC CONVERTERS.

10.1. General Equipment and Design Problems.

The principles of operation of the thermionic converter examined earlier (Section 7) and its possible design versions offer exceptional opportunities for combining the thermionic converter with a variety of energy sources, including, of course, nuclear reactors. In the latter case, we can consider two thermionic converter design configurations. In one of these, the thermionic converter is placed directly in the core of the reactor. The converter emitter becomes the fuel element clad. This allows heat liberated in the fission process to be conducted directly to the emitter, which minimizes intermediate heat transfer equipment. In the second case, the thermionic converter is located outside the reactor core and thermal energy is brought to the emitter by a coolant or by a heat pipe. The assembly of a reactor with thermionic fuel elements (TFEs), in which one or more thermionic converters are incorporated into the fuel elements, is called an in-core thermionic reactor, to distinguish it from reactors with thermionic converters external to the reactor core. Obviously, the TFE is the basic component that determines the output characteristics of the nuclear thermionic power plant as a whole. Both the internal and the external thermionic converter design versions have their own design peculiarities which one must take into consideration during their structural development and subsequent operation. However, the most complex structural design problems are encountered in the development of thermionic converters that are to be placed inside the reactor core. For this reason, we will discuss this design in greater detail. In this connection, we should first point out the main requirements placed on the thermionic reactor core and on the nuclear thermionic power plant as a whole. Basically, they consists of the following:

a. Assurance of the operating capability of the thermionic reactor design for a long period of time at high temperatures and in such aggressive media as cesium, potassium, and sodium;

b. Preservation of electrical insulation properties under these same conditions and in a nuclear radiation environment;

c. Avoidance of local overheating and boiling of the coolant;

d. Maintenance of stable properties of the zirconium hydride moderator and containment of hydrogen in the reactor core;

e. Assurance of the operating capability of all thermionic reactor control units;

f. Maintenance of the hermetic seal of all thermionic reactor cavities (cesium, control units, shield container, and others) at operating temperatures of 500-600 °C and higher;

g. Assurance of the operating capability of thermionic reactor control units while subjected to dynamic loads (spacecraft orbit insertion).

The satisfaction of these requirements makes it necessary to take special design measures in order to deal with thermal issues regarding thermionic reactor components and the nuclear power plant as a whole.

Maintenance of all thermal state parameters of the basic thermionic nuclear power plant subassemblies within prescribed limits during all stages of operation is the deciding factor in the life stability of the nuclear power plant. The thermal state requirements on the nuclear power plant components differ from each other (up to several hundred degrees) and in order to assure their operating capability, it is necessary to employ appropriate assembly configurations within the nuclear power plant, to employ special heat shielding techniques to protect thermally stressed components, and to use effective temperature control algorithms. Thus, for example, in the design of the nuclear power plant Topaz-I it was necessary to maintain definite limits on no less than 70 thermal engineering parameters pertaining to about 25 components.

10.2. Design of the Reactor and TFE.

The structural design configuration of the thermionic reactor is to a significant degree similar to that of ordinary nuclear reactors. Fundamental differences are the use of electric generating channels in the thermionic reactor instead of the commonly known fuel elements and the existence of cesium cavities that connect to the interelectrode gaps of the thermionic converters. Internal electrical connections of individual converters in the thermionic reactor should also be added to the above. Let's examine some general problems in the configuration of the thermionic converter

The coaxial TFE design is the most widely used among both the in-core and out-of-core versions. Fuel can be placed internally or externally (relative to the converter) in the coaxial TFE. In the internal version the fuel is placed inside the cylindrical emitter cavity and in the external version the emitters and other components of the thermionic converter structure are placed inside fuel blocks (Fig. 10.1).

A large mass of fuel is possible in the TFE with external fuel placement. It is easier to remove gaseous fission products in such designs because the interelectrode gap is bypassed. In addition, when the electric circuit is disrupted an excessive increase in temperature does not occur because direct contact with adjoining fuel elements will allow a portion of the generated heat to be transferred to them. Disadvantages of such designs include the need for high temperature electrical insulation between the fuel blocks within the confines of the multi-cell TFEs and between adjoining channels. In order to prevent fuel mass transfer inside the core and gas transfer between the fuel and the interelectrode gaps, the fuel blocks must be enclosed in sealed containers. Designs with external fuel placement are difficult to accomplish in thermal reactors.

Currently, the overwhelming majority of projected and completed thermionic reactors employ TFEs with internal fuel placement.

Depending on the number of cells that make up the TFE, the latter can be a single cell or multicell channel. In a single cell TFE the length of the emitter and collector is
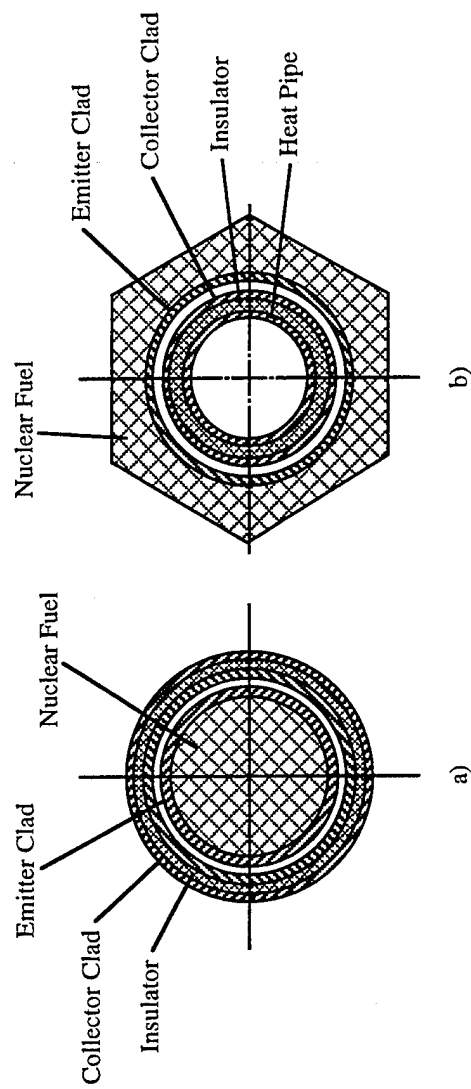
Fig. 10.1 Thermionic fuel element cross section. a) conventional topaz-type TFE; b) "inside-out" design.

equal to the core height and the emitter and collector have separate electrical terminals at the ends. Electrical connection of the TFE is made outside the core. The advantages of the single-cell TFE are the following: structural simplicity, a highly uniform longitudinal temperature field, reliable collector insulation because there is no contact with the interelectrode medium, and the converters can be tested by direct electrical heating of the emitters. A disadvantage is the relatively great length of the electrodes and, consequently, the high current flow in them, large electrical losses and a low specific power output.

The multicell TFE does not have the disadvantages inherent in the single-cell TFE, but it does have a number of other disadvantages caused by breaks in the electrodes and in the electrical connectors between the collectors and the emitters: a nonuniform temperature distribution along the electrodes, thermal energy losses through the current connectors and additional electrical losses in these connectors.

The thermionic converter structural materials should have acceptable nuclear physical properties for the built-in version and their mass in the converter should be at a minimum. The latter two requirements are important in reducing the mass and size of the converter and of the nuclear power plant as a whole.

Among the factors that are related to the operating process in the thermionic converter and which influence the structural configuration of the TFE, the following stand out: high emitter temperatures (1500-2200 K), small interelectrode gaps (0.2-0.5 mm), low electrical voltages (0.5-1 V) developed by a single TFE, the presence of cesium vapor or cesium and barium vapor in the interelectrode gap.

Among the phenomena that occur in the nuclear reactor core and which influence the thermionic converter operating process and the selection of the TFE structural configuration, the following should be noted: a change in the interelectrode gap (the danger of short circuiting the TFE electrodes due to nuclear fuel swelling); diffusion of fuel components and fission products into the interelectrode gap; a change in the mechanical and electrical characteristics of the electrode and electrical insulation materials due to the effects of neutron flux and γ radiation; nonuniform heat liberation in the core.

The individual parameters and duration of trouble-free operation of the TFE are basically determined by the converter operating temperature conditions, but they also depend significantly on the TFE configuration.

The above mentioned factors have been considered to varying degrees in existing TFE design versions. Nevertheless, certain general trends can be traced in the solution to TFE structural design problems.

The influence of electrical losses in the electrodes on the specific characteristics of the TFE was observed in comparisons of single-cell and multi-cell TFEs. In order to reduce these losses, multicell TFEs are used, that is, the length of the individual electrodes is reduced and, consequently, their electrical resistances are reduced. For this purpose, the electrode thickness is increased. In the built-in thermionic converter version, the electrode thickness affects the electrode strength and its ability to resist fuel swelling. However, the increase in thickness of the electrodes is limited by its influence on core reactivity. The number of cells in the TFE and the related number of interelement spacings also influence the neutron physical properties of the core. This influence is due to the introduction in the core of materials that absorb neutrons such as tungsten.

Attention should be paid to the fact that the number of TFEs significantly affects the emitter temperature field due to the current leads between series connected TFEs. A reduction in the emitter temperature in the region where it is connected to the current lead and the relative extent of this region depends on the dimensions of the electrodes and the current leads and on the thermal conductivity of the materials. If one considers that the dimensions of the current leads depend on their electrical resistances, and thus on the electrical losses, then it is obvious that the current lead geometry must be optimized. There is also a substantial influence on the emitter temperature field by the choice of location where the emitter is connected to the current lead. This location should be removed as far as possible from the operating surface of the emitter. Thus, the conflicting influence of the emitter and current lead dimensions on the specific parameters of the TFE makes it necessary to perform optimization calculations.

The presence of cesium vapor in the interelectrode gap requires that special measures be taken to eliminate electrical arcing between the emitters and the support tube. This is possible in a cesium atmosphere at a difference potential of several volts. On the other hand, collector insulation assembly fabrication technology and TFE assembly technology do not permit the collector to be insulated without gaps at the points where the modules of these insulation assemblies are connected. For this reason, some TFEs use special vacuum-tight metallic ceramic parts which prevent the cesium vapor from contacting the collector insulation.

Another method for eliminating the danger of electrical breakdown of the collector insulation while the output voltage is increasing is the use of a five-layer collector insulator assembly (Fig. 10.2). An intermediate metallic sheath is connected electrically to the collector output in such TFEs. This protects the external layer of the collector insulation from contacting the cesium vapor. A relatively low potential difference establishes itself between this sheath and the converter collector. It is developed in each TFE and does not present any danger of arcing. The intermediate sheath can be used as a current conductor. Such a TFE design allows one to increase the overall converter output voltage.

The small interelectrode gap and several other factors, which increase the danger of short circuiting the electrodes, require that special design steps be taken to preserve the gap. One such step is the use of spacers. These are devices that set the interelectrode gap. When the gaps are relatively large (0.4-0.5 mm), spacers are used that fix the position of the emitters at the ends. Such a design minimizes disturbance of the emitter temperature field because the region of thermal contact between the emitter and the spacer is remote from the operating surface of the emitter. With small interelectrode gaps, spacers built into the interelectrode gap will provide a more accurate mutual positioning of the electrodes. The configuration and location of the built-in spacers are chosen so as to exert the smallest possible influence on the emitter temperature field. Usually, the spacers used are washers, sprockets, spheres or short rods made of electrical insulation materials.

The high emitter component temperature has a negative effect on the ability of the fuel clad material to withstand plastic deformation due to the fission gas pressure. This naturally increases the danger of electrode short circuiting. Cathodes with thick clad and small diameters are more stable under the influence of gaseous fission products. In addition, a high emitter temperature can lead to mass transfer of the emitter material to the collector and to the electrical insulation of the collector packet and the spacer
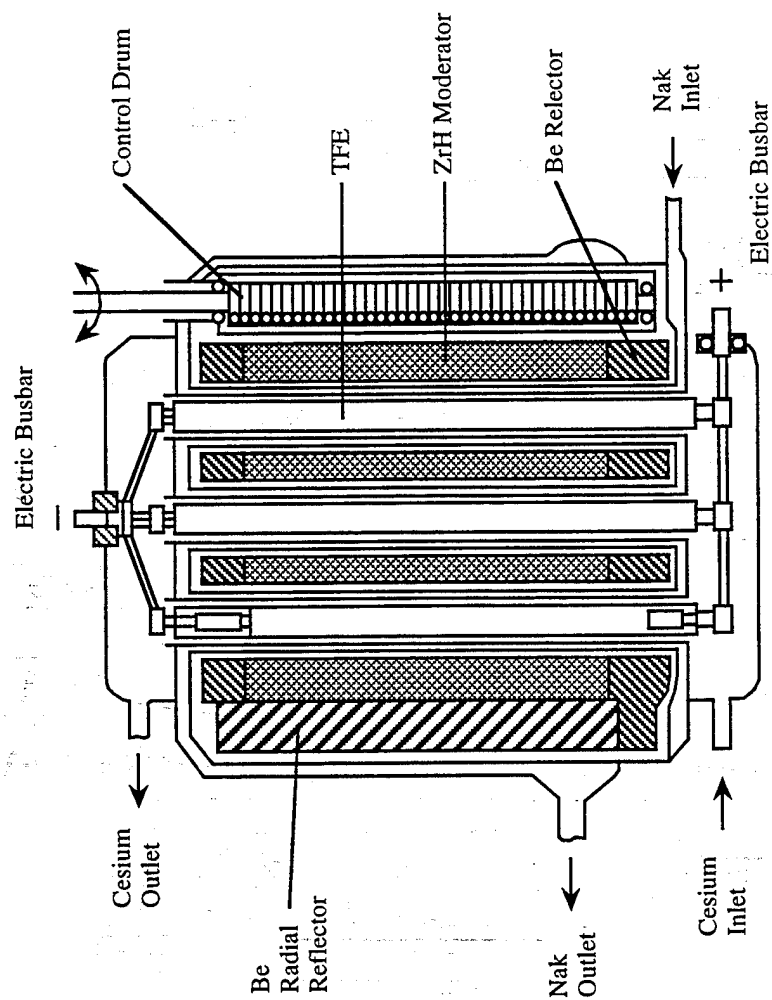
Fig. 10.2 Cutaway drawing of the topaz reactor.

Control Drum

TFE

ZrH Moderator

Be Relector

Nak
Inlet

Electric Busbar

Electric Busbar

Cesium
Outlet

Be
Radial
Reflector

Nak
Outlet

Cesium
Inlet

components. This phenomenon is the reason for changes in the emission properties of the collector and also for the reduction in the electrical resistance of the insulators. This, in turn, leads to a deterioration in the TFE characteristics. We know that the intensity of mass transfer will increase when water and oxygen appear in the gap as a result of the diffusion of oxygen from the fuel oxide and from outgassing of structural materials. Mass transfer, caused by the oxygen-hydrogen cycle, is reduced significantly by adding materials in the gap that bond with oxygen, i.e., gas absorbers (getters). Thus, when collector materials are used that contain Zr (for example, Nb-1%Zr), the mass transfer rate is reduced substantially. In order to reduce the danger of metallizing the surfaces of electrical insulation, they are placed in elevated temperature areas and shielded from emitter material deposition.

Among the negative factors, which are caused by the placement of thermionic converters in the reactor core, one should consider first the deformation of the emitter cladding due to the pressure effect of gaseous and solid fission fragments. The deformation of the shell depends on its temperature, degree of fuel burnup and the mechanical characteristics of the emitter and the fuel. Among the steps taken to lessen the effect of gas swelling of the emitter, of greatest interest is ventilation of its internal cavity, i.e. the forced removal of gaseous fission fragments. In developing a gas removal system, one should consider the possibility that the gas exhaust system could plug as a result of fuel mass transfer. We will discuss some specific gas removal designs later.

The nonuniform heat liberation in the core means that the average temperature of the emitters, and thus the average emission current density, decreases from the central TFEs to the ones at the periphery. In order that the operating point of TFEs on the core periphery does not shift to the volt-ampere characteristic region with low values of specific power and efficiency, the length of these TFEs is increased in comparison with the central ones. Thus, in designing a TFE for a core without nuclear profiling, in addition to selecting the optimum number of TFEs, one must find their optimum length.

The prolonged stay of structural and insulation materials in the core causes them to suffer radiation damage. The volume, mechanical and electrical characteristics of the materials will change. The degree of susceptibility of these materials to radiation damage depends on their composition and fabrication technology.

Electrode materials, in addition to the previously mentioned properties of fuel element clads, should have a high electrical conductivity and the lowest possible emissivity. In addition, emitter materials should have a low evaporation rate, not exceeding 3×10^{-12} m/sec. Emitters are fabricated from molybdenum, tungsten, rhenium and their alloys; collectors are fabricated from molybdenum, nickel, niobium, and electrical insulation components are fabricated from Al_2O_3, Y_2O_3, or BeO.

In conclusion, we note that in connection with the complex fabrication technology and experimental design work involved in the development of the TFE, we find it advisable to use a single universal type of TFE in nuclear power plants for different electric power outputs.

We will now proceed to a more detailed discussion of the design of the reactor-converter. For this purpose, we will use the actual development of a nuclear power plant with thermionic converters by the firm, NPO "Red Star," which was carried out under the Topaz-I program. The first reactor power plant Topaz was constructed as a

heterogeneous thermal reactor with a zirconium hydride moderator. The use of a hydride moderator made a highly compact reactor-converter design possible.

The design of the Topaz type reactor-converter is shown in Fig. 10.2. The reactor-converter core with the dimensions 280 x 360 mm contains a bank of zirconium hydride moderator disks that have holes to accommodate 79 TFEs and channels for coolant flow. The core support grid maintains the radial arrangement of the TFE banks. The moderator fraction in the transverse cross section of the core increases from the center to the periphery. This is done in order to equalize the heat liberation along the core radius. Geometric profiling is also used for this purpose, i.e., the spacing between the TFEs from the periphery to the center is decreased. The core with end reflectors is contained in the reactor-converter vessel which separate it from the side reflectors where 12 rotating control units are located. The cavities of the control units and their drive mechanisms are hermetically sealed and pressurized with an inert gas. The control units are divided into four groups with three control units in each group. The control units are kinematically connected in the groups by control mechanisms which are located at one end of the reactor-converter. Each group is controlled by its own drive mechanism. Two control unit groups fulfill the function of reactor power control, and two groups provide for reactivity compensation. The free cavities of the core are filled with an inert gas medium. In order to diminish hydrogen leakage from the hydride moderator, the maximum coolant temperature in the core is limited to ~600 °C. For the same reason, the moderator surface is coated with a special hydrogen containment coating.

The first Topaz nuclear power plant models used the TFE shown in Fig. 7.9. This is a five-element TFE with an internally connected rod design. The fissioning material (nuclear fuel) used was uranium dioxide with 95% enriched uranium-235 which was confined inside emitter shells (sealed tubes) fabricated from molybdenum alloy. The outer surface of these tubes, which were heated from the inside by the fission reaction, served as the emitter. The collector was formed by the surrounding inner surface of a niobium alloy tube. The thermal characteristics (coefficient of thermal expansion) of this alloy were compatible with the same characteristics of the beryllium oxide collector insulation material. The electric generating elements (TFEs) were insulated individually from the external stainless steel jacket of the TFE. Niobium connectors provided electrical connections between the emitters and collectors of adjoining TFEs within the confines of a single multi-cell TFE. The interelectrode gap between emitters and collectors was maintained in the 0.4-0.5 mm range. The gap spacing (maintenance of the indicated gap space) was provided by special insulators. The interelectrode gap was filled with cesium vapor during operating conditions. The length of individual elements in the TFE assembly differed in length and increased from the center of the core to the ends of the TFE. This design measure promoted equalization of heat liberation along the TFE during operating conditions and compensated for axial nonuniformity of heat liberation in the TFE as a whole. All TFEs entering into a given reactor-converter are connected electrically in series-parallel circuits in order to obtain the prescribed electrical output characteristics.

The five-layer collector insulator assembly (containing two insulation layers) is an improved version compared with the three-layer collector packet (collector-insulator-shell). It provides a much higher (by several factors) reactor-converter output voltage, which can reach ~120V. Depending on the required electrical power output of the

reactor-converter, the optimum number of individual cells that make up the TFE can change. Thus, as the power increases from several tens of kW to 100 kW, the optimum number of thermionic cells that make up a TFE falls in the range of seven to eleven.

As we noted earlier, the majority of the thermionic converter designs operate in the so-called plasma mode, i.e., the mode in which the interelectrode gaps are filled with alkali metal vapor that fulfill the appropriate functions in increasing the reactor-converter output characteristics. For this reason, the design of the system for supplying alkali metals to the interelectrode gaps is of significant interest. Cesium vapor is fed to the interelectrode gaps in the Topaz-type reactor-converter, and we will now discuss this in greater detail.

10.3. The Cesium Supply System in the Topaz-Type Reactor.

The first Topaz-I reactor-converter models used a pumped flow (circulating flow) cesium supply system (CSS) to the interelectrode gap. A liquid cesium thermostat, heated by an electric heater, was used in this system. The system was equipped with an outlet throttle device which was designed to remove gaseous fission products and a portion of the cesium vapor into special traps. The CSS also used three electromagnetically driven valves (Fig. 10.3). The vacuum system valve is used in removing condensed inert gas (i.e., the gas used in preserving the reactor-converter during storage of the nuclear power plant and during the orbit insertion period). The valve serves this same purpose while the reactor-converter is brought up to thermal power. A shut-off valve closes the vacuum channel prior to opening the actuating valve of the cesium vapor generator. After opening the cesium vapor generator, the cesium vapor is fed into the input electrical terminal chamber of the reactor-converter. Then it flows into the interelectrode gaps of all TFEs, enters the output electrical terminal chamber and passes through a throttle. The flow-through capability of this throttle determines the cesium vapor flow rate in the system under consideration. Next, the vapor enters a trap where the cesium is absorbed by a graphite layer and gaseous impurities are discharged into space. The prescribed cesium vapor pressure is assured by maintaining the "cold" region temperature of the CSS using an electric heater and a thermocouple.

Next, we will discuss the design features of the cesium supply system. Its basic component is the cesium vapor generator. Its design is shown in Fig. 10.4. The cylindrical container has a metal mesh capillary structure on the inside surface of the container. The entire cesium reserve (2.5 kg) is concentrated in this capillary structure under zero-g conditions. A heater with two sections is located in the central cavity. It supplies the necessary heat to the liquid cesium at any thermionic converter operating condition. One of the heater sections produces 50 W and operates continuously, the other section produces 130 W and is controlled by a two-position temperature regulator with inputs from two thermocouples. These thermocouples are located in the connecting pipes, which are found in openings in the CSS thermal insulation. The insulation has a coating with an emissivity no less than 0.85. Such measures assures the existence of a "cold" zone in the CSS. Disks with mesh packets increase the equivalent thermal conductivity between the electric heater and the capillary structure, thus improving the control characteristics of the CSS. The cesium vapor collector (sump) consists of two concentric shields with openings. A deflector is welded to the outer shield. The deflector prevents direct entry of
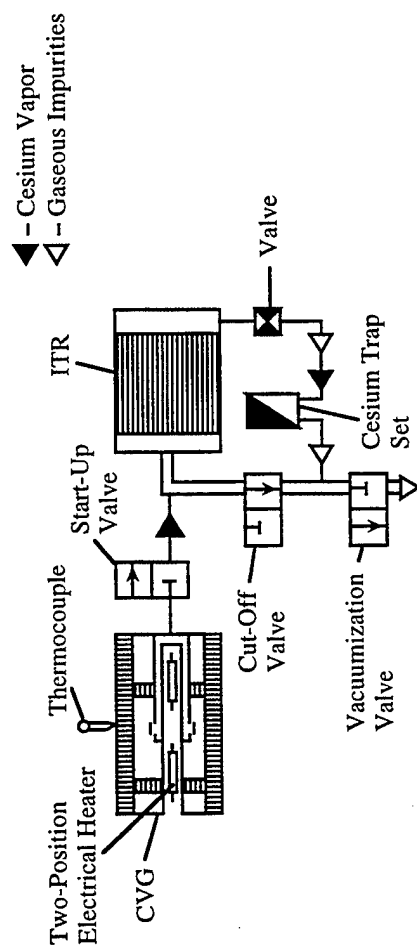
Fig. 10.3 Cesium supply system schematic.

▼ – Cesium Vapor
▽ – Gaseous Impurities

Valve

ITR

Start-Up
Valve

Thermocouple

Two-Position
Electrical Heater

CVG

Cut-Off
Valve

Vacuumization
Valve

Cesium Trap
Set

281

Valve

Heater

Startup Heater

Thermocouple Sockets

Thermal Insulation

Electrical Heater

Capillary Structure
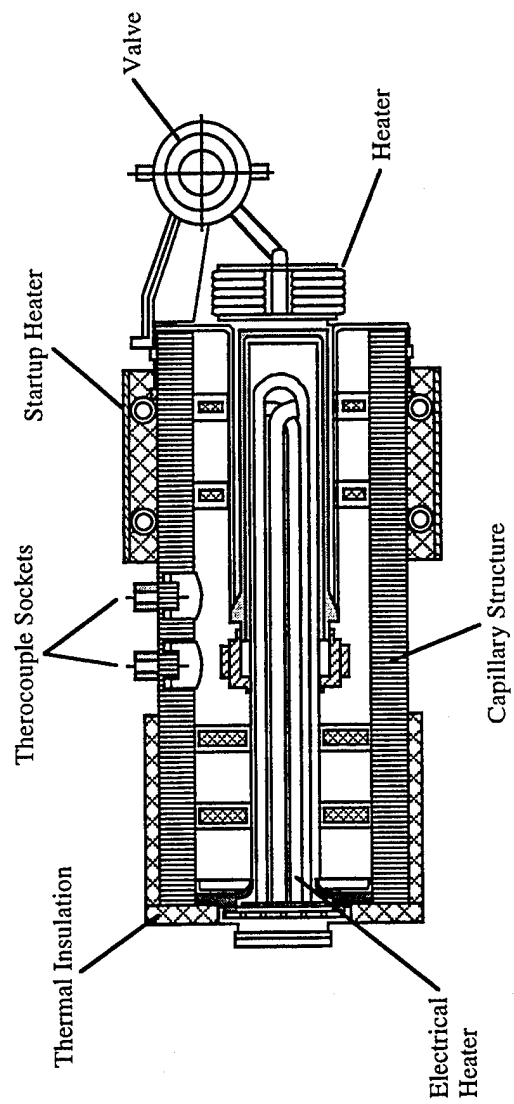
Fig. 10.4 Cesium vapor generator design.

the cesium liquid phase into the annular vapor collector. There is a vacuum gap between the vapor collector and the container. This ensures that the vapor collector is hotter than the "cold" zone, thus preventing the possibility of condensation in the vapor collector. The CSS has two additional heaters. The electric heater has a power of about 1 kW which is supplied from a ground source during prelaunch preparations. It preheats the CSS to ~600 K for a period of about 1 hour. Subsequent heating of the CSS to a prescribed temperature prior to its opening is accomplished by an electric heater during spacecraft insertion in the operating orbit. An electric heater preheats the CSS vapor collector, the startup valve and the interconnecting piping. Its power (60 W) assures that liquid cesium is removed from the vapor collector channel before the startup valve opens in the event of a hypothetical (highly unlikely) situation in which this channel is completely flooded. In order to preheat the cesium vapor supply system channel, including the valves, a startup (ground-based) electric heater of about 1 kW is used. It preheats these components to about 600 K during prelaunch preparations. The on-board electric heater of about 150 W maintains the channel temperatures at no less than 630 K prior to supplying cesium vapor into the TFE. This heater as well as heater are turned off during subsequent stages in the reactor-converter startup mode. The combination of these design measures assures that liquid cesium does not enter the cesium vapor channels during opening of the CSS and also prevents vapor condensation in the channels during the supply of vapor to the reactor-converter.

The development of a reliable system for supplying cesium vapor to a nuclear power plant with thermionic converters determines to a significant degree the stability of the output characteristics of the reactor-converter in all operating modes. For this reason, the experimental development of this system is one of the basic stages in the development of the nuclear power plant under consideration as a whole.

10.4. Cesium Vapor Supply Systems for Long Life Nuclear Power Plants with Thermionic Converters.

Thermionic nuclear power plants with long operating lives need repetitive use of cesium where the vapor flow rate in the system is not related to the cesium reserves in the CSS but is determined only by unavoidable cesium leakage. A characteristic feature of such systems is a substantial increase in the effectiveness in removing gaseous impurities from the interelectrode gaps of the TFEs due to an increase in the pumping of vapor through the system. TFEs with unseparated and separated cavities for interelectrode gaps and fuel cores can be used in reactor-converters. Fig. 10.5 shows designs of cesium supply systems with unseparated cavities. They include:

a. Unidirectional diffusion of gaseous impurities from the interelectrode gaps into the cesium chamber (a cesium channel with one end closed);

b. Bidirectional diffusion of vapor impurities from the interelectrode gaps into cesium chambers (cavities), which are located at both ends of the reactor-converter (a TFE with a continuous channel);
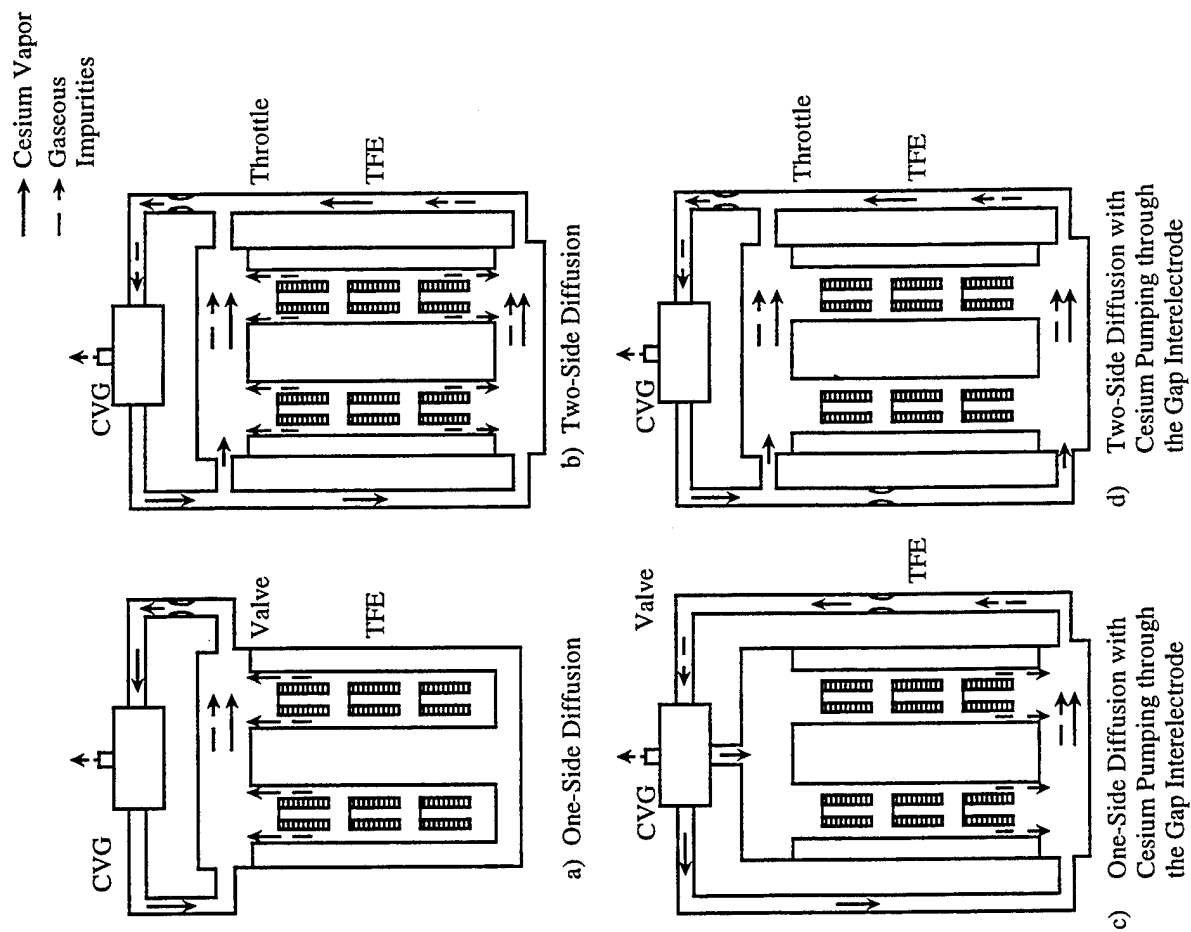
Fig. 10.5 Schemes of cesium vapor supply system for TPE with non-separated cavities of the gap interelectrode and fuel pins.

a) One-Side Diffusion

b) Two-Side Diffusion

c) One-Side Diffusion with Cesium Pumping through the Gap Interelectrode

d) Two-Side Diffusion with Cesium Pumping through the Gap Interelectrode

Cesium Vapor

Gaseous Impurities

CVG

Valve

Throttle

TFE

c and d. A combination of unidirectional and bidirectional designs with cesium vapor flow through the interelectrode gaps.

Fig. 10.6 shows cesium vapor supply system designs for a TFE with separate cavities. In this case, the removal of vapor from the interelectrode gaps can be arranged similar to the preceding. The outlets for the fuel core gas removal channels can be either in the cesium chambers or in the elevated pressure region after throttling. It is in principle possible to pump cesium successively through the interelectrode gap and the fuel core gas removal channel. Fuel core channel outlets in the elevated pressure region are possible in TFEs with three-layer collector insulation assemblies. In TFEs with five-layer collector packets, the joining of the interelectrode gap and fuel core channels is possible in the current lead region of the TFE.

A regenerative vapor generator is used in cesium supply systems. It ensures repetitive use of cesium. The cesium vapor pressure level is determined by the temperature in the vaporization zone of the generator. The cesium vapor condenses in the condensation zone and returns to the vaporization zone by way of the capillary structure. The portion of the vapor that does not condense is discharged into space. The temperature of the condensation zone should be in the 150-200 °C range in order to minimize the loss of cesium through the gas removal channel, and also to minimize the possibility of forming solid compounds of cesium with impurities that could cause clogging in the capillary structure of the cesium vapor generator. This provides the possibility of operating the system at any selected flow rate, which is determined by the flow capacity of the throttle valve at the outlet from the reactor-converter. It is in principle possible to use several independent cesium supply systems, each of which serves its own group of TFEs.

10.5. Mass and Size Characteristics of Nuclear Power Plants with Thermionic Converters in the Topaz-I and Topaz-II Programs.

The physical dimensions of the nuclear power plant are basically determined by the area of the space radiator and its placement. The long term operation of a zirconium hydride moderator in a thermal neutron reactor-converter requires that the maximum coolant temperature be limited to 600 °C. When a 10% excess space radiator area allowance is made at the outlet from the coolant piping system (or heat pipe system) to allow for the possibility of meteorite punctures, nuclear power plant electric power outputs of 30, 50 and 75 kW will require space radiator surface areas of approximately 26, 42 and 56 m^2, respectively. The assumptions made in calculating these data were a nuclear power plant life of 5 years, shielding of the coolant plena against meteorite penetration, as well as optimum relationships for the lengths of the heat input and heat output regions of the heat pipes and of other heat pipe design features. With a spacecraft instrument compartment diameter of up to about 4 m, the launch dimensions of the nuclear power plant would be about 6-7 x 2 m, which are entirely within the capabilities of modern launch vehicles.

The mass characteristics of the nuclear power plant depends to a significant degree on the allowable γ radiation dose and neutron fluence ϕ_n^* in the plane behind the radiation
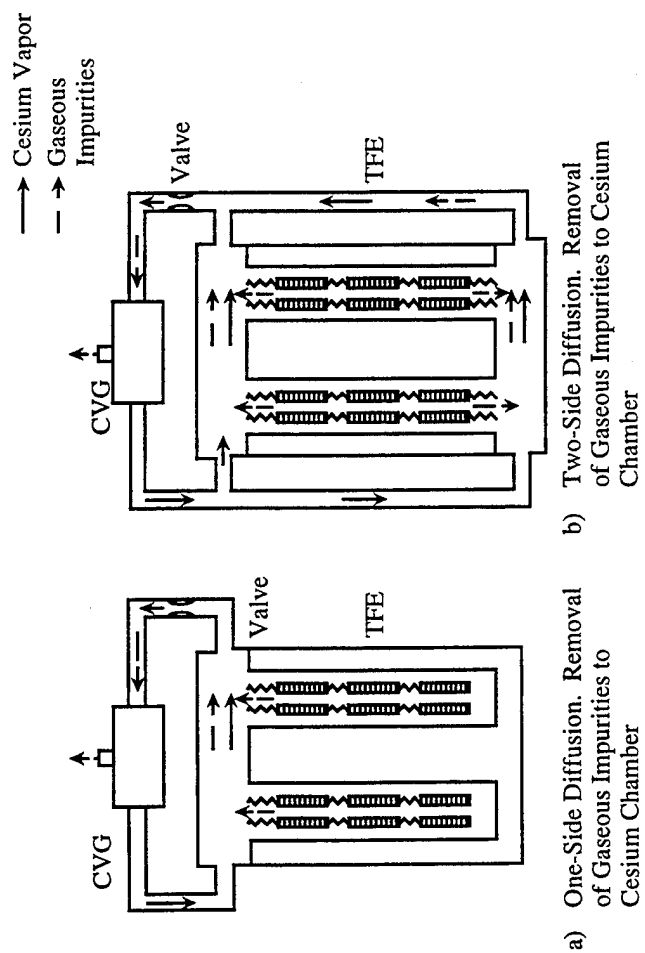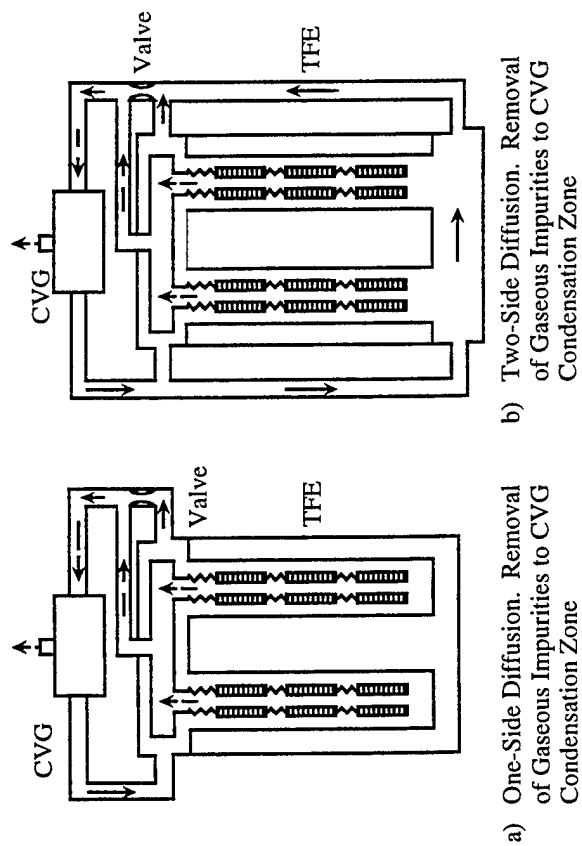
Fig. 10.6 Schemes of cesium vapor supply system for TPE with separate cavities for the interelectrode gap.

286

shield. With changes in γ radiation and ϕ_n^* in the range 10^4 - 10^6 rad and 10^4 - 10^{13} neutrons/cm² and with coolant activation accounted for even at a γ radiation level of about 10^6 rad, the achievement of a nuclear power plant without separating the instrument compartment at some distance from the shield is not likely. Separation of the nuclear power plant from the instrument compartment at a distance L requires mass optimization of the entire structure for given values of γ radiation and ϕ_n^* taking into account mass and shielding and the equipment that is separated by the distance L. Fig. 10.7 shows the relationship between mass and L for a single-loop and double-loop 30-kW nuclear power plant with a 5-year life and with single and double radiation shields (here it is assumed that the allowable γ radiation and neutron flux levels, which strike the shielded object, are within the 5 x 10^5 rad and $\phi_n^* = 10^{12}$ neutrons/cm² limits). It can be seen that with L less than 13 m, the single-loop nuclear power plant cannot be used because of an increase of up to 100% in the contribution from coolant activation by γ radiation. The optimum value of L is in this case 15-16 m. When the allowable γ radiation flux is decreased to 10^5 rad in the single-loop configuration, L_{opt} increases to 22 m, and at a γ radiation level of about 10^4 rad, L_{opt} is beyond reasonable limits.

The range of application of the double-loop configuration with a single shield at the 5 x 10^5 rad γ radiation level (L = 12-13.5 m) is quite narrow and is reduced still more when the allowable γ radiation dose is decreased. With L > 15 m the mass of the double-loop configurations differs insignificantly from the single-loop versions and the need for separate shields drops off. However, when the allowable γ radiation dose is reduced to less than 10^5 rad, one must go to the double-loop configuration. With changes in ϕ_n from 10^4 to 10^{13} neutrons/cm², the mass of the nuclear power plant changes in the ±100 kg range virtually without any shift in the optimum value of L.

Fig. 10.8 shows the relationship between mass and useful electric power output for an incore thermionic reactor space power plant with thermal (up to 100 kW) or fast (greater than 100 kW) neutrons. The figure also shows the specific mass of the nuclear power plant, and the mass of the control system together with the power conditioning systems and transmission lines.

As we have noted, all the preceding material pertains to multicell TFEs built into the core of the reactor-converter. Nuclear power plants, similar in operation but with single-cell TFEs, were built in the Topaz-II series in St. Petersburg in parallel with the Topaz-I power plant series. Some special consideration of this design are as follows:

a. It is possible to substitute special electric heaters for the nuclear fuel in the TFE in order to develop the TFE without nuclear fuel contained in it. This important advantage of the nuclear power plant under consideration sparked the interest of the American firm International Space Products, which is now testing a nonnuclear Topaz II power plant;

b. The possibility of loading and unloading nuclear fuel in a completed power plant assembly.
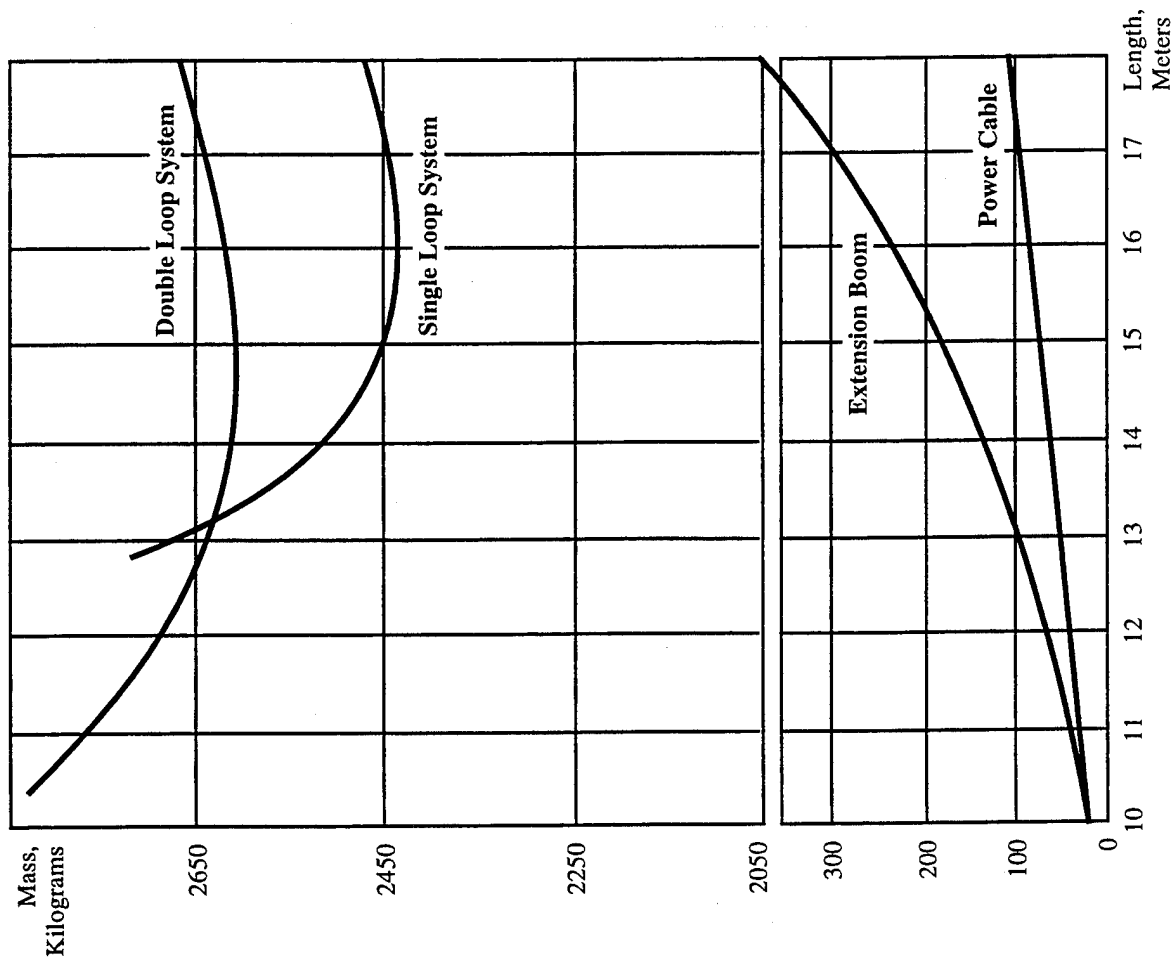
Fig. 10.7 Power system mass and reactor/payload separation distance for different heat transfer loop configurations.

288

Mass, kg

Electrical Power, kW
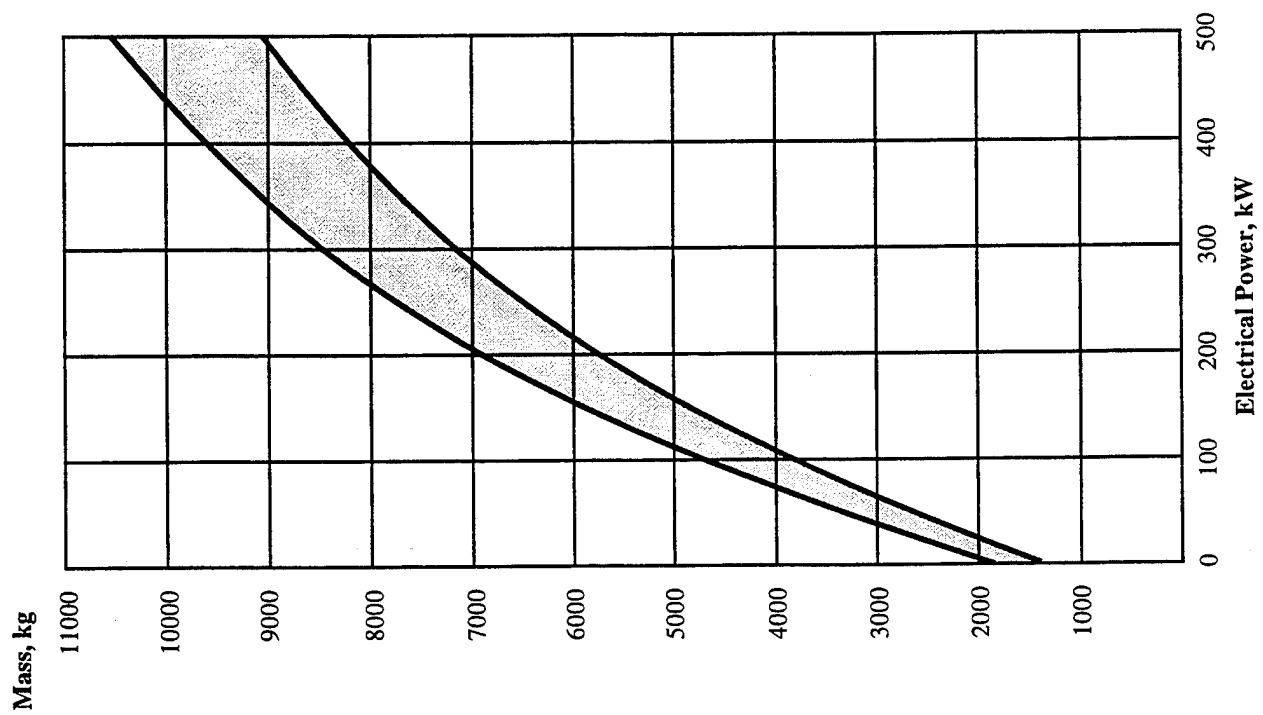
Fig. 10.8 Mass - power relationship for thermionic power plants.

The reactor unit of the Topaz-II nuclear power plant is built using a single-loop design and consists of a reactor-converter, a shadow shield, a heat rejection system, gas and cesium systems, control unit mechanisms for reactor control, control system data units, a structural framework and a cable system. An overall view of the reactor unit is shown in Fig. 10.9.

The power system consists of a consecutive assembly of the reactor, the radiation shield and a frame on which all remaining components of the reactor unit are mounted.

The zirconium hydride reactor has 37 single-cell electric generating channels built into the core and these are divided into two sections: an operating section (34 TFEs) and a pump section. The core is surrounded by a beryllium reflector with rotating control drums. A heat transfer fluid provides the cooling.

The heat rejection system consists of a tube-fin radiator, a dc electromagnetic pump, an expansion tank, oxide traps, and electric heaters for coolant preheating. The shield, which contains steel and lithium hydride, provides at a distance of 6.5 m in a 1.5 m diameter zone a fluence of $E_n > 0.1$ MeV neutrons of 5×10^{12} n/cm² and a γ radiation dose of 5×10^5 R continuously for 3 years. Cesium is fed into the interelectrode gaps of all TFEs from a single generator.

The basic technical data on the nuclear power plant are shown in Table 10.1.

Table 10.1 Topaz II Performance Summary

Electrical Power at the Output Terminals	6 kW
Voltage at the Output Terminals	6 V
Reactor Thermal Power	135 kW
Maximum Coolant Temperature	600 °C
Operating Life	Not Less than 3 Years
Weight of the Reactor System	1000 kg
Length of the Reactor System	3.9 m
Maximum Diameter	1.4 m

The reactor unit underwent experimental development in a program involving static and dynamic testing, thermal testing with electric heaters, and nuclear testing. The components of the reactor unit were subjected to 3-year life tests. Ground tests were run for 1.5 years with highly stable output characteristics. Cessation of testing was never associated with the dissipation of the operating life of the TFEs and other components. Post reactor investigations showed that the prescribed operating life parameters were within limits that would guarantee with certainty an operating life of more than 3 years.

The Topaz-II nuclear power plant can be used as a reliable and continuous power supply for space data systems (communications satellites, earth observation satellites for studying the atmosphere, plant life, resources, transportation monitoring, etc.).

The use of nuclear power plants as electric power sources for electric thrusters will allow spacecraft to be lifted from near earth orbits into geostationary orbits. The electric thruster combination will make long duration interorbital flights to different objects in the solar system possible.

As a high potential source of heat, the Topaz-II nuclear power plant can be effectively combined with machine converters, for example, the Stirling engine. Such a
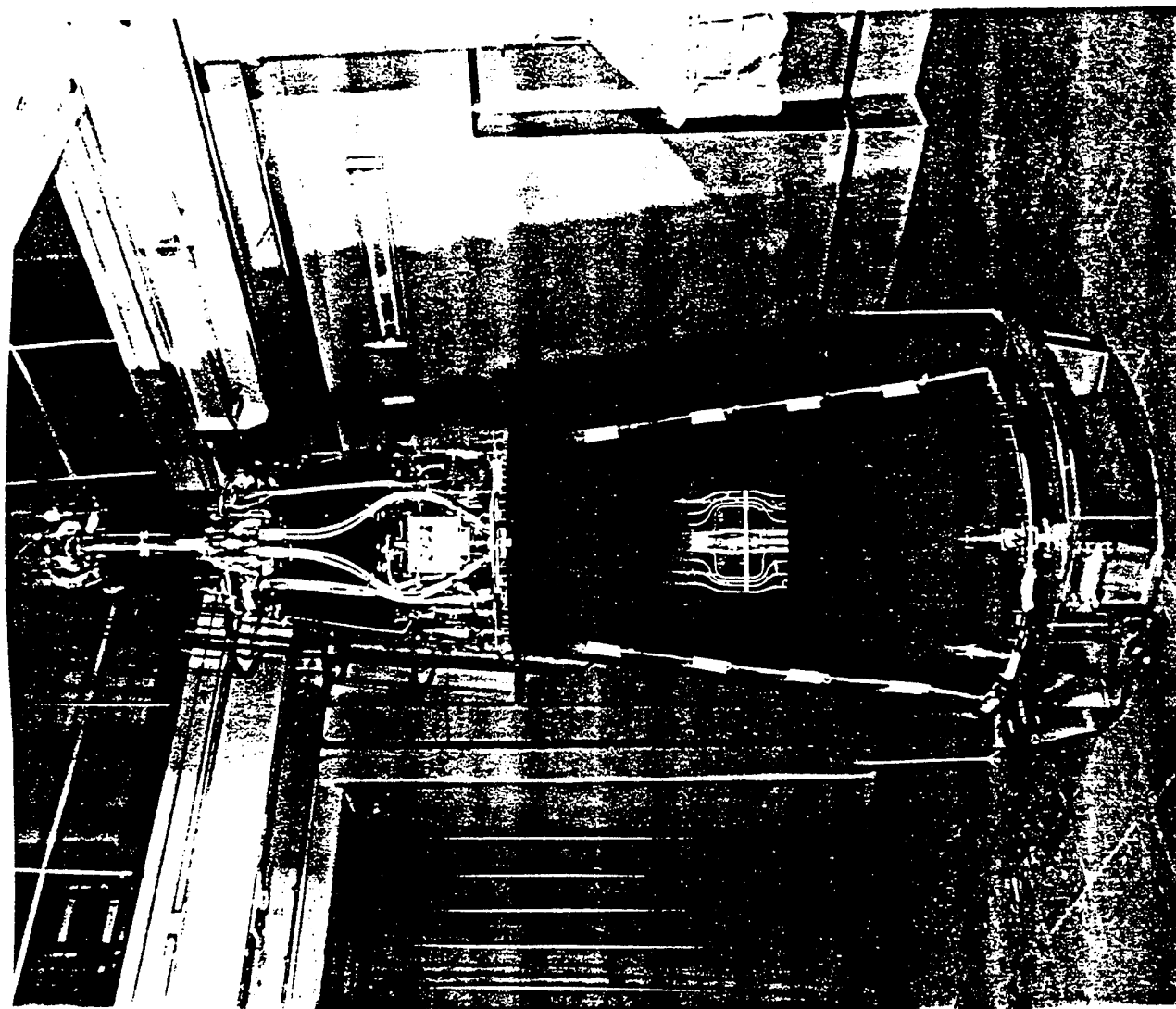
Fig. 10.9 Topaz-II space nuclear power system.

power plant combination with a power output of about 30 kW can serve as an electric power source for Moon and Mars bases, including orbiting bases (see Fig 10.10).

The expansion of nuclear power plant applications in the indicated areas will require large power outputs. The results, which have been achieved through the development of the Topaz-II nuclear power plant, will permit a sound examination of the future prospects for nuclear power plants of this kind.

In the power range of several tens of kW it is advisable to use existing TFEs with some improvements, preserve the fundamental design and construction decisions, and maximize the use of scientific design and engineering experience. An increase in power is achieved by increasing the number of TFEs in the reactor. By creating reactivity reserves it will be possible to constructively improve the TFE for the purpose of increasing its operating life and specific power. With a pessimistic value of 220 W from a TFE it is entirely realistic to obtain 300 W from a TFE with an operating life of 5-7 years, and in the future up to 400 W.

The parameters of a number of envisioned reactors and reactor units are given in the Table 10.2.

Table 10.2 Possible Designs for Future Reactors

	Topaz III/61	Topaz III/85	Topaz III/97
Number of TFEs	61	85	97
Core Dia., mm	315	370	385
Reactor Weight, kg	430	565	600
TFE Electric Power, W	220/300/400	220/300/400	220/300/400
Reactor Electric Power, kW	13.5/18.3/24	18.3/25.5/34	21/29/38
Weight of Reactor, Metric Tonnes	1.3/1.4/1.5	1.6/1.8/2.0	1.8/2.0/2.2

In the interest of objectivity in comparing nuclear power plants in the Topaz-I and Topaz-II series (i.e., power plants with multicell and single-cell TFEs) one must state the following. With electrical power requirements of 40 kW and higher (exactly such power levels are of practical interest for most space systems envisioned for global communications) the single-cell TFE, even with the most optimistic assessment, due to the unavoidable joule losses in the long electrodes, has a 20-30% lower thermionic converter efficiency in comparison with the multicell TFE. This, in turn, leads to an increase in the weight of the reactor unit by a factor of 1.5-2, and in external dimensions of the reactor unit by up to 25%.

Naturally, the weight of the radiation shielding against ionizing reactor radiation will increase by 20-30 %.

In addition, at comparatively low electric power outputs (5-10 kW) the indicated disadvantages of single-cell TFEs in the reactor unit are substantially reduced and here it will be necessary to consider other kinds of factors (economics, operating life, engineering, etc.).
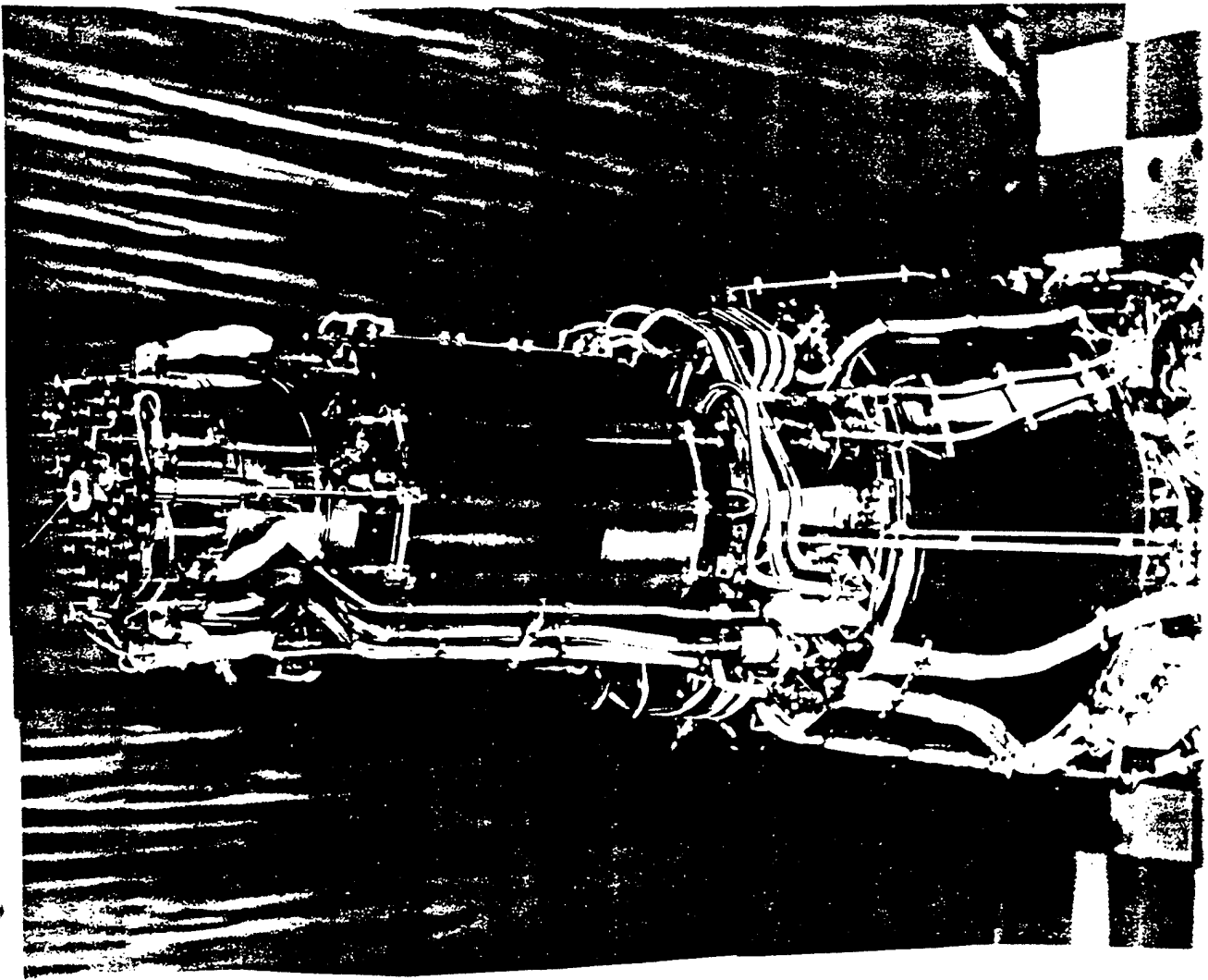
Fig. 10.10 Topaz-II reactor and shield.

10.6. Basic Results and Prospects for the Development of Thermionic Power Plants.

In the area of thermionic nuclear power Russia has always led other countries beginning with the development of the world's first reactor-converter Topaz and ending with the two tests of a nuclear power plant with thermionic converters, "Topaz-I," in space during 1987-88 on the "Cosmos" spacecraft systems (Fig 10-11). As a result of these flight design tests, all scientific and engineering aspects of the principles of designing a new series of space nuclear power plants were successfully verified.

The principal achievement in the resolution of problems in the design of nuclear power plants with thermionic conversion is the development of the concept of functional reactor-converter and nuclear power plant designs that incorporate the requirements we discussed earlier.

The first Topaz reactor with a power output of 5-7 kW was tested in 1970. It opened the path to space thermionic nuclear power plants and a new generation of nuclear power plants which are currently under development. It is appropriate here to note some problem solutions in this task.

1. The development from general laboratory investigations of thermionic converter specimens mathematical models of converters and supplementing them by reactor models. For these same purposes, special electronic models were developed and built which allowed the analysis of all possible designs for connecting individual cells and TFEs in order to optimize their parameters, to investigate the influence of nonuniform heat liberation in the reactor, breaks and short circuits in the TFE, the influence of current loads on the output characteristics (electric output power and efficiency) of the reactor-converter, and also to obtain a complete picture of the TFE emitter temperature regime in the reactor.

2. A specific problem, which directly influenced the design of the reactor, was the problem of electrical breakdown in cesium vapor. It imposed a strict limitation on the positioning of the TFE in the core and determined the minimum allowable grid spacing in the reactor. Analysis and selection of the optimum electrical connections of TFEs in the reactor, the maximum allowable voltage in the reactor-converter, the configuration and geometry of sealed conduits, electrical insulators, electrical connectors and current leads in the TFE were all determined by taking into account the arc ignition voltage as a function of the spacing between electrodes and the cesium vapor pressure. Since this relationship was unknown, it was determined and investigated for different temperatures and electrode materials and different concentrations of gas impurities during operation of the reactor-converter (xenon, krypton, hydrogen). Final investigations for the purpose of determining the boundary of safe operation from the standpoint of electrical breakdown were conducted on a specially developed reactor-converter mockup at operating temperatures, currents and voltages in the TFE, which were produced using appropriate electrical simulators.

3. The above mentioned investigations and their results were invaluable and allowed a transition to full-scale testing of the Topaz reactor. In order to avoid electrical
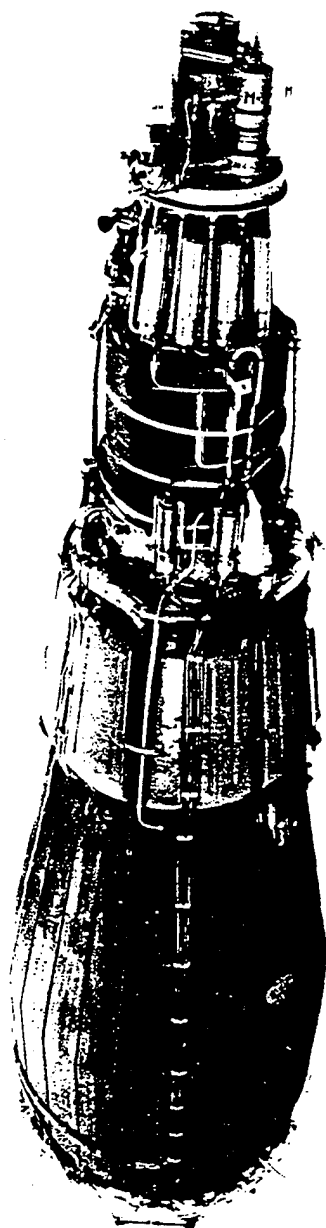
Fig. 10.11 Topaz-I reactor, flight tested in 1987-1988. World's first operational thermionic nuclear power plant.

breakdown in the transient modes (i.e., during powering up of the reactor-converter and loading it with cesium vapor when breakdown conditions are always present), the reactor operated at short circuit power. In this manner, the problem of electrical breakdown in the interelectrode gap was avoided in the nuclear power plant startup modes.

4. The important problem of shielding against ionizing reactor radiation was completely solved. It was observed that in the case of an allowable γ radiation level in the plane of the shielded object of 5×10^5 rad, as a rule, a two-loop heat removal system was advisable. Two radiation shields were used and the heat exchanger, pump and expansion tank of the primary loop were placed between them. This design measure minimized the contribution to the total dose of γ radiation activation of the coolant, which in the single loop design became intolerably high, especially during long term operation. The distance from the center of the core in the reactor-converter to the plane where the shielded object was located was chosen based on optimizing the mass of the nuclear power plant taking into account the contribution to the total dose of γ radiation activation of the coolant. The shadow angle of the truncated cone radiation shield was in the 14-18° range. The latter determined the possible diameters of the instrument compartments used on the rocket vehicles under consideration.

5. The problem of providing nuclear and radiation safety of the nuclear power plant and the thermionic converters was completely resolved during all stages of their life cycle. This important problem is discussed in the final section in this book.

6. An automatic power plant control system (ACS) was developed simultaneously with the development of the reactor-converter and nuclear power plant with thermionic converters. The ACS accomplishes reactor-converter thermal power control and regulates the cesium vapor pressure in the supply system during startup and in the nominal operating modes in accordance with optimized control algorithms. In the nominal operating mode the ACS maintains a given reactor-converter current and limits the maximum coolant temperature. The ACS includes a regulator of excess power and a pump power supply unit. The excess power regulator maintains the voltage at the output terminals at ~115 V with a given accuracy by means of redistributing the given reactor-converter current between the consumer loads on the spacecraft and a dummy load. The most promising startup power source is the sodium sulfur storage battery with a specific mass of about 10 kg/kW·hr, an energy capacity of up to 20 kW·hrs and a mass of about 200 kg.

In concluding, let's discuss some promising output characteristics of a nuclear power plant with thermionic converters which were obtained in long duration tests during the development of similar systems at NPO "Red Star." The calculations assumed that with an operating life of 5-7 years the average specific power of a reactor-converter can be 2-3 W/cm² with the emitter temperature limited to about 1600 °C. The thermionic converter efficiency at the beginning of the operating life is 10-11%, and at the end of the operating life it reduces to 8-8.5% due to degradation processes. The voltage at the output terminals of the reactor is limited to about 115 V.

Together with the long duration operating mode of the nuclear power plant, a high power mode is possible at a specific power level of 5-6 W/cm² for approximately one year.

The table below presents basic power, thermal engineering and weight characteristics of nuclear power plants with thermionic converters of different sizes.

Table 10.3 Projected Future Design Capabilities

Electric Power Output, kW	25-30	50-65	125
Life, years	5-7	5-7	5-7
Weight Characteristics			
Reactor Assembly, kg	620	905	1230
Heat Removal System, kg	535	1075	1225
Electrical Connections, kg	100	120	130
Total Nuclear Power Plant, kg	1950	3130	4055
Nuclear Power Plant Length, m	6.5	6.5	6.5
Nuclear Power Plant Diameter, m	3.0	4.0	4.0
Maximum Coolant Temp, K	873	873	1023
Neutron Spectrum	Intermediate	Intermediate	Fast

For power outputs greater than 100 kW it is advisable to use fast reactors and lithium as the coolant.

From all the material presented above one can draw the general conclusion that the majority of tasks to be resolved by future space systems can from an energy standpoint be accomplished through the use of thermionic nuclear power plants of the Topaz type. Such nuclear power plants can be developed during the course of several years without any additional expenditure of capital equipment. Their orbit insertion is entirely possible using existing launch vehicles.

In future applications of nuclear power plants in the Topaz-I series, one can add, for example, the use of the Topaz-I power plant as a lunar base power supply.

11. FUNDAMENTALS OF TESTING AND OPERATION OF SPACE NUCLEAR POWER PLANTS

11.1. General Information on Preparations for the Practical Operation of Space Nuclear Power Plants.

A significant number of papers have been published to date which are devoted to problems in theory, engineering calculation methods and the design of different kinds of nuclear power plants, including those for space applications. However, this extensive list of publications contain virtually no studies that pertain to testing and preparations for the use of nuclear power plants in space. This is not a mere coincidence. Historically, while numerous projects involving such nuclear power plants have been embarked upon, fewer projects have resulted in acquiring experience in space.

In addition, there is experience in the operation of nuclear power plants for other purposes, for example, marine, ground-based stationary and transportation. In general, these provide insight to techniques and technological processes in the testing and preparation of nuclear power plants for space use. Despite substantial differences in design, application conditions, duration of operation, methods for eliminating radioactive byproducts etc., there are some commonalities in all stages of prototype development work, including general requirements for complete nuclear and radiation safety to service personnel and in practical applications, to the earth's population.

Nuclear power plants for any application involve a number of unique and complex technical issues. Nuclear power plants for transportation uses pass through prototype development stages under stationary conditions and then under conditions close to actual. With reference to space nuclear power plants, this is the ground test and prototype development stage, and then the flight prototype test stage. After successful accomplishment of these stages and verification of all design parameters under space conditions, including the provision for nuclear and radiation safety, the nuclear power plant enters the operational phase, i.e., IOC. The operational phase of space nuclear power plants involves a whole host of activities including the transportation of the completed nuclear power plant from the fabrication and assembly plant, storage at the launch site, and a variety of inspection and measurement activities prior to launching the spacecraft with the nuclear power plant. The operational phase of space nuclear power plants also includes the whole range of precautions taken to provide nuclear and radiation safety during the entire life cycle of the nuclear power plant, including proper functioning of the spacecraft and the possibility of accidents.

In this section we will mainly discuss ground prototype and flight prototype testing of nuclear power plants. Our principal focus will be on a discussion of these issues as they pertain to the Topaz-I and Topaz-II nuclear thermionic power plant program. Substantial attention will also be paid to problems of nuclear and radiation safety. The broad practical use of any space nuclear power plant depends on their solution.

11.2. Ground Test and Prototype Development Work.

298

Nuclear power plants are extremely complex technical systems. Their practical development and operational use take years (up to 5-7 years) of work beginning with preliminary design and ending in multipurpose and multifaceted prototype testing. The latter is, in turn, divided into ground test (in test stands) and flight prototype test phases. Each of these two kinds of test phases has its advantages and disadvantages and specific objectives. Of course, the final decision to transition the nuclear power plant from prototype to operational use (IOC) can be made only after prototype development testing has confirmed all design data.

In this section we will examine prototype development using the thermionic Topaz series as the example.

11.2.1. Tasks, Contents and Results of Prototype Development.

Ground development work on nuclear reactor power plants in the Topaz program included the following basic stages:

a. Separate development of components, assemblies, and nuclear power plant systems with thermal, hydraulic, electrical, mechanical and other kinds of testing;

b. Testing of different kinds of full-scale nuclear power plant mockups without nuclear fuel in order to resolve problems in thermophysics, strength and reliability, and in engineering preparations for launch of the spacecraft assembly;

c. Nuclear power plant power tests in test stands together with automatic control systems and simulated on-board control systems. This stage also included nuclear power tests of individual reactor converters and several types of reactor converter channel assemblies. Ground development work showed that positive results from separate tests and tests on mockups of power plants without nuclear fuel did not provide assurance that an actual (full-scale) nuclear power plant would operate properly because the following remained unknown;

d. Operating life changes in the parameters;

e. The behavior of processes during control of the nuclear power plant by the automatic control system (ACS);

f. Agreement of nuclear power plant output electrical parameters with electric generating channel assembly test results obtained in a high power stationary reactor (the so called "loop" tests);

g. Operating capability of full-scale nuclear power plant components and subassemblies, especially the cesium system;

h. The probability of determining the state of a nuclear power plant from a given number of telemetered parameters.

These problems can be resolved either in ground testing and in costly nuclear power plant power tests or directly during flight prototype testing.

In the Topaz program, the first alternative was recognized as optimum for the following reasons:

1) The telemetry system provides less data volume and accuracy than test stand control and measurement facilities;

2) Elimination of local defects in the nuclear power plant and continuation of testing are possible only under ground conditions, including duplicate test stands;

3) Determination of the true reasons for failures during flight prototype testing is virtually impossible in most cases. Under test stand conditions, such reasons are found by dismantling the nuclear power plant in a "hot" cell. This provides safety in the work that needs to be done;

4) Special research spacecraft would be needed in order to perform maintenance on the nuclear power plant during flight prototype testing. This would add a substantial cost to the program.

Significant resources are also required by test stand power tests because a unique test stand is needed to carry them out.

The great technical complexity of the test stand is due to the following:

a. The requirement for reliable nuclear and radiation safety and regard for the great fire hazard and toxicity of the working fluids used;

b. The requirement for a highly reliable test system in order to minimize the risk of having to terminate testing of costly nuclear power plants due to faults in this system;

c. Lack of direct control of the internal parameters of the nuclear power plant, which requires the development of unique facilities and measurement techniques;

d. Very long test durations;

e. The need to duplicate space conditions as closely as possible.

Such a test stand was developed at the Physical Energetics Institute (Obninsk). A schematic of this test stand is shown in Fig. 11.1. The stand permits work on the nuclear power plant in the autonomous operating mode and together with test stand equipment. The stand is equipped with a vacuum pumping system, a liquid metal loop, special control and measurement systems, etc. The stand has a vertical vacuum chamber (VC) with a hood under which the nuclear power plant to be tested is mounted. All the connections to the nuclear power plant pass through the hood. The VC is enclosed in a concrete shield.
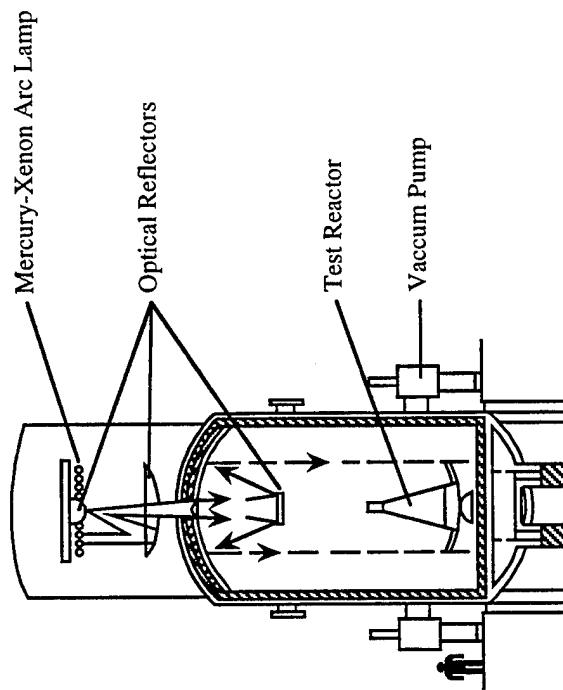
Fig. 11.1 Schematic of the topaz reactor test stand developed at the Physical Energetics Institute, Obninsk, Russia.

Mercury-Xenon Arc Lamp

Optical Reflectors

Test Reactor

Vaccum Pump

In addition, this is used as the compartment for post reactor tests ("hot" chamber) and for the burial of waste following dismantling of the nuclear power plant in the "hot" chamber.

In all, seven power tests were conducted on the stand. All nuclear power plants tested were equipped with additional data recorders and test stand connections to several nuclear power plant systems, such as, for example, the cesium system, the electomagnetic pump power (EMP) supply system, and the coolant expansion tank. A number of reactor control components were also switched on by fast acting test stand drive mechanisms. All this made it possible to continue prolonged testing of a nuclear power plant even when defects or failures occurred in its systems.

The plan for developing the Topaz nuclear power plant, in which the basic stage was power testing for about half a year, permitted to the maximum degree possible the resolution of a number of very important problems on the ground. We will continue with a discussion of their nature, contents and results relative to prototype tests of a reactor in which electric generating channels with monocrystal cathodes were used. Testing of this prototype was carried out for 5000 hours in a test stand with heat removal systems and was concluded with the full operating capability of the reactor. The results are given in Table 11.1.

Table 11.1. Results of Topaz-I Testing

Electric Power, kW	7
Thermal Power, Beginning of Test, kW	152
Thermal Power, End of Test, kW	160
Coolant Temperature, inlet, $^\circ$C	480
Coolant Temperature, outlet, $^\circ$C	550
Conversion Efficiency, Start of Test, %	5.8
Conversion Efficiency, End of Test, %	5.5
Optimum Cs pressure, Start of Test, Torr	4.5
Optimum Cs pressure, End of Test, Torr	2.5

A summary of the basic results follows:

1) *The cesium system.* One of the most complex systems to develop was the cesium system. The fundamental problems were:

a. Determining the relationship between the pressure in the system and the "cold" region temperature in the cesium vapor generator (CVG);

b. Investigation of the temperature state of the cesium system components in all regimes;

c. Selection of an algorithm for bringing the cesium system to a given temperature;

d. Investigation of the influence of dynamic loads, including small loads in a zero-g environment, on CVG operation.

302

The results that followed were:

a. A CVG design that contained 2.5 kg of cesium and maintained a "cold" region temperature in the 300-340 °C range while influenced by external factors;

b. A trap design that provided reliable absorption of the entire quantity of cesium at 200-400 °C;

c. Design of electromagnetic valves for one-time operation.

2) *Heat removal system.* A great deal of development work was done on electromagnetic pumps (EMP) and space radiators (radiator). Problems in the development of EMPs were:

a. Investigation of flow, head and volt-ampere characteristics;

b. Investigation of cavitation in the start-up mode;

c. EMP optimization for the minimum required current;

d. Determination of the mechanical strength of the EMP structure.

As a result, a three-channel EM conduction pump was developed with a hydraulic power of about 150 W and with an efficiency of about 12% at a supply current of up to 1100 A. The stability of the EMP characteristics was verified in tests lasting for about one year.

The following had to be done in separate tests of the radiator:

a. Establish the actual load capacity of a shielded tube radiator for all design conditions;

b. Verify the vibration resistance of the design;

c. Verify the required heat rejection effectiveness;

d. Determine the hydraulic characteristics of the radiator;

e. Verify the life stability of the heat rejection characteristics.

The tests that were carried out demonstrated that the radiator designs developed had a high margin of strength and a high heat rejection effectiveness. The life stability of the radiator is determined by the radiating characteristics of the thermal control coatings. There were virtually no changes in these during continuous testing for about one year.

Tasks in developing the start-up system were:

a. Providing the proper coolant temperature during orbit insertion and nuclear power plant start-up;

b. Providing an acceptable coolant flow rate with the EMP power supplied by the start-up unit;

c. Investigating processes during transition of EMP power from the start-up unit to the pump section of the reactor.

Solutions to these tasks were achieved by:

a. Selecting the liquid metal coolant start-up power;

b. Selecting the EMP start-up unit electrical parameters;

c. Determining the safe conditions for disconnecting the start-up unit from the EMP;

d. Applying a thermal covering over the radiator surfaces.

3) *Radiation shielding*. Both mockup and actual radiation shields were tested under static and dynamic load conditions. A design with an adequate margin of strength and which was feasible for incorporation in the nuclear power plant structure was found. Investigations conducted on the attenuation of x-ray radiation in the radiation shield permitted fabrication quality criteria to be established.

4) *ACS and storage batteries*. Separate development of ACS components was carried out using simulated thermionic generators and simulation of the nuclear power plant electric circuit. In addition, the ACS was worked out with state certified on-board systems and loads using simulated nuclear power plants. In the development of storage batteries, discharge characteristics, life capabilities of storage batteries in supplying power to the nuclear power plant startup unit and to the telemetry system after startup were investigated. ACS and storage battery equipment were subjected to a full cycle of mechanical tests. The radiation resistance of the ACS and storage batteries was also verified.

5) *Remaining nuclear power plant components and systems.* Control unit drives, electrical switches, electrical couplings, contacts, the startup unit, neutron flux recorders, temperature and pressure recorders and other electrical devices were developed and tested separately. Test conditions simulated to the maximum degree possible state certified operating conditions.

Mechanical tests under all load conditions were conducted on the structural framework between the reactor, radiation shield, space radiator and spacecraft compartment equipment.

6) *Thermophysical and mechanical testing of nuclear power plant mockups.* Thermophysical and mechanical testing of nuclear power plant mockups of different sizes and complexity was conducted for the following purposes:

a. To determine prestartup heating by duplicating the heat transfer conditions that exist as the launch rocket passes through the atmosphere;

b. To prevent freezing of the coolant during orbit insertion for up to 2 hours;

c. To verify that there were no "cold" spots while cesium vapor was admitted into the reactor;

d. To determine the temperature state of components and systems and develop thermal shielding;

e. To verify strength characteristics in static and dynamic loading;

f. To determine the amplitude-frequency characteristics, resonance frequencies and inherent frequencies of the nuclear power plant.

Results of calculations and separate development work were verified and refined in tests on about ten mockups. Measures for thermal shielding of all components and systems were found to be sound and the static and dynamic strength of the nuclear power plant structures was substantiated. No interelectrode short circuiting occurred when the nuclear power plant structure was subjected to vibration loads.

7) *Ground power tests.* The nuclear power plant tested was assembled according to state standards together with certified automatic control system equipment and modified to provide nuclear safety in the ground test stand. This was done in order to obtain needed information apart from that obtained from uncertified telemetry recorders.
The principal tasks in the power tests were:

a. Verification of the basic operating capability criterion:

$$\dot{Q}_{el}(t) \geq \dot{Q}_{el,min} \text{ at } t \leq t_{req} \qquad ,$$

where t_{req} is the required operating life of the Topaz nuclear power plant during ground testing; t_{req} was about 4500 hours;

b. Verification of the accuracy of control algorithms in all regimes and that the parameters being controlled were maintained accurately;

c. Verification that component and nuclear power plant system parameters conformed with established requirements in all operating regimes;

d. The working out of methods for identifying the state of the nuclear power plant under actual conditions and determine the optimum number of telemetered parameters.

The first automatic startup of the nuclear power plant with an ACS was accomplished in 1979. These tests verified the essential accuracy of the startup mode algorithm, which included the following operations:

a. Programmed increase in reactor thermal power to a prescribed level;

b. Bringing the vapor generator to a prescribed temperature and admitting cesium vapor into the reactor internal cavities, which were pumped down during the preheat period;

c. Verification that the current in the basic reactor section was 300-400 A and that the terminal voltage was no more than 5-6 V;

d. A one step transition to the useful load;

e. Switching the voltage and current regulators to the nominal regime.

The accuracy of control algorithms was also verified in the nominal regime based on the current in the output section of the reactor. Changes in current translated into corrections in thermal power and channel temperature while the maximum allowable coolant temperature at the exit from the reactor was maintained at about 600 °C.

In 1982-84, two additional nuclear power plant power tests were conducted with an ACS in the automatic mode by using spacecraft command and control simulation in order to prepare for flight testing. In the first of these tests, an electric generating channel was used in which the cathode was fabricated from single-crystal molybdenum with a single-crystal tungsten coating; the second test used an electric generating channel with cathodes fabricated from single-crystal molybdenum. The first unit was tested for a 4500-hour life, the second for about a 7000-hour life. It should be pointed out that in the development of the nuclear power plant for flight testing, there were no design and technological measures considered in the Topaz nuclear power plant for providing a life time greater than several thousand hours.

The test results led to the following:

a. Complete verification of the accuracy of the control algorithms in the startup and nominal modes;

b. Verification that component and system parameters conformed with prescribed values and that temperature restrictions were observed;

c. Establishment of the life degradation of electrical characteristics. This showed up as increases in thermal power by approximately 30 kW (or by 20% of the power at the start of testing) during the 4500 hours;

d. Life changes in reactivity of the reactor exceeded 80%, which was caused by hydrogen loss from the core. This loss increased substantially beyond 3000 hours.

It should be noted that during testing the internal resistance of the output section changed insignificantly. R_i in the first unit at the beginning of testing was about 0.12 ohm and at the end 0.14 ohm. The change in R_i took place during the first 2500 hours. In the second unit, R_i remained virtually unchanged during the entire test period and was about 0.15 ohm. This shows that the reason for degradation may be due to internal short circuiting in the electric generating channels.

The most probable reason for degradation was the presence of gas impurities in the interelectrode gaps in the electric generating channels. The gas impurity concentration increased with the operating time. Testing demonstrated a correlation between changes in reactivity, gas flows from the interelectrode cavities, thermal power and coolant temperature. The gas flows from the interelectrode gaps consisted of more than 90% hydrogen. The composition stabilized after 10 - 15 days of testing. The magnitude of the flow increased with increases in coolant temperature. With a 10 g/day cesium vapor flow in the cesium system and a hydrogen flow of $3 - 5 \times 10^{-4}$ W, reached in 3000 - 3500 hours, the hydrogen pressure in the IEG of the TFE should be at the 650 Pa level. At such pressures, increasing plasma loss and heat transfer factors in the TFE IEGs should appear. Analytical and experimental investigations of these factors show that they provide an entirely adequate explanation for the observed degradation in efficiency of the reactor.

Fundamental tasks in ground testing and development work on specific components in the Topaz family of nuclear power plants have been discussed above. However, it makes sense in keeping with the objectives of this book to discuss some general problems relevant to any class of space nuclear power plants. We will begin the discussion with the physical startup of a reactor, an important operation which pertains to any kind of nuclear power plant. Physical startup will be accomplished in vacuum chambers that meet the stated requirements for the chambers in which the Topaz power plant was tested.

11.2.2. Physical Startup of a Reactor.

Physical startup is the process of bringing a reactor from an initial state to a subcritical state in which a fission chain reaction begins and the thermal power reaches a minimum controlled level (MCL).

The objective of physical reactor startup is the resolution of a number of tasks. The basic ones are:

1. Verification of the accuracy of core loading.

2. Determination of the critical positions of control devices.

3. Determination of the effectiveness of control devices and the neutron physics characteristics of the reactor.

4. Determination of reactor power.

5. Determination of the temperature coefficient of reactivity, etc.

The condition of the reactor during physical startup and operation at the MCL is controlled by using pulsed neutron counters. In order to obtain the required accuracy in measuring low neutron flux densities, the counters are included in a measurement circuit with a large time constant. The main danger during physical startup is that there may be a delay in control system reaction to a rapid rise in neutron flux. This can lead to run-away of the reactor (uncontrolled rise in power). During the physical startup of any reactor, the reactor must be maintained in the subcritical state at neutron flux densities that are quite high. For this purpose, an external neutron source can be used with a power of about 10^6-10^8 neutrons/sec. This corresponds to an MCL of about 10^{-4} - 10^{-6} nominal reactor power.

Let's examine the physical reactor startup sequence, for example, the determination of the critical position of the control rods (with a control system that uses control devices).

Deployment of emergency shielding and raising the control rods to the extreme position where initiation of a fission chain reaction is excluded are stipulated as initial operations in this case. When the control rods reaches a certain position specified earlier in special instructions, and a neutron power source S is installed, conditions are created in the core for a fission chain reaction: the reactor transitions to the subcritical state.

The neutron multiplication process begins. In fact, the neutrons obtained in 1 sec after the installation of the neutron source S result in the formation of $S \cdot k_{eff}$ new neutrons. As a result, in the reactor there will be $S + S \cdot k_{eff} = S(1 + k_{eff})$ first generation neutrons. In still another second they will form $S \cdot k_{eff}(1 + k_{eff})$ new neutrons, and, taking the neutron source into account, this will be $S\left[1 + k_{eff} + k_{eff}^2 + ...k_{eff}^{n-1}\right]$ neutrons. Note that the series within the brackets forms a geometric progression with the common ratio $k_{eff} < 1$. The sum of this series is equal to $S/(1 - k_{eff})$. It is finite and characterizes the number of neutrons in the reactor at an arbitrary instant of time. Thus, if $k_{eff} = 0.99$ and the power of the neutron source, $S = 10^7$ neutrons/sec, there will always be 10^9 neutrons in the reactor. Essentially, as k_{eff} increases, the number of neutrons in the reactor will increase.

$M = 1/(1-k_{eff})$ is called the neutron multiplication factor, and $(1-k_{eff})/S$ is the inverse multiplication factor which is more convenient for practical use. At first, the number of pulses recorded, N_o, corresponds to the rated power of the neutron source. Then the control devices begin to shift to the earlier established mark. In the new control device position (the control device could be an absorbing rod, reflector drum, etc. In the case of Topaz, it was a rotating reflector drum with absorber on one side), the corresponding number of participating neutrons is measured (the so called neutron count), which will now be, let's say, N_1. This value corresponds with the neutron multiplication factor, $M = N_1/N_o$, and also with the inverse multiplication factor M^{-1}. Generally M^{-1} is multiplied by a factor of a thousand for practical problems. With $k_{eff} > 1$ we see that $M \rightarrow \infty$. This is the most crucial moment in the physical startup process of a reactor. Therefore, one must approach the critical mode with great caution. A very strict

procedure is followed in practice. The essence of this procedure is to shift the control devices to the critical position in a definite order.

After determining the factor M^{-1}, on the graph (Fig. 11.2) using M^{-1}, H coordinates (H is an arbitrary value that characterizes the position of the control devices) point 1 (M_1^{-1}, H_1) is plotted. Next, the control devices are shifted to mark H_2, which is also calculated the same way. The neutron count is again taken and new values for the factors M_2^{-1} and H_2 are found. Point 2 is plotted on the graph (M_2^{-1}, H_2). A straight line intersecting with the abscissa is drawn through points 1 and 2. The first extrapolated critical position of the control devices, H_{cr1}, is obtained at the point of intersection. Subsequent gradual shifting of the control devices from mark H_2 to mark H_3 derives from the condition $H_3 = H_2 + \Delta H_2$, where $\Delta H_2 = 0.25 \times (H_1 - H_2)$. M_3 and M_3^{-1} are determined. Point 3 is plotted on the graph (M_3^{-1}, H_3) and the entire process of plotting is repeated. Shifting of the control devices continues until the quantity $1000 \cdot M^{-1}$ reaches about 2.

After connecting the last two points, a point is found on the abscissa which characterizes the critical position of the control devices, H_{cr}. We note that the value of H_{cr} can differ even for nuclear power plants in the same series. For this reason, determination of H_{cr} is an exceptionally crucial operation. The reactor period, T, is determined at this position. Reactor operation is first stabilized in this mode at the minimum controlled level. The control devices are then moved slightly into the supercritical region and the reactor begins to increase power. A continuous neutron count is made and at a certain instant of time (let's say, after 100 arbitrary units of neutron counts), a time interval is measured in which the number of neutrons has increased by the factor e. This interval is the reactor period.

As we observed, the physical startup of a reactor also includes a determination of the effectiveness (integral and differential) of the control devices and a computation of the reactor power. We will briefly discuss the content of these operations.

The effectiveness of control devices is determined from an analysis of how the reactivity introduced depends on the travel of the control devices, the so called rod travel calibration. The calibration is accomplished in the following sequence. The neutron multiplication factor, M_1, is computed in the initial position. The control rods are then shifted some distance and a new multiplication factor, M_2, is computed. Based on the neutron multiplication obtained, the effectiveness of the control devices is determined for the distance traveled from the equation

$$\rho_{1,2} = 1000\left(\frac{1}{M_2} - \frac{1}{M_1}\right) \qquad (11.1)$$

Such measurements are carried out at fixed positions over the entire range of control device coordinates.

Fig. 11.3 shows one of the characteristic calibration curves. As can be seen, the effectiveness of the control devices estimated by ρ, is not the same over the entire travel path: it is least at the start and end sections and increases approximately linearly towards the center section.
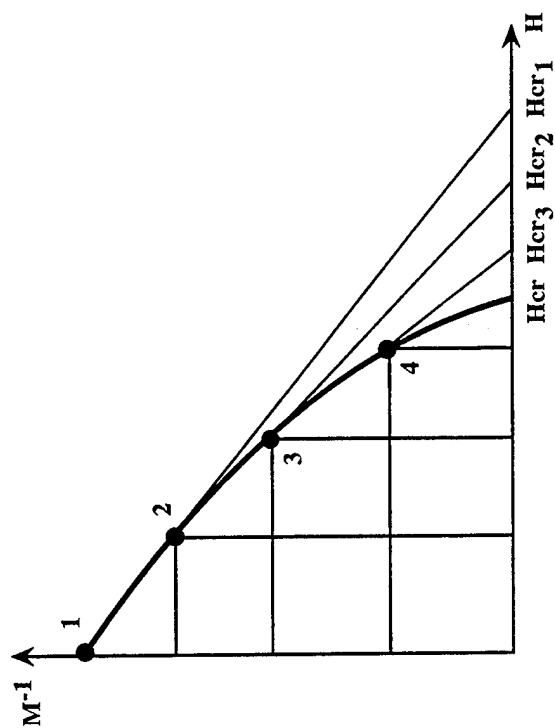
Fig. 11.2 Determining the critical position of reactor controls using the inverse of the neutron multiplication factor, M, and a control coordinate, H.
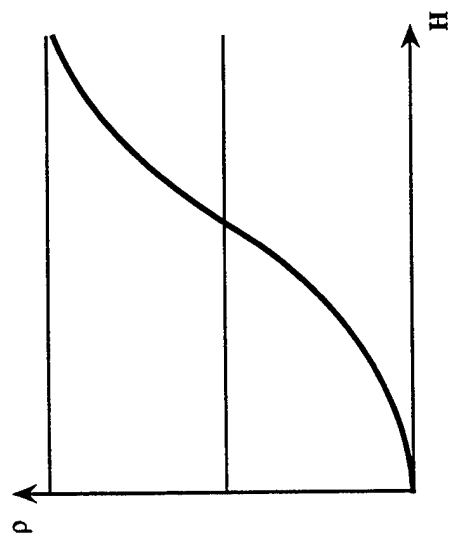
Fig. 11.3 Typical calibration curve for reactivity, ρ, versus control coordinate, H.

311

The magnitude of the reactivity permits one with a uniform movement of the control rods to determine the rate at which reactivity is introduced. As was observed in Section 3, this rate must be such that the margin of reactivity, Δk_{eff}, does not exceed the delayed neutron fraction.

In conclusion, we will discuss the determination of the minimum controlled thermal power level, which is called the "absolute" physical power rating. The magnitude of this power is used, in particular, in tuning ionization chambers prior to verifying their effectiveness. It also needs to be determined in order to establish the power level for nuclear power plant preheating during reactor startup and in transitioning to the nominal operating regime.

There are two methods for determining the "absolute" physical power of a reactor: 1) based on the spectral density of reactor noise, which is determined by the fission reaction rate at different points in the core; 2) through the use of an ionization chamber. The first method is based on measuring the noise frequency spectrum of the reactor. It reflects the statistical regularities in nuclear fission processes. The noise frequency spectrum depends on the kind of reactor and is in the range from zero to several kHz. Fast reactors are distinguished by a broader spectrum. From analyses of typical noise spectra in "cold" reactors it follows that independently of the kind of reactor, there is always an upper and lower frequency limit. Practical experience shows that the noise spectrum in regions beyond the lower and upper frequency limits depends only slightly on frequency. This circumstance must be taken into account in determining the "absolute" physical reactor power by this method.

The second method is based on measuring the rate of increase in the neutron count by using pulse neutron counters. The time needed to collect a certain number of pulses (as a rule, 1000 or more) is measured at the critical position of the control devices. The count rate is found from this data, and the "absolute" physical power is computed from the simple equation

$$\dot{Q}_{abs} = \frac{N_p}{t} K_o \qquad , \qquad (11.2)$$

where N_p is the number of pulses; t is the time of the count; K_o is an empirical conversion factor which is determined for a specific reactor.

It should be noted that physical startup of a reactor is in a number of cases carried out after full scale "hot" tests of the nuclear power plant in vacuum chambers, that is, under conditions that closely approach actual conditions. The objective of such a controlled startup is to determine the neutron physics characteristics of the reactor and the control devices (in particular, the temperature effect of reactivity). Preheating of the nuclear power plant with the coolant present is taken into account. The method for conducting a controlled physical startup of any reactor is virtually identical to the method described above.

11.2.3. Some Problems in Modeling During Testing in Vacuum Chambers.

Here we will restrict ourselves to only a discussion of thermal tests associated with the rejection of waste heat in the nuclear power plant from a space radiator to surrounding space.

The main requirement in these tests is to create conditions in the vacuum chamber that simulate heat rejection in space from the nuclear power plant being tested (primarily from the radiator). Consequently, a vacuum must be developed in the vacuum chamber such that the convective heat flux, $\dot{Q}''_{conv}$, and the heat flux by thermal conductance through the medium, $\dot{Q}''_{cond}$, will be negligibly small in comparison with the radiation heat flux, $\dot{Q}''_{rad}$. In other words, it is important to satisfy the inequalities $\dot{Q}''_{conv} \ll \dot{Q}''_{rad}$ and $\dot{Q}''_{conv} \ll \dot{Q}''_{rad}$. The heat fluxes $\dot{Q}''_{conv}$ and $\dot{Q}''_{cond}$ depend primarily on the pressure in the vacuum chamber. It is not difficult to show (analytically and experimentally) that if the clearance between the object being tested and the walls of the vacuum chamber is commensurate with the dimensions of the object being tested, then the vacuum chamber pressure at which the above stated inequalities are satisfied will not exceed 10^{-2} - 10^{-3} Pa (10^{-3}-10^{-4} mm Hg). Such a vacuum can easily be achieved even in large size vacuum chambers. Therefore, the first requirement for vacuum chambers is not difficult to satisfy.

The second vacuum chamber requirement is to make sure that the effect of the chamber walls on the radiation heat transfer process is as low as possible. In limited volume vacuum chambers, this requirement depends on the temperature and emissivity of the surfaces of the cooled object and the chamber walls. The radiation heat flux from a cooled object at a constant surface temperature and with mutual radiation with the chamber walls is determined from the well known Stefan-Boltzmann equation

$$\dot{Q}''_{rad} = \varepsilon_{1,2}\sigma\left(\overline{T}_1^4 - \overline{T}_2^4\right) \qquad , \qquad (11.3)$$

where

$$\varepsilon_{1,2} = \left\{ \frac{1}{\dfrac{1}{\varepsilon_1} + \left(\dfrac{1}{\varepsilon_2} - 1\right)\dfrac{A_1}{A_2}} \right\}$$

is the normalized emissivity; ε_1, A_1 and $\overline{T}_1$ are the emissivity, surface area and temperature of the hot object, and ε_2, A_2 and $\overline{T}_2$ correspond to the vacuum chamber walls.

If we compare the radiation flux from the cooled object in an infinite vacuum, that is, the ideal (Q''_∞) and that during testing (Q''_{test}), we obtain the following relationship which can serve as a measure of the quality of simulating external space conditions:

$$\frac{\dot{Q}''_\infty}{\dot{Q}''_{test}} = \frac{\varepsilon_{1,2}}{\varepsilon_1}\left[1 - \left(\frac{\overline{T}_2}{\overline{T}_1}\right)^4\right] \qquad . \qquad (11.4)$$

Good modeling of external conditions requires a small difference between $\dot{Q}''_\infty$ and $\dot{Q}''_{test}$. First of all, a normalized emissivity $\varepsilon_{1,2}$ must be chosen in an appropriate manner and the vacuum chamber walls must be cooled effectively. However, the vacuum chamber cooling system will in some cases require special coolant fluids. Thus, when $\varepsilon_{1,2} \approx \varepsilon_1$, and $\overline{T}_2 / \overline{T}_1 < 0.32$, then $\dot{Q}''_\infty$ will differ from $\dot{Q}''_{test}$ by no more than 1%, which is entirely acceptable. The indicated ratio in a water-cooled vacuum chamber corresponds to $\overline{T}_1 \approx 1000\,K$. However, if $\overline{T}_1 < 1000\,K$, then for acceptable modeling low boiling point liquids must be used instead of water. For example, liquid nitrogen cooling of the vacuum chamber will result in the same difference in $\dot{Q}''_\infty$ and $\dot{Q}''_{test}$ with $\overline{T}_1 \approx 400\,K$.

It follows from (11.4) that the ratio $\dot{Q}''_\infty / \dot{Q}''_{test}$ is influenced also by the emissivity and surface area of the vacuum chamber walls. By way of illustration, Fig. 11.4 shows $\dot{Q}''_\infty / \dot{Q}''_{test}$ as a function of A_1/A_2 for different values of ε_2. Analysis of this relationship shows that during testing in relatively small size vacuum chambers the wall emissivity requirement is quite rigorous. Thus, when $A_1/A_2 = 1/2$, then $\varepsilon_{1,2} \approx \varepsilon_1$ when $\varepsilon_2 > 0.9$.

The combined influence of $\overline{T}_2$ and ε_2 increases the difference between $\dot{Q}''_\infty$ and $\dot{Q}''_{test}$. For example, during testing in a water-cooled vacuum chamber of objects with diameters equal to 0.1 m, emissivity $\varepsilon_1 = 0.9$ and $\varepsilon_2 = 0.8$; and temperature $\overline{T}_1 = 700\,K$ and $\overline{T}_2 = 290\,K$, we obtain $\varepsilon_{1,2} = 0.88$, and the difference between $\dot{Q}''_\infty$ and $\dot{Q}''_{test}$ is more than 5%. Thus, in space the test object will dissipate 5% more thermal power than in the vacuum chamber. This difference is substantial and it obviously needs to be taken into account in predicting the output characteristics of the object being tested.

It should be noted that the difference in $\dot{Q}''_\infty$ and $\dot{Q}''_{test}$ can in some cases be put to good use. Thus, if the object under test will be subjected to solar radiation in space, then one can select values for A_1/A_2, such that there will be a small difference in $\dot{Q}''_\infty / \dot{Q}''_{test}$ from unity in the test mode. Since the radiation flux from the sun, $Q''_{solar} = 1.4\,kW/m^2$, such modeling is possible only when the cooled object is at comparatively low temperatures ($\overline{T}_1 < \sim 1000\,K$). If we consider that the tested object will radiate heat from all sides in space and that solar radiation is incident on one of its sides, then the indicated temperature $\overline{T}_1$ must be reduced, for example, for a cylinder by approximately 20% and for a sphere by 30%.

Thus, the main condition for good modeling of space conditions in vacuum chamber tests is to maintain a high emissivity of the internal walls of the vacuum chamber and provide adequate cooling, including the use of cryogenic liquids.

Regardless of the quality in simulating actual operating conditions during nuclear power plant testing in a vacuum chamber, there will always be certain differences between the operating processes that occur in power plants in test stands and those that occur in space. We will examine these differences by looking at three basic nuclear power plant parameters:

a. Rejected thermal power, $\dot{Q}''_{rad}$;
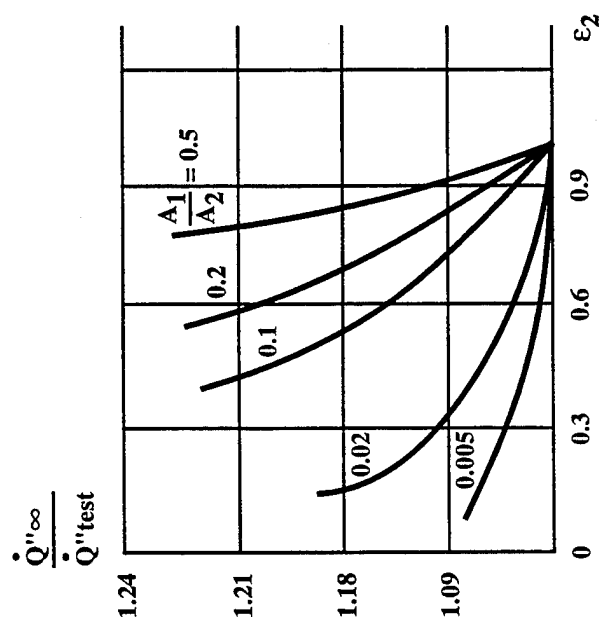
Fig. 11.4 Thermal power correction factor as a function of vacuum chamber wall emissivity ε_2. The larger ε_2 is, and the larger the vacuum chamber is, the better the actual heat removal will correspond to the situation in space.

315

b. The thermal flux incident on the space radiator;

c. Coolant temperature at the outlet of a reactor operating in the nominal mode at design conditions (recall that we are discussing thermal testing of nuclear power plants without bringing the reactor to nominal power).

Heat rejection by radiation from a nuclear power plant in a vacuum chamber is always less than under actual conditions for two reasons. First, as we noted earlier, the repeated reflection of radiation flux in the "space radiator-vacuum chamber wall" system will lower the normalized emissivity of the surfaces of the cooled object, and consequently, the thermal power it rejects will be reduced. Second, this power will be influenced by the unavoidable shading of individual sections of the space radiator surfaces by structural components of the test stand (by structural fastening members of the nuclear power plant inside the vacuum chamber, etc.). In order to account for these factors in the intensity of radiation heat rejection from the nuclear power plant during testing in a vacuum chamber, the concept of the equivalent space radiator surface area is introduced, A_{eq}.

In order to determine A_{eq}, one can use one of two nuclear power plant test modes in a vacuum chamber: preheating of all nuclear power plant components to a nominal temperature and separate heating of the space radiator.

In the first case, the space radiator will dump heat carried to it by the coolant and heat conducted to it from other nuclear power plant components (plumbing, converter housing, pumps, etc.). We will only discuss the separate space radiator heating mode, although, of course, this mode conforms to a lesser degree to actual conditions. In this case, one can determine A_{eq} from a differential equation which describes a heat balance on an elementary annular section of a cylindrical radiator:

$$\dot{M}_c \bar{c}_p dT_c = \varepsilon_{1,2} \sigma \left(\overline{T}_1^4 v_f - \overline{T}_2^4 \right) dA_{eq} \tag{11.5}$$

where $\dot{M}_c$ is the coolant flow per second through the isolated section, $\bar{c}$ is the average heat capacity of the coolant; T_c is the coolant temperature along the length of the isolated section; $\overline{T}_1$ is the radiator channel wall temperature along the length of the isolated section (as we noted in Section 4, $T_c = T_1$ can be assumed for liquid metal coolants); v_f is the fin factor which accounts for a reduction in temperature along the height of the fin; $\overline{T}_2$ is the average wall temperature of the vacuum chamber.

We conclude with these examples our discussion of specific operations involved in ground testing and development, and we will proceed to a discussion of flight prototype testing of nuclear power plants. However, we will first discuss the many precautions that need to be taken to provide radiation and nuclear safety.

11.4. Problems in Providing Radiation and Nuclear Safety.

11.4.1. Radiation Safety.

As we have stated, one of the three basic conditions for using nuclear power plants, including those for use in space, is the assurance of nuclear and radiation safety for service personnel and the population. This must be accomplished in all stages beginning with development work in plants and factories, during delivery of the nuclear power plant to the spacecraft launch site, and ending with the space flight mission itself. Of course, accidents can occur during all stages and allowances for the consequences must be made in the development of the safety system. The nuclear power plant is above all a source of ionizing radiation. In addition to the reactor, the radiation shield is also a source of ionizing radiation and the intensity increases with the operating life of the reactor. As we have mentioned, the radiation shield contains a slab of lithium hydride supplemented with steel, tungsten and other materials that are excellent absorbers of γ quanta. Radioactive isotopes, which determine the activity that results from nuclear power plant operation and which are dangerous to humans, include:

a. Isotopes in the fuel rods ranging from krypton-85 to europium-157 (products of uranium-235 fission);

b. Activation products in the beryllium reflector, such as Chromium-51, manganese-54, iron-59, cobalt-58, cobalt-60 isotopes;

c. Isotopes in the shield--mainly, manganese-54 and cobalt-60.

The remainder of the nuclear power plant structure and the spacecraft structure is virtually devoid of radioactivity.

In order to assess possible conditions for infractions of nuclear safety, we will begin with the operational use of nuclear space power plants. Orbit selection is of fundamental importance here. In general, we are talking about the so called radiation safe orbits (RSO) in which the residence time of the spacecraft after the nuclear power plant ceases to operate is sufficient to reduce the ionizing radiation from the fission products and the nuclear power plant to minimum acceptable levels.

There are also low earth orbits (LEO) in space where this condition is not satisfied and where safety is assured by taking appropriate, effective steps. Thus, when nuclear power plants are used in low orbits, *basic and backup* radiation safety systems (BRSS) must be used. The basic system must be able to transfer the nuclear power plant compartment into long duration orbits. The backup safety system is intended to disperse (scatter) core materials and other nuclear reactor components that are sources of ionizing radiation into particles of insignificant size. The dispersion of these particles and their density must be such that when they fall to earth, they do not present any radiation danger to the population (the relevant radiation standard is that this radiation must not exceed 0.5 rems/year or 0.5×10^{-2} eV/year). This approach to the safe use of nuclear space power plants was incorporated in United Nations documents and approved by a resolution of the UN General Assembly in 1981.

Let's discuss orbit selection. A significant time after the nuclear power plant ceases to operate, the activity of the reactor structure is determined by the presence of the Co^{60} isotope. After more than 100 years, the activity of the fission products (and the

317

activity of the reactor as a whole) is determined by the isotopes Cs^{137} and Sr^{90}. The time it takes for the activity to fall to the 0.5 rem/year (0.1 Curie) level can be determined from the relationship

$$\tau_{0.5Rem} = 43.3\left(2.56 + \ln\int_{0}^{T}\dot{Q}_t(t)dt\right) \qquad ,\qquad (11.6)$$

where $\dot{Q}_t(t)$ is the thermal power of the reactor at any instant of time; T is the operating life of the reactor in years.

It is obvious that the lowest radiation safe orbit, H_o, must satisfy the condition: $\tau(H_o) \geq \tau_{0.5Rem}$ is the spacecraft residence time at the altitude H_o.

For $\dot{Q}_e > 10$ kW and life T > 3 years the needed time will exceed 400 years. Typically, an orbit of 800-1000 km is high enough to guarantee this.

The problem of providing radiation safety during the operation of nuclear power plants in low and intermediate orbits requires special attention. Here, the system for placing the nuclear power plant in a radiation safe orbit plays the principal role. This system functions to a great degree in response to failures in spacecraft systems: spacecraft orientation and stabilization systems, temperature control of instrumentation in telemetry and electrical supply systems.

The orbit transfer system contains command and control equipment which is housed in a separate spacecraft compartment. It performs the following functions: reactor shutdown ("extinguishing"), orientation and stabilization of the spacecraft, separation of parts of the spacecraft from the transfer compartment, starting the transfer thrusters (as a rule, solid rocket engines). The total mass of the transfer compartment including the fuel mass constitutes up to 40% of the nuclear power plant mass and the initial mass of the transfer compartment.

The nuclear power plant orbit transfer system must be activated under the following emergency situations:

a. Failures in the spacecraft orientation and stabilization system and deviations of the longitudinal axis of the spacecraft from the flight orientation;

b. Failures in the instrument compartment temperature control system and increases in temperature inside the compartment to a level above which the command equipment will fail to operate;

c. Failures in the electrical supply system and increases or reductions in voltage to levels that are the minimum acceptable for electrical circuit operation.

The system for dispersing the space power plant reactor, that is, the mandatory system for partitioning its structure in the event of emergency conditions on the spacecraft, must be activated when:

a. The temperature of reactor components increases to a level beyond which relevant mechanisms will not continue to function and beyond which the geometric dimensions and clearances within the reactor cannot be maintained;

b. Aerodynamic damage begins to occur to the nuclear power plant structure and the spacecraft during reentry into the upper layers of the atmosphere.

c. Possible failures in the spacecraft orbit transfer system and in the system for partitioning the reactor structure must be considered in all stages of operation of these systems, including failures in discrete command and control links.

The probability of simultaneous failures of the orbit transfer system and the system for partitioning the reactor structure, which are independent events, is estimated to be 10^{-4} or less. This provides adequate radiation safety reliability when nuclear power plants are used on low orbit spacecraft.

We will now discuss some details of the backup radiation safety system. A very promising backup radiation safety system is one that employs aerodynamic dispersion of nuclear fuel, fission products and reactor components with induced radiation. The development of an aerodynamic dispersion system has been the subject of numerous experimental studies in special experimental structures with simulated aerodynamic heating and velocities that occur during reentry into the dense layers of the atmosphere. The experimental installations permitted the study of:

a. The mechanism of aerodynamic disintegration of reactor core materials, including nuclear fuel specimens of uranium and its compounds;

b. The thermal state and the order of disintegration of reactor scale models;

c. The order and characteristics of the dispersion of full size fuel rods and electric generating channels fabricated to technical specifications;

d. Mechanisms and characteristics of aerodynamic disintegration into particles and dispersion of core structural components during their descent into the lower layers of the earth's atmosphere.

Reactor models of the Cosmos-954 type and the zirconium hydride moderated Topaz type reactor have both been tested. The test units consisted of cylindrical rods, sleeves, and four and six sided prisms with cylindrical channels through them. A velocity head in the 10-200 kPa range and heating temperatures up to 800-1200 °C at the ends of the specimens were simulated during testing.

The principal result of the experimental studies in simulating reentry in the dense layers of the atmosphere was conclusive data on the breakup and disintegration of the moderator into particles no larger than 10 mm and with a surface area to mass ratio of about 0.5 cm²/g. Consequently, aerodynamic disintegration of the basic nuclear power plant components was adopted as a method for providing radiation safety. Later on, the

aerodynamic dispersion system was used in nuclear power plants on the Cosmos-1402 and Cosmos-1900 spacecraft. Such a system for the Topaz reactor family is based on the following principles:

a. Extraction of the electric generating channel assemblies from the nuclear reactor;

b. Bringing these assemblies intact to altitudes of about 60-80 km where the velocity head and aerodynamic heat flux will reach 700 kg/m² and 1500 kW/m², respectively (accounting for the use of heat shields);

c. Gradual disintegration of the shields, electric generating channel assemblies, their containers and releasing the cathode components.

The uranium dioxide solid fuel core or fuel consisting of individual tablets disintegrated due to thermal stress and melting, including melting of particle sizes up to several millimeters. As a result of these processes, a particle cloud with particle sizes of no more than several tenths of millimeters formed at altitudes extending over several kilometers. This cloud spread for a distance of several tens of kilometers.

Calculations of the fall-out from these particles showed that with a total activity of the nuclear fuel in the reactor of about 10^5 Curies (about 10 days of operation with an energy liberation of about 600 kW/yr), the maximum activity of the particle fallout on earth will not exceed 10^{-4} Curie/m², and the area traced by such radiation activity will be about 1000 km². At a density of about 10^{-4} Curie/m², the dose from external radiation for a limited portion of the population will be less than the allowable limit (0.5 rem/yr). In the remaining territories, the external radiation dose from particle fall-out will be at the natural background level. Certain difficulties arise with the dispersion of hydride moderators from thermal reactors with thermionic converters. As the above mentioned modeling showed, solid moderator plates of zirconium hydride with diameters equal to the core diameter will not disperse due to insufficient heating under any atmospheric reentry conditions. One possible approach to solving this problem is to develop a moderator design consisting of individual slabs of zirconium hydride, for example, a six-sided shape around each electric generating channel. Another possibility is explosive dispersion of the reactor structure after ejection of the electric generating assemblies as the nuclear power plant enters into the dense layers of the atmosphere. Destruction of reactor structural components by the accumulative effect of exploding materials and subsequent aerodynamic disintegration of the fragments will result in fallout on earth with particle sizes substantially less than the allowable.

The experimental verification of such a system and demonstration of its efficacy was subsequently accomplished in the Topaz program.

An actual system for orbit transfer of a nuclear power plant and partitioning the reactor structure in order to disintegrate its components aerodynamically were installed on "Cosmos-1900," a spacecraft intended for observations of ocean surfaces. This spacecraft was launched into orbit on Dec. 12, 1987. The situation on the spacecraft after loss of

radio contact with the earth on Apr. 4, 1988 and failure to respond to a command for orbit transfer on Apr. 13, 1988 was as follows:

a. Nuclear power plant separation failed to occur on command from earth;

b. Orbit corrections on command from earth were stopped;

c. Orientation and stabilization systems operated normally based on measurements of flight trajectory parameters;

d. The nuclear power plant operated normally.

As the satellite orbit decreased to an altitude of 100 km in stable flight, triggering of the nuclear power plant separation system could be accomplished by two commands based on indications of a voltage drop in the electrical supply circuit and a mismatch in the spacecraft stabilization angle.

Satellite flight in the 95 to 100 km altitude range is characterized by additional aerodynamic heat fluxes on the space radiator. This reduces the temperature drop in the thermoelectric converters of heat which, in turn, drops the power and voltage to below acceptable limits.

During descent in the 90 to 95 km altitude range, aerodynamic heating results in triggering of the reactor structure separation system and ejection of the fuel element assembly on command from the aerodynamic heating data recorders.

Cosmos 1900 reentered the atmosphere at an altitude of 100 km on Sep. 30, 1988. This had been predicted to occur on Oct. 5, 1988. During the night of Sep. 30, 1988 in the initial portion of the next orbit at an altitude of about 180 km, the system for sending the nuclear power plant into a higher orbit and ejecting the fuel element assembly from the reactor into a parking orbit triggered into action. The parking orbit has an apogee of 773 km and a perigee of 725 km with a residence time of about 200 years. The fuel assembly orbit has an apogee of 764 km and a perigee of 708 km giving it a residence time of more than 300 years. These orbit lives are entirely adequate to reduce the radiation levels of the nuclear reactor components to acceptable levels. Thus, radiation safety of the "Kosmos-1900" satellite was assured.

The adoption and determination of radiation safety during the operation of nuclear power plants have become well known during the last decade to a broad segment of the population. This is due to accidents and their consequences, such as at the atomic electric power stations at Chernobyl (1986), and also in other devices for stationary and transport purposes. People are aware that calculations of characteristic levels and ionizing radiation absorption parameters differ significantly. For this reason, we will recall basic findings that characterize radiation safety for personnel associated with the operation of space nuclear power plants.

From a biological point of view, of greatest importance is that γ radiation and elementary particles that strike living tissue will lose their energy to its atoms and molecules and thus destroy the normal functioning of biological cells. Water, which is contained in biological cells, can convert to free radicals, such as H, OH, H_2O_2, HO_2, etc.

Because the human body consists mainly of water, particle radiation can influence the organism significantly. In addition, radiation can cause direct injury to tissues by which several molecules are damaged, particularly the DNA molecule, which controls cell growth and formation. Danger of serious damage to the thyroid gland can occur by accumulation of the I^{135} isotope in the gland. The gastrointestinal tract is very sensitive to radioactive substances that can form in test cells and which can enter the human organism during breathing.

In order to evaluate the biological effects of ionizing radiation, a number of special terms need to be introduced. The first one of these is the absorbed radiation dose, D, which characterizes the energy transferred to one gram of irradiated biological tissue. The unit of the absorbed dose is one gram-roentgen (100 rads) and is equal to 1 joule/kg. It is virtually impossible to measure the γ radiation dose directly in living tissue. However, the absorption of γ radiation in a substance, including tissue, depends on the number of chemical elements that compose it. Substances which differ little in the value of Z from biological tissues are called tissue equivalents. They are used in measuring γ radiation doses in tissue. The simplest method is to measure γ radiation by the ionization of a tissue equivalent substance, air.

Practical dosimetry for measuring absorbed radiation doses uses another unit, the roentgen. One roentgen is equal to a dose of X-ray or γ radiation in which in 1 cm^3 of air at normal atmospheric pressure ions are formed which carry a charge of 3.33×10^{-10} coulomb. In the conversion to absorbed dose in air, 1 roentgen = 0.0089 gram-roentgen (0.89 rad), and in living tissue, 1 roentgen = 0.0093 gram-roentgen (0.90 rad).

The biological effect of radiation on living tissue depends also on the specific kind of radiation. Doses of proton and neutron and γ radiation have a significantly greater biological effect than equal doses of x-ray or γ radiation.

The biological effect of radiation takes into account a radiation quality factor, QF. This factor indicates by what multiple the biological effect of a given kind of radiation exceed that of an equal dose of γ radiation. For example, for α particles the qualitative factor is equal to 10, for β^- particles, the factor equals 1, and for thermal neutrons, the factor equals 3, etc. The product of the absorbed dose D of a given kind of radiation and its qualitative factor QF is called the equivalent dose, $D_{eq} = D \cdot QF$. The unit of the equivalent dose is the rem. It equals the dose of any kind of radiation which causes the same biological effect as a 1 rad dose of x-ray or γ radiation.

The biological effect of radiation on an organism depends on the dose rate and increases as the latter increases. Therefore, in work compartments it is necessary to control not only the radiation dose but also the dose rate.

For personnel involved in the operation of different nuclear power plants a maximum allowable dose, MAD, has been established. It is selected on the condition that the annual radiation level with a uniform dose accumulation for 50 years would not cause any unfavorable changes in health. For this condition, MAD is 5 rem/yr.

In order to provide radiation safety in all operations carried out by personnel in the operation of a nuclear power plant, special clothing must be worn and each worker is required to wear an individual dosimeter.

11.4.2. Nuclear Safety.

Let's now turn to a discussion of the second factor dealing with safety in nuclear power plant operation, nuclear safety.

By *nuclear hazards* we understand potent processes that arise as a result of an uncontrolled reactor run-away up to the critical and beyond into the supercritical mode. Of course, such processes are accompanied by a rapid deterioration in radiation safety.

Practically all stages in the preparation of nuclear power plants for application and subsequent operation have a certain probability of accidents in which the fission process in the nuclear reactor can go out of control. However, this probability is most characteristic of such processes as the delivery of the nuclear power plant from the fabrication facility to the launch assembly facility, transfer to the launch pad, and during portions of the launch of the spacecraft with the nuclear power plant into the design orbit. After fabrication of the nuclear power plant, the basic stages in preparing it for application are:

a. Transportation from the fabrication facility. In general, transportation follows storage of a nuclear power plant under factory conditions and also subsequent to storage under the technological conditions of the launch complex. Transportation of the nuclear power plant is possible by rail, water and air. However, the requirement for nuclear and radiation safety remains unchanged, regardless of the diverse conditions under which it has to be provided.

Emergency situations during transportation by rail and air that can occur are: shock and vibration loads during possible collisions by transport vehicles. During transportation by ship or river boats an especially dangerous situation can occur in which the nuclear power plant may become immersed in water. Finally, in all situations one must consider climatic effects (changes in temperature and air pressure, moisture, dust, etc.);

b. Prestart preparation and launch of the carrier rocket. The following emergency situations are possible: effects on the nuclear power plant by exploding rocket fuel, immersion in hot fuel, impact of the launch rocket in the launch area;

c. Introduction into orbit. Emergency situation: fall of the nuclear power plant from different altitudes;

d. Functioning in orbit. Emergency situations: failures in the control system, heat transfer system, etc.

The consensus regarding nuclear safety in all the above mentioned emergency situations is based on the following principles:

a. Different design measures can ensure subcriticality of a nuclear reactor;

b. The spread of radioactive and toxic aerosols from rocket fuel explosions and fires can be confined to the launch facility area where appropriate safety measures are provided;

c. Physical startup of a reactor during nuclear power plant fabrication stages can be limited to a few watts (a minimum controllable power level) for several hours, and the time from the last physical startup to the launch of the spacecraft with the nuclear power plant can be made long enough to reduce the radioactivity in the reactor to allowable levels;

d. Startup of the nuclear power plant reactor is made possible only after the spacecraft has reached the operating orbit by blocking the reactor control device drive mechanism and removing it only by special command after the orbit trajectory parameters have been verified.

At the present time, depending on the nature of any emergency situation, a variety of measures are taken to provide nuclear safety. The most essential of these are:

a. During shocks and vibration loads beyond specifications, the rotating control devices may shift with respect to maximum subcriticality, thus introducing positive reactivity. In order to reduce this effect, the following design steps can be taken:

    i. decrease the moment of the shock forces affecting the rotating control devices owing to a maximum possible shift of the center of mass of the rotating control devices from the axis of rotation;

    ii. Create a weak spot in the construction of the side reflectors which will cause portions of the reflectors and the control devices to deploy at overloads limited to less than those which are unsafe for rotation of the control devices (i.e. adding positive reactivity);

    iii. Lock the rotating control devices during transportation of the nuclear power plant and during spacecraft orbit insertion;

    iv. Replace the standard reflector units during the nuclear power plant transportation process with suitable simulators made of materials which are poor reflectors but which are excellent absorbers of neutrons.

b. Introduction into the reactor core of additional safety rods, which are made of materials that are good absorbers of neutrons. The functioning of the safety rods involves the following:

    a. After the completion of physical startups and fabrication of the reactor, the safety rods are introduced into the core and kept there;

    b. The safety rods are located in the core during transportation of the nuclear power plant and kept there until the spacecraft has reached the design orbit;

c. After successful orbit insertion and verification of the trajectory parameters, the safety rods are withdrawn from the core and the reactor stands ready to enter the design operating mode.

d. An important safety rod design requirement is that the rods must not be removed from the core as a result of the variety of shock loads that may occur during accidents.

c. The application of resonance absorbers in the core with a neutron resonance absorption range that is sufficiently low in terms of its influence on reactivity under normal operating conditions but sufficiently high to assure the requisite subcriticality in emergency situations. Isotopes of gadolinium, europium, samarium, etc. can be used as resonance absorbers. The obvious advantages of resonance absorbers compared with safety rods are the absence of any moving parts and absorber retainers in the core and also the assurance that subcriticality will be maintained in the event the nuclear power plant is immersed in water. These measures increase the reliability of nuclear safety systems. The disadvantage of these systems is inevitable losses in reactivity which is compensated for by increasing the core volume and the mass of the nuclear power plant. Moreover, resonance absorbers cannot compensate for changes in reactivity during accidental compression of reactor components.

In conclusion, we note the following. Experience in working on radiation safety problems relevant to space nuclear power plants and in their operation has shown that it is sufficient to use two separate systems: a system for orbit transfer and a system for dispersing the reactor by actively partitioning its structure. This conclusion is substantiated by the position adopted by the UN Committee on the Uses of Space for Peaceful Purposes following discussions in scientific-technical and judicial subcommittees.

The technical, engineering and experimental investigations carried out in Russia and design development, technology and testing attest to the effectiveness of radiation and nuclear safety systems. Their operating capabilities and requisite reliability under normal operating conditions and during emergency situations on spacecraft were also confirmed. The successful launches in past years of spacecraft in the Cosmos series with thermoelectric and thermionic nuclear power plants on board testify to this.

11.3. Basic Tasks and Results of Design Prototype Flight Testing of Nuclear Power Plants in the Topaz Program.[1]

11.3.1. Tasks and test objectives.

Space nuclear power plants are unique devices. Problems in the design prototype flight testing of nuclear power plants with thermionic converters are being resolved for the first time in the world. For this reason, despite the methodological bent of this book which is to present more general issues including the development of space nuclear power plants, we find it advisable to discuss design prototype flight testing of nuclear power plants as it was done in the Topaz program.

Moreover, one can expect that during the initial period of preparing any nuclear power plant for application, the relevant tasks in prototype flight testing and their analysis will differ little from those discussed in this section.

Two experimental nuclear power plant models in this program, in particular, Topaz-I, underwent successful prototype flight testing on spacecraft in the Cosmos series during 1987-88.

The fundamental objectives of prototype flight testing, which should provide insight to the operating capabilities of thermionic nuclear power plants, were:

a. Verification that nuclear power plant output parameters obtained in ground tests agreed with those obtained during flight testing;

b. Substantiation that the thermionic reactor operated properly after experiencing mechanical loads during portions of spacecraft orbit insertion;

c. Verification that the reactors and servicing systems operated properly under the combined effects of space conditions;

d. Final confirmation of the control algorithms used during startup and in the nominal operating modes of the nuclear power plant.

The achievement of a prolonged life during flight testing was not attempted. The design and technological decisions adopted in the nuclear power plant were to provide adequate operational stability of the nuclear power plant for several thousand hours.

The Topaz-I nuclear power plant flight models incorporated the following:

a. A reactor with control device mechanisms;

b. Control device drives divided into four groups;

c. A cesium supply system;

---

[1] Based on materials from NPO "Red Star."

326

d. A heat rejection system;

e. A startup system;

f. An automatic control system with storage batteries.

In the reactor, which incorporated zirconium hydride moderator and beryllium reflectors, the electric generating channels were commutated in two independent sections: the output section for supplying the spacecraft equipment and the pump section for supplying the electromagnetic pumps in the heat rejection system. Single-crystal molybdenum (first model) and single-crystal molybdenum with a single-crystal tungsten coating (second model) were used as the cathode materials. Gaseous fission product venting was accomplished from the sealed cathode components of the electric generating channels directly into the interelectrode gaps. A three-layer anode packet was used. A niobium alloy was used as the anode material. Aluminum oxide was used as insulation, and the electric generating channel containers were made from stainless steel.

The electrical connections of the output and pump sections of the electric generating channels were made in the upper and lower commutation chambers in cesium vapor. The output section had six electric generating channel circuits in parallel, each containing 8 to 12 series connected electric generating channels. All electric generating channels in the pump section were connected in parallel. Current output from the commutation chamber was accomplished through metallic ceramic seals.

12 rotating cylinders with sectored boron carbide inserts were located in the lateral reflector. The control devices were divided into four groups with three rotating drums in each. Two groups were used for control, and two were used for reactivity compensation.

The reactor used a cesium flow system in which cesium vapor passed through the interelectrode gaps in order to remove gaseous fission products directly to space. The cesium system had a thermostat controlled cesium vapor generator with electric heaters which helped maintain the required pressure. The maximum quantity of cesium was 2.5 kg in the cesium generator design used. Depending on the vapor flow rate, this clearly placed a limitation on the operating life of the nuclear power plant.

Table 11.2 presents the basic characteristics of the reactor in the Topaz-I nuclear power plant.

Table 11.2. Basic Characteristics of the Topaz-I Reactor.

Characteristic	Value
Emitter Diameter, mm	10
Generating Channel Outside Diameter, mm	14.6
Number of TFEs	79
Number Included in the Operating Section	63
Average Moderator Fraction	0.72
Core Diameter, mm	280
Core Height, mm	360
U-235 Loading, kg	12

Effectiveness of the 12 Rotating Control Drums, % k_{eff}	7.0
Subcriticality of the Reactor, in "Cold" State, % k_{eff}	6.2
Temperature Effect of Reactivity, k_{eff}	1.8

The automatic control system and storage batteries were placed in the instrument compartment. The automatic control system provided for:

a. Bringing the power plant up to thermal and electrical power;

b. Sustaining a given operating regime;

c. Sustaining a given voltage at the output terminals;

d. Power plant shutdown by signals from on-board equipment.

The required electrical power of the reactor in the nominal mode was provided by maintaining a given current in the output section of the reactor through appropriate corrections to the thermal power of the reactor.

A restriction was placed on the coolant temperature at the reactor exit. This temperature was not allowed to exceed 610 °C.

The cesium vapor generator temperature regulator made it possible to operate in three modes based on the temperature in the cold region within about 25° intervals. The cesium vapor pressure was changed on command from earth in order to fine tune the optimum level for nuclear power plant operation. The basic parameters of the Topaz-I nuclear power plant flight model are given in Table 11.3.

Table 11.3. Basic Parameters of the Nuclear Power Plant.

Characteristic	Value
Electric Output Power, kW	6
Output Voltage, V	32
Output Section Current	180
Voltage at Pump Section Terminals, V	1.1
Pump Section Current	1200
Maximum Coolant Outlet Temp, °C	610
Coolant Preheat Temp, °C	80
Cesium Vapor Flow Rate, g/day	6-20
Cesium Vapor Pressure, Pa	266-730
Nuclear Power Plant Mass (less batteries), kg	1200
Length, m	4.7
Diameter,m	1.3

The startup algorithms included the following:

a. Bringing the reactor up to the preheat thermal power level;

b. Preheating of the structures sufficiently to eliminate the possibility of "cold spots" in the cesium vapor channels while opening the thermostat;

c. Filling the interelectrode gaps of the reactor electric generating channels with cesium vapor and regulating the current close to the short circuit current in the output section of the reactor for a limited time sufficient to completely stabilize the cesium vapor pressure distribution in the reactor channels;

d. Switching the output section of the reactor to the spacecraft loads, simultaneously turning the fast-acting voltage regulator on.

11.3.2. Results of Flight Prototype Testing of the Topaz-I Nuclear Power Plant.

Startup of both nuclear power plant models was accomplished in complete agreement with the control algorithms adopted. The nuclear power plant was brought to a thermal power level that supplied the required preheating of the cesium system. There were no anomalies discovered in either model that could be traced to "cold spots" in the channels while the current was increased in the output section as the cesium vapor generator opened and as the reactor filled with cesium vapor. In the first model, the reactor output section transitioned to the short circuit current regulation mode in 70 minutes, and in the second model, 55 minutes after startup began.

The transition time from the short circuit current regulation mode to the nominal mode was about 90 sec in both nuclear power plant models.

The first Topaz-I nuclear power plant model. The initial "cold zone" cesium vapor generator temperature (about 324 °C) corresponded to a cesium vapor pressure of about 600 Pa based on data obtained in ground development work. This pressure proved to be approximately optimum for the output section of the reactor and below optimum for the pump section. After 53 days, the cesium vapor generator temperature was switched to 336 °C by radio command from earth. The resultant vapor pressure proved to be virtually optimum for the pump section and somewhat below optimum for the output section. Flight testing of the first nuclear power plant model was continued at this temperature. Diagnostic signs of cesium depletion in the vapor generator appeared in 123 days. This corresponded with data obtained during ground testing. The initial reserve of cesium (2.5 kg) was completely exhausted after 143 days. This time was in good agreement with an analytical prognosis made by using the relationship $p_{Cs} = f(T_{Cs})$. As the remaining cesium depleted and thus reduced the reactor output and pump section currents, at a certain instant of time the output section current became less than that required by the spacecraft systems. The voltage at the reactor terminals consequently dropped and based on this signal of a voltage drop below the permissible level, the automatic control system placed the reactor rotating control drums in the position of maximum subcriticality.

The cessation of operation of the reactor was verified by telemetry data obtained during subsequent communication sessions with the spacecraft.

The second Topaz-I nuclear power plant model. In this model, the startup temperature in the cesium vapor generator was 312 °C which agreed with the anticipated optimum pressure level for cathodes with single-crystal tungsten coatings. At this temperature, the vapor pressure proved to be close to optimum for the pump section and higher than optimum for the output section. 92 days after the start of testing the generator temperature was changed to 302 °C upon command from earth. This temperature provided an approximately optimum pressure for the output section. This pressure proved to be below optimum for the pump section. Flight testing continued at this temperature. We note that toward completion of the testing this temperature began to approximate the optimum for the reactor pump section.

The cesium reserve was completely depleted after 342 days. During this period, diagnostic indications of cesium depletion in the vapor generator were recorded. The process of shutting down the reactor proceeded in the same way as in the first model.

11.3.3. Analysis of Results of Flight Prototype Testing of the Topaz-I Nuclear Power Plant Models.

The difference in the operating duration of the first and second nuclear power plant models was caused entirely by the less than optimum cesium vapor pressure level. As a consequence, the cesium consumption rate was lower in the second model than in the first. This, in turn, resulted in a larger vacuum work function of the single-crystal tungsten compared with the single-crystal molybdenum.

Life changes in reactivity of the reactor were determined during the flight prototype tests based on the angle of rotation of the control drums relative to that determined experimentally during the fabrication stages of these nuclear power plants. The observed changes in reactivity where caused basically by hydrogen losses from the reactor core (approximately 80-85% of the total change in reactivity). The relatively large hydrogen loss, which in the second model reached about 4% of the initial quantity of hydrogen in the zirconium hydride, was caused by the fact that due to the short design life no special steps to guard against hydrogen loss were taken. Such design steps would be taken for operating life times of more than 4000 hours.

Even with such high hydrogen losses, the time limited operation due to loss in reactivity exceeded two years. This time is substantially greater than the time for complete depletion of the cesium reserve. A portion of the hydrogen escaping from the core entered the interelectrode gaps in the electric generating channels. The appearance of hydrogen in the interelectrode gap during ground testing was identified in 250-300 hours after testing began.

Analysis of the results of prototype flight testing together with ground-based power test results showed that there was a sufficiently clear link between the rate of reactivity changes, the reactor thermal power and the coolant temperature at the reactor core exit.

An evaluation of hydrogen pressure in electric generating channel interelectrode gaps was carried out based on experimental data on changes in reactivity during prototype flight testing and ground testing.

Investigations of the influence of hydrogen on the electrical characteristics of the thermionic converter showed that this influence can be explained by the following:

a. An increase in plasma losses due to energy transfer by the vibration level of the hydrogen molecule;

b. An increase in the recombination coefficient and an increase in the cesium atom ionization coefficients;

c. An increase in the thermal conductance of the interelectrode gaps in the electric generating channels.

The possibility of chemical reactions of hydrogen cannot be ruled out, for example, reactions with carbon monoxide that produce hydrocarbons can lead to changes in the radiation and emissive properties of the electrodes.

At 67-133 Pa hydrogen pressures in the interelectrode gaps of the electric generating channels, the effect of these factors is entirely sufficient to explain the degradation in electrical characteristics observed during flight prototype testing and in ground tests. On the average, this degradation showed up as a decrease in the original conversion efficiency at a rate of $5\text{-}7 \times 10^{-4}$ %/hr.

Analysis of telemetry data obtained during the flight prototype tests showed that the parameters of all basic systems of the nuclear power plant (the cesium system, the heat rejection system, the automatic control system) agreed with required values and remained stable during the entire test period. The nature of thermal, hydraulic and electrical processes in the nuclear power plant was virtually the same in the flight prototype tests as in the ground tests. Especially noteworthy is the operating ability of the cesium vapor supply system. Filling the interelectrode gaps upon opening the vapor generator, maintaining a given temperature in the cold zone of the generator, transitioning from one temperature to another, and depleting the cesium reserves in the generator were processes during flight prototype testing which were fundamentally identical to those observed in the ground power tests. The temperatures of components and subassemblies during flight test conditions were found to be in good agreement with the reactor thermal power and with test stand data.

The cesium vapor generator temperature mode selected provided fine tuning of the anticipated optimum pressures for the output and pump sections of the reactor.

The automatic control system maintained the current accurately while functioning through the current channel and maintained the coolant temperature accurately at the reactor exit while functioning through the temperature channel. The cesium vapor generator temperature was also accurately maintained.

This leads to the conclusion that space conditions exert no noticeable influence on the operating capability of nuclear power plants and on their characteristics.

The flight prototype test program was carried out to completion with both nuclear power plant models. The results obtained verified the validity of the design decisions made and of the control algorithms used in all operating modes. The results validated that the output parameters and the nature of basic processes during flight testing agreed with those observed during ground testing and that the reactor and the systems servicing it operated stably under space conditions. Thus, the operating capability and high effectiveness of nuclear power plants with thermionic converters have to all practical purposes substantiated their use in resolving problems in space both in the near and foreseeable future.

12. FORMING A RATIONAL NUCLEAR POWER PLANT DESIGN

12.1. Features in the Design of Nuclear Power Plants.

A distinctive feature of nuclear power plants compared with other types of autonomous (space) power plants is the need to provide radiation safety to the consumers of electric energy, i.e. the spacecraft payload systems.

Another characteristic of nuclear power plants, as their practical development demonstrates, is that the design and development of flight power plant models require a significant expenditure of real time (10 and more years). In other words, the nuclear power plant is always the "time consuming" element in space power development. For this reason, in the advanced design phase it is very difficult to produce a sound requirement for the quality characteristics of the nuclear power plant.

Important properties of a nuclear power plant are: output, reliability (dependability), operating life and safety. They correspond to such characteristic qualities of the nuclear power plant as generated electrical power, dependable duration of operation, in-flight mass, and the magnitude of the neutron and γ radiation flux beyond the radiation shield.

The required electrical power and the duration of its generation as well as the allowable radiation flux are determined by the kinds of spacecraft payloads and their properties. The spacecraft payloads are designed and developed simultaneously ("in parallel") with the development of the nuclear power plant. The allowable mass of the nuclear power plant, i.e. the mass which can be identified as the fraction it will occupy on the spacecraft, is determined by the launch capability of the rocket. This is again developed or improved in "parallel" with the development of the nuclear power plant, and it depends on the mass of the payloads and other required spacecraft systems, which are also undergoing development or improvement.

This means that in the advanced nuclear power plant design stage it is in principal impossible to describe accurately its quantitative requirements. In an objective sense, they can only be described probabilistically. One needs to make responsible design solutions with a priori uncertainties in the initial data.

The problem in designing a nuclear power plant with uncertainties in the initial data is closely tied to the problem of the universality of a nuclear power plant, i.e. the problem of developing an all-purpose power plant which is capable of successfully supplying electrical power to a broad class of consumers. Onboard consumers can differ substantially in power and in the duration of the power requirement as well as in the allowable integrated radiation dose, which is not the same, for example, for unmanned and manned spacecraft. It is obvious for economic reasons that each kind of consumer cannot be provided with its own optimum nuclear power plant. It is basically necessary to design a single power plant (in the extreme case, two or three) capable of adequately serving all consumers of a given class.

In order to solve the problem of an all-purpose nuclear power plant one needs to estimate the consumer requirements in advance of actual data. Thus, in order to solve the nuclear power plant design problem with uncertainties in the initial data, a probabilistic description of the power plant requirements is needed. We know that with an unlimited

333

number of tests the frequency of occurrence of some event will coincide with its probability of occurrence. Objectively, several atypical consumers will exist in the all-purpose nuclear power plant problem. In the problem of designing a nuclear power plant with uncertainties the power plant is intended for servicing consumers of one kind, but the characteristics of this kind is not accurately known a priori. It is obvious that with a sufficiently large total number of consumers the uncertainty in the characteristics of a consumer can be interpreted as the a priori uncertainty of its kind. Therefore, despite the substantive differences in the all-purpose nuclear power plant design problem and the problem of designing a nuclear power plant with a priori uncertainties in the initial data, identical formal (mathematical) methods can be used in their solution.

12.2 Substantive Statement of the Problem.

The nuclear power plant is intended to supply electrical power to the spacecraft payloads for a prescribed time period. Consequently, the functional requirements on the nuclear power plant can be formulated in the following manner. The output electrical power, $\dot{Q}_e$, of the power plant should be equal to the power, $\dot{Q}_{e,pl}$, required by the payloads:

$$\dot{Q}_e = \dot{Q}_{e,pl} \qquad . \qquad\qquad (12.1)$$

and the duration, τ_{op}, of trouble-free operation should not be less than the time, τ_{pl}, of the active functioning of the payloads:

$$\tau_{op} \geq \tau_{pl} \qquad\qquad (12.2)$$

As a rule, the consumers require a specific quality (voltage) of electric power. Therefore, the output voltage, V_o, developed by the nuclear power plant should agree with the voltage, V_{pl}, required by the payloads:

$$V_o = V_{pl} \qquad\qquad (12.3)$$

Special shielding is needed to provide payload radiation safety. Its characteristics should be chosen such that the γ radiation dose, D_γ [MeV/m²], and the neutron radiation dose, D_n [neutrons/m²], that the payloads receive during a time of nuclear power plant operation will not exceed the allowable doses, $D_{a,\gamma}$ and $D_{a,n}$:

$$D_\gamma\left(\tau_{pl}\right) \leq D_{a,\gamma} \quad ; D_n\left(\tau_{pl}\right) \leq D_{a,n} \qquad . \qquad\qquad (12.4)$$

The total mass of the nuclear power plant, M_{pp}, should not exceed the allowable value, $M_{a,pp}$:

$$M_{pp} \leq M_{a,pp} \qquad . \qquad\qquad (12.5)$$

In addition to the above, other requirements should be placed on the nuclear power plant, for example, limitations on the cost and duration of its development and fabrication, and limitations on the maximum dimensions of the power plant. In this study we will limit our discussion to the above requirements since, despite their incompleteness, they will permit us to adequately demonstrate the methods employed in the complex approach to forming a rational nuclear power plant design.

Obviously, the common objective in developing and using a nuclear power plant is attained only when the combination of functional (12.1) - (12.3) and technical/operational (12.4)-(12.5) requirements are fulfilled simultaneously. The problem that arises is in selecting the optimum parameters of the nuclear power plant and the best way (in a certain sense) to attain the stated objective.

12.3. A Systems Engineering Mathematical Model of a Nuclear Power Plant.

The systems engineering mathematical model of a nuclear power plant should establish objectively the existing interrelationships between its qualitative characteristics, i.e. the left side of equations (12.1) - (12.5). In order to develop this model, we will avoid the approach to designing a single purpose (narrowly specialized) nuclear power plant in which, based on a priori accurately known power plant requirements, all power plant parameters are uniquely determined, both design and mode parameters. The calculation of each mode parameter, for example, specific power output, coolant flow rate, temperature, precede the calculation of the design parameters, i.e., the geometric and mass characteristics of the nuclear power plant components.

We will assume that the nuclear power plant has been designed and fabricated, i.e., its design parameters have been chosen. Whether this choice was the right one will remain open to question. For the same design parameters, one can realize different combinations of mode parameters in a nuclear power plant through appropriate adjustments (control), certainly within the limits set by the design parameters chosen. The main purpose of system engineering and mathematical modeling is to obtain a description of the most significant interrelationships that exist between the nuclear power plant mode parameters with fixed design parameters.

By way of example, we will discuss the mathematical modeling of a most promising nuclear power plant, the in-core nuclear thermionic power plant, i.e. a power plant in which the source of heat and the converters make up a single assembly called the reactor.

The components of the in-core thermionic nuclear power plant are, in addition to the reactor: the space radiator, the electromagnetic pump and the radiation shield. We will assume that the payload and the electromagnetic pump are connected in parallel to the reactor in the electrical circuit.

The output electrical power, $\dot{Q}_e$, of the nuclear power plant is equal to the difference in power generated by the reactor and the power used by the electromagnetic pump:

$$\dot{Q}_e = \dot{Q}_{e,gen} - \dot{Q}_{e,emp} \qquad . \qquad (12.6)$$

A most important mathematical description of a specific reactor is its control characteristics which is established by its generated electrical power, $\dot{Q}_{e,gen}$, as a function of the required (high temperature) thermal power, $\dot{Q}_t$, the temperature of the coolant at the inlet, T_{ci}, and at the outlet, T_{co}, from the converter, the voltage, V_o, at the load and the pressure, p_{Cs}, of the cesium working fluid in the interelectrode gap:

$$Q_{e,gen} = f_Q(Q_t, T_{ci}, T_{co}, V_o, p_{Cs})$$ (12.7)

Wide control of the electrical power generated by the reactor, $Q_{e,gen}$, allowing it to be increased by a factor of 10 for short durations, can be accomplished by changing the thermal power liberated, Q_t, using rotating control drums or segments located in the side reflector. Fine control (for a fixed value of Q_t) is provided by changing the heat rejection conditions (T_{ci} and T_{co}), the parameters of the electrical circuit, V_o, and the interelectrode plasma, p_{Cs}.

The operating life of a high temperature nuclear power plant is determined principally by the duration of trouble-free operation of the reactor. This is a monotonically decreasing function of the maximum temperature, $T_{e,max}$, of the emitter, which is the most thermally stressed component in the power plant. Consequently,

$$\tau_{op} = f_\tau(T_{e,max}) \quad ; \quad \frac{d\tau}{dT_{e,max}} < 0$$ (12.8)

The maximum emitter temperature, $T_{e,max}$, in the reactor depends on the same parameters that determine its generated electrical power:

$$T_{e,max} = f_T(Q_t, T_{ci}, T_{co}, V_o, p_{Cs})$$ (12.9)

The thermal power of the reactor is

$$\dot{Q}_t = \dot{Q}''' V_f n_{TFE}$$

where $\dot{Q}'''$ is the average volume density of heat liberation in the fuel core; V_f is the volume of the fuel core in a single TFE, and n_{TFE} is the number of TFEs in the core.

The volume density of heat liberation should not exceed some maximum allowable value:

$$\dot{Q}''' < \dot{Q}'''_{max}$$

therefore, the reactor thermal power is limited:

$$\dot{Q}_t < \dot{Q}_{t,max} \quad ; \quad \dot{Q}_{t,max} = \dot{Q}'''_{max} V_f n_{TFE}$$ (12.10)

The pressure, p_{Cs}, of the interelectrode gap filler can be changed only within some range:

$$p_{Cs,min} \leq p_{Cs} \leq p_{Cs,max} \qquad \cdot \qquad (12.11)$$

The waste heat,

$$\dot{Q}_{rad} = \dot{Q}_t - \dot{Q}_e \qquad (12.12)$$

is rejected to surrounding space by the radiator.

The influence of external heat flows from celestial bodies on the space radiator must not be neglected. In this situation, the following approximate equation applies to the rejection of thermal power to surrounding space by the space radiator:

$$\dot{Q}_{rad} = \sigma \varepsilon_{rad} \alpha_{rad} v_t A_{rad} T_{rad}^4 \quad ; \qquad v_t = \frac{3t^3}{1+t+t^2} \qquad ; \qquad (12.13)$$

$$t = T_{ci}/T_{co}; \qquad \cdot \qquad (12.14)$$

A_{rad} is the surface area of the space radiator; $v_t < 1$ is a factor that accounts for the coolant temperature drop along the length of the space radiator; $\alpha_{rad} < 1$ is a temperature distribution nonuniformity factor that accounts for the nonuniform radiator surface temperature along the width of the space radiator and its difference (on the decreasing side) from the coolant temperature; ε_{rad} is the emissivity of the space radiator; and σ is the Stefan-Boltzmann constant.

The temperature distribution nonuniformity factor, α_{rad}, is convenient in that it is determined by the materials and geometric characteristics of the space radiator. It is virtually independent of the coolant temperature in high temperature radiators.

The thermal power, $\dot{Q}_{rad}$, transferred from the reactor to the space radiator is proportional to the coolant flow rate, $\dot{M}_c$:

$$\dot{Q}_{rad} = \dot{M}_c \bar{c}_p (T_{co} - T_{ci}) \qquad , \qquad (12.15)$$

where $\bar{c}_p$ is the average coolant heat capacity in the temperature range from T_{ci} to T_{co}.

Equations (12.13) through (12.15) establish an implicit relationship between the coolant temperature at the inlet, T_{ci}, and the outlet, T_{co}, of the reactor and the space radiator area, A_{rad}, the thermal power, $\dot{Q}_{rad}$, rejected by it, and the coolant flow rate, $\dot{M}_c$:

$$T_{ci} = T_{ci}\left(A_{rad}, \dot{Q}_{rad}, \dot{M}_c\right) \quad ; \qquad T_{co} = T_{co}\left(A_{rad}, \dot{Q}_{rad}, \dot{M}_c\right) \qquad (12.16)$$

The electrical power, $\dot{Q}_{e,emp}$, required by the electromagnetic pump is determined by the coolant flow rate, $\dot{M}_c$:

$$\dot{Q}_{e,emp} = \dot{Q}_{e,emp}(\dot{M}_c) \tag{12.17}$$

$$\dot{M} \le \dot{M}_{max} \tag{12.18}$$

where $\dot{m}_{max}$ is the maximum possible output of the electromagnetic pump.

Equation (12.12) for the unused thermal power takes the following form when (12.6) and (12.17) are taken into account:

$$\dot{Q}_{rad} = \dot{Q}_t - \dot{Q}_{e,gen} + \dot{Q}_{e,emp}(\dot{M}_c) \tag{12.19}$$

By taking (12.19) into account, equation (12.16) can be written differently:

$$T_{ci} = T_{ci}\left(A_{rad}, \dot{Q}_t, \dot{Q}_{e,gen,}\dot{M}_c\right) \quad ; \quad T_{co} = T_{co}\left(A_{rad}, \dot{Q}_t, \dot{Q}_{e,gen}, \dot{M}_c\right) . \tag{12.20}$$

By combining (12.6), (12.7), (12.17) and (12.20), we obtain the expression for the control characteristics of the nuclear power plant as a whole:

$$\dot{Q}_e = f_Q\left(\dot{Q}_t, T_{ci}\left(A_{rad}, \dot{Q}_t, \dot{Q}_{e,gen}, \dot{M}_c\right), T_{co}\left(A_{rad}, \dot{Q}_t, \dot{Q}_{e,gen}, \dot{M}_c\right), V_o, p_{Cs}\right) - \dot{Q}_{e,emp}(\dot{M}_c) . \tag{12.21}$$

where $\dot{Q}_t$, p_{Cs} and $\dot{M}_c$ must satisfy the limits in (12.10), (12.11) and (12.18).

Equation (21) determines implicitly the output electrical power, Q_e, of the nuclear power plant as a function of the thermal power, Q_t, of the reactor, the surface area, A_{rad}, of the space radiator, the flow rate, $\dot{m}$, of the coolant through the electromagnetic pump, the voltage, V_o, at the load and the pressure, p_{Cs}, of the filler in the interelectrode gap:

$$\dot{Q}_e = f_Q\left(\dot{Q}_t, A_{rad}, \dot{M}_c, V_o, p_{Cs}\right) \tag{12.22}$$

Taking (20) into account, equation (9) takes the following form:

$$T_{e,max} = f_T\left(\dot{Q}_t, A_{rad}, \dot{M}_c, V_o, p_{Cs}\right) . \tag{12.23}$$

The design and fabrication of the nuclear power plant is characterized entirely by a specific set of "inflexible" design parameters, which cannot be changed quickly before their use. The nuclear power plant design parameters include: the design thermal power of the reactor, the design flow capacity of the electromagnetic pump, and the surface area, of the space radiator. Control of the output electrical power of the nuclear power plant can be accomplished by changing the "flexible" mode parameters: the actual thermal power of the reactor, the actual flow rate of the coolant, the voltage at the load and the pressure p_{Cs} of the cesium reservoir. Thus, the nuclear power plant as an object of control has in

338

principle four degrees of freedom. If the consumer needs electrical power of a certain specified voltage, the nuclear power plant has but three degrees of freedom.

With any changes in mode parameters ($\dot{Q}_t$, $\dot{M}_c$ and p_{Cs}) simultaneously with changes in the output electrical power of the nuclear power plant, the maximum temperature of the emitter $T_{e,max}$ will change in accordance with (23) and, consequently, the predicted duration, τ_{op}, of trouble-free operation of the power plant will change. Common sense shows that with other conditions being the same, it is advisable to adjust the nuclear power plant before its use such that emitter temperature is minimized.

We will designate $\vec{X} = \langle \dot{Q}_t, \dot{m}, p_{Cs} \rangle$ as the mode parameter control (regulation) vector and $\{X^a\}$ as the product of the allowable values of the mode parameters that are described by equations (12.10), (12.11), (12.18) and (12.22):

$$\{X^a\} = \left\{ \begin{array}{l} \dot{Q}_t < \dot{Q}_{t,max}; \ p_{Cs,min} \leq p_{Cs} \leq p_{Cs,max}; \ \dot{M}_c \leq \dot{M}_{cmax} \\ \dot{Q}_e = f_Q\left(\dot{Q}_t, A_{rad}, \dot{M}_c, V_o, p_{Cs}\right) \end{array} \right\} \tag{12.24}$$

Equation (23) will then take on the following form:

$$T_{e,max} = f_T\left(\vec{X}, A_{rad}, V_o, \dot{Q}_e\right) \tag{12.25}$$

The problem of optimum control (regulation) of the nuclear power plant prior to its use consists in finding a value of the mode parameter vector X from the product (12.24) of the allowables such that it will result in a minimum value of the function (12.25):

$$\vec{X}_* = \vec{X}_*(A_{rad}, V_o, \dot{Q}_e) = \text{Arg min } f_T\left(\vec{X}, A_{rad}, V_o, \dot{Q}_e\right); \quad \vec{X} \in \{X^a\} . \tag{12.26}$$

$$\left(T_{e,max}\right)_{min} = f_T\left(\vec{X}_*, A_{rad}, V_o, \dot{Q}_e\right) \tag{12.27}$$

It is obvious that the maximum allowable value of the output electrical power, $Q_{e,max}$, of the nuclear power plant is attained for $\dot{Q}_t = \dot{Q}_{t,max}$ and the corresponding optimum mode parameters $\dot{Q}_t$ and p_{Cs}:

$$Q_{e,max} = \text{max}\left\{ f_Q\left(Q_t, A_{rad}, \dot{m}, V_o, p_{Cs}\right) \right\}$$

Consequently, equations (12.26) and (12.27) have solutions only for $Q_e \leq Q_{e,max}$.

The above analysis has permitted the establishment of a sufficiently complex interrelationship between the left sides of the equations, (12.1) to (12.3). In accordance with (12.8) and (12.27), an optimally tuned nuclear power plant can generate electrical power, N_{np}, at a voltage, V_{np}, for the period of time

$$\tau_{op} = f_\tau \left(\left(T_{e,max} \right)_{min} \right) = f_\tau \left(f_T \left(\bar{X}_* \left(A_{rad}, V_o, \dot{Q}_e \right), A_{rad}, V_o, \dot{Q}_e \right) \right) \quad .$$

Let's turn to an analysis of the left side of the inequalities (12.4) and (12.5).

The γ radiation, D_γ, and neutron radiation, D_n, doses imparted to the payload are directly proportional to the duration, τ_{op}, of trouble-free nuclear power plant operation:

$$D_\gamma \left(\tau_{op} \right) = J\tau_{op} \quad ; \qquad D_n \left(\tau_{op} \right) = \phi\tau_{op} \qquad , \qquad (12.28)$$

where J and ϕ are the intensity of γ radiation and the neutron flux density at the payload surface closest to the nuclear power plant.

J and ϕ are proportional to the intensity J_o of γ radiation and neutron flux density ϕ_o at the reactor core surface and decrease with an increasing thickness (δ_n and δ_γ) of the neutron and γ shield. If the payload is separated from the center of the reactor core by a distance L that significantly exceeds a radius R_e of an equivalent spherical core, then

$$J = B_{en} J_o \frac{R_e^2}{L^2} \left(1 - \frac{R_e}{L} \right) \exp\left(-\mu_n \delta_n - \mu_\gamma \delta_\gamma \right) \qquad , \qquad (12.29)$$

$$\phi = \phi_o \frac{R_e^2}{L^2} \left(1 - \frac{R_e}{L} \right) \exp\left(-\sigma_n \delta_n - \sigma_\gamma \delta_\gamma \right) \qquad , \qquad (12.30)$$

where $B_{en} > 1$ is an energy accumulation or buildup factor, which accounts for scattering of γ quanta; μ_γ and μ_n are linear attenuation coefficients of γ quanta by neutron and gamma shield materials; σ_γ and σ_n are exposure cross sections of neutron and gamma shield materials.

The γ radiation intensity J_o and the neutron flux density ϕ_o at the core surface are directly proportional to the reactor thermal power, $\dot{Q}_t$:

$$J_o = \frac{\alpha_\gamma \dot{Q}_t}{2\mu_\Sigma V_e} \left[1 - \frac{1}{2\mu_\Sigma R_e} \left(1 - e^{-2\mu_\Sigma R_e} \right) \right] \qquad , \qquad (12.31)$$

$$\phi_o = \frac{\alpha_n \dot{Q}_t}{A_e} \left(1 - e^{-B^2 \tau} \right) \qquad , \qquad (12.32)$$

where $\alpha_\gamma = 38.75 \times 10^{10}$ (MeV/sec)/W is the specific γ radiation power (the γ radiation power being produced in 1 watt of reactor thermal power); $\alpha_n = 7.7 \times 10^{10}$ (neutron/sec)/W is the specific neutron power (the number of fast neutrons being formed in one second in the reactor core during the liberation of 1 watt of thermal power); μ_Σ is the total γ quanta linear attenuation coefficient for the core materials; τ is the "neutron age" in the moderator material (1/6 the mean square straight line distance through which a

neutron passes during moderation from its point of origin to the point where it becomes thermalized);

$$A_{sph} = 4\pi R_{sph}^2 \quad ; \qquad V_{sph} = \frac{4}{3}\pi R_{sph}^3 = \pi R_{core}^2 H_{core} \qquad , \qquad (12.33)$$

A_{sph} and V_{sph} are the surface area and volume of an equivalent spherical core; R_{core} and H_{core} are the radius and height of the cylindrical core;

$$B^2 = \left(\frac{2.405}{R_{e,core}}\right)^2 + \left(\frac{\pi}{H_{e,az}}\right)^2$$

is the geometric buckling of the reactor as described in Chapter 3; $R_{e,core}$, and $H_{e,core}$ are the effective radius and height of the core,

$$R_{e,core} = R_{core} + \Delta R \quad , \qquad H_{e,core} = H_{core} + 2\Delta H \qquad ,$$

where

$$\Delta R = 1.2l \tanh\left(\frac{\delta_{sref}}{l}\right) \quad , \qquad \Delta H = 1.2l \tanh\left(\frac{\delta_{eref}}{l}\right)$$ are the extrapolated lengths to

the geometric dimensions of the core, l is the diffusion length of thermal neutrons in the reflector material; δ_{sref} is the thickness of the neutron side reflector; δ_{eref} is the thickness of the neutron end reflector and tanh refers to the hyperbolic tangent function. As discussed in Chapter 3, the extrapolated lengths provides a slightly estimate of the neutron flux profile, using the buckling approximation. The extrapolation length approximates helps correct for the discontinuity between the core and neutron reflector.

The regulation of a nuclear power plant to a specific value of output electrical power, $\dot{Q}_e = \dot{Q}_1$, is accompanied by unavoidable changes in both the thermal power $\dot{Q}_t$ of the reactor and in the predicted duration τ_{op} of trouble-free power plant operation. According to equations (12.28)-(12.32), the radiation dose absorbed by the payload will also change. Consequently, the left sides of the inequalities (12.1), (12.2) and (12.4) are interrelated in a complex manner.

In order to establish the interrelationships between the geometric characteristics of the nuclear power plant components and the payload, one must analyze the structural design makeup of the nuclear power plant. For definitive purposes, we will examine an actual structural design which has practical application. The space radiator and both radiation shields of the nuclear power plant are truncated cones with the same cone angle ß. This provides a smooth transition from the cylindrical reactor to the cylindrical payload compartment of radius R_{pl}.

Let's examine the mass of other nuclear power plant components as a function of their design parameters. The mass of the reactor is made up of the mass of the

341

components that form the core and the mass of the reflector assembly with the control units contained in it:

$$m_{reac} = m_{core} + m_{ref} \qquad (12.34)$$

The mass m_{core} of the components that make up the core is proportional to the number of TFEs:

$$m_{core} = (1 + K_{core})n_{TFE}m_{TFE}$$

where m_{TFE} is the mass of the TFE; K_{core} is an empirical factor that accounts for the mass of additional core components (coolant, TFE grid fasteners, etc.).

The mass of the TFE is a function of several geometric variables, including its length and width:

$$m_{TFE} = m_{TFE}(L, w, ...) \qquad (12.35)$$

The mass m_{ref} of the side reflector with the control units contained in it is roughly proportional to its thickness δ_{ref} and the lateral surface area A_{core} of the core:

$$m_{ref} = (1 + K)\rho_{ref}\delta_{ref}A_{core} \quad ; \qquad A_{core} = 2\pi R_{core}H_{reac}$$

where ρ_{ref} is the density of the side reflector material; and K is an empirical factor that accounts for the additional mass of the control units and the structural components.

The mass m_{rad} of the space radiator is approximately proportional to its radiating surface area, A_{rad}:

$$m_{rad} = m'' A_{rad}$$

where m'' is the specific mass of the space radiator.

The mass m_{emp} of the electromagnetic pump is a monotonically increasing function of its design (operational) hydraulic power, $\dot{Q}_{h,max,emp}$:

$$M_{emp} = \Psi(\dot{Q}_{h,max,emp}) \qquad (12.36)$$

The actual hydraulic power $\dot{Q}_{h,emp}$ of the electromagnetic pump is a directly controlled parameter which must satisfy the condition

$$\dot{Q}_{h,emp} \leq \dot{Q}_{h,emp,max} \qquad (12.37)$$

and is determined in the following manner:

$$\dot{Q}_{h,emp} = \frac{\Delta p \dot{M}_c}{\rho_c} \quad ; \qquad \Delta p = \chi \dot{M}_c{}^2 \quad ; \qquad \chi = \chi_{reac} + \chi_{rad} \qquad (12.38)$$

where Δp is the hydraulic pressure difference developed by the electromagnetic pump; ρ_c is the coolant density; χ_{reac} and χ_{rad} are factors that characterize the coolant pressure losses in the reactor and space radiator.

The electrical power $\dot{Q}_{e,emp}$ required by the electromagnetic pump is proportional to the hydraulic power:

$$\dot{Q}_{h,emp} = \eta_{emp} \dot{Q}_{e,emp}$$

where η_{emp} is the electromagnetic pump efficiency.

By combining (12.37) and (12.38), we obtain

$$\dot{Q}_{h,emp} = \frac{\chi \dot{M}_c^3}{\rho_c} \leq \dot{Q}_{h,emp,max} \quad ; \qquad \text{or} \quad \dot{M}_c = \left(\frac{\rho_c \dot{Q}_{h,emp}}{\chi} \right)^{1/3} \qquad (12.39)$$

By equating (12.18) and (12.39), we come to the conclusion that

$$\dot{M}_{c,max} = \left(\frac{\rho_c \dot{Q}_{h,emp}}{\chi} \right)^{1/3}$$

When equation (12.39) is taken into account, the expression for $\dot{Q}_{h,emp}$ takes the following form:

$$\dot{M}_{c,max} = \left(\frac{\rho_c \dot{Q}_{h,emp,max}}{\chi} \right)^{1/3}$$

The electrical power $\dot{Q}_{e,emp}$ required by the electromagnetic pump is proportional to the cube of the coolant flow rate $\dot{m}$. For this reason, with $\dot{Q}_1 \ll \dot{Q}_{e,emp,max}$ the limiting of the coolant flow rate will involve a substantial reduction in power $\dot{Q}_{e,emp}$ which can be advantageous from the point of view of increasing the duration τ_{op} of trouble-free nuclear power plant operation.

The total mass of the nuclear power plant is the sum of the masses of the reactor, space radiator, radiation shields and the electromagnetic pump:

$$m_{pp} = m_{reactor} + m_{core} + m_{rad} + m_{shield} + m_{emp}$$

The maximum allowable mass $M_{pp,max}$ of the nuclear power plant is determined by the equation:

$$m_{pp,max} = m_{launch} - m_{pl} - m_{subsys}$$

where m_{launch} is the launch capacity of the rocket vehicle which is to place the spacecraft with the nuclear power plant in the operational orbit; m_{pl} is the mass of the spacecraft payload system; m_{subsys} is the mass of other required spacecraft systems.

Among the numerous design parameters of the nuclear power plant components, only some are independent. Apart from the TFE geometric characteristics, the following will be assumed as independent design parameters of the reactor: the number of concentric rings of TFEs within the core, n_{TFE}, the grid spacing x, the thicknesses of the side and end neutron reflectors. We can consider the following as independent design parameters of the remaining nuclear power plant components: the thicknesses (δ_n and δ_γ) of the shield layers, the length L_{rad} of the space radiator, the maximum hydraulic power $\dot{Q}_{h,emp,max}$ of the electromagnetic pump. Thus, the vector of the independent nuclear power plant design parameters is

$$\vec{Y} = \left\langle n_{TFE}, x_T \delta_{eref}, \delta_{sref}, \delta_n, \delta_\gamma, \dot{Q}_{h,emp,max} \right\rangle$$

In order to continue investigating the mathematical model of a nuclear power plant, one must classify data (factors, parameters) that figure in the criteria for its applicability.

12.4. Information Classification.

The data relevant to the nuclear power plant being investigated are divided into external and internal data. The external data pertains invariably to the technical aspects (structure and parameters) of the system. In other words, the factors that characterize external data can be determined in the complete absence of data on nuclear power plant design aspects. The following pertains to external data in the present problem: electrical power $\dot{Q}_{e,req}$ and voltage V_{pl} required by the payload, duration τ_{op} of active payload operation; the maximum allowable γ radiation, $D_{\gamma,max}$, and neutron radiation, $D_{n,max}$, doses; the launch capacity, m_{launch}, of the rocket vehicle; the mass of the payload system m_{pl} and the total mass, m_{subsys}, of other required spacecraft systems.

All remaining data pertain to internal data: data on the structure of the nuclear power plant, its structural assembly and the parameters of individual power plant components.

Depending on the research task (relevant to the nuclear power plant design), the data is subdivided into basic (known) and desired (unknown) data. External data are, as a rule, always known and represents factors that the designer has no control over. Internal known data form the Designer. To this pertain the nomenclature of competing space power components, the materials used in them and the allowable or envisioned characteristics resulting from design improvements to components (functional relationships or specific parameters) that are not the subject of a systems engineering study.

344

The materials used in the problem under consideration will not be specified. Therefore, the internal known data, apart from the nuclear power plant structure chosen, consists of the functional relationships for the reactor (12.7)-(12.9), radiation shielding parameters, space radiator parameters; coolant parameters and so forth.

The desired or unknown data consists of controlled reactions (parameters or functions) which can be managed (regulated) by the Designer in solving the problem of integrating a rational nuclear power plant design. In the general case, the Designer will first of all strive to select from the numerous competing space power components the necessary optimum subset of components, i.e., to accomplish a nuclear power plant design optimization. Therefore, the desired or unknown data are primarily a judgment regarding the rational design of the nuclear power plant. In addition, within the framework of a given design the Designer should select the best nuclear power plant design parameters ("rigorously" established in the "internal" design process) which are also desired data. Finally, considering that an engineered system is, as a rule, capable of flexible reactions (adjustment, adaptation) to changes in its configuration and use, the desired data can be the principles of operational control of its individual components or their control parameters (mode parameters).

The necessary condition for the realization of control principles and (or) making adjustments is the possibility of obtaining additional data on changes in system configuration and use. If such (current) data is absent, any control principle or form of adjustment cannot be realized. A sufficient condition for control is the presence in the system of control units that require additional physical (material) expenditures. An adaptable system is therefore more resourceful.

In the problem under consideration the structure and component assembly design of the nuclear power plant has been presented heuristically. The identification of the design and mode parameters of the nuclear power plant was accomplished above during the development of its mathematical model.

During the time of entry, the data can be conditionally subdivided into a priori and current data. A priori data are data which is available to the Designer and which is pertinent in solving the problem of an optimum "external" design of the nuclear power plant. Current data are information on changes in conditions relevant to system configuration and operation. These data can be found, respectively, only in its "internal" design processes and from its intended use. The possibility of obtaining current data and its useful application is established in comprehensive studies. In the nuclear power plant "external" design process, the Designer has only a priori data available. The actual possibility (or impossibility) of obtaining and using additional data later on must be reflected without fail in the mathematical modeling of operations in making and using the nuclear power plant (in the criteria for its applicability in achieving the intended objectives). Accounting (or lack of accounting) for this circumstance can influence significantly the decision on the optimum nuclear power plant configuration.

We must emphasize that a priori and current data constitute information on one and the same factors. A priori data are knowledge of the range of possible changes (the law of probability distribution) in a wittingly unknown (contingent) factor; current data are knowledge of the value this factor will assume in a given actual event.

Factors determined by a priori data are assumed to be subdivided into determinate (uniquely determined), contingent (conjecturally determined) and indeterminate factors. An indeterminate factor is one for which only the region of its possible values is reliably known, and information on the frequency at which this factor will take on one or another value from the given region is lacking.

In the problem of forming a rational nuclear power plant design all the external input data is a priori contingent data. The greater portion of internal input data is a priori contingent data. Exceptions are the physical constants such as the Stefan-Boltzmann constant and the specific power of γ radiation and neutron radiation, and the physical-technical constants which uniquely characterize the materials being used (density, heat capacity, linear coefficient of attenuation of γ quanta, exposure cross section, and so on).

The contingency of the functional relationships (12.7) - (12.9), (12.35) and (12.36) that enter into the mathematical model of the nuclear power plant is interpreted in the following manner. The result of computing a function for fixed values of its arguments is a mathematical expectancy of its true value which is a priori contingent. Analysis of statistical data or results of expert inquiry allows one to evaluate the variation factor for this contingent value and come up with a hypothesis of its simplest (two-parameter) law of distribution.

The data classification presented, which figures in the nuclear power plant suitability criteria, is shown in a conditional diagram in Fig. 12.2.

APPENDIX A. VARIABLE LIST AND RUSSIAN COUNTERPART

English	Russian	Meaning plus typical units.
A	A	Total number of nucleons, dimensionless.
A	A	Richardson constant, 120 A/cm²K.
A_b	$S_в$	Cross sectional area of thermoelement branch, cm².
A_{eq}	$S_{хиэкв}$	Equivalent radiator area, m².
A_{flow}	$S_{\Sigma т}$	Cross sectional flow area, m².
A_{fuel}	$S_{\Sigma твэл}$	Sum of surface area of fuel cladding, m².
A_{holes}	$S_{\Sigma отв}$	Area of holes in support grid, m².
A_{sph}	$S_{эк}$	Surface area of an equivalent spherical reactor, cm².
A_{stab}	$Z_{стаб}$	Most stable number of nucleons.
B_{en}	$B_{эн}$	Energy buildup factor, dimensionless.
B_g	$B_г$	Geometric "buckling" factor, cm⁻².
B_l	B_l	Creep factor, sec⁻¹.
B^2	B^2	Reactor "buckling" paramter, cm⁻².
$B^2_{g,crit}$	$B^2_{г.кр}$	Critical reactor geometric "buckling," cm⁻².
c	C	Speed of light 2.998 x 10⁸ m/sec.
c	c	Fin conductance parameter, dimensionless.
$\bar{c}_p$	$\bar{c}$	Specific heat, W/kgK.
c_{vent}	$c_{уд}$	Mass divided by energy content, kg/kWhr.
C	C	Collision rate (sec⁻¹).
d_{fuel}	$d_{твэл}$	Diameter of fuel element, cm.
D	D	Rigidity, Nm.
D	D	Diffusion coefficient (used with φ), centimeters.
D		Diamter of a cylindrical reactor core, cm.
D_i	$D_{к.вн}$	Internal channel diameter, cm.
D_n	D_n	Neutron dose, neutrons/m².
D_o	$D_к$	Outer channel diameter, cm.
D_o	D_o	Diffusion coefficient (used with N_n), cm.
D_γ	D_γ	Gamma ray dose, MeV/m².
E	E	Energy, J.
E	E	Thermal electromotive force, V.
E	E	Modulus, Pa.
E_{ac}	$E_{ак}$	Activation energy, MeV.
E_b	$E_{св}$	Nuclear binding energy, MeV.
E_d	$E_{д.я}$	Energy of daughter nucleus, MeV.
$E_{d,tot}$	$E_{р.пол}$	Total decay energy, W or MeV.
E_f	g_f	Fission energy which is converted to heat, J.
E_f	E_0	Fermi energy, eV.
E_i	E_i	Ionization potential, eV.
E_{is}	$E_{из}$	Isotopic Energy, MeV.
E_{na}	$E_{я.пр}$	Energy of nuclear attraction, MeV.
E_{pair}	$E_{ч.н.}$	Pairing energy, MeV.

Symbol	Symbol (Russian)	Definition
$E_{release}$	$E_{\text{выд}}$	Energy release from fission, MeV.
E_{rep}	$E_{\text{эл.от.}}$	Coulomb energy of repulsion, MeV.
$E_{\alpha d}$	$E_{\alpha p}$	Energy of alpha decay, MeV.
E_{α}	E_{α}	Energy of alpha particle within nucleus, MeV.
E_1, E_2	E_1, E_2	Neutron energies before and after the collision, respectively; usually MeV.
ΔE_{max}	ΔE_{max}	Maximum energy loss in a single collision, MeV.
E_s	E_c	Total density of solar Radiation, W/m^2
$E_{\beta d}$	$E_{\beta \rho}$	Energy of beta decay, MeV.
$E_{\beta tot}$	$E_{\beta\text{р.пол}}$	Total (useful) energy of beta decay, MeV.
$E_{ke}^{''}$,	$E_{\text{уд}}$	Specific particle kinetic energy, Jkg/sec^{-2}.
f	f	Particle flux density, kg/cm^2, and v the average impact velocity, m/sec).
f	f	Non 1/v factor, dimensionless.
f	θ	Thermal neutron utilization, dimensionless.
h	$\bar{\alpha}$	Newton's cooling coefficient, W/m^{2}K.
h	h	Planck's constant, 6.626 x 10^{-34} J-sec.
H	H_p	Height of a fin, cm.
H, H_{core}	$H_a, H_{\text{аз}}$	Height (actual) of a cylindrical reactor core, cm.
H_e	$H_{\text{эк}}$	Extrapoloated height of a cylindrical reactor core, cm.
ΔH	ΔH	Extrapolation distance (height) for a reactor core, cm.
I	I	Current, amps.
I	I	neutron flux intensity sec^{-1}cm^{-2}.
I	I	Resonance Integral, cm^2.
I	I	Current, amps.
I_{sc}	$I_{\text{к.з}}$	Maximum (short circuit) current in a thermoelement, amps.
J	J_n	Neutron current, n/cm^{2}sec.
J	J	Intensity of gamma radiation, MeV/m^{2}sec.
J_o	J_o	Gamma ray intensity, MeV/cm^{2}sec.
$J_i^{''}$	j_i	Ion current density, Amp/cm^2.
$J^{''}$	j	Electron emission current density, Amp/cm^2.
$J_c^{''}$	j_a	Collector emission current density, Amp/cm^2.
$J_{cs}^{''}$	j_{as}	Collector saturation current density, Amp/cm^2.
$J_e^{''}$	$j_{\text{к}}$	Emitter current density, Amp/cm^2.
$J_{es}^{''}$	$j_{\text{кs}}$	Emitter saturation current density, Amp/cm^2.
$J_s^{''}$	j_s	Saturation electron current density, Amp/cm^2.
k	k	Boltzmann constant, 8.62 x 10^{-5} eV/K.
k	$\bar{\lambda}$	Thermal conductivity, W/m°C.
k_p	k_p	Coefficient of conicity, dimensionless.
k_{plasma}	$k_{\text{пл}}$	Thermal conductivity of a plasma, W/cm°C.
k_{∞}	k_{∞}	Infinite medium neutron multiplication factor, dimensionless.
K	k	Thermal conductance, W/°C.

K_B	KB	Breeding factor, dimensionless.
K_n	k_n	Thermal conductance of n material, W/$^\circ$C.
K_p	k_p	Thermal conductance of p material, W/$^\circ$C.
Δk_{pois}	$\Delta k_{отр}$	Reactivity change due to "poisoning," dimensionless.
l	l	Neutron diffusion length, cm.
$\bar{l}$	$\bar{l}$	Neutron average lifetime, sec.
$\bar{l}$	$\bar{\lambda}$	Mean free path, cm^{-1}
L	L	Interelectrode space, cm.
L^2	L^2	Neutron diffusion area, cm^2
L_v	L	Latent heat of vaporization, J/kg.
m	$A_{ат}$	Atomic mass, grams
m	$M_{хи}$	Mass of radiator, kg.
m	m	Relative resistance of thermoelement external circuit, dimensionless.
m	m	Mass of meteorite, g.
m_{core}	$M_{аз}$	Reactor core mass, kg.
m_d	$m_{д.я}$	Mass of daughter nucleus, MeV/c^2.
m_e	m_e	Rest mass of electron, MeV/c^2.
m_{emp}	$M_{эн}$	Mass of electromagnetic pump, kg.
m_{fuel}	$m_{твэл}$	Mass of fuel, kg.
m_{grid}	m_p	Mass of support grid, kg.
m_i	$A_{атi}$	Atomic mass of ith element, grams.
m_{launch}	$M_{рн}^{г}$	Launch capacity, kg.
$m_{max\ eff}$	m_η	Relative resistance corresponding to maximum efficiency, dimensionless.
$m_{max\ pwr}$	m_N	Relative resistance corresponding to maximum power, dimensionless.
m_n	m_n	Mass of neutron ~1 atomic mass unit
m_{pl}	$M_{цс}$	Payload mass, kg.
m_{pp}	$M_{эу}$	Mass of power plant, kg.
m_{reac}	$M_{рп}$	Reactor mass, kg.
m_{ref}	$M_{бо}$	Reactor reflector mass, kg.
m_{rad}	$M_{хи}$	Mass of radiator, kg.
m_{shield}	$M_{рз}$	Mass of radiation shield, kg.
m_{subsys}	M_{oc}^{Σ}	Mass of payload subsystems, kg.
m_{te}	m_{te}	Mass of thermoelements, g.
m_π	m_π	Rest mass of π-meson, MeV/c^2.
m''	μ	Radiator specific mass (area), kg/m^2.
M_n	$M_я$	Mass of nucleus, MeV/c^2.
M_{rad}	$M_{рад}$	Mass of radiator, kg.
M_{sp}	$M_{ти.m}, \overline{M}_{ти}$	Radiator specific mass (power), kgm^2/W.
M_{burn}^{235}	$M_{выг}^{5}$	Burnup mass of uranium, kg.
M_{cr}^{235}	$M_{кр}^{5}$	Critical mass of U-235, kg.

Symbol	Russian	Description
M_{ltr}''	$M_{\text{н.т.s}}$	Low temperature radiator mass per unit area, kg/m^2.
$\dot{M}_c$	M_c	Coolant mass flow per second through the core, kg/sec.
n	n	Number of meteorites impacting per unit time on a unit surface, $m^{-2}sec^{-1}$.
n_a	n_a	Number of atoms colliding with electrode surface, dimensionless.
n_c	$n_{\text{ст}}$	Average number of neutron collisions, dimensionless.
n_{cell}	$n_{\text{ед}}$	Number of thermionic cells, dimensionless.
n_e	n_e	Number of electrons present in interelectrode space, dimensionless.
n_i	n_i	Number of ions incident on electrode surface, dimensionless.
n_s	n_c	Number of radiator sections, dimensionless.
n_x, n_y, n_z	n_x, n_y, n_z	Loading (accelearation), measure in g's ($1g = 9.81$ m/sec^2).
N	N	Total number of neutrons, dimensionless.
N_{abs}	$N_{\text{n,погл}}$	Neutron absorption, neutrons/cm^3.
N_A	$A_\text{В}$	Avogadro's number, 6.023×10^{24} atoms/mol.
N_{gen}	$N_{\text{n,обр}}$	Neutron generation, neutrons/cm^3.
N_{leak}	$N_{\text{n,ут}}$	Neutron leakage , neutrons/cm^3.
N_n	$N_\text{я}$	Number of nucleii, nuclei/cm^3.
N_n	ρ_n, N_n	Neutron density, neutrons/cm^3.
$N_{n,i}$	$\rho_{i.\text{спл}} \quad \rho_{i.\text{xc}}$	Nuclear density of ith element, atoms/cm^3 (спл = alloy, xc = chemical compound; the distinction is typically not carried for this context in American convention).
$N_{n,tot}$	not used	Total nuclear density, atoms/cm^3
$N(U^{238})$	N^8	Atomic density of U^{238} atoms, atoms per cm^3.
p	φ	Resonance escape probability, dimensionless.
p_{cap}	$P_\text{к}$	Capillary pressure difference, Pa.
p_{cr}	$p_{\text{кр}}$	Critical pressure, Pa.
p_{Cs}	P_{Cs}	Cesium pressure, Torr.
p_g	$p_\text{г}$	Pressure of gas, Pa.
p_{liq}	$P_\text{ж}$	Pressure difference in liquid section, Pa.
$p_{nonleak}$	$p_{\text{ут.з}}$	Nonleakage probability, dimensionless
p_v	$P_\text{п}$	Pressure difference in vapor section, Pa.
p^*	P^*	Stagnation pressure, Pa.
Δp	Δp	Pressure difference, Pa.
Δp_{ev}	$\Delta P_{\text{пи}}$	Pressure drop in evaporator section, Pa.
Δp_a	ΔP_a	Pressure drop in adiabatic section, Pa.
Δp_{con}	$\Delta P_{\text{пк}}$	Pressure drop in condensor section, Pa.
$P_{1,2}$	$\Gamma_{1,2}$	Peltier coefficient, associated with materials 1 and 2, volts.
PR^*_{comp}	$\Pi_\text{к}$	Compressor pressure ratio, dimensionless.
PR^*_{turb}	$\Pi_\text{т}$	Turbine pressure ratio, dimensionless.
q_f	$q_\text{п}$	Fin effectiveness, dimensionless.

q'', $\dot{Q}''$	q	Heat flux, W/m^2
q''	$(N_{ти})_p$	Heat radiated from one fin, W/m^2.
q''	$N_{ти}$	Radiant heat flux from radiator, W/m^2
$q''_{entrain}$	q	Heat pipe entrainment heat flux limit, W/m^2.
q''_{sonic}	q_{max}	Heat pipe sonic heat flux limit, W/m^2.
q''_w	$(N_{ти.s})_к$	Heat radiated from channel wall, W/m^2
q^*_a	q'_π	Temperature parameter, K^4.
Q_{comp}	$L_к$	Compressor Work, J.
Q_e	$E_{эл.уд}$	Electric Energy, J.
Q_{net}	$L_{пол}$	Net output energy (useful work), J.
Q_{tur}	$L_т$	Turbine output energy, J.
$\dot{Q}_{cond}$	N_{tt}, $N_{тепл}$	Heat transferred by thermal conduction, W.
$\dot{Q}_e$	$N_{эл.уд}$	Electric Power, W.
$\dot{Q}_{e,emp}$	$N_{эн}$	Electric power consumed by electromagnetic pump, W.
$\dot{Q}_{e,gen}$	$N_{рп}$	Electric Power generated, W.
$\dot{Q}_{e,int}$	$N_{эл.с.н}$	Power consumed for internal power plant needs, W.
$\dot{Q}_{e,pl}$	$N_{цс}$	Electrical power required by spacecraft payload, W.
$\dot{Q}_{e,spec}$	$N_{эл.v}$	Specific electric power , W/kg.
$\dot{Q}_{h,emp}$	$Q_{эн}$	Hydraulic power of electromagnetic pump, W.
$\dot{Q}_{h,max,emp}$	$Q^M_{эн}$	Maximum hydraulic power of electromagnetic pump, W.
$\dot{Q}_i$	N_{T1}	Input thermal power, W.
$\dot{Q}_j$	$N_{дж}$	Joule heating, W.
$\dot{Q}_P$	$N_п$	Power released or absorbed via Peltier effect , W.
$\dot{Q}_t$	$N_{т.р}$	Reactor thermal power, kW.
$\dot{Q}_t$	N_t	Thermal power, W.
$\dot{Q}_{Thm}$	$N_{томс}$	Power released or absorbed via the Thompson effect, W.
$\dot{Q}''_e$	$N_э$	Electrical power density, W/cm^2.
$\dot{Q}''_{ecool}$	$N_{эа.s}$	Collector electron cooling flux, W/cm^2.
$\dot{Q}''_{ecool}$	$N_{эк.s}$	Emitter electron cooling flux, W/cm^2.
$\dot{Q}''_{rad}$	$N_{ти.s}$	Radiative heat flux, W/cm^2.
$\dot{Q}''_{test}$	$q_{л.д}$	Experimentally measured radiative heat flux, W/cm^2.
$\dot{Q}''_\infty$	$q_{л.и}$	Ideal radiative heat flux, W/cm^2.
$\dot{Q}'''$	N_{tv}	Thermal power per unit volume, W/m^3.
$\dot{Q}'''_c$	$N_{tv.ц}$	Maximum power per unit volume, in the center of the core (r=0; z=0), W/m^3.
r	r	distance from sun, m.
r	r	Internal resistance of a thermoelement, ohms.
r_c	r_a	Collector radius, cm.

351

r_{cap}	$r_{пор}$	Effective radius of capillaries (porosity) in wick, m.
$\bar{r}_d$	$\bar{r}_д$	Migration distance, cm.
r_e	$r_к$	Emitter radius, cm.
$\bar{r}_{hs}$	$\bar{\rho}_{к.н}$	Electrical resistance of hot shoe, ohm.
r_α	l_α	Range, m.
R	R	Resistance, ohms.
R, R_{core}	$R_a, R_{аз}$	Radius (actual) of a cyldindrical reactor core, cm.
R_c	R_a	Resistance of collector, ohms.
R_e	$R_к$	Resistance of emitter, ohms.
R_e	$R_{эк}$	Extrapolated radius of a cylindrical reactor core, cm.
R_{eq}	$R_{эк}$	Equivalent radius of spherical reactor, cm.
R_{grid}	R_p	Radius of support grid, m.
R_i	$R_i, R_{вн}$	Internal resistance, ohms.
R_L	$R_н$	Resistance of the external load, ohms.
R_n	$R_я$	Radius of the nucleus, cm.
R_o	R_o	Radius of a single nucleon, m.
R_{par}	$r_{пар}$	Resistance of parallel loads, ohms.
R_{pl}	$R_{цс}$	Radius of payload compartment, m.
ΔR	ΔR	Extrapolation distance (Radius) of reactor core.
S	$S_{рб}$	Neutron source in infinite reactor, neutrons/cm^{3}sec
t	τ	time, sec
T	T	Tangential stress, Pa.
T_{avg}	$T_{ст}$	Average coolant temperature, °C
T_c	T_a	Collector (anode) temperature, K.
T_c	T_x	Cold temperature of thermelement, K.
T_{cd}	$T_{x.x}$	Cooling device temperature, K.
T_{ci}	$T_{тн}$	Inlet coolant temperature, °C.
T_{clad}	$T_{ст}$	Cladding temperature, °C.
T_{co}	$T_{тв}$	Outlet coolant temperature, °C.
T_{cool}	T_t	Coolant temperature, °C.
T_{Cs}	T_{Cs}	Effective cesium reservoir temperature, K.
T_e	$T_к$	Emitter (cathode) temperature, K.
T_{elec}	T_e	Electron temperature in plasma, K.
T_h	$T_г$	Hot temperature of a thermoelement, K.
T_{hs}	$T_{г.и}$	Heat source temperature, K.
T_{in}	$T_{т.вх}$	Inlet coolant temperature, °C
T_n	T_n	Temperature of neutrons, K.
T_{out}	$T_{т.вых}$	Outlet coolant temperature, °C
T_w	$T_к$	Wall temperature, °C.
T^*	T^*	Stagnation temperature, K.
ΔT_{tot}	$\Delta T_{общ}$	Total temperature drop in thermoelement, K.
u	u	Neutron lethargy (logarithmic energy decrease), dimensionless.
v	ω	Velocity, m/sec.
$\bar{v}$	$\bar{w}$	Coolant flow speed, m/sec

$\bar{v}_e$	$\bar{v}_e$	Electron velocity, m/sec.
$\bar{v}_i$	$\bar{v}_i$	Ion velocity, m/sec.
$\bar{v}_n$	$\bar{v}_n$	Neutron average velocity, usually cm/sec or m/sec
V	U	Voltage, volts.
V_{arc}	$U_д$	Arc voltage drop, volts.
V_{cyl}	$V_{цил}$	Cylindrical reactor volume, cm^3.
V_E	$V_э$	Electrode voltage drop, volts.
V_{ext}	$U_г$	Extinguishing voltage, volts.
V_f	V_f, V_k	Volume containing nuclear fuel, m^3.
V_g	$V_г$	Volume of fission gas space, m^3.
V_{ig}	$U_п$	Ignition voltage, volts.
V_L	$U_н$	Load voltage, volts.
$V_{n,p}$	$V_{n,p}$	Volume of thermoelement branches, cm^3.
V_{oc}	U_{xx}	Open-circuit voltage, volts.
V_{lead}	$U_{пр}$	Lead voltage drop, volts.
$V_{max\ eff}$	$U_η$	Voltage required to achieve maximum efficiency, volts.
V_{pl}	$U_{пс}$	Payload voltage requirement, volts.
V_{sph}	$V_{сф}$	Equivalent spherical reactor volume, cm^3.
w_n, w_p	B_n, B_p	Width of thermoelements, cm.
W	W	Reactor poisoning, cm^2.
W_{perf}	$W_{перф}$	Buckling of a perforated plate, m^{-3}.
W_{sol}	$W_{сплош}$	Buckling of a solid, m^{-3}.
$\vec{X}$	X	Mode control parameter vector.
Z	Z	Total number of protons
$\bar{Z}_{n,p}$	$\bar{Z}_{n,p}$	Thermoelectric figure of merit, K^{-1}.
α	α	absorptivity, dimensionless.
α	α	Temperature coefficient, K^{-1}.
α	α	Charge compensation parameter, dimensionless.
α_n	α_n	Specific neutron radiation power, (neutrons/sec)/W.
α_γ	α_γ	Specific gamma radiation factor, (MeV/sec)/W.
α_{rad}	$\alpha_{хи}$	Temperature nonuniformity coefficient, dimensionless.
$\alpha_{1,2}$	$\alpha_{1,2}$	Differential thermal emf factor of conductors 1 and 2, V/K.
β	β	Delayed neutron fraction, dimensionless.
β_i	β_i	Ionization fraction, dimensionless.
β_m	β_m	Allowance coefficient, dimensionless
γ	γ	Relative buckling, dimensionless.
γ	γ	Cone angle, radians.
δ	δ_p	Fin thickness, m.
δ	δ	Surface potential arising from cesium dipole, eV.
δ_{clad}	$\delta_{об}$	Deformation of cladding, m.
δ_{con}	$\delta_{к.п}$	Contact thickness, cm.
δ_e	$\delta_{эк}$	Extrapolation distance, cm.
δ_{eff}	$\delta_{эф}$	Effective extrapolation distance, cm.
δ_{eref}	$\delta_{то}$	Thickness of the neutron end reflector, cm.

δ_{is}	$\delta_{из}$	Insulator thickness, cm.
δ_n	δ_n	Neutron shield thickness, cm.
δ_{ref}	$\delta_{отр}^{\delta}$	Reflector thickness, cm.
δ_{sref}	$\delta_{бо}$	Thickness of the neutron side reflector, cm.
δ_w	$\delta_к$	Wall thickness, cm.
δ_γ	δ_γ	Gamma shield thickness, cm.
Δ	Δ	Penetration depth of a meteorite, cm.
ε	ε	Fast fission factor.
ε	ε	Emissivity, dimensionless.
ε	ε	Strain, dimensionless.
ε_{eq}	$\varepsilon_{эк}$	Equivalent emissivity, dimensionless.
η	η	Fast neutron yield, dimensionless.
η_{cond}	$\eta_{тепл}$	Thermal conduction efficiency, dimensionless.
η_{eg}	$\eta_{эг}$	Electrogenerator efficiency, dimensionless.
η_{emp}	$\eta_{эн}$	Electromagnetic pump efficiency, dimensionless.
η_m	η_m	Second allowance coefficient, dimensionless.
$\eta_{n,p}$	$\eta_{н.п}$	Thermoelectric efficiency factor, dimensionless.
η_{int}	$\eta_{c.н}$	Efficiency factor due to power plant internal needs.
$\eta_{nonisothermal}$	$\eta_{неиз}$	Efficiency due to temperature nonuniformity, dimensionless.
η_{load}	$\eta_{д.н}$	Additional load efficiency, dimensionless.
η_{mech}	$\eta_{мех}$	Mechanical efficiency, dimensionless.
η_{te}	$\eta_{тэ}$	Efficiency of a thermoelement, dimensionless.
η_{comp}^*	η_{comp}^*	Compressor efficiency, dimensionless.
η_{turb}^*	η_{turb}^*	Turbine efficiency, dimensionless.
θ	θ	Degree of cesium coverage, dimensionless.
θ	θ	Scattering angle, radians.
κ	$\kappa_з$	Moderation factor, dimensionless.
κ	κ	Plate stiffness factor, dimensionless.
$\bar{\kappa}_R, \bar{\kappa}_H$	$\bar{\kappa}_R, \bar{\kappa}_H$	Flux averaging factors, dimensionless.
λ	λ	Wavelength, m.
λ_e	$\bar{l}_e$	Electron mean free path, cm.
$\bar{\lambda}_s$	$\bar{l}_s$	Scattering mean free path, cm^{-1}.
$\bar{\lambda}_{tr}$	$\bar{l}_{тр}$	Transport mean free path, cm^{-1}.
μ	μ	Viscosity, kgm/sec.
μ	μ	Poisson's ratio, dimensionless.
μ_Σ	μ_Σ	Total gamma radiation attenuation coefficient, cm^{-1}.
$\bar{\mu}$	$\bar{\mu}$	Average scattering angle cosine, dimensionless.
ν_p	ν	Fin efficiency factor, dimensionless.
ν_t	ν_t	Fin length correction factor, dimensionless.
$\bar{\nu}$	$\bar{\nu}$	Number of neutrons per fission, dimensionless.
ξ	ξ	Neutron moderation parameter, dimensionless.

ξ	ξ	Neutron moderation parameter, dimensionless.
ρ	ρ	Density, g/cm^3.
ρ	ρ	Reactivity, dimensionless.
ρ_i	$\gamma_{спл}$	Mass density of alloy, kg/m^3.
ρ_m	ρ_M	Density of meteorites, g/cm^3.
ρ_{ref}	$\rho_{бо}$	Reflector density, g/cm^3.
σ	σ	Stefan-Boltzmann constant = 5.72 x 10^{-8} w/m^{2}K^4.
σ	σ	Stress, Pa.
σ	σ	Cross section 10^{-24} cm^2 or cm^2.
σ_a	σ_a	Absorption cross section 10^{-24} cm^2 or cm^2
$\bar{\sigma}_{al}$	$\bar{\sigma}_{al}$	Resonance absorption cross section, 10^{-24} cm^2 or cm^2.
σ_c	σ_c	Radiative capture cross section 10^{-24} cm^2 or cm^2
σ_f	σ_f	Fission cross section 10^{-24} cm^2 or cm^2
σ_s	σ_s	Scattering cross section 10^{-24} cm^2 or cm^2
σ_{liq}	$\sigma_ж$	Capillary force, Nm.
σ_{plumb}	$\sigma_{г.пр}$	Gas plumbing pressure loss factor, dimensionless.
σ_{rad}	$\sigma_{хи}$	Radiator pressure loss factor, dimensionless.
σ_{reac}	$\sigma_{яр}$	Reactor pressure loss factor, dimensionless.
σ_α	σ_α	Circumferential stress, Pa.
σ_θ	σ_θ	Longitudinal stress, Pa.
σ_Σ	σ_Σ	Total pressure loss factor, dimensionless.
$\bar{\Sigma}$	$\bar{\Sigma}$	Macroscopic cross section cm^{-1}.
Σ_a	Σ_a	Macroscopic absorption cross section cm^{-1}.
$\bar{\Sigma}_{at}$	$\bar{\Sigma}_{at}$	Thermal neutron absorption cross section cm^{-1}.
Σ_c	Σ_c	Macroscopic radiative capture cross section cm^{-1}.
Σ_f	Σ_f	Macroscopic fission cross section cm^{-1}.
Σ_g	$\Sigma_г$	Macroscopic exposure cross section, cm^{-1}.
Σ_s	Σ_s	Macroscopic scattering cross section cm^{-1}.
$\bar{\Sigma}_{at}^{fuel}$	$\bar{\Sigma}_{at}^{r}$	Thermal neutron absorption cross section in fuel only, cm^{-1}.
τ	τ	Neutron "age" parameter, cm^2.
τ	$\tau_{гр}$	Time duration for pulsed operation of thermal load, sec.
τ_o	τ_Σ	Time duration for pulsed operation of thermal load, accounting for duty cycle, sec.
τ_{op}	τ_ρ	Operating lifetime, years.
τ_{pl}	$\tau_{пс}$	Required operating lifetime for payload, years.
$\tau_{0.5Rem}$	$\tau_в$	Time for radioactivity levels to decay to 0.5 Rem/year, years.
τ_1	τ_1	Thompson factor, volts.
ϕ_n	ϕ_n	Neutron flux, neutrons/cm^{2}sec.
ϕ_n	ϕ_n	Neutron fluence, neutrons/cm^2.
φ	φ	Electronic work function, eV.
φ_c	φ_a	Collector (anode) work function, eV.
φ_e	φ_c	Emitter (cathode) work function, eV.

Φ	Φ	Quality criterion for working fluids, W/m².
χ(E)	χ(E)	Neutron fission spectrum, neutrons/MeV.
χ_{reac}	$\chi_{рп}$	Reactor pressure loss factor, kg⁻¹m⁻¹.
χ_{rad}	$\chi_{хи}$	Radiator pressure loss factor, kg⁻¹m⁻¹.
ψ	ψ	Surface barrier potential, eV.